

Functional Analysis of Zinc Finger Proteins  
in the Arbuscular Mycorrhiza Symbiosis of  
*Medicago truncatula* Suggests a  
Regulatory Involvement of the PALM1  
Transcription Factor

Von der Naturwissenschaftlichen Fakultät der  
Gottfried Wilhelm Leibniz Universität Hannover

zur Erlangung des Grades  
Doktor der Naturwissenschaften (Dr. rer. nat.)

genehmigte Dissertation

von

Arne Christopher Alexander Petersen, M. Sc.

2022

Referent: Prof. Dr. rer. nat. Helge Küster

Korreferent: Dr. rer. nat. Sascha Offermann

Tag der Promotion: 12.07.2022

## Abstract

The arbuscular mycorrhizal (AM) symbiosis is a widespread beneficial association of ~80% of vascular plant species with a variety of soil-dwelling fungi. Establishing and maintaining this symbiosis and in particular the arbuscule as its central intracellular interface requires major transcriptional reprogramming of the host cells in the root cortex. Although major efforts have been successful in identifying key members of signaling pathways contributing to the regulation of the AM symbiosis, mechanisms for finetuning the association with respect to the hormonal and nutritional status of the host plant are still largely unknown. As part of this study, four *Medicago truncatula* genes encoding Zinc finger (ZF) proteins were identified to be transcriptionally upregulated in roots colonized by *Rhizophagus irregularis*. Of these genes, *MtZf1*, *MtZf2* and *MtZf3* were not characterized prior to this study, while *MtPalm1*, encoding a C2H2-family transcription factor, had been identified to act as a regulator in *M. truncatula* compound leaf development. As part of a functional analysis, the activity of these genes was confirmed to be strongly correlated with the growth of intraradical AM fungal structures via transcript measurements and histochemical localizations. These studies also indicated the involvement of upstream/overlapping ORFs in the regulation of these genes, in particular *MtPalm1*. Additionally, three separate gene silencing experiments via RNA-interference demonstrated that roots deficient in MtPALM1, MtZF1 and MtZF2 were quantitatively hampered in AM fungal colonization, with functional disruption of *MtPalm1* yielding average ~50% reductions in arbuscule formation. These phenotypes were confirmed for *MtPalm1* and *MtZf2* in stable *Tnt1*-insertion mutant lines and could be rescued through complementation via the introduction of a functional gene copy. Transcriptome profiles obtained from MtPALM1-deficient mycorrhized roots suggested this TF to act as a potential link between AM-symbiotic signaling involving strigolactones and other phytohormones, most crucially auxin. Conversely, heterologous protein interaction studies via a Yeast 2-Hybrid library mating suggested that the putative RING domain protein MtZF1 functions in targeted ubiquitination prior to AM fungal colonization. Furthermore, promoter-binding assays performed in a Yeast 1-Hybrid system gave indications of the position of the four ZFs studied in known AM regulatory networks, with protein-DNA interactions pointing to an involvement of key regulators such as RAM1, NSP2 and AM-related NF-Y-proteins in the regulation of *MtPalm1*-, *MtZf1*- and *MtZf3*-expression.

As a whole, the present thesis provides novel insights into the previously unknown contributions of ZF proteins to the fine-tuning of AM-symbiotic interactions, including the surprising role of the leaf developmental regulator MtPALM1 in modulating the level of AM-colonization, possibly by integrating hormonal signals during mycorrhization.

Keywords: Arbuscular mycorrhiza, symbiosis, transcription factor, Zinc finger, expression profiling, RNASeq, RNA interference, phytohormone, Yeast 1-hybrid, Yeast 2-hybrid

## Zusammenfassung

Die arbuskuläre Mykorrhizasymbiose (AM) ist eine weitverbreitete mutualistische Assoziation, die von ~80% der Gefäßpflanzenarten und einer Reihe von bodenlebenden Pilzen eingegangen wird. Diese Symbiose – und insbesondere die Arbuskel als ihre zentrale intrazelluläre Schnittstelle – zu etablieren und aufrechtzuerhalten setzt massive Veränderungen in der Genexpression seitens der Wirtszelle in der Wurzelrinde voraus. Vorangegangene Arbeiten konnten bereits Schlüsselfaktoren in Signalwegen für die basale Regulation der Mykorrhizasymbiose identifizieren, während Mechanismen für die feinere Steuerung und Verschaltung von hormonellen und Nährstoff-Stimuli noch immer weitestgehend unbekannt sind. Im Zuge dieser Studie wurden vier Zinkfinger-codierende *Medicago truncatula* Gene identifiziert, die in mit *Rhizophagus irregularis* kolonisierten Wurzeln transkriptionell induziert sind. Drei dieser Gene, *MtZf1*, *MtZf2* und *MtZf3* wurden vor dieser Arbeit noch nicht charakterisiert, wohingegen der von *MtPalm1* codierte C2H2-Typ Transkriptionsfaktor (TF) zuvor als Regulator der Entwicklung zusammengesetzter Blätter von *M. truncatula* identifiziert wurde. Messungen der Transkriptmengen dieser Gene sowie histochemische Lokalisationen wiesen eine starke Korrelation mit intraradikalen AM-Pilzstrukturen als Andeutung eines funktionellen Zusammenhangs auf. Dies wurde mittels dreier separater RNA-Interferenz-Experimente überprüft, bei denen sich in *MtPALM1*-, *MtZF1*- und *MtZF2*-defizienten Wurzeln signifikante quantitative Reduktionen der AM-Kolonisierung beobachten ließen. Insbesondere einhergehend mit der Reduktion von *MtPalm1*-Transkripten wurde ein signifikanter Rückgang der Menge von Arbuskeln um ~50% festgestellt. Diese Phänotypen ließen sich in *Tnt1*-Insertions-Mutantenlinien für *MtPalm1* und *MtZf2* bestätigen und durch Einbringen einer funktionalen Kopie des jeweiligen Gens komplementieren. Transkriptom-Daten aus *MtPALM1*-defizienten mykorrhizierten Wurzeln gaben Hinweise darauf, dass dieser TF eine potenzielle Schnittstelle darstellt zwischen AM-Signalwegen, bei denen Strigolactone eine Rolle spielen und der Wirkung verschiedener anderer Phytohormone. Darüber hinaus ließ sich in Yeast 2-Hybrid Interaktionsstudien für das RING-Domänen-beinhaltenende Protein *MtZF1* eine mögliche Funktion in der gezielten Proteolyse in der Vorbereitung für symbiontische Kolonisierung feststellen. Schließlich wurden Yeast 1-Hybrid Assays dazu verwendet, um DNA-Bindungen einiger bekannter AM-regulatorischer TFs mit den Promotoren der vier ZF-Gene zu untersuchen. Einige der dabei gefundenen Interaktionen mit AM-Schlüsselregulatoren wie RAM1, NSP2 und NF-Y-Proteinen lieferten Hinweise für die Regulation der Expression von *MtPalm1*, *MtZf1* und *MtZf3*.

Insgesamt bringt diese Arbeit neue Erkenntnisse über die zuvor unbekannt Funktionen von ZF-Proteinen in der Abstimmung von AM-symbiontischen Interaktionen und demonstriert die überraschende Funktion des Blattentwicklungs-Regulators *MtPALM1* in der Modulation der AM-Kolonisierung, möglicherweise durch die Integration hormoneller Signale.

Schlüsselwörter: Arbuskuläre Mykorrhiza, Symbiose, Transkriptionsfaktor, Zinkfinger, Expressionsprofil, RNASeq, RNA-Interferenz, Phytohormone, Hefe, Yeast 1-hybrid, Yeast 2-hybrid



# 1 Table of Contents

Abstract	III
Zusammenfassung	IV
1 Contents	V
1.1 List of Figures	VIII
1.2 List of Tables	X
2 Introduction	1
2.1 Arbuscular mycorrhiza symbiosis	1
2.2 <i>Medicago truncatula</i> and <i>Rhizophagus irregularis</i> as model-legume and -AM-fungus respectively	2
2.3 Major transcriptional reprogramming induces physiological changes required for fungal colonization and arbuscule formation	4
2.3.1 Pre-contact stage and early signaling	4
2.3.2 Establishment and life cycle of an arbuscule	6
2.3.3 Formation of the periarbuscular membrane via exocytosis	7
2.3.4 AM-dependent lipid biosynthesis	7
2.3.5 Regulation of nutritional exchange in AM	8
2.3.6 A network of GRAS-TFs involved in arbuscule formation and maintenance	10
2.3.7 Hormonal influences on AM symbiosis	11
2.4 <i>M. truncatula</i> ZF genes with a potential role in AM-symbiosis	13
2.5 Outline and objectives for this thesis	19
3 Material and Methods	20
3.1 Plasmids generated and used	20
3.2 Primers used	34
3.3 Other materials used	42
3.4 Nucleic acid extraction from plants and quantification	48
3.4.1 Extraction of genomic DNA from <i>M. truncatula</i>	48
3.4.2 Extraction of RNA from <i>M. truncatula</i>	48
3.4.3 Quantification of nucleic acids via the Nanodrop spectrophotometer	49
3.4.4 Estimation of RNA quality via Bioanalyzer capillary electrophoresis	49
3.5 PCR-based methods	49
3.5.1 Standard PCR protocol	49
3.5.2 Reverse Transcriptase (RT)-PCR	50
3.5.3 Detection of mutants via direct PCR screening	51
3.5.4 Semi-quantitative real-time RT-PCR	51
3.5.5 Purification of PCR- and Klenow-reaction volumes	53
3.6 Bacterial cultures	53
3.6.1 Growth conditions for bacterial cultures	53
3.6.2 Production of chemically competent <i>E. coli</i> for heat-shock transformation	54
3.6.3 Heat-shock transformation of chemically competent <i>E. coli</i>	55
3.6.4 Electroporation for transformation of <i>Rhizobium</i> -strains	55
3.6.5 Long-term storage of bacterial strains using glycerol	56
3.6.6 Quick plasmid-isolation for testing purposes	56
3.6.7 Plasmid purification from <i>E. coli</i>	56
3.6.8 Plasmid isolation from <i>Rhizobium</i> strains	57
3.7 Cloning methods	57
3.7.1 Classical cloning via Type-II restriction endonucleases	57
3.7.2 Fill-in of single-stranded 5'-overhangs using the Klenow-Fragment	58
3.7.3 Golden-Gate cloning via Type-IIs restriction endonucleases	58
3.7.4 Gateway-cloning	59
3.8 Plant treatment and cultivation	60
3.8.1 Seed sterilization and germination	60

3.8.2	Plant growth conditions	60
3.8.3	Induction of transgenic roots	60
3.8.4	Detection and screening of transgenic roots using the <i>dsRed</i> reporter	61
3.8.5	Mycorrhization by inoculation with <i>R. irregularis</i> spores	61
3.8.6	Histochemical detection of $\beta$ -Glucuronidase activity	62
3.8.7	Staining of fungal structures	63
3.8.8	Randomized quantification of intraradical AMF structures via the Gridline Intersection method	63
3.8.9	Arbuscule size measurements	64
3.8.10	Cloning and application of RNAi-based knockdown constructs	64
3.8.11	<i>Tnt1</i> -lines and complementation	66
3.8.12	RNASeq transcriptome analyses	66
3.8.13	Enrichment analyses	67
3.9	Yeast cultivation and applications	67
3.9.1	Yeast 1-Hybrid	67
3.9.2	Replica plating for yeast autoactivity tests	69
3.9.3	Yeast 2-Hybrid	69
3.9.4	Bait-autoactivation test	70
3.9.5	Yeast direct mating	70
3.9.6	Yeast library mating	70
3.10	Protein binding-assays via Bimolecular Fluorescence Complementation	72
3.10.1	Principle of BiFC	72
3.10.2	Cloning of BiFC constructs	72
3.10.3	Infiltration of <i>A. tumefaciens</i> into <i>N. benthamiana</i> leaves	73
3.10.4	YFP signal detection via confocal laser scanning microscopy	73
4	Results	75
4.1	The Zinc finger genes <i>MtPalm1</i> , <i>MtZf1</i> , <i>MtZf2</i> and <i>MtZf3</i> are upregulated during the AM-symbiosis of <i>M. truncatula</i>	75
4.2	Functional analysis of <i>MtPalm1</i> under AM-conditions	77
4.2.1	Exclusion of a putative oORF from the <i>MtPalm1</i> promoter increases the intensity of histochemical stains	77
4.2.2	Activity of the <i>MtPalm1</i> promoter is strongly correlated with arbuscule containing cells of mycorrhized roots	79
4.2.3	<i>MtPalm1</i> promoter activity is strongly diminished in the <i>ram1-1</i> and <i>pt4-2</i> mutants	80
4.2.4	Overexpression of <i>MtPalm1</i> had no significant effect on the AM symbiosis	81
4.2.5	An RNAi-mediated knockdown of <i>MtPalm1</i> leads to a reduction in overall AM colonization and in the rate of arbuscules	83
4.2.6	Negative effects of a MtPALM1-KO on the arbuscule rate and overall AM colonization were partially rescued via the introduction of a functional gene copy	86
4.2.7	Transcriptome analysis of <i>MtPalm1</i> -knockdown roots via RNASeq reveals a potential involvement in hormonal signaling networks	89
4.3	Functional analysis of <i>MtZf1</i> under AM-conditions	103
4.3.1	Promoter activity of <i>MtZf1</i> is stimulated in the presence of fungal structures and during early AM infection	103
4.3.2	<i>MtZf1</i> promoter activity is not impaired in <i>ram1-1</i> and <i>pt4-2</i> mutant backgrounds	104
4.3.3	Overexpression of <i>MtZf1</i> had no significant effect on the AM symbiosis	105
4.3.4	An RNAi-mediated knockdown of <i>MtZf1</i> led to decreased AM-colonization only in roots exhibiting substantially reduced target gene expression	107
4.4	Functional analysis of <i>MtZf2</i> under AM-conditions	110
4.4.1	A partially truncated <i>MtZf2</i> promoter exhibits activity around strongly AM colonized areas of the roots	110

4.4.2	AM-related promoter activity of <i>MtZf2</i> is abolished in <i>ram1-1</i> but not in <i>pt4-2</i> mutant backgrounds	112
4.4.3	Overexpression of <i>MtZf2</i> led to a significant reduction in AM marker gene expression as well as in the sizes of arbuscules	113
4.4.4	Successful RNAi-mediated knockdowns of <i>MtZf2</i> negatively affected AM-symbiosis	115
4.4.5	Negative effects of an MtZF2-KO on the overall mycorrhization rate were partially rescued via the introduction of a functional gene copy	117
4.5	Functional analysis of <i>MtZf3</i> under AM-conditions	121
4.5.1	Activity of the <i>MtZf3</i> promoter is increased in the presence of functional arbuscular mycorrhiza	121
4.5.2	<i>MtZf3</i> promoter activity depends on the presence of functional arbuscules	122
4.5.3	An RNAi-mediated knockdown of <i>MtZf3</i> had slightly negative effects on overall AM colonization	123
4.6	Yeast 2-Hybrid interaction analyses involving MtPALM1, MtZF1 and MtZF2 as well as MtARF-proteins	127
4.6.1	Y2H bait strains expressing <i>MtPalm1</i> , <i>MtZf2</i> and <i>MtArf12</i> exhibit some level of autoactivity	129
4.6.2	A Y2H library mating revealed potential interaction candidates for MtZF1	131
4.7	Identification of AM-related TFs interacting with <i>MtPalm1</i> , <i>MtZf1</i> , <i>MtZf2</i> and <i>MtZf3</i> promoters via Yeast 1-Hybrid direct mating	135
4.7.1	A diverse group of TFs including AP2/ERF, GRAS, and NF-YA potentially bind to the <i>MtPalm1</i> promoter	136
4.7.2	Binding to the <i>MtZf1</i> promoter was possible for members of an NF-Y-complex as well as a number of other AM-related TFs	139
4.7.3	The <i>MtZf2</i> promoter exhibits binding properties in combination with numerous different TFs from various families	141
4.7.4	The <i>MtZf3</i> promoter is putatively bound by the AM-related GRAS-TFs MtRAM1, MtNSP1 and MtNSP2	143
4.7.5	Yeast 1-Hybrid mating results indicate functional regulatory relationships between <i>MtZf</i> -gene expression and AM-related TFs	145
5	Discussion	147
5.1	The four <i>M. truncatula</i> Zinc finger genes <i>MtPalm1</i> , <i>MtZf1</i> , <i>MtZf2</i> and <i>MtZf3</i> feature distinct activation patterns during AM-development and -maintenance	147
5.2	Insights into the involvement of <i>M. truncatula</i> ZF proteins in the development and maintenance of the AM-symbiosis	152
5.2.1	The CCCH ZF protein encoded by <i>MtZf3</i> plays a minor role during AM-symbiosis	152
5.2.2	The RING-domain protein encoded by <i>MtZf1</i> is involved in AM signaling and might contribute to targeted proteolysis in preparation of fungal colonization	152
5.2.3	The C2H2 Zinc finger TFs encoded by <i>MtPalm1</i> and <i>MtZf2</i> are important for the full functionality of AM symbiotic program	156
5.3	MtPALM1 acts as a mediator between AM symbiotic processes and hormonal stimuli, especially auxin	161
5.4	Conclusion and outlook	165
6	References	170
7	Supplements	185
S1.	<i>MtPalm1</i> bait-autoactivity was too severe to identify clear interaction partners in direct mating analyses	200
S2.	Interaction partners of MtZF2 could not be identified due to sporadic growth of the Y2H bait strain	201
S3.	BiFC-matrix of AM-related GRAS-proteins reveals novel potential interaction pairs	203
8	Danksagung	207

## 1.1 List of Figures

Figure 1 – Example of a fluorescence-stained arbuscular mycorrhiza colonized root fragment	2
Figure 2 – Arbuscular mycorrhiza early signaling and the intraradical fungal life cycle	5
Figure 3 – Schematic overview of the arbuscule life cycle	6
Figure 4 – Overview of the nutrient exchange in an arbuscocyte	9
Figure 5 – Schematic overview of the GRAS-domain	11
Figure 6 – In silico expression analysis of several putative AM-related <i>M. truncatula</i> Zinc finger genes	14
Figure 7 – Regulatory pathway for <i>M. truncatula</i> compound leaf development involving <i>MtPalm1</i>	16
Figure 8 – Principle of Golden-Gate cloning via Typell's restriction endonucleases	59
Figure 9 – Overview of the RNAi-knockdown target regions	65
Figure 10 – Principle of the Yeast 1-Hybrid system employed	68
Figure 11 – Principle of the Yeast 2-Hybrid system employed	71
Figure 12 – Bimolecular fluorescence complementation assay	74
Figure 13 – Measurements of AM-induced Zinc finger genes in a <i>M. truncatula</i> mycorrhization time course via sqRT-PCR	75
Figure 14 – Comparative analysis of AM-induced <i>MtPalm1</i> -promoter activity in a full and 3'-truncated version	78
Figure 15 – Histochemical localization of <i>MtPalm1</i> promoter activity in wild-type mycorrhized roots	79
Figure 16 – Histochemical localization of <i>MtPalm1</i> promoter activity in mycorrhized roots of <i>ram1-1</i> and <i>pt4-2</i> mutants	80
Figure 17 – Effects of <i>MtPalm1</i> -overexpression on AM-colonization and arbuscule sizes	82
Figure 18 – <i>MtPalm1</i> -RNAi-knockdown results on AM marker <i>MtPt4</i> and overall AM-colonization	84
Figure 19 – Effects of a <i>MtPalm1</i> - <i>Tnt1</i> -knockout and -complementation on the expression of AM-marker <i>MtPt4</i> and overall AM-colonization	88
Figure 20 – Expression of <i>MtPalm1</i> and <i>RiαTub</i> in the RNA-samples used for the RNASeq analysis	89
Figure 21 – Overview of differentially regulated genes in mycorrhized roots expressing an <i>MtPalm1</i> -RNAi construct	90
Figure 22 – Known or putative AM-related genes downregulated in mycorrhized roots expressing <i>MtPalm1</i> -RNAi	92
Figure 23 – Overlap between <i>MtPalm1</i> -downregulation and the AM-transcriptional program	94
Figure 24 – GO-enrichment analyses of groups of genes differentially regulation in the absence of <i>MtPALM1</i>	96
Figure 25 – Terpenoid and carotenoid biosynthetic pathways exhibiting differential regulation in <i>MtPALM1</i> -deficient mycorrhized roots	101
Figure 26 – Selection of phytohormone signaling pathways exhibiting differential regulation in roots expressing <i>MtPalm1</i> -RNAi	102
Figure 27 – Histochemical localization of <i>MtZf1</i> promoter activity in wild-type mycorrhized roots	104
Figure 28 – Histochemical localization of <i>MtZf1</i> promoter activity in mycorrhized roots of <i>ram1-1</i> and <i>pt4-2</i> mutants	105
Figure 29 – Effects of <i>MtZf1</i> -overexpression on AM-colonization and arbuscule sizes	106
Figure 30 – <i>MtZf1</i> -RNAi-knockdown results on AM marker <i>MtPt4</i> and overall AM-colonization	109
Figure 31 – A <i>gus</i> -fusion construct of the -1,572/-3 <i>MtZf2</i> promoter region shows no activity in wild-type mycorrhized roots	110
Figure 32 – Histochemical localization of <i>MtZf2</i> promoter (-2,059/-184) activity in wild-type mycorrhized roots	111

Figure 33 – Histochemical localization of MtZf2 promoter activity in mycorrhized roots of ram1-1 and pt4-2 mutants	113
Figure 34 – Effects of MtZf2-overexpression on AM-colonization and arbuscule sizes	114
Figure 35 – MtZf2-RNAi-knockdown results on AM marker MtPt4 and overall AM-colonization	116
Figure 36 – Effects of a MtZf2-Tnt1-knockout and -complementation on the expression of AM-marker MtPt4 and overall AM-colonization	119
Figure 37 – Histochemical localization of MtZf3 promoter activity in wild-type mycorrhized roots	121
Figure 38 – Histochemical localization of MtZf3 promoter activity in mycorrhized roots of ram1-1 and pt4-2 mutants	123
Figure 39 – MtZf3-RNAi-knockdown results on AM marker MtPt4 and overall AM-colonization	125
Figure 40 – Autoactivation-test for Y2H-bait strains produced during this work	130
Figure 41 – Yeast 1-Hybrid assay revealing potential binding of the MtPalm1 promoter by multiple TFs important during AM	138
Figure 42 – Yeast 1-Hybrid assay revealing potential binding of the MtZf1 promoter by multiple TFs important during AM	140
Figure 43 – Yeast 1-Hybrid assay revealing potential binding of the MtZf2 promoter by multiple TFs important during AM	142
Figure 44 – Yeast 1-Hybrid assay revealing potential binding of the MtZf3 promoter by multiple TFs important during AM	144
Figure 45 – Patterns of promoter activity observed for the different MtZf genes	148
Figure 46 – Major patterns of MtRam1 and MtZf gene activity during the arbuscular life cycle	151
Figure 47 – Model for the AM-based induction and activity of MtZf1	154
Figure 48 – Model for the promotion of mycorrhization via different influences on the AM-specific activation of MtPalm1	160
Figure 49 – Proposed model integrating MtPALM1 with hormonal stimuli and AM-signaling	163

## 1.2 List of Tables

Table 1 – Nomenclature of MtZf and MtArf3-like candidate genes subject to this study	17
Table 2 – List of microbial strains carrying plasmids constructed/used during this work	20
Table 3 – Primers used during this work	34
Table 4 – Buffers used	42
Table 5 – Chemicals used	43
Table 6 – Enzymes used	45
Table 7 – Commercial kits used	45
Table 8 – Materials used	46
Table 9 – Machines and devices	46
Table 10 – Software used	47
Table 11 – Standard PCR setup	49
Table 12 – RT-PCR setup	50
Table 13 – Direct PCR setup	51
Table 14 – sqRT-PCR setup	52
Table 15 – Strains of bacteria and corresponding media	53
Table 16 – Standard media for bacterial cultures	54
Table 17 – Antibiotic solutions	54
Table 18 – Golden-gate cloning reaction setup	59
Table 19 – Cloning and staining procedures for promoter-gus constructs	62
Table 20 – Differentially regulated genes annotated as part of biosynthetic and signaling pathways	99
Table 21 – Information concerning candidate genes for the protein-interaction studies	127
Table 22 – Relative autoactivity of any Y2H bait-strains used in this work	131
Table 23 – Y2H direct mating results for MtZF1	132
Table 24 – Results for the MtZF1 Library mating	134
Table 25 – Summary of Yeast 1-Hybrid direct mating results	146
Table 26 – List of Abbreviations	167

## 2 Introduction

### 2.1 Arbuscular mycorrhiza symbiosis

The term “Mycorrhiza” derives from the Greek words “*mykes*” for fungus and “*rhiza*” for root and was first introduced by Albert Bernard Frank, (1885) to describe the mutualistic association between a diverse group of fungi and over 90% of all terrestrial plant families (Wang and Qiu, 2006). These symbiotic interactions can be subdivided based on the morphology of the association with the host roots: in ectomycorrhizae, fungal hyphae form a sheath on the outside of the root and are only able to grow between the root cells to form a so called Hartig Net, but do not typically invade individual cells. Endomycorrhizae, in contrast, involve fungal structures penetrating the cell walls of cortical cells within the root (Parniske, 2008). This category comprises a number of distinct mycorrhizal associations such as arbuscular, arbutoid, ericoid, monotropoid and orchid mycorrhizas (Peterson *et. al*, 2004).

By far the most widespread type of endomycorrhiza is the arbuscular mycorrhiza (AM; Fitter and Moyersoen, 1996) formed by over 240 species of fungi from the phylum *Glomeromycota* (Redecker *et. al*, 2000; Redecker *et. al*, 2013; Heijden *et. al*, 2015). Fossil records suggest that AM-symbiosis first evolved approximately 400 – 450 million years ago and may have been instrumental for the initial spread of plants from the water to terrestrial habitats (Pirozynski and Malloch, 1975; Kistner and Parniske, 2002). AM symbiosis is characterized by hyphae not merely invaginating individual cortical cells within the roots, but developing highly branched structures inside them. These “arbuscules” (from latin “*arbusculum*” for little tree, see also Figure 1b for a visual example) represent the interface at which the symbiotic exchange of nutrients occurs: The host plant benefits from the hyphae increasing the surface area capable of absorbing and translocating water and minerals from the soil, thereby measurably increasing the fitness of AM-colonized plants. In particular, uptake of the typically limiting nutrient phosphate contributes to this positive effect, though the supply of other macronutrients such as nitrogen, sulfur and potassium (Govindarajulu *et. al*, 2005; Allen and Shachar-Hill, 2009; Garcia *et. al*, 2017) also plays a relevant role, as do enhanced tolerances to drought and heavy metal stresses (Miller *et. al*, 1995; Berruti *et. al*, 2015). In exchange, the obligate biotrophic fungi are supplied with organic carbon to sustain the mycelium inside and outside of the root systems, where the ultimate formation of new spores takes place as well (Bago *et. al*, 2000).

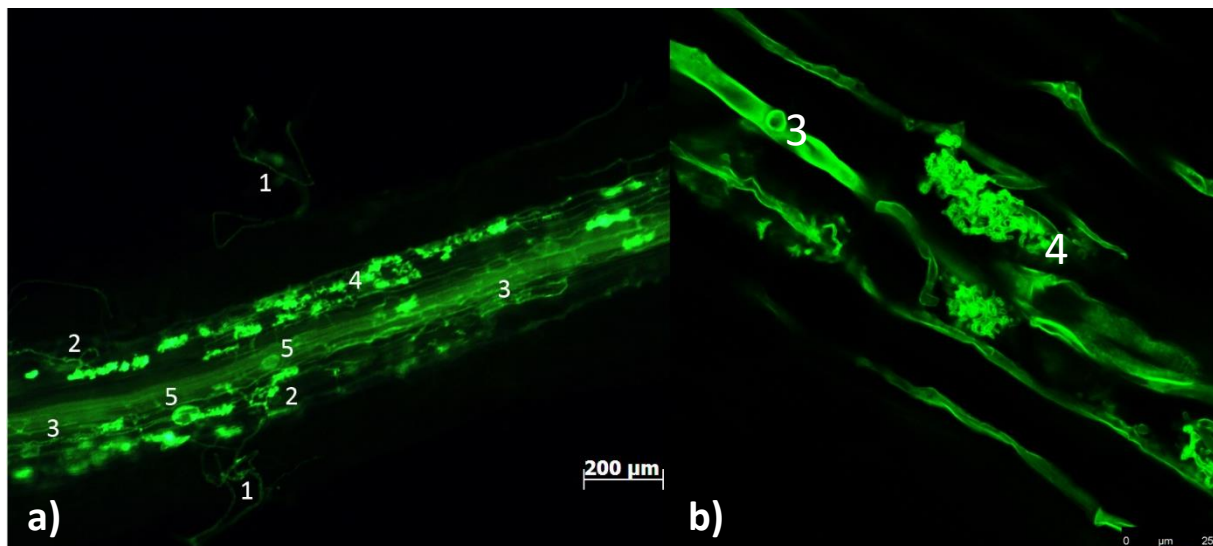


**Figure 1 – Example of a fluorescence-stained fragment of an arbuscular mycorrhiza colonized root**

a) Representative overview of a *M. truncatula* root colonized by *R. irregularis*. AM fungal structures were stained using Alexa488-WGA, images were captured via fluorescence microscopy. (1) indicates extraradical hyphae connected to the root. Fungal hyphopodia used as entry points into the roots are marked by (2). (3) points to intraradical hyphae. A number of arbuscules are clustered in a row around (4). Fungal storage vesicles within the roots are indicated by (5). b) shows a closeup of single arbuscules connected to the wider hyphal network by their respective trunks.

## 2.2 *Medicago truncatula* and *Rhizophagus irregularis* as model-legume and -AM-fungus respectively

The barrel medic *Medicago truncatula* is an established model plant for the *Fabaceae* or legume family that includes important crops such as soybean as well as various types of beans, peas and lentils. As part of this family, *M. truncatula* is capable of establishing AM symbiotic relationships with a variety of fungi as well as the formation of root nodules harboring *Rhizobium*-bacteria able to fix nitrogen. *M. truncatula* plants are relatively small and self-fertile, while having a short generation time of only 3-6 months, making them compatible with a laboratory setting. Additionally, its comparatively small, diploid genome of approximately 500 Mbp across  $2n = 16$  chromosomes facilitates genetic accessibility, a prerequisite of a suitable model organism (Young *et. al*, 2005).

Initial efforts in transcript sequencing led to the first expressed sequence tag (EST) based cDNA arrays and – together with genomic sequences – to the subsequent design of an Affymetrix GeneChip. The resulting collection of transcriptome datasets over time consolidated into the *Medicago truncatula* Gene Expression Atlas (MtGEA, data currently hosted at <https://lipm-browsers.toulouse.inra.fr/pub/expressionAtlas/app/mtgeav3/>), making this information readily available to researchers (Liu *et. al*, 2003; Frenzel *et. al*, 2005; Benedito *et. al*, 2008; Carrere *et. al*, 2021). Further efforts to obtain sequence data on all nuclear encoded genes as part of the *Medicago*



*truncatula* Genome Project have, by March 2021 led to the reference genome database ver5.1.8 (<https://medicago.toulouse.inra.fr/MtrunA17r5.0-ANR/>), comprising more than 430 Mbp of the *M. truncatula* Jemalong A17 gene space with 44,623 protein coding genes (Pecrix *et. al*, 2018). Mutant databases for functional analysis of genes of interest generated via fast neutron bombardment or random insertion of the *Tnt1*-retrotransposon (Transposon from *Nicotiana tabacum*) are also available (<https://medicago-mutant.dasnr.okstate.edu/mutant/index.php>; Tadege *et. al*, 2008; Sun *et. al*, 2019). Additionally, a number of transformation protocols for the production of transgenic plants have been developed over time (Trinh *et. al*, 1998; Wright *et. al*, 2006; Jiang *et. al*, 2019), as have protocols for root-transformation using *Agrobacterium rhizogenes* (Limpens *et. al*, 2004; Vieweg *et. al*, 2004), together comprising a set of tools for the investigation of gene functions.

*Rhizophagus irregularis*, previously known as *Glomus intraradices*, is an arbuscular mycorrhizal fungus (AMF) of the order *Glomeromycota* naturally occurring in soils (Schenck and Smith, 1982; Kruger *et. al*, 2012). It lives as an obligate symbiont in association with a variety of host plants such as maize, rice onions, tomatoes, or legumes and is used as microbial inoculant in horticulture or agriculture to improve access to nutrients enhancing plant growth and overall health (Toro *et. al*, 1997; Cavagnaro *et. al*, 2006). *R. irregularis* reproduces asexually and is able to efficiently colonize plants from spores, hyphae, or other infected root fragments (Klironomos and Hart, 2002). The haploid genome of *R. irregularis* strain DAOM 197198 has been partially sequenced and assembled to a size of approximately 91.1 Mbp with 30,282 annotated gene models (JGI Mycorrhizal Genomics Initiative, <http://genome.jgi.doe.gov/Gloin1/Gloin1.home.html>, Tisserant *et. al*, 2013). As part of the same effort, transcriptome data sets are available as well, together comprising a basis for future research with this model AMF (Tisserant *et. al*, 2012).

## 2.3 Major transcriptional reprogramming induces physiological changes required for fungal colonization and arbuscule formation

### 2.3.1 Pre-contact stage and early signaling

Establishing the symbiotic relationship between the plant and AM fungi requires a network of signals triggering transcriptional and subsequent physiological changes (outlined in Figure 2). Various components of this network are conserved between AM-symbiosis and nodulation as part of the so-called common symbiotic signaling pathway (CSSP) and are thus at least partially understood (Gutjahr *et. al*, 2008): Prior to physical contact between the fungus and the root, specific carotenoids called strigolactones exuded by the plant are perceived by AM-fungi (Akiyama *et. al*, 2005; Besserer *et. al*, 2006). In turn, fungal growth, as well as production of chito- and lipochitooligosaccharides (COs and LCOs, respectively), is stimulated (Maillet *et. al*, 2011; Czaja *et. al*, 2012; Hohnjec *et. al*, 2015). These signal molecules bind to and activate Leucine-rich repeat and Lysine-motif receptor like kinases (LRR- / LysM-RLKs) such as DMI2 (“Does not Make Infection 2”, SYMRK in *Lotus japonicus*) and NFP (Nod Factor Perception, Stracke *et. al*, 2002; Maillet *et. al*, 2011; Camps *et. al*, 2015). This triggers the activation of the enzyme 3-hydroxy-3-methylglutaryl coenzyme A reductase 1 (HMGR1) and thereby the production of mevalonate which in turn leads to oscillations of Ca<sup>2+</sup>-concentration in the nuclei of root cells (Kevei *et. al*, 2007; Venkateshwaran *et. al*, 2015). This calcium-spiking is facilitated by the K-channels CASTOR and POLLUX/DMI1 (Ané *et. al*, 2004; Charpentier *et. al*, 2008), the nucleoporins NUP85, NUP133 and NENA (Kanamori *et. al*, 2006; Saito *et. al*, 2007; Groth *et. al*, 2010) and three cyclic nucleotide-gated channels (Charpentier *et. al*, 2016), all located in the nuclear membrane. In response to these Ca<sup>2+</sup>-spikes, the calcium/calmodulin-dependent kinase DMI3 phosphorylates the transcriptional regulator IPD3 (CYCLOPS) (Yano *et. al*, 2008). The TF IPD3 is able to directly bind to a *cis*-regulatory element called “AM-CYC box” (Pimprikar *et. al*, 2016) present in a variety of different promoter regions including those of key AM-regulating GRAS-TFs NSP2 (Nodulation Signaling Pathway 2) and RAM1 (Reduced Arbuscular Mycorrhiza 1). These two factors have been demonstrated to form heterodimers and have the capacity to bind to promoters (Hirsch *et. al*, 2009; Gobbato *et. al*, 2012) and to directly or indirectly activate a variety of further downstream genes, including genes required for lipid-biosynthesis such as the glycerol-3-phosphate acyltransferase MtrAM2 (Gobbato *et. al*, 2013), the acyl-ACP (acyl carrier protein) thioesterase *FatM* (Bravo *et. al*, 2017) or the arbuscule-specific phosphate transporter *Pt4* (Harrison *et. al*, 2002; Pimprikar *et. al*, 2016).

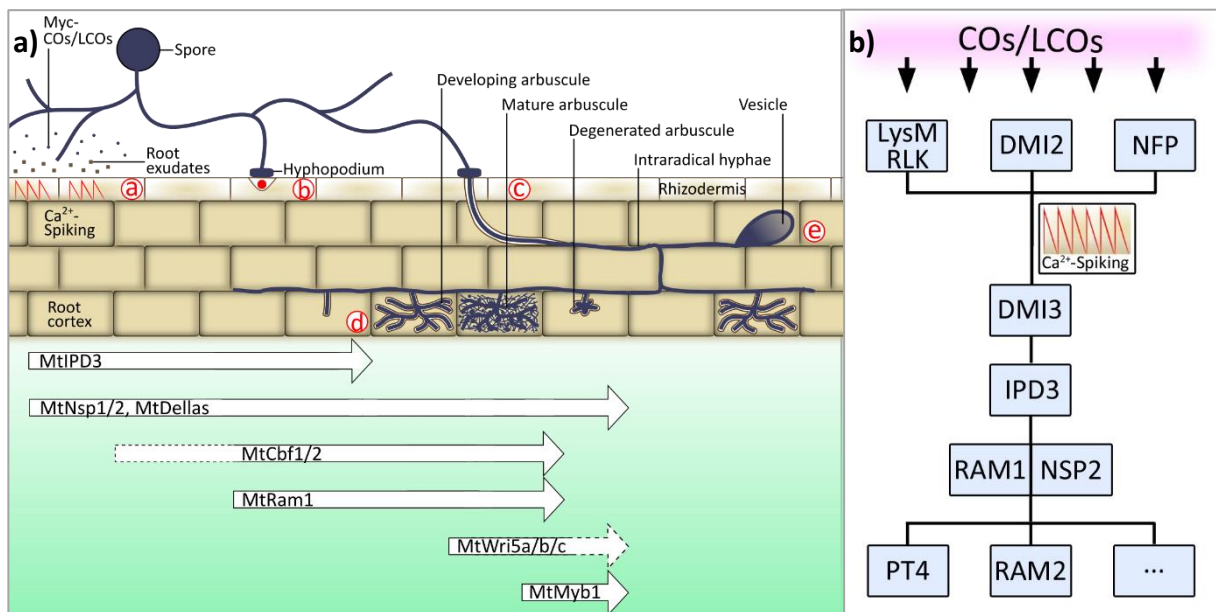


**Figure 2 – Arbuscular mycorrhiza early signaling and the intraradical fungal life cycle**

During the pre-contact phase (a), root exudates including strigolactones stimulate hyphal branching and growth towards the root surface. Myc-(lipo-)chitoooligosaccharides (COs/LCOs) in turn stimulate rhizodermal cells, ultimately initiating nuclear  $\text{Ca}^{2+}$ -spiking. When contact is made (b), the hyphal tips differentiate into a hyphopodium. The contacted cell forms the pre-penetration apparatus in preparation for invagination of the AMF into the cell and further through the outer cortex (c). In the inner cortex, individual cells are colonized to facilitate the symbiotic exchange through arbuscules that themselves go through the life cycle outlined under d). The AMF uses carbon supplied by the host plant to sustain the rest of the mycelium, including the formation of lipid storage bodies within the roots called vesicles (e). Arrows below indicate activity of a selection of important AM symbiosis genes: The helix-loop-helix TF IPD3/CYCLOPS is crucial during both the pre- and early contact phases as well as during the establishment of individual arbuscules. The GRAS-TFs NSP1/2 and DELLA-proteins are likewise important early and continue to control various processes throughout the life cycle of arbuscules. TFs like CCAAT-box binding factors 1 and 2 (Cbf1/2) or RAM1 are specifically active in the presence of an AMF symbiont. In contrast, genes encoding TFs like WR15-like proteins are specifically expressed in the mature stage of arbuscules, while MYB1 has been demonstrated to coordinate arbuscule degeneration. The diagram on the right (b) outlines the initial signaling processes during AM pre-contact/early contact: LCOs stimulate LRR- or Lysine-motif receptor like kinases (LysM-RLKs) like DMI2 and NFP (Nod factor perception) among others. Through  $\text{Ca}^{2+}$ -Spiking as a signal, DMI3 activates IPD3/CYCLOPS, which as a TF enables transcription of the *Ram1* and *Nsp2* genes. The resulting proteins dimerize and are able to activate a variety of crucial AM-dependent genes (Adapted from: Parniske, 2008; Oldroyd, 2013; Pimprikar and Gutjahr, 2018).

### 2.3.2 Establishment and life cycle of an arbuscule

Upon contact to the root, the fungal hyphae differentiate to form a thickened structure called a hyphopodium (or more generally an appressorium; Genre *et. al*, 2005). As a result of the signaling cascade detailed above, epidermal root cells reorganize their cytoskeleton and cluster the endoplasmic reticulum and Golgi-apparatus below the point of fungal contact (Blancaflor *et. al*, 2001; Genre *et. al*, 2008). This membrane aggregation is subsequently able to facilitate the invagination of the fungus through the epidermal cell and further into the cortical cell layers. Here, the intraradical hyphae can infect individual cells, where they branch out extensively to form arbuscules (see also Figure 2a).

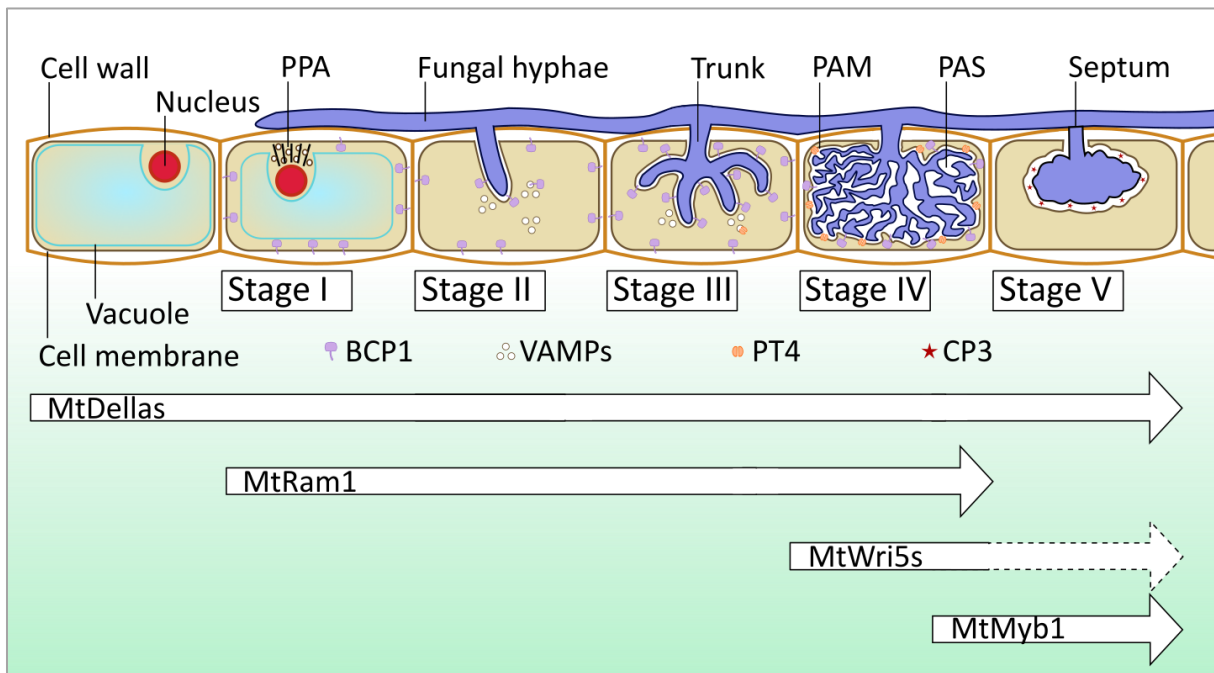


**Figure 3 – Schematic overview of the arbuscule life cycle**

During the initial Stage I, an intraradical hypha makes contact with the prospective cortical host cell. In response, nuclear movements are initiated and components of the cytoskeleton as well as elements from the cytoplasm and ER form a cytoplasmic bridge called the pre-penetration apparatus (PPA). Initial symbiotic marker genes encoding the GRAS-TFs RAM1 and the blue copper protein 1 (BCP1) are already active at this stage. The fungus is then able to penetrate into the cell along the path pre-defined via PPA, initiating Stage II. During the entire process, the fungus is enveloped by the plant-derived periarbuscular membrane, built up by exocytotic vesicles. This process directs membrane-proteins to the periarbuscular membrane (PAM), illustrated via the vesicle-associated membrane proteins (VAMPs). Low-order branching of the hyphae forms structures resembling a “bird’s foot” in Stage III. Continually finer branching leads to the formation of arbuscules facilitating the symbiotic exchange. During this mature Stage IV, the host plant releases hexoses and C16 fatty acids into the periarbuscular space (PAS) for uptake by the fungus in exchange for nutrients, especially phosphate that is transported into the plant cytosol through the phosphate transporter 4 (PT4) present in the PAM. Wrinkled 5-like (Wri5) TFs from the AP2/ERF family activating FA-biosynthetic processes are crucial during this stage. After a few days, the arbuscule is degenerated by the host plant through hydrolases such as the cysteine protease 3 (CP3) activated by the TF MYB1. During this Stage V, the arbuscule is cut off from the syncytial fungal network via the introduction of a septum. A number of genes required for full arbuscule development such as those encoding DELLA-proteins are constitutively expressed. Adapted from: Gutjahr and Parniske (2013); Pimprikar and Gutjahr (2018).

An individual arbuscule, as the interface unit for the symbiotic nutrient exchange, itself only has a short lifespan of several days, while going through a variety of developmental stages during this time (Alexander *et. al*, 1989, see also Figure 3). In the first stage, the pre-penetration apparatus (PPA) is formed, following the early signaling pathway. Then, the hypha – the subsequent “trunk” of the forming arbuscule – invades the cortical cell enveloped in a newly built-up periarbuscular membrane (PAM), initiating Stage II. This hypha now begins to branch out, first rather coarsely into a structure resembling a “birdsfoot” (Stage III), then into increasingly finer structures forming a large surface area. This mature Stage IV of arbuscule life is central to the symbiotic nutrient exchange between plant and fungus (Luginbuehl and Oldroyd, 2017). After several days of this mature stage, the arbuscule is broken down by the host-plant (Stage V) and is ultimately cut off from the fungal network via a cytoplasmic barrier called a “septum” (Alexander *et. al*, 1989; Kobae *et. al*, 2014; Uhe *et. al*, 2018).

### 2.3.3 Formation of the periarbuscular membrane via exocytosis

The formation of the plant-derived PAM requires the buildup of new membranes and the incorporation of specific proteins (Pumplin and Harrison, 2009). To that end, exocytosis of vesicles from the *trans*-Golgi network has been shown to play a major role: the two vesicle-associated membrane proteins VAMP721d and VAMP721e are necessary for the formation of properly branched mature arbuscules (Ivanov *et. al*, 2012; see also Figure 3, Stages II and III). Similarly, a structurally related protein VAPYRIN is required for proper root infection and arbuscule initiation (Pumplin *et. al*, 2010). VAPYRIN itself binds to other secretion proteins including the contain the EXOCYST-complex subunit EXO70I, which has been demonstrated as necessary for the incorporation of the ABC transporters STR and STR2 (stunted arbuscule) and is required for full arbuscule development (Genre *et. al*, 2012; Zhang *et. al*, 2015). This interaction might suggest that VAPYRIN directs EXO70I to the PAM in order to facilitate its buildup. Additionally, the t-SNARE protein SYP132A is also important for the development of the PAM (Pan *et. al*, 2016).

### 2.3.4 AM-dependent lipid biosynthesis

PAM formation requires the synthesis of fatty acids to form the phospholipids necessary for membrane-buildup. Likewise, fungal growth, branching, as well as the formation of vesicles as lipid storage bodies necessitate the AMF to be supplied by the symbiotic host plant with lipids, since AMF lack genes encoding fatty acid synthases (Wewer *et. al*, 2014; Tang *et. al*, 2016). This is facilitated by a proposed linear fatty acid synthesis pathway largely dependent on regulation by RAM1, as illustrated in the left of Figure 4. As the initial step of this process, 2C-ACP molecules are condensed to 4C-ACP by

the  $\alpha$ -keto-acyl-ACP synthase KASIII. These 4C-ACP are further elongated to C16-ACP by the  $\beta$ -keto-acyl ACP synthase encoded by Dis (disorganized arbuscule; Keymer *et. al*, 2017). These C16 fatty acids are subsequently released from the ACP by AM-specific acyl thioesterase FatM (fat required for arbuscular mycorrhiza symbiosis, Bravo *et. al*, 2016; Bravo *et. al*, 2017). RAM2 then converts these C16-FAs to C16- $\beta$ -monoacylglycerol (Gobbato *et. al*, 2013; Bravo *et. al*, 2017). These are then transferred to the periarbuscular space (PAS) via half-size ATP binding cassette transporter subfamily G (ABCG) STR/STR2 (Zhang *et. al*, 2010; Gutjahr *et. al*, 2012; Jiang *et. al*, 2017). Besides regulation by RAM1, three Apetala 2 (AP2) transcription factors orthologous to the *A. thaliana* “Wrinkled 5” TF called WR15A, B and C have recently been demonstrated to also play a major enhancing role in this AM-dependent fatty acid biosynthesis- and delivery-pathway. This is accomplished by either direct or indirect activation of the fatty acid biosynthesis enzymes outlined above, as well as direct binding to the promoter of the *Str*-gene (Luginbuehl *et. al*, 2017; Jiang *et. al*, 2018).

### 2.3.5 Regulation of nutritional exchange in AM

The arbuscule represents the central interface for the symbiotic exchange of nutrients, an overview of which is presented in Figure 4. Here, the obligate biotrophic AMF are supplied by the host plant with organic carbon representing up to 20% of the host plant’s photoassimilates (Bago *et. al*, 2000). Monoacylglycerols (MAG) that the *Glomeromycota* fungi are believed to be unable to produce, synthesized through the process outlined in the prior section, are delivered to the fungus via the half-size ABCG-transporters STR/STR2 (Trépanier *et. al*, 2005; Gutjahr *et. al*, 2012; Jiang *et. al*, 2017). Besides this lipid supply, sugars have long been known to be delivered as well (Parniske, 2008). To that end, AM-specifically expressed sucrose-cleaving enzymes such as SucS1 (Sucrose Synthase 1) or apoplastic invertases (Schaarschmidt *et. al*, 2006) provide the hexoses glucose and fructose for supply of the fungus, as evidenced by the impairment of the symbiosis in the absence of SucS1 (Hohnjec *et. al*, 2003; Baier *et. al*, 2010). The hexoses are believed to be exported into the PAS through a class of monosaccharide transporters called SWEET (Chen *et. al*, 2010b; Manck-Götzenberger and Requena, 2016). On the fungal side, the supplied sugars are subsequently taken up through a variety of monosaccharide transporters (MST) to be used as energy or converted into trehalose and glycogen for transport and storage (Pfeffer *et. al*, 1999; Schüssler *et. al*, 2006; Helber *et. al*, 2011).

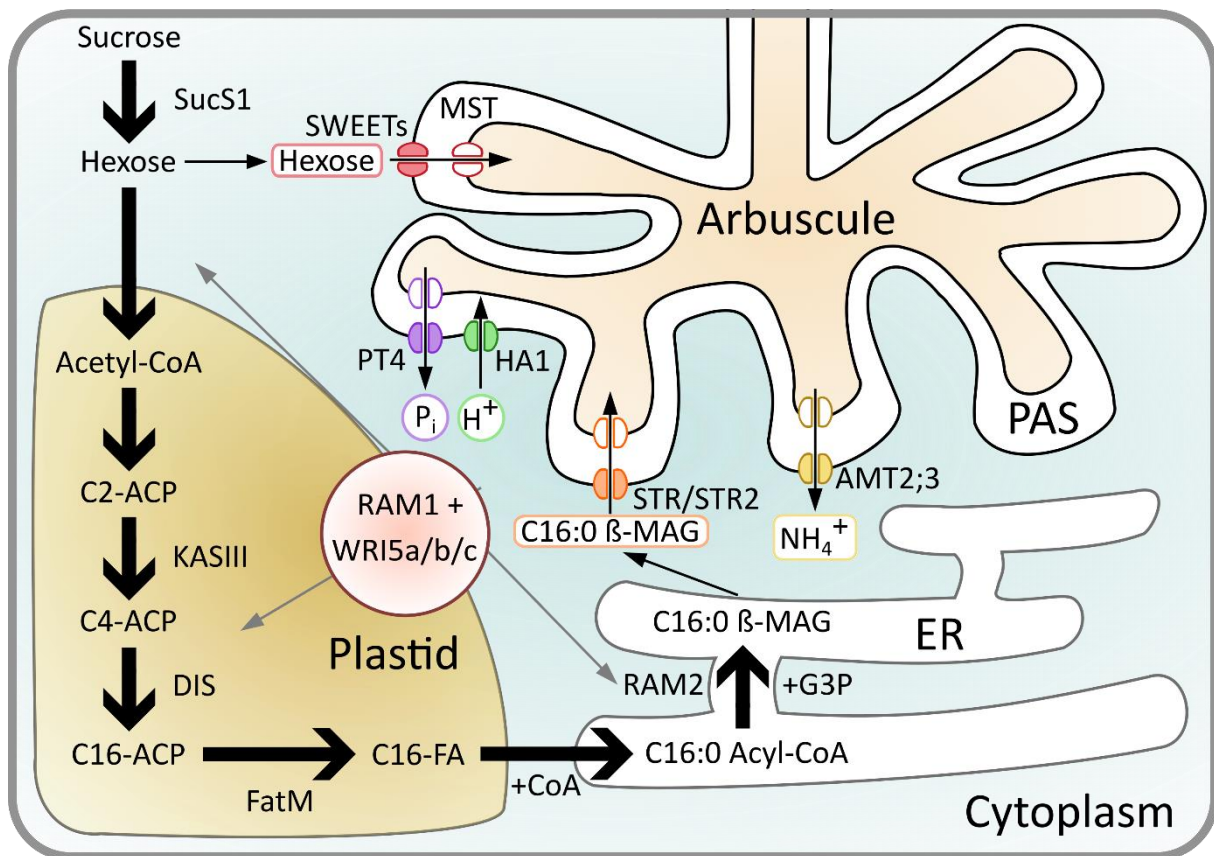


**Figure 4 – Overview of the nutrient exchange in an arbusocyte**

The AMF is supplied by the host plant with sugars and C16-fatty acids as carbon sources. The hexose sugars, produced by breaking down sucrose via enzymes such as SucS1 or apoplastic invertases (not depicted), are transported into the periarbuscular space (PAS) through SWEET sugar transporters and subsequently taken up by the fungus through the MST transporter. Lipids used for the supply of the symbiotic partner are synthesized *de novo* by the plant: in the plastids, from initial Acetyl-CoA, a C2-body fused to an Acyl carrier protein (ACP) is synthesized. These C2-ACPs are condensed into C4-ACP by KASIII ( $\beta$ -keto-acyl ACP synthase III), which are in turn converted to C16-ACP by the enzyme DIS (disorganized arbuscule). FatM (fatty acid required for mycorrhization) then creates C16 fatty acids. In the ER, RAM2 (reduced arbuscular mycorrhiza 2, a glycerol-3-phosphate acyltransferase) subsequently is able to create C16  $\beta$ -monoacylglycerol. These processes are transcriptionally controlled by AP2/ERF-TFs Wri5a/b/c and the GRAS-TF RAM1. The two half-size ATP binding cassette transporter subfamily G (ABCG) STR/STR2 membrane proteins are able to facilitate transport of these lipids to the PAS. The transporter on the AMF side is still unknown. In exchange, the major nutrient phosphate is delivered to the PAS and taken up the phosphate transporter PT4, requiring a proton-gradient produced by the ATPase HA1. Ammonium translocated to the PAS by the fungus is transported into the plant cell via ammonium transporter AMT2;3. Information based on: Garcia *et. al* (2016); Keymer *et. al* (2017); Roth and Paszkowski (2017); Choi *et. al* (2018); Jiang *et. al* (2018).



In exchange for this considerable carbon cost, the host plant receives the benefit of a significantly improved nutrient status facilitated by the expansive, fine mycelium in the soil (Smith and Smith, 2011). Specifically, the nutrients phosphate and ammonium are taken up by specific transporters expressed in extraradical hyphae (Harrison and van Buuren, 1995; Benedetto *et. al*, 2005; López-Pedrosa *et. al*, 2006) and are transported to the arbuscules in the form of polyphosphates and arginine, respectively (Ezawa *et. al*, 2002; Cruz *et. al*, 2007). Phosphate and ammonium are then released into the PAS by as of yet unknown process (Luginbuehl and Oldroyd, 2017). Uptake of these nutrients by the arbuscule containing cell (arbuscocyte) has been studied extensively and is outlined in the right of Figure 4: The phosphate transporter PT4, expressed exclusively under AM-conditions is responsible for the uptake of phosphate from the PAS. In the absence of this transporter, arbuscules are degenerated prematurely via the MYB1-activated pathway illustrated in Stage V of Figure 3, demonstrating the ability of the host plant to sense the supplied phosphate-levels (Javot *et. al*, 2007). Additionally, a proton gradient produced by the H<sup>+</sup>-ATPase HA1 is required for phosphate-import, with mutant plants exhibiting similar impairment in mycorrhization (Krajinski *et. al*, 2014; Wang *et. al*, 2014). A number of genes encoding ammonium transporters have been reported as upregulated during AM-interactions, indicating functional involvement for MtAMT2;3, 2;4 and 2;5. Interestingly, uptake of nitrogen via AMT2;3 has been shown to suppress the premature arbuscule degeneration (PAD) phenotype brought on by a nonfunctional PT4, indicating that nitrogen starved conditions can be enough to enable a functional AM-symbiosis (Javot *et. al*, 2011; Breuillin-Sessoms *et. al*, 2015).

Potential transporters for other ions involved in the AM-symbiotic exchange such as for potassium or sulfate have been identified, though a critical impact like for Pi and NH<sub>4</sub><sup>+</sup> was not observed as of yet (Sieh *et. al*, 2013; Giovannetti *et. al*, 2014; Garcia *et. al*, 2017).

### 2.3.6 A network of GRAS-TFs involved in arbuscule formation and maintenance

The previously mentioned key AM-regulators RAM1, NSP1 And NSP2 belong to a superfamily of plant-specific transcriptional regulators called GRAS named after the initially described members Gibberelic Acid Insensitive (GAI), Repressor of GAI (RGA) and Scarecrow (SCR) (Di Laurenzio *et. al*, 1996; Peng *et. al*, 1997; Pysh *et. al*, 1999). They are characterized into different subfamilies by conserved C-terminal regions shown in Figure 5 in addition to variable N-termini facilitating different protein- and DNA-binding properties (Sun *et. al*, 2011).



DELLA proteins – comprised of three members in the *M. truncatula* genome – are one such family and have been demonstrated to be crucial during early AM-signaling by forming a complex with IPD3/CYCLOPS (Pimprikar *et. al*, 2016). In this function, DELLA-proteins appear to act upstream of RAM1 and are capable of driving the expression of AM-symbiosis genes by themselves (Floss *et. al*, 2016). Likewise, *M. truncatula* plants with deficient DELLA-proteins 1 and 2 are severely hampered in overall mycorrhization as further evidence of the importance during AM-symbiosis (Floss *et. al*, 2013). It is therefore no surprise that a number of other GRAS-TFs have been observed to act in concert with this DELLA-CYCLOPS-RAM1-complex such as RAD1 (Required for Arbuscule Development) (Xue *et. al*, 2015; Floss *et. al*, 2016) and MIG1 (Mycorrhiza-induced GRAS; Heck *et. al*, 2016). Similarly, MtGRAS1 (TF80), a close homologue of MtrAM1 and potential interactor might enhance arbuscule-development as part of a feedback-loop with MtrAM1 (Park *et. al*, 2015; Hartmann *et. al*, 2019). A number of other AM-induced GRAS-TF genes (*MtGras4*, 6 and 7) might also play a role in fine tuning the arbuscular lifecycle, though no concrete functions are known thus far (Hartmann *et. al*, 2019).



**Figure 5 – Schematic overview of the GRAS-domain**

GRAS transcription factors contain a conserved region at their carboxyl-termini. Two Leucine-Heptad-Repeats flank a VHIID-motif containing a conserved sequence of P-N-H-D-Q-L-residues. The region following that contains a PFYRE-motif and finally a SAW-region with the following conserved amino acid-pairs: R-E, W-G and WW (Modified from: (Pysh *et. al*, 1999)

During later stages of AM (Figure 3, Stage V), a DELLA-NSP1-heterodimer has been demonstrated to form a complex with the TF MYB1 for the induction of protease and chitinase genes triggering the process of arbuscule degeneration (Floss *et. al*, 2017). As such, differential expression- and interaction patterns accompany the entire arbuscular lifecycle.

### 2.3.7 Hormonal influences on AM symbiosis

Besides the numerous developmental processes specific to AM fungal infection and arbuscule formation outlined above, signals delivered through phytohormones have been demonstrated to have a strong influence in finetuning colonization levels as well (Liao *et. al*, 2018). The carotene-derived strigolactone (SL) phytohormones have already been mentioned as signals enhancing growth of the AMF to initiate symbiotic contact. Consistent with this, experiments involving host plants unable to produce SLs were quantitatively hampered in AM-colonization, but produced morphologically normal

arbuscules (Kohlen *et. al*, 2012; Kobae *et. al*, 2018). In this early signaling function, biosynthesis of SLs in roots is induced by phosphate-deprivation (López-Ráez *et. al*, 2008) and also heavily depends on regulation by the NSP1/2 GRAS-TFs (Liu *et. al*, 2011). Various abiotic stresses also appear to affect SL-production and release (van Ha *et. al*, 2014).

Abscisic acid (ABA), another phytohormone synthesized from carotenoids, has also been suggested to promote production of SLs (López-Ráez *et. al*, 2010). Outside of this function, this hormone, commonly associated with stress responses (Liu *et. al*, 2018), was shown to have a crucial quantitative effect on promoting AM-symbiosis, as deficient mutants exhibited quantitative effects on AMF spread and arbuscule formation (Herrera-Medina *et. al*, 2007; Martín-Rodríguez *et. al*, 2011). This observation appears to be a dose-dependent effect, since a supply of large amounts of ABA likewise led to impaired AM-symbiosis (Charpentier *et. al*, 2014).

Levels of gibberelic acid, (GA) a hormone normally involved in a variety of basic developmental processes such as controlling germination or flowering (van de Velde *et. al*, 2017), have also been observed to be elevated in mycorrhized roots (Shaul-Keinan *et. al*, 2002). When investigated, higher GA-levels were observed to negatively affect the AM-symbiosis with external supplementation of large concentrations blocking colonization entirely (El Ghachtouli *et. al*, 1996). By now, this effect could also be observed at natural concentrations with GA-signaling being proposed as a mechanism for suppression of AM-symbiosis in the presence of sufficient phosphate supply (Nouri *et. al*, 2021). Conversely, GA-deficient plants were demonstrated to contain more arbuscules, though overall colonization was largely unaffected (Foo *et. al*, 2013). Consistent with this, DELLA-proteins that act antagonistically to GA-signaling were found to be promoters of overall colonization and arbuscule formation (Floss *et. al*, 2013; Yu *et. al*, 2014). Similarly, ABA has been suggested to counteract negative effects of external GA-supplementation by inducing the expression of *Della* (Martín-Rodríguez *et. al*, 2016). However, a lack of GAs also appears to negatively affect arbuscule formation by specifically inhibiting hyphal branching, overall suggesting the necessity of a balance between these signals for the regulation of colonization and arbuscule formation (Takeda *et. al*, 2015).

Finally, auxin, key regulator of a variety of processes in plants and crucially for Pi-stress induced lateral root formation (Pérez-Torres *et. al*, 2009) was found to be present at elevated levels in mycorrhized roots (Jentschel *et. al*, 2007). Further evidence obtained from mycorrhized roots externally supplied with auxins showed an increase in overall colonization, while conversely auxin-responsive genes were demonstrated to be specifically upregulated in mycorrhized roots and arbuscocytes (Chen *et. al*, 2017; Campanella *et. al*, 2008). Consistent with this, the microRNA *miR393*, which negatively regulates auxin-perception by degrading the TIR1 (Transporter Inhibitor Response) receptor protein is downregulated during AM while its overexpression leads to hampered AM-colonization (Etemadi *et. al*, 2014). Further,

downregulation of the IAA27 protein, an inhibitor of downstream auxin-responses via Auxin Response Factor (ARF) TFs, leads to numerically hampered AM as well. Interestingly, these results also suggest the integration of auxin and SL signaling (Guillotin *et. al*, 2017; Agusti *et. al*, 2011) that was evidenced before via experiments with mutants producing less auxin that also exhibited lower SL-levels (Hanlon and Coenen, 2011).

## 2.4 *M. truncatula* ZF genes with a potential role in AM-symbiosis

Despite the extensive knowledge presented prior, many signaling pathways for the fine-tuning of AM-development are likely still unknown. To gain insight into new potential candidates for such regulatory roles, transcriptomes of single cell-types such as arbuscocytes and surrounding cortical cells in comparison to epidermal cells were obtained via laser-microdissection (Gomez *et. al*, 2009; Hogeekamp *et. al*, 2011; Gaude *et. al*, 2012). Appressoria, as the fungal entry-points into the roots were likewise analyzed in comparison to non-appressorial epidermal cells. These cell-specific measurements revealed a variety of putative TFs from different families, especially the ERF and GRAS-categories detailed above to be specifically active in or around arbuscule-containing cells (Hogeekamp *et. al*, 2011; 2013). When examining this data further, a number of as of yet uncharacterized genes emerge as transcriptionally induced, including TFs.

Two of these putative AM-upregulated candidate-TFs encode C2H2-Type Zinc finger proteins. As such, these two genes are part of one of the largest and most ubiquitous superfamilies of transcription factors that control a multitude of essential biological processes including various processes of plant organ development and stress responses among other signaling roles (Englbrecht *et. al*, 2004). More specifically, the C2H2 family comprises proteins with conserved motifs containing two cysteine and two histidine-residues coordinating a Zinc cation (Takatsuji, 1999). This structure confers the ability to specifically bind to target sequences of DNA, but also RNA-molecules or other proteins, allowing such proteins to act in transcriptional regulation pathways (Hall, 2005). While ZF proteins have thus far not been reported to play a role in AM-signaling, some proteins from this family have previously been demonstrated to play roles in the root nodule symbiosis such as MtRSD (Regulator of symbiosome differentiation) or CgZF1 (Senjuti Sinharoy *et. al*, 2013; Diédhiou *et. al*, 2014). Interestingly, GRAS/DELLA-proteins crucial for AM-symbiosis development have been previously reported to interact with ZF-proteins from the C2H2- and RING-domain families, suggesting a potential integration with hormonal responses in general and GA-signaling in particular (Park *et. al*, 2013; Yoshida *et. al*, 2014; Davière and Achard, 2016; Aoyanagi *et. al*, 2020).

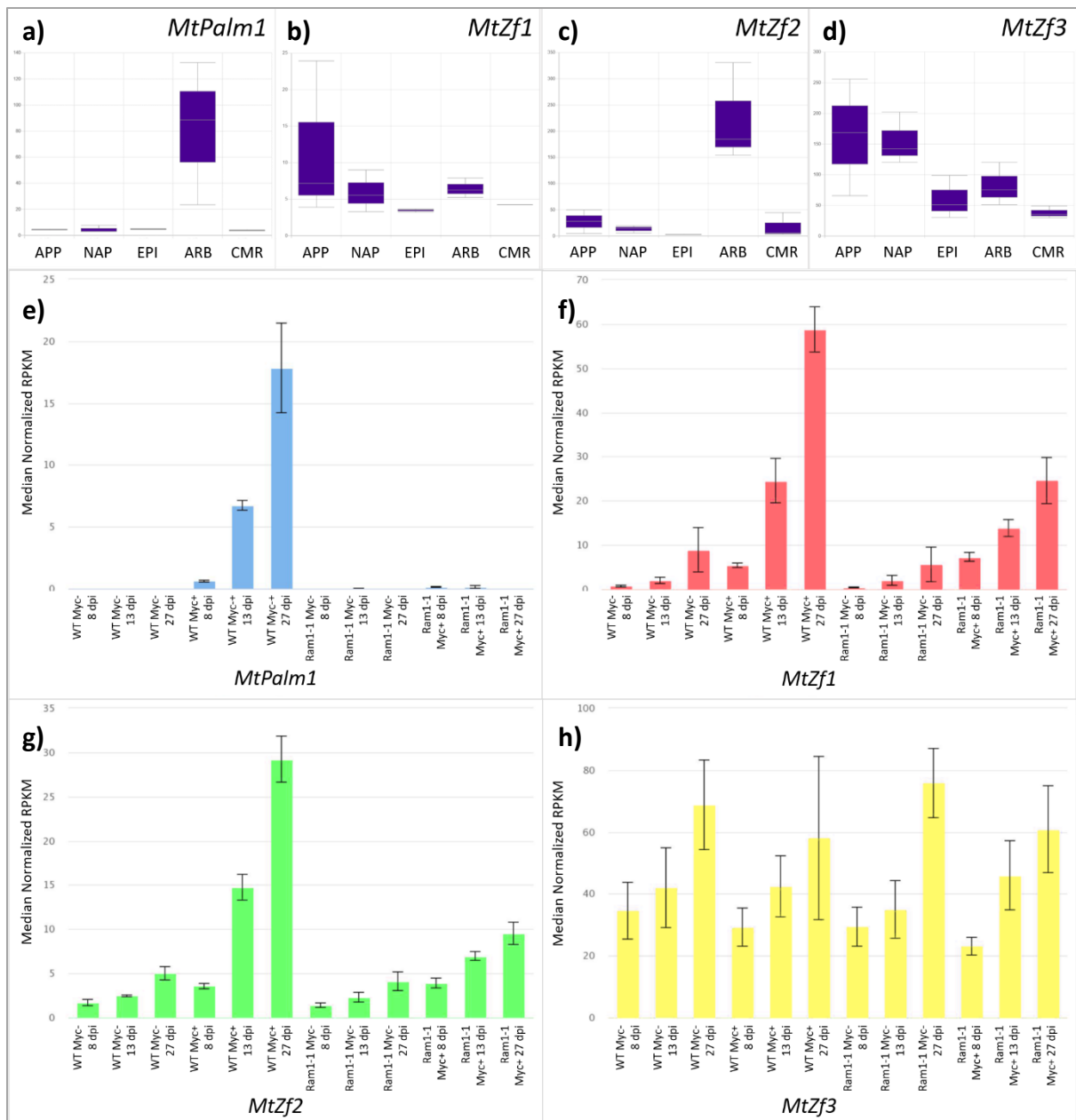


**Figure 6 – *In silico* expression analysis of several putative AM-related *M. truncatula* Zinc finger genes**

Box plots under a-d were compiled from GeneChip data from Hogekamp *et. al* (2011), available at the Medicago truncatula Gene Expression Atlas (<https://lipm-browsers.toulouse.inra.fr/pub/expressionAtlas/app/mtgeav3>): Data points represent expression levels of the *MtPalm1*, *MtZf1*, *MtZf2* and *MtZf3* genes in different cell types of *R. irregularis* mycorrhized roots isolated via laser-microdissection: APP = appressoria at 6 dpi, NAP = epidermal cells without appressoria at 6 dpi, EPI = epidermal cells at 21 dpi, ARB = arbuscocytes at 21 dpi and CMR = cortical cells around fungal hyphae at 21 dpi. Bar charts in e)-h) depict RNASeq expression data (RPKM: Reads Per Kilobase Million) available as part of the MtSSPdb (<https://mtsspdb.zhaolab.org/atlas-internal/3880/transcript/profile/0>, Boschiero *et. al*, 2020), derived from a mycorrhization time course performed by Luginbuehl *et. al* (2017) with 8, 13 and 27 dpi *R. irregularis* inoculated *M. truncatula* A17 root systems. RNA from non-mycorrhized (Myc-) roots grown in parallel is represented by the three charts to the left. Additionally, the same experiment was performed with mycorrhized- and non-mycorrhized roots in MtRAM1-deficient roots (Ram1-1\_Myc+/Myc-). Expression profiles depicted represent *MtPalm1* (blue), *MtZf1* (red), *MtZf2* (green) and *MtZf3* (yellow). Error bars indicate the respective 95% confidence intervals from variation between four biological replicates.

The first of the two AM-upregulated C2H2 Zinc finger TFs genes was identified to be *MtPalm1* or “*Palmate-like pentafoliata 1*” (for detailed attributions of GeneIDs see Table 1). Mutations in this gene were shown to cause defects in compound-leaf development of *M. truncatula* trifoliates, leading to the formation of two additional leaflets for a total of five (Chen *et. al*, 2010a). In this function, MtPALM1 was demonstrated to act as a transcriptional regulator by specifically binding to and negatively regulating the promoter region of *MtSgl1* (*Single leaflet 1*, Ge *et. al*, 2010), see also Figure 7a. The LFY-type TF MtSGL1 itself is active in the shoot apical meristem and emerging leaf primordia, responding to local auxin maxima caused by polar efflux through the PIN10 carrier (Wang *et. al*, 2008; Peng and Chen, 2011, Figure 7b). During lateral leaf (LL) initiation, expression of *MtSgl1* is restricted to the terminal leaflets (TL) by MtPALM1. Without this negative regulation in the emerging LLs, MtSGL1 causes the initiation of additional lateral leaves, leading to pentafoliates. As part of this process, *MtPalm1* itself is negatively regulated by MtARF3 (Auxin Responsive Factor 3) due to the presence of auxin responsive elements (ARE) in its promoter region. *MtArf3* is specifically expressed in the abaxial region of LL primordia and is thus able to cause MtPALM1 to be localized more to the adaxial domain (Peng *et. al*, 2017, Figure 7).

Consistent with this, evidence from Uppalapati *et. al* (2012) suggests that *MtPalm1* mutants also have some disturbances in the Ad- abaxial leaf identity: Here, the *MtPalm1* gene has been designated as *MtIrg1* for “*inhibitor of rust germ tube differentiation 1*”, since the loss of function leads to a severe reduction in infections by fungal rust pathogens in leaves. This effect was attributed to the lack of long fatty acids produced in the absence of regulation by MtIRG1/PALM1 and subsequent reductions in abaxial cuticular wax deposition that the rust pathogens require to germinate (Uppalapati *et. al*, 2012). As such, connections to auxin-dependent growth regulation and fatty-acid production are known for MtPALM1 in leaves.

Interestingly, all three *MtArf3*-like genes identified in a genome-wide analysis performed by Shen *et. al*, (2015), exhibit a slight induction in the presence of a symbiotic partner in roots, including the gene demonstrated to negatively regulate *MtPalm1* in leaves, also called MtARF3 in this work. The genes MtARF7, MtARF12 and another putative ARF3-orthologue not subject of the work by Shen and colleagues (MtARF25) might thus act as potential regulators of *MtPalm1*-expression under AM-conditions (see also Table 1).

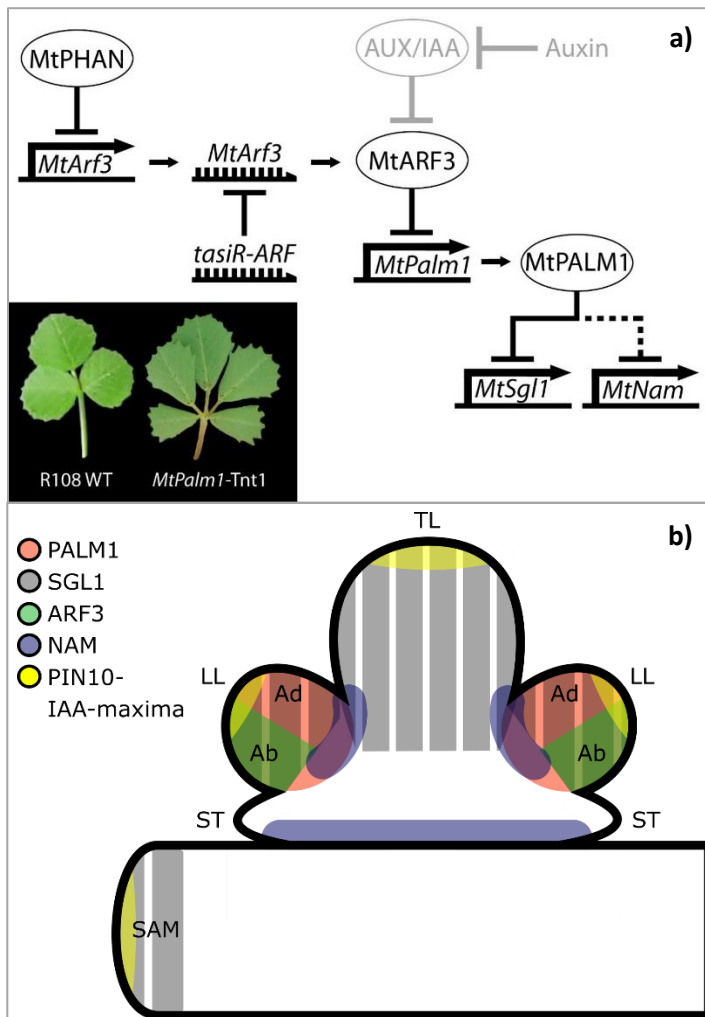


**Figure 7 – Regulatory pathway for *M. truncatula* compound leaf development involving *MtPalm1***

a) *M. truncatula* plants carrying a mutation in the *MtPalm1*-gene (*MtPalm1-Tnt1*) exhibit palmate leaves instead of the typical trifoliate (R108 WT). This was shown to be due to the MtPALM1-TF acting as a negative regulator of SINGLE LEAFLET 1 (*MtSgl1*) which is itself responsible for the initiation of additional lateral leaflet (LL)-formation (Chen et al., 2010; Wang et al., 2008; Ge et al., 2010). Either direct or indirect inhibition of NO APICAL MERISTEM (*MtNam1*), which, among other functions, also controls part of lateral leaflet formation has also been reported (Cheng et al., 2012). Transcription of *MtPalm1* is in itself negatively regulated by the AUXIN RESPONSE FACTOR 3 (MtARF3) protein (Peng et al., 2017). *MtArf3* is subject to negative transcriptional regulation by Myb-TF PHANTASTICA (MtPHAN), a regulator of ad- abaxial leaf polarity (Ge et al., 2014). Abundance of the *MtArf3*-mRNA is additionally controlled by the *trans*-acting short interfering RNA *tasiR-ARF* (Montgomery et al., 2008; Peng et al., 2017).

Finally, ARF3-proteins are bound and thereby blocked by AUX/IAA-proteins which in turn are subject to ubiquitination and degradation in the presence of elevated auxin-levels (Dharmasiri et al., 2005). The pathway depicted for *A. thaliana* was observed in tomato leaves, but has not yet been confirmed in *M. truncatula* and is thus grayed out (David-Schwartz et al., 2009; Hayashi, 2012; Piya et al., 2014). Regulatory scheme modified from Peng et al. (2017). b) Spatiotemporal expression patterns in leaf primordia suggest activity of MtSGL1 (gray) to be restricted to terminal leaflets (TL) by MtPALM1 (red). From there, MtSGL1 is able to control LL-initiation along with MtNAM at the organ boundaries (blue). Activity of MtARF3 (green) in the abaxial domain forces *MtPalm1* to be expressed stronger adaxially. These processes depend on auxin (IAA) maxima (yellow) produced by the PIN10 efflux carrier. (Abbreviations: ST = stipule, SAM = shoot apical meristem, Zhou et al., 2011; Wang and Chen, 2013; Mo et al., 2021).

In the context of roots, *MtPalm1* expression was only measurable under AM-conditions and in arbuscule containing cells (Hogekamp et al., 2011; Hogekamp and Küster, 2013). This observation is compounded by other gene expression data: a genome-wide analysis of C2H2-Type Zinc finger TFs excluding AM-conditions found no evidence of *MtPalm1*-activity in roots (Jiao et al., 2020) while RNASeq-data from a mycorrhization time course by Luginbuehl et al., (2017) (available at <http://mtsspdb.noble.org/>) suggests that expression of *MtPalm1* in roots requires the presence of AM, while implying a dependency on the key AM- regulator MtRAM1. These data points as well as subsequent transcriptome data elucidated below are shown in Figure 6.

*MtZf2*, the other C2H2-Type Zinc finger TF reported to be upregulated by Hogekamp *et. al* (2011; 2013) does not exhibit the same kind of arbuscule-specific expression pattern but instead also shows some activity in the presence of appressoria and cortical cells surrounding mycorrhized regions. Likewise, the RNASeq time course data shows some basal expression in roots under non-mycorrhized conditions while showing strong upregulation as AMF-infection progresses (Table 1 and Figure 6).

Subsequent to these initial two candidate genes putatively active during AM-infection, two other genes (Table 1) encoding further ZF-domain containing proteins were identified to be upregulated under AM-conditions. *MtZf1*, the first of these genes is annotated to contain a C3HC4 motif, also known as a RING domain (*really interesting new gene*). This structure coordinates two Zinc-ions to form a type of “cross-brace” structure that often enables protein-binding capabilities. As such, many proteins from this family act as ubiquitin-ligases in targeted protein-degradation (Kosarev *et. al*, 2002) and thus play roles in various signaling cascades including those responding to phytohormones such as auxin, jasmonic acid and ABA (Hotton and Callis, 2008). Still, factors acting as more traditional transcriptional regulators also exist within this family (Kentsis *et. al*, 2001).

The expression pattern for *MtZf1* shown in Figure 6 suggests induction in the presence of appressoria and arbuscules in particular. In the RNASeq data, *MtZf1* is only weakly expressed during the later time points of the non-mycorrhized control roots, while exhibiting strong induction over the course of AM-colonization. In *MtRAM1*-deficient roots, *MtZf1* transcript amounts were slightly reduced compared to the mycorrhized WT, while still much more abundant compared to conditions without the symbiotic fungus (Figure 6).

**Table 1 – Nomenclature of *MtZf* and *MtArf3*-like candidate genes subject to this study**

Gene names based on Ge *et. al* (2010); Uppalapati *et. al* (2012) and (Shen *et. al* (2015). Gene IDs were taken from the *M. truncatula* version 4 (Tang *et. al*, 2014) and 5 genome-annotations (Pecrix *et. al*, 2018). Affymetrix GeneChip ver1 IDs are indicated to the right (Benedito *et. al*, 2008).

Trivial name	Subfamily	Version 4 Gene ID	Version 5 Gene ID	GeneChip ID Ver1
MtPalm1/ Mtlrg1	C2H2	Medtr5g014400	MtrunA17_Chr5g0400571	Mtr.25270.1.S1_at
MtZf1	C3HC4	Medtr5g026730	MtrunA17_Chr5g0409211	Mtr.9667.1.S1_at
MtZf2	C2H2	---	MtrunA17_Chr7g0268961	Mtr.28153.1.S1_at Mtr.30759.1.S1_at
MtZf3	C3H	Medtr3g103960	MtrunA17_Chr3g0135351	Mtr.8678.1.S1_at
MtArf3	ARF3	Medtr2g014770	MtrunA17_Chr2g0282961	Mtr.10529.1.S1_at
MtArf7	ARF3	Medtr2g093740	MtrunA17_Chr2g0326281	Mtr.26216.1.S1_at
MtArf12	ARF3	Medtr4g060460	MtrunA17_Chr4g0029671	---
MtArf25	ARF3	Medtr4g088210	MtrunA17_Chr4g0046371	Mtr.38753.1.S1_at

The final putative Zinc finger TF-encoding candidate gene chosen for further analysis concerning AM symbiosis is *MtZf3*. In this case, the cell-type specific expression data shows upregulation in arbuscule-containing cells, as well as around appressoria (Figure 6). In contrast, the RNASeq-time course data shows no specific increase in whole-root expression between mycorrhized and non-mycorrhized conditions. A dependence on MtRAM1 is also not apparent based on this data.

The annotation categorizes the protein encoded by *MtZf3* to be part of the CCCH family of Zinc fingers, known to act by binding to RNA molecules and thereby being involved in processing, inhibition and degradation processes. A genome-wide analysis of all 34 *M. truncatula* CCCH-ZF genes (as of genome version 3.5) revealed *MtZf3* (there referred to as *MtC3H11*) to be one of only two genes from this family to be specifically expressed in roots (Zhang *et. al*, 2013). Further analysis suggested this gene to potentially have a role in stress responses, as it was more strongly expressed during drought and treatment with abscisic acid.



## 2.5 Outline and objectives for this thesis

Initially, the expression of putatively AM-induced Zinc finger genes is to be measured individually over the time course of colonization by the AM-symbiotic fungus *R. irregularis*. The aim of this experiment is to confirm the available transcriptome data presented above and to obtain additional confirmation for the relevance of these genes to the AM symbiosis. In addition, promoter reporter-gene studies performed in mycorrhized root systems of WT plants as well as mutants for key symbiotic genes will allow for further insights into patterns of gene activity on the cellular level and reveal any potential correlation with intraradical AMF-structures.

Since these putative TFs induced under AM-conditions might act as positive or negative regulators of downstream target genes and processes, an overexpression study is to be performed for possible evidence of either scenario. Conversely, any potential adverse effects on the AM-symbiosis brought on by the absence of *MtPalm1*, *MtZf1*, *MtZf2* and *MtZf3* expression are to be studied via RNAi-based gene silencing approaches. Moreover, the examination of mycorrhized *Tnt1*-mutant plants with non-functional copies of the *MtZf* candidate genes may lead to further evidence in this direction. Using RNA-samples obtained from this material, quantification of mRNA amounts either for the entire transcriptome or for AM-marker genes in particular might suggest possible direct or indirect regulatory targets or more general cellular processes influenced by these ZF proteins.

Furthermore, protein-interaction assays are to be employed to gain insights into the potential functional networks between known AM-related TFs as well as with the novel ZF-proteins. In particular, heterologous Yeast 2-Hybrid assays will be used to examine possible dimerization between the Zinc finger candidates and other factors. Promoter-binding of a number of AM-related TFs is to be assayed via Yeast 1-Hybrid approaches. In this context, the previously indicated binding of ARF3-proteins to the promoter of *MtPalm1* is of particular interest.

In summary, the ultimate objective of this thesis is to elucidate potential roles of the Zinc finger proteins encoded by the *MtPalm1*, *MtZf1*, *MtZf2* and *MtZf3* genes during arbuscular mycorrhiza symbiosis development and maintenance in *M. truncatula*.

### 3 Material and Methods

#### 3.1 Plasmids generated and used

Table 2 – List of microbial strains carrying plasmids constructed/used during this work

Plasmid	Organism	Size (kb)	Resistance/ Auxotrophy	Description of the construct	Reference
813p9RFP-D35s-Expr “pGolm35s”	<i>E. coli</i> Top10	12.6	Spec50	Binary empty vector; contains mcs surrounded by 2x35s-promoter and 35s-terminator as well as dsRed for visual screening	Devers <i>et. al</i> (2013)
pDONR: <i>MtDella1</i>	<i>E. coli</i> DH5α mcr'	4,2	Kan50	pDONR221-derivative containing the CDS of <i>MtDella1</i> (Medtr3g065980) without the Stop-codon (1621 bp); cloned via BP-recombination	This work
pDONR: <i>MtDella2</i>	<i>E. coli</i> DH5α mcr'	4,1	Kan50	pDONR221-derivative containing the CDS of <i>MtDella2</i> (contig_52215) without the Stop-codon (1599 bp); cloned via BP-recombination	This work
pDONR: <i>MtDella3</i>	<i>E. coli</i> DH5α mcr'	4	Kan50	pDONR221-derivative containing the CDS of <i>MtDella3</i> (contig_55897) without the Stop-codon (1503 bp); cloned via BP-recombination	This work
pDONR: <i>MtGras1</i>	<i>E. coli</i> DH5α mcr'	3.9	Kan50	pDONR221-derivative containing the CDS of <i>MtGras1</i> (Medtr3g022830) without the Stop-codon (1314 bp); cloned via BP-recombination	BH
pDONR: <i>MtGras4</i>	<i>E. coli</i> DH5α mcr'	4.2	Kan50	pDONR221-derivative containing the CDS of <i>MtGras4</i> (Medtr7g109580) without the Stop-codon (1668 bp); cloned via BP-recombination	BH
pDONR: <i>MtGras5</i>	<i>E. coli</i> DH5α mcr'	3,9	Kan50	pDONR221-derivative containing the CDS of <i>MtGras5</i> (Medtr1g069725) without the Stop-codon (1404 bp); cloned via BP-recombination	This work
pDONR: <i>MtGras6</i>	<i>E. coli</i> DH5α mcr'	3,9	Kan50	pDONR221-derivative containing the CDS of <i>MtGras6</i> (Medtr2g099100) without the Stop-codon (1374 bp); cloned via BP-recombination	This work
pDONR: <i>MtGras7</i>	<i>E. coli</i> DH5α mcr'	4	Kan50	pDONR221-derivative containing the CDS of <i>MtGras7</i> (Medtr1g086970) without the Stop-codon (1440 bp); cloned via BP-recombination	This work
pDONR: <i>MtGrasX</i>	<i>E. coli</i> DH5α mcr'	4,3	Kan50	pDONR221-derivative containing the CDS of <i>MtGrasX</i> (Medtr7g069740) without the Stop-codon (1755 bp); cloned via BP-recombination	This work
pDONR: <i>MtNsp1</i>	<i>E. coli</i> DH5α mcr'	4.2	Kan50	pDONR221-derivative containing the CDS of <i>MtNsp1</i> (Medtr8g020840) without the Stop-codon (1662 bp); cloned via BP-recombination	This work
pDONR: <i>MtNsp2</i>	<i>E. coli</i> DH5α mcr'	4.1	Kan50	pDONR221-derivative containing the CDS of <i>MtNsp2</i> (Medtr3g072710) without the Stop-codon (1524 bp); cloned via BP-recombination	This work
pDONR: <i>MtPalm1</i> -RNAi-1	<i>E. coli</i> DH5α mcr'	2,65	Kan50	pDONR221-derivative containing a 100 bp fragment starting at position 334 of the CDS of <i>MtPalm1</i> (Medtr5g014400); cloned via BP-recombination	This work
pDONR: <i>MtPalm1</i> -RNAi-2	<i>E. coli</i> DH5α mcr'	2,7	Kan50	pDONR221-derivative containing a 188 bp fragment starting at position 556 of the CDS of <i>MtPalm1</i> (Medtr5g014400); cloned via BP-recombination	This work
pDONR: <i>MtRad1</i>	<i>E. coli</i> DH5α mcr'	4.1	Kan50	pDONR221-derivative containing the CDS of <i>MtRad1</i> (Medtr4g104020) without the Stop-codon (1536 bp); cloned via BP-recombination	This work
pDONR: <i>MtRam1</i>	<i>E. coli</i> DH5α mcr'	4.6	Kan50	pDONR221-derivative containing the CDS of <i>MtRam1</i> (Medtr7g027190) without the Stop-codon (2022 bp); cloned via BP-recombination	This work
pDONR: <i>MtZf1</i> -RNAi-1	<i>E. coli</i> DH5α mcr'	2,6	Kan50	pDONR221-derivative containing a 44 bp fragment starting at position 485 of the CDS of <i>MtZf1</i> (Medtr5g026730); cloned via BP-recombination	This work

pDONR: <i>MtZf1</i> -RNAi-2	<i>E. coli</i> DH5 $\alpha$ mcr'	2,65	Kan50	pDONR221-derivative containing a 120 bp fragment starting at position 34 of the 3'-UTR of <i>MtZf1</i> (Medtr5g026730); cloned via BP-recombination	This work
pDONR: <i>MtZf2</i> -RNAi-1	<i>E. coli</i> DH5 $\alpha$ mcr'	2.75	Kan50	pDONR221-derivative containing a 202 bp fragment starting at position 128 of the CDS of <i>MtZf2</i> (MtrunA17_Chr7g0268961); cloned via BP-recombination	This work
pDONR: <i>MtZf2</i> -RNAi-2	<i>E. coli</i> DH5 $\alpha$ mcr'	2.65	Kan50	pDONR221-derivative containing a 120 bp fragment starting at position 561 of the CDS of <i>MtZf2</i> (MtrunA17_Chr7g0268961); cloned via BP-recombination	This work
pDONR: <i>MtZf3</i> -RNAi-1	<i>E. coli</i> DH5 $\alpha$ mcr'	2,8	Kan50	pDONR221-derivative containing a 247 bp fragment starting in the 5'-UTR and ending at position 169 of the CDS of <i>MtZf3</i> (Medtr3g103960); cloned via BP-recombination	This work
pDONR: <i>MtZf3</i> -RNAi-2	<i>E. coli</i> DH5 $\alpha$ mcr'	2,7	Kan50	pDONR221-derivative containing a 178 bp fragment starting at position 540 of the CDS of <i>MtZf3</i> (Medtr3g103960); cloned via BP-recombination	This work
pDONR: <i>pMtPalm1</i>	<i>E. coli</i> DH5 $\alpha$ mcr'	4.5	Kan50	pDONR221-derivative containing the -1981/-1 promoter region of <i>MtPalm1</i> (Medtr5g014440) cloned via BP-recombination	This work
pDONR: <i>pMtZf1</i>	<i>E. coli</i> DH5 $\alpha$ mcr'	4.0	Kan50	pDONR221-derivative containing the -1455/-1 promoter region of <i>MtZf1</i> (Medtr5g026730) cloned via BP-recombination	This work
pDONR: <i>pMtZf2</i>	<i>E. coli</i> DH5 $\alpha$ mcr'	4.4	Kan50	pDONR221-derivative containing the -2060/-184 promoter region of <i>MtZf2</i> (MtrunA17_Chr7g0268961) cloned via BP-recombination	This work
pDONR: <i>pMtZf3</i>	<i>E. coli</i> DH5 $\alpha$ mcr'	3.6	Kan50	pDONR221-derivative containing the -1016/-1 promoter region of <i>MtZf3</i> (Medtr3g103960) cloned via BP-recombination	This work
pGADT7: <i>Mt15867</i>	<i>E. coli</i> DH5 $\alpha$ mcr'	9.1	Amp100	Y2H prey vector containing the 1071 bp CDS of <i>Mt15867</i> (Medtr4g130270) in-frame with GAL4-activation domain; cloned via <i>SmaI</i>	LH
pGADT7: <i>Mt25005</i>	<i>E. coli</i> DH5 $\alpha$ mcr'	9.4	Amp100	Y2H prey vector containing the 1392 bp CDS of <i>Mt25005</i> (Medtr7g011630) in-frame with GAL4-activation domain; cloned via <i>SmaI</i>	LH
pGADT7: <i>Mt460730</i>	<i>E. coli</i> DH5 $\alpha$ mcr'	9.1	Amp100	Y2H prey vector containing the 1101 bp CDS of <i>Mt460730</i> (Medtr2g460730) in-frame with GAL4-activation domain; cloned via <i>SmaI</i>	LH
pGADT7: <i>MtArf3</i>	<i>E. coli</i> DH5 $\alpha$ mcr'	9,8	Amp100	Y2H prey vector containing the 2049 bp CDS of <i>MtArf3</i> (Medtr2g014770) in-frame with GAL4-activation domain; cloned via <i>SmaI</i>	This work
pGADT7: <i>MtArf7</i>	<i>E. coli</i> DH5 $\alpha$ mcr'	10,5	Amp100	Y2H prey vector containing the 2433 bp CDS of <i>MtArf7</i> (Medtr2g093740) in-frame with GAL4-activation domain; cloned via <i>SmaI</i>	This work
pGADT7: <i>MtArf12</i>	<i>E. coli</i> DH5 $\alpha$ mcr'	10,4	Amp100	Y2H prey vector containing the 2379 bp CDS of <i>MtArf12</i> (Medtr4g060460) in-frame with GAL4-activation domain; cloned via <i>SmaI</i>	This work
pGADT7: <i>MtArf25</i>	<i>E. coli</i> DH5 $\alpha$ mcr'	10,1	Amp100	Y2H prey vector containing the 2106 bp CDS of <i>MtArf25</i> (Medtr4g088210) in-frame with GAL4-activation domain; cloned via <i>XhoI</i>	This work
pGADT7: <i>MtCbf1</i>	<i>E. coli</i> DH5 $\alpha$ mcr'	8.4	Amp100	Y2H prey vector containing the 360 bp CDS of <i>MtCbf1</i> (Medtr2g081600) in-frame with GAL4-activation domain; cloned via <i>NdeI/BamHI</i>	SK
pGADT7: <i>MtCbf2</i>	<i>E. coli</i> DH5 $\alpha$ mcr'	8.4	Amp100	Y2H prey vector containing the 354 bp CDS of <i>MtCbf2</i> (Medtr2g081630) in-frame with GAL4-activation domain; cloned via <i>NdeI/BamHI</i>	SK
pGADT7: <i>MtCbf3</i>	<i>E. coli</i> DH5 $\alpha$ mcr'	8.6	Amp100	Y2H prey vector containing the 609 bp CDS of <i>MtCbf3</i> (Medtr8g091720) in-frame with GAL4-activation domain; cloned via <i>EcoRI/BamHI</i>	SK

pGADT7: <i>MtColE</i>	<i>E. coli</i> DH5α mcr'	9.2	Amp100	Y2H prey vector containing the 1236 bp CDS of <i>MtColE</i> (Medtr3g082630) in-frame with GAL4-activation domain; cloned via <i>SmaI</i>	SK
pGADT7: <i>MtDella1</i>	<i>E. coli</i> DH5α mcr'	9.6	Amp100	Y2H prey vector containing the 1644 bp CDS of <i>MtDella1</i> (Medtr3g065980) in-frame with GAL4-activation domain; cloned via <i>SmaI</i>	RH
pGADT7: <i>MtDella2</i>	<i>E. coli</i> DH5α mcr'	9.6	Amp100	Y2H prey vector containing the 1602 bp CDS of <i>MtDella2</i> (contig_52215) in-frame with GAL4-activation domain; cloned via <i>SmaI</i>	RH
pGADT7: <i>MtDella3</i>	<i>E. coli</i> DH5α mcr'	9.5	Amp100	Y2H prey vector containing the 1506 bp CDS of <i>MtDella3</i> (contig_55897) in-frame with GAL4-activation domain; cloned via <i>SmaI</i>	RH
pGADT7: <i>MtGras1</i>	<i>E. coli</i> DH5α mcr'	9.3	Amp100	Y2H prey vector containing the 1332 bp CDS of <i>MtGras1</i> (Medtr3g022830) in-frame with GAL4-activation domain; cloned via <i>SmaI</i>	RH
pGADT7: <i>MtGras4</i>	<i>E. coli</i> DH5α mcr'	9.4	Amp100	Y2H prey vector containing the 1671 bp CDS of <i>MtGras4</i> (Medtr7g109580) in-frame with GAL4-activation domain; cloned via <i>SmaI</i>	RH
pGADT7: <i>MtGras5</i>	<i>E. coli</i> DH5α mcr'	9.4	Amp100	Y2H prey vector containing the 1407 bp CDS of <i>MtGras5</i> (Medtr1g069725) in-frame with GAL4-activation domain; cloned via <i>SmaI</i>	RH
pGADT7: <i>MtGras7</i>	<i>E. coli</i> DH5α mcr'	9.4	Amp100	Y2H prey vector containing the 1443 bp CDS of <i>MtGras7</i> (Medtr1g086970) in-frame with GAL4-activation domain; cloned via <i>SmaI</i>	RH
pGADT7: <i>MtNF-YA1</i>	<i>E. coli</i> DH5α mcr'	9	Amp100	Y2H prey vector containing the 999 bp CDS of <i>MtNF-YA1</i> (Medtr1g056530) in-frame with GAL4-activation domain; cloned via <i>SmaI</i>	SK
pGADT7: <i>MtNF-YA2</i>	<i>E. coli</i> DH5α mcr'	9	Amp100	Y2H prey vector containing the 1002 bp CDS of <i>MtNF-YA2</i> (Medtr7g106450) in-frame with GAL4-activation domain; cloned via <i>SmaI</i>	SK
pGADT7: <i>MtNF-YA3</i>	<i>E. coli</i> DH5α mcr'	8.7	Amp100	Y2H prey vector containing the 708 bp CDS of <i>MtNF-YA3</i> (Medtr2g041090) in-frame with GAL4-activation domain; cloned via <i>SmaI</i>	SK
pGADT7: <i>MtNF-YA4</i>	<i>E. coli</i> DH5α mcr'	9	Amp100	Y2H prey vector containing the 1044 bp CDS of <i>MtNF-YA4</i> (Medtr2g099490) in-frame with GAL4-activation domain; cloned via <i>SmaI</i>	SK
pGADT7: <i>MtNF-YA5</i>	<i>E. coli</i> DH5α mcr'	9	Amp100	Y2H prey vector containing the 990 bp CDS of <i>MtNF-YA5</i> (Medtr3g061510) in-frame with GAL4-activation domain; cloned via <i>SmaI</i>	SK
pGADT7: <i>MtNF-YA6</i>	<i>E. coli</i> DH5α mcr'	8.6	Amp100	Y2H prey vector containing the 624 bp CDS of <i>MtNF-YA6</i> (Medtr2g030170) in-frame with GAL4-activation domain; cloned via <i>SmaI</i>	SK
pGADT7: <i>MtNF-YA7</i>	<i>E. coli</i> DH5α mcr'	8.9	Amp100	Y2H prey vector containing the 915 bp CDS of <i>MtNF-YA7</i> (Medtr8g037270) in-frame with GAL4-activation domain; cloned via <i>SmaI</i>	SK
pGADT7: <i>MtNF-YA8</i>	<i>E. coli</i> DH5α mcr'	8.9	Amp100	Y2H prey vector containing the 903 bp CDS of <i>MtNF-YA8</i> (Medtr8g019540) in-frame with GAL4-activation domain; cloned via <i>SmaI</i>	SK
pGADT7: <i>MtNsp1</i>	<i>E. coli</i> DH5α mcr'	9.4	Amp100	Y2H prey vector containing the 1665 bp CDS of <i>MtNsp1</i> (Medtr8g020840) in-frame with GAL4-activation domain; cloned via <i>BamHI/EcoRI</i>	RH
pGADT7: <i>MtNsp2</i>	<i>E. coli</i> DH5α mcr'	9.5	Amp100	Y2H prey vector containing the 1527 bp CDS of <i>MtNsp2</i> (Medtr3g072710) in-frame with GAL4-activation domain; cloned via <i>SmaI</i>	RH
pGADT7: <i>MtPalm1</i>	<i>E. coli</i> DH5α mcr'	8.8	Amp100	Y2H prey vector containing the 756 bp CDS of <i>MtPalm1</i> (Medtr5g014400) in-frame with GAL4-activation domain; cloned via <i>SmaI</i>	This work
pGADT7: <i>MtRad1</i>	<i>E. coli</i> DH5α mcr'	9.4	Amp100	Y2H prey vector containing the 1566 bp CDS of <i>MtRad1</i> (Medtr4g104020) in-frame with GAL4-activation domain; cloned via <i>SmaI</i>	RH
pGADT7: <i>MtRam1</i>	<i>E. coli</i> DH5α mcr'	10	Amp100	Y2H prey vector containing the 2025 bp CDS of <i>MtRam1</i> (Medtr7g027190) in-frame with GAL4-activation domain; cloned via <i>SmaI</i>	RH

pGADT7: <i>MtWri5a</i>	<i>E. coli</i> DH5α mcr'	9.2	Amp100	Y2H prey vector containing the 1221 bp CDS of <i>MtWri5a</i> (Medtr8g468920) in-frame with GAL4-activation domain; cloned via <i>SmaI</i>	LH
pGADT7: <i>MtWri5b</i>	<i>E. coli</i> DH5α mcr'	9.2	Amp100	Y2H prey vector containing the 1188 bp CDS of <i>MtWri5b</i> (Medtr7g009410) in-frame with GAL4-activation domain; cloned via <i>SmaI</i>	LH
pGADT7: <i>MtWri5c</i>	<i>E. coli</i> DH5α mcr'	9.2	Amp100	Y2H prey vector containing the 1146 bp CDS of <i>MtWri5c</i> (Medtr6g011490) in-frame with GAL4-activation domain; cloned via <i>SmaI</i>	LH
pGADT7: <i>MtZf1</i>	<i>E. coli</i> DH5α mcr'	8.5	Amp100	Y2H prey vector containing the 528 bp CDS of <i>MtZf1</i> (Medtr5g026730) in-frame with GAL4-activation domain; cloned via <i>SmaI</i>	This work
pGADT7: <i>MtZf2</i>	<i>E. coli</i> DH5α mcr'	9.5	Amp100	Y2H prey vector containing the 1566 bp CDS of <i>MtZf2</i> (MtrunA17_Chr7g0268961) in-frame with GAL4-activation domain; cloned via <i>SmaI</i>	This work
pGADT7: <i>Mt15867</i>	<i>S. cerevisiae</i> Y187	9.1	Leu	Y2H prey vector containing the 1071 bp CDS of <i>Mt15867</i> (Medtr4g130270) in-frame with GAL4-activation domain; cloned via <i>SmaI</i>	LH
pGADT7: <i>Mt25005</i>	<i>S. cerevisiae</i> Y187	9.4	Leu	Y2H prey vector containing the 1392 bp CDS of <i>Mt25005</i> (Medtr7g011630) in-frame with GAL4-activation domain; cloned via <i>SmaI</i>	LH
pGADT7: <i>Mt460730</i>	<i>S. cerevisiae</i> Y187	9.1	Leu	Y2H prey vector containing the 1101 bp CDS of <i>Mt460730</i> (Medtr2g460730) in-frame with GAL4-activation domain; cloned via <i>SmaI</i>	LH
pGADT7: <i>MtArf3</i>	<i>S. cerevisiae</i> Y187	9,8	Leu	Y2H prey vector containing the 2049 bp CDS of <i>MtArf3</i> (Medtr2g014770) in-frame with GAL4-activation domain; cloned via <i>SmaI</i>	This work
pGADT7: <i>MtArf7</i>	<i>S. cerevisiae</i> Y187	10,5	Leu	Y2H prey vector containing the 2433 bp CDS of <i>MtArf7</i> (Medtr2g093740) in-frame with GAL4-activation domain; cloned via <i>SmaI</i>	This work
pGADT7: <i>MtArf12</i>	<i>S. cerevisiae</i> Y187	10,4	Leu	Y2H prey vector containing the 2379 bp CDS of <i>MtArf12</i> (Medtr4g060460) in-frame with GAL4-activation domain; cloned via <i>SmaI</i>	This work
pGADT7: <i>MtArf25</i>	<i>S. cerevisiae</i> Y187	10,1	Leu	Y2H prey vector containing the 2106 bp CDS of <i>MtArf25</i> (Medtr4g088210) in-frame with GAL4-activation domain; cloned via <i>XhoI</i>	This work
pGADT7: <i>MtCbf1</i>	<i>S. cerevisiae</i> Y187	8.4	Leu	Y2H prey vector containing the 360 bp CDS of <i>MtCbf1</i> (Medtr2g081600) in-frame with GAL4-activation domain; cloned via <i>NdeI/BamHI</i>	SK
pGADT7: <i>MtCbf2</i>	<i>S. cerevisiae</i> Y187	8.4	Leu	Y2H prey vector containing the 354 bp CDS of <i>MtCbf2</i> (Medtr2g081630) in-frame with GAL4-activation domain; cloned via <i>NdeI/BamHI</i>	SK
pGADT7: <i>MtCbf3</i>	<i>S. cerevisiae</i> Y187	8.6	Leu	Y2H prey vector containing the 609 bp CDS of <i>MtCbf3</i> (Medtr8g091720) in-frame with GAL4-activation domain; cloned via <i>EcoRI/BamHI</i>	SK
pGADT7: <i>MtCoIE</i>	<i>S. cerevisiae</i> Y187	9.2	Leu	Y2H prey vector containing the 1236 bp CDS of <i>MtCoIE</i> (Medtr3g082630) in-frame with GAL4-activation domain; cloned via <i>SmaI</i>	SK
pGADT7: <i>MtDella1</i>	<i>S. cerevisiae</i> Y187	9.6	Leu	Y2H prey vector containing the 1644 bp CDS of <i>MtDella1</i> (Medtr3g065980) in-frame with GAL4-activation domain; cloned via <i>SmaI</i>	RH
pGADT7: <i>MtDella2</i>	<i>S. cerevisiae</i> Y187	9.6	Leu	Y2H prey vector containing the 1602 bp CDS of <i>MtDella2</i> (contig_52215) in-frame with GAL4-activation domain; cloned via <i>SmaI</i>	RH
pGADT7: <i>MtDella3</i>	<i>S. cerevisiae</i> Y187	9.5	Leu	Y2H prey vector containing the 1506 bp CDS of <i>MtDella3</i> (contig_55897) in-frame with GAL4-activation domain; cloned via <i>SmaI</i>	RH
pGADT7: <i>MtGras1</i>	<i>S. cerevisiae</i> Y187	9.3	Leu	Y2H prey vector containing the 1332 bp CDS of <i>MtGras1</i> (Medtr3g022830) in-frame with GAL4-activation domain; cloned via <i>SmaI</i>	RH
pGADT7: <i>MtGras4</i>	<i>S. cerevisiae</i> Y187	9.4	Leu	Y2H prey vector containing the 1671 bp CDS of <i>MtGras4</i> (Medtr7g109580) in-frame with GAL4-activation domain; cloned via <i>SmaI</i>	RH

pGADT7: <i>MtGras5</i>	<i>S. cerevisiae</i> Y187	9.4	Leu	Y2H prey vector containing the 1407 bp CDS of <i>MtGras5</i> (Medtr1g069725) in-frame with GAL4-activation domain; cloned via <i>SmaI</i>	RH
pGADT7: <i>MtGras7</i>	<i>S. cerevisiae</i> Y187	9.4	Leu	Y2H prey vector containing the 1443 bp CDS of <i>MtGras7</i> (Medtr1g086970) in-frame with GAL4-activation domain; cloned via <i>SmaI</i>	RH
pGADT7: <i>MtNF-YA1</i>	<i>S. cerevisiae</i> Y187	9	Leu	Y2H prey vector containing the 999 bp CDS of <i>MtNF-YA1</i> (Medtr1g056530) in-frame with GAL4-activation domain; cloned via <i>SmaI</i>	SK
pGADT7: <i>MtNF-YA2</i>	<i>S. cerevisiae</i> Y187	9	Leu	Y2H prey vector containing the 1002 bp CDS of <i>MtNF-YA2</i> (Medtr7g106450) in-frame with GAL4-activation domain; cloned via <i>SmaI</i>	SK
pGADT7: <i>MtNF-YA3</i>	<i>S. cerevisiae</i> Y187	8.7	Leu	Y2H prey vector containing the 708 bp CDS of <i>MtNF-YA3</i> (Medtr2g041090) in-frame with GAL4-activation domain; cloned via <i>SmaI</i>	SK
pGADT7: <i>MtNF-YA4</i>	<i>S. cerevisiae</i> Y187	9	Leu	Y2H prey vector containing the 1044 bp CDS of <i>MtNF-YA4</i> (Medtr2g099490) in-frame with GAL4-activation domain; cloned via <i>SmaI</i>	SK
pGADT7: <i>MtNF-YA5</i>	<i>S. cerevisiae</i> Y187	9	Leu	Y2H prey vector containing the 990 bp CDS of <i>MtNF-YA5</i> (Medtr3g061510) in-frame with GAL4-activation domain; cloned via <i>SmaI</i>	SK
pGADT7: <i>MtNF-YA6</i>	<i>S. cerevisiae</i> Y187	8.6	Leu	Y2H prey vector containing the 624 bp CDS of <i>MtNF-YA6</i> (Medtr2g030170) in-frame with GAL4-activation domain; cloned via <i>SmaI</i>	SK
pGADT7: <i>MtNF-YA7</i>	<i>S. cerevisiae</i> Y187	8.9	Leu	Y2H prey vector containing the 915 bp CDS of <i>MtNF-YA7</i> (Medtr8g037270) in-frame with GAL4-activation domain; cloned via <i>SmaI</i>	SK
pGADT7: <i>MtNF-YA8</i>	<i>S. cerevisiae</i> Y187	8.9	Leu	Y2H prey vector containing the 903 bp CDS of <i>MtNF-YA8</i> (Medtr8g019540) in-frame with GAL4-activation domain; cloned via <i>SmaI</i>	SK
pGADT7: <i>MtNsp1</i>	<i>S. cerevisiae</i> Y187	9.4	Leu	Y2H prey vector containing the 1665 bp CDS of <i>MtNsp1</i> (Medtr8g020840) in-frame with GAL4-activation domain; cloned via <i>BamHI/EcoRI</i>	RH
pGADT7: <i>MtNsp2</i>	<i>S. cerevisiae</i> Y187	9.5	Leu	Y2H prey vector containing the 1527 bp CDS of <i>MtNsp2</i> (Medtr3g072710) in-frame with GAL4-activation domain; cloned via <i>SmaI</i>	RH
pGADT7: <i>MtPalm1</i>	<i>S. cerevisiae</i> Y187	8.8	Leu	Y2H prey vector containing the 756 bp CDS of <i>MtPalm1</i> (Medtr5g014400) in-frame with GAL4-activation domain; cloned via <i>SmaI</i>	This work
pGADT7: <i>MtRad1</i>	<i>S. cerevisiae</i> Y187	9.4	Leu	Y2H prey vector containing the 1566 bp CDS of <i>MtRad1</i> (Medtr4g104020) in-frame with GAL4-activation domain; cloned via <i>SmaI</i>	RH
pGADT7: <i>MtRam1</i>	<i>S. cerevisiae</i> Y187	10	Leu	Y2H prey vector containing the 2025 bp CDS of <i>MtRam1</i> (Medtr7g027190) in-frame with GAL4-activation domain; cloned via <i>SmaI</i>	RH
pGADT7: <i>MtWri5a</i>	<i>S. cerevisiae</i> Y187	9.2	Leu	Y2H prey vector containing the 1221 bp CDS of <i>MtWri5a</i> (Medtr8g468920) in-frame with GAL4-activation domain; cloned via <i>SmaI</i>	LH
pGADT7: <i>MtWri5b</i>	<i>S. cerevisiae</i> Y187	9.2	Leu	Y2H prey vector containing the 1188 bp CDS of <i>MtWri5b</i> (Medtr7g009410) in-frame with GAL4-activation domain; cloned via <i>SmaI</i>	LH
pGADT7: <i>MtWri5c</i>	<i>S. cerevisiae</i> Y187	9.2	Leu	Y2H prey vector containing the 1146 bp CDS of <i>MtWri5c</i> (Medtr6g011490) in-frame with GAL4-activation domain; cloned via <i>SmaI</i>	LH
pGADT7: <i>MtZf1</i>	<i>S. cerevisiae</i> Y187	8.5	Leu	Y2H prey vector containing the 528 bp CDS of <i>MtZf1</i> (Medtr5g026730) in-frame with GAL4-activation domain; cloned via <i>SmaI</i>	This work
pGADT7: <i>MtZf2</i>	<i>S. cerevisiae</i> Y187	9.5	Leu	Y2H prey vector containing the 1566 bp CDS of <i>MtZf2</i> (MtrunA17_Chr7g0268961) in-frame with GAL4-activation domain; cloned via <i>SmaI</i>	This work
pGBKT7: <i>Mt25005</i>	<i>E. coli</i> DH5 $\alpha$ mcr'	8.7	Kan50	Y2H bait vector containing the 1392 bp CDS of <i>Mt25005</i> (Medtr7g011630) in-frame with GAL4-binding domain; cloned via <i>SmaI</i>	LH

pGBKT7: <i>MtArf3</i>	<i>E. coli</i> DH5α mcr'	9.4	Kan50	Y2H bait vector containing the 2049 bp CDS of <i>MtArf3</i> (Medtr2g014770) in-frame with GAL4-DNA-binding domain; cloned via <i>SmaI</i>	This work
pGBKT7: <i>MtArf7</i>	<i>E. coli</i> DH5α mcr'	9.8	Kan50	Y2H bait vector containing the 2433 bp CDS of <i>MtArf7</i> (Medtr2g093740) in-frame with GAL4-DNA-binding domain; cloned via <i>SmaI</i>	This work
pGBKT7: <i>MtArf12</i>	<i>E. coli</i> DH5α mcr'	9.7	Kan50	Y2H bait vector containing the 2379 bp CDS of <i>MtArf12</i> (Medtr4g060460) in-frame with GAL4-DNA-binding domain; cloned via <i>SmaI</i>	This work
pGBKT7: <i>MtArf25</i>	<i>E. coli</i> DH5α mcr'	9.4	Kan50	Y2H bait vector containing the 2106 bp CDS of <i>MtArf25</i> (Medtr4g088210) in-frame with GAL4-DNA-binding domain; cloned via <i>XhoI</i>	This work
pGBKT7: <i>MtCbf1</i>	<i>E. coli</i> DH5α mcr'	7.7	Kan50	Y2H bait vector containing the 360 bp CDS of <i>MtCbf1</i> (Medtr2g081600) in-frame with GAL4-DNA-binding domain; cloned via <i>NdeI/BamHI</i>	SM
pGBKT7: <i>MtCbf2</i>	<i>E. coli</i> DH5α mcr'	7.7	Kan50	Y2H bait vector containing the 354 bp CDS of <i>MtCbf2</i> (Medtr2g081630) in-frame with GAL4-DNA-binding domain; cloned via <i>NdeI/BamHI</i>	SM
pGBKT7: <i>MtCbf3</i>	<i>E. coli</i> DH5α mcr'	7.9	Kan50	Y2H bait vector containing the 609 bp CDS of <i>MtCbf3</i> (Medtr8g091720) in-frame with GAL4-DNA-binding domain; cloned via <i>EcoRI/BamHI</i>	SM
pGBKT7: <i>MtGras1</i>	<i>E. coli</i> DH5α mcr'	8.6	Kan50	Y2H bait vector containing the 1332 bp CDS of <i>MtGras1</i> (Medtr3g022830) in-frame with GAL4-DNA-binding domain; cloned via <i>SmaI</i>	RH
pGBKT7: <i>MtGras4</i>	<i>E. coli</i> DH5α mcr'	8.6	Kan50	Y2H bait vector containing the 1671 bp CDS of <i>MtGras4</i> (Medtr7g109580) in-frame with GAL4-DNA-binding domain; cloned via <i>SmaI</i>	RH
pGBKT7: <i>MtGras6</i>	<i>E. coli</i> DH5α mcr'	8.7	Kan50	Y2H bait vector containing the 1377 bp CDS of <i>MtGras6</i> (Medtr1g069725) in-frame with GAL4-DNA-binding domain; cloned via <i>SmaI</i>	RH
pGBKT7: <i>MtGras7</i>	<i>E. coli</i> DH5α mcr'	8.7	Kan50	Y2H bait vector containing the 1443 bp CDS of <i>MtGras7</i> (Medtr1g086970) in-frame with GAL4-DNA-binding domain; cloned via <i>SmaI</i>	RH
pGBKT7: <i>MtNsp1</i>	<i>E. coli</i> DH5α mcr'	9	Kan50	Y2H bait vector containing the 1665 bp CDS of <i>MtNsp1</i> (Medtr8g020840) in-frame with GAL4-DNA-binding domain; cloned via <i>SmaI</i>	RH
pGBKT7: <i>MtPalm1</i>	<i>E. coli</i> DH5α mcr'	8.1	Kan50	Y2H bait vector containing the 756 bp CDS of <i>MtPalm1</i> (Medtr5g014400) in-frame with GAL4-DNA-binding domain; cloned via <i>SmaI</i>	This work
pGBKT7: <i>MtWri5a</i>	<i>E. coli</i> DH5α mcr'	8.5	Kan50	Y2H bait vector containing the 1221 bp CDS of <i>MtWri5a</i> (Medtr8g468920) in-frame with GAL4-DNA-binding domain; cloned via <i>SmaI</i>	LH
pGBKT7: <i>MtWri5b</i>	<i>E. coli</i> DH5α mcr'	8.5	Kan50	Y2H bait vector containing the 1188 bp CDS of <i>MtWri5b</i> (Medtr7g009410) in-frame with GAL4-DNA-binding domain; cloned via <i>SmaI</i>	LH
pGBKT7: <i>MtWri5c</i>	<i>E. coli</i> DH5α mcr'	8.5	Kan50	Y2H bait vector containing the 1196 bp CDS of <i>MtWri5c</i> (Medtr6g011490) in-frame with GAL4-DNA-binding domain; cloned via <i>SmaI</i>	LH
pGBKT7: <i>MtZf1</i>	<i>E. coli</i> DH5α mcr'	8.5	Kan50	Y2H bait vector containing the 528 bp CDS of <i>MtZf1</i> (Medtr5g026730) in-frame with GAL4-DNA-binding domain; cloned via <i>SmaI</i>	This work
pGBKT7: <i>MtZf2</i>	<i>E. coli</i> DH5α mcr'	9.5	Kan50	Y2H bait vector containing the 1566 bp CDS of <i>MtZf2</i> (MtrunA17_Chr7g0268961) in-frame with GAL4-DNA-binding domain; cloned via <i>SmaI</i>	This work
pGolm-true- empty	<i>E. coli</i> DH5α mcr'	11.8	Spec50	Empty binary vector formed by removing the <i>MtPt4</i> -promoter from 315p9RFP-Pt4-Expr	This work
pGolm-true- empty	<i>R. rhizogenes</i> ARqua1	11.8	Strep600/ Spec50	Empty binary vector formed by removing the <i>MtPt4</i> -promoter from 315p9RFP-Pt4-Expr	This work
pGolm35s: <i>MtPalm1</i> -CDS	<i>E. coli</i> DH5α mcr'	13.4	Spec50	Overexpression vector with the 756 bp CDS of <i>MtPalm1</i> (Medtr5g014400) under control of a CMV 35s-promoter; cloned via <i>SmaI</i>	This work

pGolm35s: <i>MtZf1</i> -CDS	<i>E. coli</i> DH5α mcr'	13.2	Spec50	Overexpression vector with the 528 bp CDS of <i>MtZf1</i> (Medtr5g026730) under control of a CMV 35s-promoter; cloned via <i>SmaI</i>	This work
pGolm35s: <i>MtZf2</i> -CDS	<i>E. coli</i> DH5α mcr'	14.2	Spec50	Overexpression vector with the 1566 bp CDS of <i>MtZf2</i> (MtrunA17_Chr7g0268961) under control of a CMV 35s-promoter; cloned via <i>SmaI</i>	This work
pGolm: <i>MtPalm1</i> - Comp	<i>E. coli</i> DH5α mcr'	15.5	Spec50	Expression vector containing 3768 bp fragment of <i>MtPalm1</i> (Medtr5g014400) with the 1979 bp promoter, 756 bp CDS and 1033 bp terminator region; cloned via <i>SmaI</i>	This work
pGolm: <i>MtZf2</i> -Comp	<i>E. coli</i> DH5α mcr'	17.9	Spec50	Expression vector containing 6145 bp fragment of <i>MtZf2</i> (MtrunA17_Chr7g0268961) with the 1867 bp promoter, coding region and 1185 bp terminator region; cloned via <i>SmaI</i>	This work
pGUS-INT	<i>E. coli</i> DH5α mcr'	5.4	Amp100	Empty cloning vector; contains <i>gusA</i> int-gene.	Küster <i>et. al</i> (1995)
pGUS-Int: p <i>MtPalm1</i>	<i>E. coli</i> DH5α mcr'	7.4	Amp100	pGUS-Int-derivative with the -1981/-1 promoter region of <i>MtPalm1</i> (Medtr5g014440) directionally cloned with <i>EcoRI/HindIII</i>	This work
pGUS-Int: p <i>MtPalm1</i> _ver2	<i>E. coli</i> DH5α mcr'	7.4	Amp100	pGUS-Int-derivative with the -1981/-38 promoter region of <i>MtPalm1</i> (Medtr5g014440) directionally cloned with <i>EcoRI/HindIII</i>	This work
pGUS-Int: p <i>MtZf2</i>	<i>E. coli</i> DH5α mcr'	7.3	Amp100	pGUS-Int-derivative with the -2060/-184 promoter fragment of <i>MtZf2</i> (MtrunA17_Chr7g0268961), cloned via <i>SphI/HindIII</i>	HP
pGUS-Int: p <i>MtZf3</i>	<i>E. coli</i> DH5α mcr'	6.4	Amp100	pGUS-Int-derivative with the -1016/-1 promoter region of <i>MtZf3</i> (Medtr3g103960) directionally cloned with <i>EcoRI/HindIII</i>	This work
pMWR#2	<i>E. coli</i> One Shot ccdB Survival 2 T1R	7.77	Amp100	Y1H Destination vector with a HIS3 reporter gene modified to contain a Gateway cassette with attR4 and attL1 recombination sites.	Deplancke <i>et. al</i> (2004); RH
pMWR#3	<i>E. coli</i> One Shot ccdB Survival 2 T1R	10.39	Amp100	Y1H Destination vector with a <i>lacZ</i> reporter gene modified to contain a Gateway cassette with attR4 and attL1 recombination sites.	Deplancke <i>et. al</i> (2004); RH
pMWR#2: p <i>MtPalm1</i>	<i>E. coli</i> DH5α mcr'	7.5	Amp100	Derivative of pMWR#2 containing the -1981/-1 promoter region of <i>MtPalm1</i> (Medtr5g014440) upstream of a HIS3-reporter; cloned via LR-recombination	This work
pMWR#2: p <i>MtZf1</i>	<i>E. coli</i> DH5α mcr'	7.1	Amp100	Derivative of pMWR#2 containing the -1455/-1 promoter region of <i>MtZf1</i> (Medtr5g026730) upstream of a HIS3-reporter; cloned via LR-recombination	This work
pMWR#2: p <i>MtZf2</i>	<i>E. coli</i> DH5α mcr'	7.3	Amp100	Derivative of pMWR#2 containing the -2060/-184 promoter region of <i>MtZf2</i> (MtrunA17_Chr7g0268961) upstream of a HIS3-reporter; cloned via LR-recombination	This work
pMWR#2: p <i>MtZf3</i>	<i>E. coli</i> DH5α mcr'	6.5	Amp100	Derivative of pMWR#2 containing the -1016/-1 promoter region of <i>MtZf3</i> (Medtr3g103960) upstream of a HIS3-reporter; cloned via LR-recombination	This work
pMWR#3: p <i>MtPalm1</i>	<i>E. coli</i> DH5α mcr'	10.2	Amp100	Derivative of pMWR#3 containing the -1981/-1 promoter region of <i>MtPalm1</i> (Medtr5g014440) upstream of a LacZ-reporter; cloned via LR-recombination	This work
pMWR#3: p <i>MtZf1</i>	<i>E. coli</i> DH5α mcr'	9.8	Amp100	Derivative of pMWR#3 containing the -1455/-1 promoter region of <i>MtZf1</i> (Medtr5g026730) upstream of a LacZ-reporter; cloned via LR-recombination	This work
pMWR#3: p <i>MtZf2</i>	<i>E. coli</i> DH5α mcr'	10.1	Amp100	Derivative of pMWR#3 containing the -2060/-184 promoter region of <i>MtZf2</i>	This work



				(MtrunA17_Chr7g0268961) upstream of a LacZ-reporter; cloned via LR-recombination	
pMWR#3: pMtZf3	<i>E. coli</i> DH5α mcr'	9.3	Amp100	Derivative of pMWR#3 containing the -1016/-1 promoter region of <i>MtZf3</i> (Medtr3g103960) upstream of a LacZ-reporter; cloned via LR-recombination	This work
pMWR: pMtPalm1	<i>S. cerevisiae</i> YM4271	--	His/Ura	Co-integrant of both pMWRs containing the -1981/-1 promoter region of <i>MtPalm1</i> (Medtr5g014440) upstream of a HIS3-reporter and a LacZ-reporter	This work
pMWR: pMtZf1	<i>S. cerevisiae</i> YM4271	--	His/Ura	Co-integrant of both pMWRs containing the -1455/-1 promoter region of <i>MtZf1</i> (Medtr5g026730) upstream of a HIS3-reporter and a LacZ-reporter	This work
pMWR: pMtZf2	<i>S. cerevisiae</i> YM4271	--	His/Ura	Co-integrant of both pMWRs containing the -2060/-184 promoter region of <i>MtZf2</i> (MtrunA17_Chr7g0268961) upstream of a HIS3-reporter and a LacZ-reporter	This work
pMWR: pMtZf3	<i>S. cerevisiae</i> YM4271	--	His/Ura	Co-integrant of both pMWRs containing the -1016/-1 promoter region of <i>MtZf3</i> (Medtr3g103960) upstream of a HIS3-reporter and a LacZ-reporter	This work
pK18	<i>E. coli</i> DH5α mcr'	2.66	Kan50	Empty cloning vector; contains <i>lacZ</i> -gene; B/W-selection possible.	Pridmore (1987)
pK18: <i>MtPalm1</i> -CDS	<i>E. coli</i> DH5α mcr'	3.4	Kan50	Cloning vector containing the 756 bp CDS of <i>MtPalm1</i> (Medtr5g014400) cloned via <i>SmaI</i>	This work
pK18: <i>MtZf1</i> - CDS	<i>E. coli</i> DH5α mcr'	3.2	Kan50	Cloning vector containing the 528 bp CDS of <i>MtZf1</i> (Medtr5g026730) cloned via <i>SmaI</i>	This work
pK18: <i>MtZf2</i> - CDS	<i>E. coli</i> DH5α mcr'	4.2	Kan50	Cloning vector containing the 1566 bp CDS of <i>MtZf2</i> (MtrunA17_Chr7g0268961) cloned via <i>SmaI</i>	This work
pK18: <i>MtPalm1</i> - Comp.	<i>E. coli</i> DH5α mcr'	6.2	Kan50	Cloning vector containing a 3768 bp fragment of <i>MtPalm1</i> (Medtr5g014400) with the 1979 bp promoter, 756 bp CDS and 1033 bp terminator region; cloned via <i>SmaI</i>	This work
pK18: <i>MtZf2</i> - Comp.	<i>E. coli</i> DH5α mcr'	8.8	Kan50	Cloning vector containing a 6145 bp fragment of <i>MtZf2</i> (Medtr5g014400) with the 1876 bp promoter, coding region and 1185 bp terminator region; cloned via <i>SmaI</i>	This work
pK18: pMtPalm1	<i>E. coli</i> DH5α mcr'	4,6	Kan50	Cloning vector containing the -1979/-1 promoter fragment of <i>MtPalm1</i> (Medtr5g014400), cloned via <i>EcoRI/HindIII</i>	This work
pK18: pMtZf1	<i>E. coli</i> DH5α mcr'	4,1	Kan50	Cloning vector containing the -1455/-1 promoter fragment of <i>MtZf1</i> (Medtr5g026730), cloned via <i>EcoRI/PstI</i>	This work
pK18: pMtZf2	<i>E. coli</i> DH5α mcr'	4,5	Kan50	Cloning vector containing the -2060/-184 promoter fragment of <i>MtZf2</i> (MtrunA17_Chr7g0268961), cloned via <i>SphI/HindIII</i>	HP
pK18: pMtZf3	<i>E. coli</i> DH5α mcr'	3,6	Kan50	Cloning vector containing the -1016/-1 promoter fragment of <i>MtZf3</i> (Medtr3g103960), cloned via <i>EcoRI/HindIII</i>	This work
pK7GWIWG2- dsRed	<i>E. coli</i> DB3.1	15.4	Spec50	Empty binary Gateway destination vector for generation of RNAi-constructs; contains dsRed expression cassette for visual screening	Limpens <i>et. al</i> (2004)
pK7GW:gus	<i>E. coli</i> OmniMax	13.1	Spec50	pK7GWIWG2-dsRed-derivative containing two opposed 263 bp fragments of a <i>gus</i> -gene starting at position 920; cloned via LR-recombination	DA
pK7GW: <i>MtPalm1</i> - RNAi-1	<i>E. coli</i> OmniMax	13,7	Spec50/ Cloro15	pK7GWIWG2-dsRed-derivative containing two opposed 100 bp fragments starting at position 334 of the CDS of <i>MtPalm1</i> (Medtr5g014400); cloned via LR-recombination	This work

pK7GW: <i>MtPalm1</i> - RNAi-2	<i>E. coli</i> OmniMax	13,9	Spec50/ Cloro15	pK7GWIWG2-dsRed-derivative containing two opposed 188 bp fragment starting at position 556 of the CDS of <i>MtPalm1</i> (Medtr5g014400); cloned via LR-recombination	This work
pK7GW: <i>MtZf1</i> -RNAi-1	<i>E. coli</i> OmniMax	13,6	Spec50/ Cloro15	pK7GWIWG2-dsRed-derivative containing two opposed 44 bp fragments starting at position 485 of the CDS of <i>MtZf1</i> (Medtr5g026730); cloned via LR-recombination	This work
pK7GW: <i>MtZf1</i> -RNAi-2	<i>E. coli</i> OmniMax	13,7	Spec50/ Cloro15	pK7GWIWG2-dsRed-derivative containing two opposed 120 bp fragments starting at position 34 of the 3'-UTR of <i>MtZf1</i> (Medtr5g026730); cloned via LR-recombination	This work
pK7GW: <i>MtZf2</i> -RNAi-1	<i>E. coli</i> OmniMax	13,9	Spec50/ Cloro15	pK7GWIWG2-dsRed-derivative containing two opposed 202 bp fragments starting at position 128 of the CDS of <i>MtZf2</i> (MtrunA17_Ch7g0268961); cloned via LR-recombination	This work
pK7GW: <i>MtZf2</i> -RNAi-2	<i>E. coli</i> OmniMax	13,7	Spec50/ Cloro15	pK7GWIWG2-dsRed-derivative containing two opposed 120 bp fragments starting at position 561 of the CDS of <i>MtZf2</i> (MtrunA17_Ch7g0268961); cloned via LR-recombination	This work
pK7GW: <i>MtZf3</i> -RNAi-1	<i>E. coli</i> OmniMax	14	Spec50/ Cloro15	pK7GWIWG2-dsRed-derivative containing two opposed 247 bp fragment starting in the 5'-UTR and ending at position 169 of the CDS of <i>MtZf3</i> (Medtr3g103960); cloned via LR-recombination	This work
pK7GW: <i>MtZf3</i> -RNAi-2	<i>E. coli</i> OmniMax	13,9	Spec50/ Cloro15	pK7GWIWG2-dsRed-derivative containing two opposed 178 bp fragment starting at position 540 of the CDS of <i>MtZf3</i> (Medtr3g103960); cloned via LR-recombination	This work
pK7GW: <i>MtPalm1</i> - RNAi-1	<i>R.</i> <i>rhizogenes</i> ARqua1	13,7	Strep600/ Spec100	pK7GWIWG2-dsRed-derivative containing two opposed 100 bp fragments starting at position 334 of the CDS of <i>MtPalm1</i> (Medtr5g014400); cloned via LR-recombination	This work
pK7GW: <i>MtPalm1</i> - RNAi-2	<i>R.</i> <i>rhizogenes</i> ARqua1	13,9	Strep600/ Spec100	pK7GWIWG2-dsRed-derivative containing two opposed 188 bp fragment starting at position 556 of the CDS of <i>MtPalm1</i> (Medtr5g014400); cloned via LR-recombination	This work
pK7GW: <i>MtZf1</i> -RNAi-1	<i>R.</i> <i>rhizogenes</i> ARqua1	13,6	Strep600/ Spec100	pK7GWIWG2-dsRed-derivative containing two opposed 44 bp fragments starting at position 485 of the CDS of <i>MtZf1</i> (Medtr5g026730); cloned via LR-recombination	This work
pK7GW: <i>MtZf1</i> -RNAi-2	<i>R.</i> <i>rhizogenes</i> ARqua1	13,7	Strep600/ Spec100	pK7GWIWG2-dsRed-derivative containing two opposed 120 bp fragments starting at position 34 of the 3'-UTR of <i>MtZf1</i> (Medtr5g026730); cloned via LR-recombination	This work
pK7GW: <i>MtZf2</i> -RNAi-1	<i>R.</i> <i>rhizogenes</i> ARqua1	13,9	Strep600/ Spec100	pK7GWIWG2-dsRed-derivative containing two opposed 202 bp fragments starting at position 128 of the CDS of <i>MtZf2</i> (MtrunA17_Ch7g0268961); cloned via LR-recombination	This work
pK7GW: <i>MtZf2</i> -RNAi-2	<i>R.</i> <i>rhizogenes</i> ARqua1	13,7	Strep600/ Spec100	pK7GWIWG2-dsRed-derivative containing two opposed 120 bp fragments starting at position 561 of the CDS of <i>MtZf2</i> (MtrunA17_Ch7g0268961); cloned via LR-recombination	This work
pK7GW: <i>MtZf3</i> -RNAi-1	<i>R.</i> <i>rhizogenes</i> ARqua1	14	Strep600/ Spec100	pK7GWIWG2-dsRed-derivative containing two opposed 247 bp fragment starting in the 5'-UTR and ending at position 169 of the CDS of <i>MtZf3</i> (Medtr3g103960); cloned via LR-recombination	This work
pK7GW: <i>MtZf3</i> -RNAi-2	<i>R.</i> <i>rhizogenes</i> ARqua1	13,9	Strep600/ Spec100	pK7GWIWG2-dsRed-derivative containing two opposed 178 bp fragment starting at position 540 of the CDS of <i>MtZf3</i> (Medtr3g103960); cloned via LR-recombination	This work

pRedRoot	<i>E. coli</i> DH5α mcr'	13.5	Kan50	Empty binary vector; contains <i>DsRed</i> -gene under control of a <i>ubiquitin</i> -promoter	Limpens <i>et. al</i> (2004)
pRedRoot:pMtPalm1-gus	<i>E. coli</i> DH5α mcr'	17,8	Kan50	pRedRoot-derivative with the -1981/-1 promoter region of <i>MtPalm1</i> (Medtr5g014440) fused to the <i>gusAint</i> reporter gene; cloned using <i>EcoRI/XbaI</i> -cleavage filled in by Klenow	This work
pRedRoot:pMtPalm1-gus_ver2	<i>E. coli</i> DH5α mcr'	17,8	Kan50	pRedRoot-derivative with the -1981/-38 promoter region of <i>MtPalm1</i> (Medtr5g014440) fused to the <i>gusAint</i> reporter gene; cloned using <i>EcoRI/HindIII</i>	This work
pRedRoot:pMtZf1-gus	<i>E. coli</i> DH5α mcr'	17,2	Kan50	pRedRoot-derivative with the -1455/-1 promoter region of <i>MtZf1</i> (Medtr5g026730) fused to the <i>gusAint</i> reporter gene; cloned using <i>XmaI/HindIII</i>	This work
pRedRoot:pMtZf2-gus	<i>E. coli</i> DH5α mcr'	17,2	Kan50	pRedRoot-derivative with the -1572/-3 of <i>MtZf2</i> (MtrunA17_Chr7g0268961) fused to the <i>gusAint</i> reporter gene via a <i>BsaI</i> -site; cloned using <i>XmaI/HindIII</i> sites	This work
pRedRoot:pMtZf2-gus_ver2	<i>E. coli</i> DH5α mcr'	17,4	Strep600/ Kan100	pRedRoot-derivative with the -2060/-184 promoter fragment of <i>MtZf2</i> (MtrunA17_Chr7g0268961), fused to the <i>gusAint</i> reporter gene; cloned using <i>SpeI</i> and filled in by Klenow	HP
pRedroot:pMtZf3-gus	<i>E. coli</i> DH5α mcr'	16,9	Kan50	pRedRoot-derivative with the -1016/-1 promoter region of <i>MtZf3</i> (Medtr3g103960) fused to the <i>gusAint</i> reporter gene; cloned using <i>SpeI</i> and filled in by Klenow	This work
pRedRoot:pMtPalm1-gus	<i>R. rhizogenes</i> ARqua1	17,8	Strep600/ Kan100	pRedRoot-derivative with the -1981/-1 promoter region of <i>MtPalm1</i> (Medtr5g014440) fused to the <i>gusAint</i> reporter gene; cloned using <i>EcoRI/XbaI</i> -cleavage filled in by Klenow	This work
pRedRoot:pMtPalm1-gus_ver2	<i>R. rhizogenes</i> ARqua1	17,8	Strep600/ Kan100	pRedRoot-derivative with the -1981/-38 promoter region of <i>MtPalm1</i> (Medtr5g014440) fused to the <i>gusAint</i> reporter gene; cloned using <i>EcoRI/XbaI</i> -cleavage filled in by Klenow	This work
pRedRoot:pMtZf1-gus	<i>R. rhizogenes</i> ARqua1	17,2	Strep600/ Kan100	pRedRoot-derivative with the -1455/-1 promoter region of <i>MtZf1</i> (Medtr5g026730) fused to the <i>gusAint</i> reporter gene; cloned using <i>XmaI/HindIII</i>	This work
pRedRoot:pMtZf2-gus	<i>R. rhizogenes</i> ARqua1	17,2	Strep600/ Kan100	pRedRoot-derivative with the -1572/-3 of <i>MtZf2</i> (MtrunA17_Chr7g0268961) fused to the <i>gusAint</i> reporter gene via a <i>BsaI</i> -site; cloned using <i>XmaI/HindIII</i> sites	This work
pRedRoot:pMtZf2-gus_ver2	<i>R. rhizogenes</i> ARqua1	17,4	Strep600/ Kan100	pRedRoot-derivative with the -2060/-184 promoter fragment of <i>MtZf2</i> (MtrunA17_Chr7g0268961), fused to the <i>gusAint</i> reporter gene; cloned using <i>SpeI</i> and filled in by Klenow	This work
pRedroot:pMtZf3-gus	<i>R. rhizogenes</i> ARqua1	16,9	Strep600/ Kan100	pRedRoot-derivative with the -1016/-1 promoter region of <i>MtZf3</i> (Medtr3g103960) fused to the <i>gusAint</i> reporter gene; cloned using <i>SpeI</i> and filled in by Klenow	This work
pSPYCE:35s-GW	<i>E. coli</i> One Shot ccdB Survival 2 T1R	13,7	Kan50	Binary Gateway-compatible empty vector containing an C-terminal YFP-fragment (aa 156-239); via LR-recombination, a CDS lacking the Stop-codon can be introduced upstream of the YFP-fragment	Walter <i>et. al</i> (2004)
pSPYCE-empty-control	<i>E. coli</i> DH5α mcr'	13.4	Kan50	pSPYCE:35s-GW-derivative with the GW-cassette removed using <i>SmaI</i> . Contains only the C-terminal YFP fragment and a linker.	This work
pSPYCE:MtDella1	<i>E. coli</i> DH5α mcr'	13.7	Kan50	pSPYCE:35s-GW-derivative containing the CDS of <i>MtDella1</i> (Medtr3g065980) without the Stop-codon (1621 bp) fused to the C-terminal YFP-fragment; cloned via LR-recombination	This work

pSPYCE: <i>MtDella2</i>	<i>E. coli</i> DH5 $\alpha$ mcr'	13.7	Kan50	pSPYCE:35s-GW-derivative containing the CDS of <i>MtDella2</i> (contig_52215) without the Stop-codon (1599 bp) fused to the C-terminal YFP-fragment; cloned via LR-recombination	This work
pSPYCE: <i>MtDella3</i>	<i>E. coli</i> DH5 $\alpha$ mcr'	13.6	Kan50	pSPYCE:35s-GW-derivative containing the CDS of <i>MtDella3</i> (contig_55897) without the Stop-codon (1503 bp) fused to the C-terminal YFP-fragment; cloned via LR-recombination	This work
pSPYCE: <i>MtGras1</i>	<i>E. coli</i> DH5 $\alpha$ mcr'	13.4	Kan50	pSPYCE:35s-GW-derivative containing the CDS of <i>MtGras1</i> (Medtr3g022830) without the Stop-codon (1314 bp) fused to the C-terminal YFP-fragment; cloned via LR-recombination	This work
pSPYCE: <i>MtGras4</i>	<i>E. coli</i> DH5 $\alpha$ mcr'	13.7	Kan50	pSPYCE:35s-GW-derivative containing the CDS of <i>MtGras4</i> (Medtr7g109580) without the Stop-codon (1668 bp) fused to the C-terminal YFP-fragment; cloned via LR-recombination	This work
pSPYCE: <i>MtGras5</i>	<i>E. coli</i> DH5 $\alpha$ mcr'	13.5	Kan50	pSPYCE:35s-GW-derivative containing the CDS of <i>MtGras5</i> (Medtr1g069725) without the Stop-codon (1404 bp) fused to the C-terminal YFP-fragment; cloned via LR-recombination	This work
pSPYCE: <i>MtGras6</i>	<i>E. coli</i> DH5 $\alpha$ mcr'	13.5	Kan50	pSPYCE:35s-GW-derivative containing the CDS of <i>MtGras6</i> (Medtr2g099100) without the Stop-codon (1374 bp) fused to the C-terminal YFP-fragment; cloned via LR-recombination	This work
pSPYCE: <i>MtGras7</i>	<i>E. coli</i> DH5 $\alpha$ mcr'	13.5	Kan50	pSPYCE:35s-GW-derivative containing the CDS of <i>MtGras7</i> (Medtr1g086970) without the Stop-codon (1440 bp) fused to the C-terminal YFP-fragment; cloned via LR-recombination	This work
pSPYCE: <i>MtGrasX</i>	<i>E. coli</i> DH5 $\alpha$ mcr'	13.9	Kan50	pSPYCE:35s-GW-derivative containing the CDS of <i>MtGrasX</i> (Medtr7g069740) without the Stop-codon (1755 bp) fused to the C-terminal YFP-fragment; cloned via LR-recombination	This work
pSPYCE: <i>MtNsp1</i>	<i>E. coli</i> DH5 $\alpha$ mcr'	13.8	Kan50	pSPYCE:35s-GW-derivative containing the CDS of <i>MtNsp1</i> (Medtr8g020840) without the Stop-codon (1662 bp) fused to the C-terminal YFP-fragment; cloned via LR-recombination	This work
pSPYCE: <i>MtNsp2</i>	<i>E. coli</i> DH5 $\alpha$ mcr'	13.6	Kan50	pSPYCE:35s-GW-derivative containing the CDS of <i>MtNsp2</i> (Medtr3g072710) without the Stop-codon (1524 bp) fused to the C-terminal YFP-fragment; cloned via LR-recombination	This work
pSPYCE: <i>MtRad1</i>	<i>E. coli</i> DH5 $\alpha$ mcr'	13.6	Kan50	pSPYCE:35s-GW-derivative containing the CDS of <i>MtRad1</i> (Medtr4g104020) without the Stop-codon (1536 bp) fused to the C-terminal YFP-fragment; cloned via LR-recombination	This work
pSPYCE: <i>MtRam1</i>	<i>E. coli</i> DH5 $\alpha$ mcr'	14.1	Kan50	pSPYCE:35s-GW-derivative containing the CDS of <i>MtRam1</i> (Medtr7g027190) without the Stop-codon (2022 bp) fused to the C-terminal YFP-fragment; cloned via LR-recombination	This work
pSPYCE- empty- control	<i>R. radiobacter</i> GV3101	13.4	Rif100/Gent a15/Kan50	pSPYCE:35s-GW-derivative with the GW-cassette removed using Smal. Contains only the C-terminal YFP fragment and a linker.	This work
pSPYCE: <i>MtDella1</i>	<i>R. radiobacter</i> GV3101	13.7	Rif100/Gent a15/Kan50	pSPYCE:35s-GW-derivative containing the CDS of <i>MtDella1</i> (Medtr3g065980) without the Stop-codon (1621 bp) fused to the C-terminal YFP-fragment; cloned via LR-recombination	This work
pSPYCE: <i>MtDella2</i>	<i>R. radiobacter</i> GV3101	13.7	Rif100/Gent a15/Kan50	pSPYCE:35s-GW-derivative containing the CDS of <i>MtDella2</i> (contig_52215) without the Stop-codon (1599 bp) fused to the C-terminal YFP-fragment; cloned via LR-recombination	This work
pSPYCE: <i>MtDella3</i>	<i>R. radiobacter</i> GV3101	13.6	Rif100/Gent a15/Kan50	pSPYCE:35s-GW-derivative containing the CDS of <i>MtDella3</i> (contig_55897) without the Stop-codon (1503 bp) fused to the C-terminal YFP-fragment; cloned via LR-recombination	This work

pSPYCE: <i>MtGras1</i>	<i>R. radiobacter</i> GV3101	13.4	Rif100/Gent a15/Kan50	pSPYCE:35s-GW-derivative containing the CDS of <i>MtGras1</i> (Medtr3g022830) without the Stop-codon (1314 bp) fused to the C-terminal YFP-fragment; cloned via LR-recombination	This work
pSPYCE: <i>MtGras4</i>	<i>R. radiobacter</i> GV3101	13.7	Rif100/Gent a15/Kan50	pSPYCE:35s-GW-derivative containing the CDS of <i>MtGras4</i> (Medtr7g109580) without the Stop-codon (1668 bp) fused to the C-terminal YFP-fragment; cloned via LR-recombination	This work
pSPYCE: <i>MtGras5</i>	<i>R. radiobacter</i> GV3101	13.5	Rif100/Gent a15/Kan50	pSPYCE:35s-GW-derivative containing the CDS of <i>MtGras5</i> (Medtr1g069725) without the Stop-codon (1404 bp) fused to the C-terminal YFP-fragment; cloned via LR-recombination	This work
pSPYCE: <i>MtGras6</i>	<i>R. radiobacter</i> GV3101	13.5	Rif100/Gent a15/Kan50	pSPYCE:35s-GW-derivative containing the CDS of <i>MtGras6</i> (Medtr2g099100) without the Stop-codon (1374 bp) fused to the C-terminal YFP-fragment; cloned via LR-recombination	This work
pSPYCE: <i>MtGras7</i>	<i>R. radiobacter</i> GV3101	13.5	Rif100/Gent a15/Kan50	pSPYCE:35s-GW-derivative containing the CDS of <i>MtGras7</i> (Medtr1g086970) without the Stop-codon (1440 bp) fused to the C-terminal YFP-fragment; cloned via LR-recombination	This work
pSPYCE: <i>MtGrasX</i>	<i>R. radiobacter</i> GV3101	13.9	Rif100/Gent a15/Kan50	pSPYCE:35s-GW-derivative containing the CDS of <i>MtGrasX</i> (Medtr7g069740) without the Stop-codon (1755 bp) fused to the C-terminal YFP-fragment; cloned via LR-recombination	This work
pSPYCE: <i>MtNsp1</i>	<i>R. radiobacter</i> GV3101	13.8	Rif100/Gent a15/Kan50	pSPYCE:35s-GW-derivative containing the CDS of <i>MtNsp1</i> (Medtr8g020840) without the Stop-codon (1662 bp) fused to the C-terminal YFP-fragment; cloned via LR-recombination	This work
pSPYCE: <i>MtNsp2</i>	<i>R. radiobacter</i> GV3101	13.6	Rif100/Gent a15/Kan50	pSPYCE:35s-GW-derivative containing the CDS of <i>MtNsp2</i> (Medtr3g072710) without the Stop-codon (1524 bp) fused to the C-terminal YFP-fragment; cloned via LR-recombination	This work
pSPYCE: <i>MtRad1</i>	<i>R. radiobacter</i> GV3101	13.6	Rif100/Gent a15/Kan50	pSPYCE:35s-GW-derivative containing the CDS of <i>MtRad1</i> (Medtr4g104020) without the Stop-codon (1536 bp) fused to the C-terminal YFP-fragment; cloned via LR-recombination	This work
pSPYCE: <i>MtRam1</i>	<i>R. radiobacter</i> GV3101	14.1	Rif100/Gent a15/Kan50	pSPYCE:35s-GW-derivative containing the CDS of <i>MtRam1</i> (Medtr7g027190) without the Stop-codon (2022 bp) fused to the C-terminal YFP-fragment; cloned via LR-recombination	This work
pSPYCE: <i>MtTf124</i>	<i>R. radiobacter</i> GV3101	13.7	Rif100/Gent a15/Kan50	pSPYCE:35s-GW-derivative containing the CDS of <i>MtTf124</i> (Medtr8g442410) without the Stop-codon (1608 bp) fused to the C-terminal YFP-fragment; cloned via LR-recombination	This work
pSPYNE:35s- GW	<i>E. coli</i> One Shot ccdB Survival 2 T1R	13,7	Kan50	Binary Gateway-compatible empty vector containing an N-terminal YFP-fragment (aa 1-155); via LR-recombination, a CDS lacking the Stop-codon can be introduced upstream of the YFP-fragment	Walter <i>et. al</i> (2004)
pSPYNE- empty- control	<i>E. coli</i> DH5α mcr'	13.4	Kan50	pSPYNE:35s-GW-derivative with the GW-cassette removed using <i>Sma</i> I. Contains only the N-terminal YFP fragment and a linker	This work
pSPYNE: <i>MtDella1</i>	<i>E. coli</i> DH5α mcr'	13.7	Kan50	pSPYNE:35s-GW-derivative containing the CDS of <i>MtDella1</i> (Medtr3g065980) without the Stop-codon (1621 bp) fused to the N-terminal YFP-fragment; cloned via LR-recombination	This work
pSPYNE: <i>MtDella2</i>	<i>E. coli</i> DH5α mcr'	13.7	Kan50	pSPYNE:35s-GW-derivative containing the CDS of <i>MtDella2</i> (contig_52215) without the Stop-codon (1599 bp) fused to the N-terminal YFP-fragment; cloned via LR-recombination	This work
pSPYNE: <i>MtDella3</i>	<i>E. coli</i> DH5α mcr'	13.6	Kan50	pSPYNE:35s-GW-derivative containing the CDS of <i>MtDella3</i> (contig_55897) without the Stop-	This work

				codon (1503 bp) fused to the N-terminal YFP-fragment; cloned via LR-recombination	
pSPYNE: <i>MtGras1</i>	<i>E. coli</i> DH5 $\alpha$ mcr'	13.4	Kan50	pSPYNE:35s-GW-derivative containing the CDS of <i>MtGras1</i> (Medtr3g022830) without the Stop-codon (1314 bp) fused to the N-terminal YFP-fragment; cloned via LR-recombination	BH
pSPYNE: <i>MtGras4</i>	<i>E. coli</i> DH5 $\alpha$ mcr'	13.7	Kan50	pSPYNE:35s-GW-derivative containing the CDS of <i>MtGras4</i> (Medtr7g109580) without the Stop-codon (1668 bp) fused to the N-terminal YFP-fragment; cloned via LR-recombination	BH
pSPYNE: <i>MtGras5</i>	<i>E. coli</i> DH5 $\alpha$ mcr'	13.5	Kan50	pSPYNE:35s-GW-derivative containing the CDS of <i>MtGras5</i> (Medtr1g069725) without the Stop-codon (1404 bp) fused to the N-terminal YFP-fragment; cloned via LR-recombination	This work
pSPYNE: <i>MtGras6</i>	<i>E. coli</i> DH5 $\alpha$ mcr'	13.5	Kan50	pSPYNE:35s-GW-derivative containing the CDS of <i>MtGras6</i> (Medtr2g099100) without the Stop-codon (1374 bp) fused to the N-terminal YFP-fragment; cloned via LR-recombination	This work
pSPYNE: <i>MtGras7</i>	<i>E. coli</i> DH5 $\alpha$ mcr'	13.5	Kan50	pSPYNE:35s-GW-derivative containing the CDS of <i>MtGras7</i> (Medtr1g086970) without the Stop-codon (1440 bp) fused to the N-terminal YFP-fragment; cloned via LR-recombination	This work
pSPYNE: <i>MtGrasX</i>	<i>E. coli</i> DH5 $\alpha$ mcr'	13.9	Kan50	pSPYNE:35s-GW-derivative containing the CDS of <i>MtGrasX</i> (Medtr7g069740) without the Stop-codon (1755 bp) fused to the N-terminal YFP-fragment; cloned via LR-recombination	This work
pSPYNE: <i>MtNsp1</i>	<i>E. coli</i> DH5 $\alpha$ mcr'	13.8	Kan50	pSPYNE:35s-GW-derivative containing the CDS of <i>MtNsp1</i> (Medtr8g020840) without the Stop-codon (1662 bp) fused to the N-terminal YFP-fragment; cloned via LR-recombination	This work
pSPYNE: <i>MtNsp2</i>	<i>E. coli</i> DH5 $\alpha$ mcr'	13.6	Kan50	pSPYNE:35s-GW-derivative containing the CDS of <i>MtNsp2</i> (Medtr3g072710) without the Stop-codon (1524 bp) fused to the N-terminal YFP-fragment; cloned via LR-recombination	This work
pSPYNE: <i>MtRad1</i>	<i>E. coli</i> DH5 $\alpha$ mcr'	13.6	Kan50	pSPYNE:35s-GW-derivative containing the CDS of <i>MtRad1</i> (Medtr4g104020) without the Stop-codon (1536 bp) fused to the N-terminal YFP-fragment; cloned via LR-recombination	This work
pSPYNE: <i>MtRam1</i>	<i>E. coli</i> DH5 $\alpha$ mcr'	14.1	Kan50	pSPYNE:35s-GW-derivative containing the CDS of <i>MtRam1</i> (Medtr7g027190) without the Stop-codon (2022 bp) fused to the N-terminal YFP-fragment; cloned via LR-recombination	This work
pSPYNE- empty- control	<i>R.</i> <i>radiobacter</i> GV3101	13.4	Rif100/Gent a15/Kan50	pSPYNE:35s-GW-derivative with the GW-cassette removed using <i>Sma</i> I. Contains only the N-terminal YFP fragment and a linker.	This work
pSPYNE: <i>MtDella1</i>	<i>R.</i> <i>radiobacter</i> GV3101	13.7	Rif100/Gent a15/Kan50	pSPYNE:35s-GW-derivative containing the CDS of <i>MtDella1</i> (Medtr3g065980) without the Stop-codon (1621 bp) fused to the N-terminal YFP-fragment; cloned via LR-recombination	This work
pSPYNE: <i>MtDella2</i>	<i>R.</i> <i>radiobacter</i> GV3101	13.7	Rif100/Gent a15/Kan50	pSPYNE:35s-GW-derivative containing the CDS of <i>MtDella2</i> (contig_52215) without the Stop-codon (1599 bp) fused to the N-terminal YFP-fragment; cloned via LR-recombination	This work
pSPYNE: <i>MtDella3</i>	<i>R.</i> <i>radiobacter</i> GV3101	13.6	Rif100/Gent a15/Kan50	pSPYNE:35s-GW-derivative containing the CDS of <i>MtDella3</i> (contig_55897) without the Stop-codon (1503 bp) fused to the N-terminal YFP-fragment; cloned via LR-recombination	This work
pSPYNE: <i>MtGras1</i>	<i>R.</i> <i>radiobacter</i> GV3101	13.4	Rif100/Gent a15/Kan50	pSPYNE:35s-GW-derivative containing the CDS of <i>MtGras1</i> (Medtr3g022830) without the Stop-codon (1314 bp) fused to the N-terminal YFP-fragment; cloned via LR-recombination	This work

pSPYNE: <i>MtGras4</i>	<i>R. radiobacter GV3101</i>	13.7	Rif100/Gent a15/Kan50	pSPYNE:35s-GW-derivative containing the CDS of <i>MtGras4</i> (Medtr7g109580) without the Stop-codon (1668 bp) fused to the N-terminal YFP-fragment; cloned via LR-recombination	This work
pSPYNE: <i>MtGras5</i>	<i>R. radiobacter GV3101</i>	13.5	Rif100/Gent a15/Kan50	pSPYNE:35s-GW-derivative containing the CDS of <i>MtGras5</i> (Medtr1g069725) without the Stop-codon (1404 bp) fused to the N-terminal YFP-fragment; cloned via LR-recombination	This work
pSPYNE: <i>MtGras6</i>	<i>R. radiobacter GV3101</i>	13.5	Rif100/Gent a15/Kan50	pSPYNE:35s-GW-derivative containing the CDS of <i>MtGras6</i> (Medtr2g099100) without the Stop-codon (1374 bp) fused to the N-terminal YFP-fragment; cloned via LR-recombination	This work
pSPYNE: <i>MtGras7</i>	<i>R. radiobacter GV3101</i>	13.5	Rif100/Gent a15/Kan50	pSPYNE:35s-GW-derivative containing the CDS of <i>MtGras7</i> (Medtr1g086970) without the Stop-codon (1440 bp) fused to the N-terminal YFP-fragment; cloned via LR-recombination	This work
pSPYNE: <i>MtGrasX</i>	<i>R. radiobacter GV3101</i>	13.9	Rif100/Gent a15/Kan50	pSPYNE:35s-GW-derivative containing the CDS of <i>MtGrasX</i> (Medtr7g069740) without the Stop-codon (1755 bp) fused to the N-terminal YFP-fragment; cloned via LR-recombination	This work
pSPYNE: <i>MtNsp1</i>	<i>R. radiobacter GV3101</i>	13.8	Rif100/Gent a15/Kan50	pSPYNE:35s-GW-derivative containing the CDS of <i>MtNsp1</i> (Medtr8g020840) without the Stop-codon (1662 bp) fused to the N-terminal YFP-fragment; cloned via LR-recombination	This work
pSPYNE: <i>MtNsp2</i>	<i>R. radiobacter GV3101</i>	13.6	Rif100/Gent a15/Kan50	pSPYNE:35s-GW-derivative containing the CDS of <i>MtNsp2</i> (Medtr3g072710) without the Stop-codon (1524 bp) fused to the N-terminal YFP-fragment; cloned via LR-recombination	This work
pSPYNE: <i>MtRad1</i>	<i>R. radiobacter GV3101</i>	13.6	Rif100/Gent a15/Kan50	pSPYNE:35s-GW-derivative containing the CDS of <i>MtRad1</i> (Medtr4g104020) without the Stop-codon (1536 bp) fused to the N-terminal YFP-fragment; cloned via LR-recombination	This work
pSPYNE: <i>MtRam1</i>	<i>R. radiobacter GV3101</i>	14.1	Rif100/Gent a15/Kan50	pSPYNE:35s-GW-derivative containing the CDS of <i>MtRam1</i> (Medtr7g027190) without the Stop-codon (2022 bp) fused to the N-terminal YFP-fragment; cloned via LR-recombination	This work
pSPYNE: <i>MtTf124</i>	<i>R. radiobacter GV3101</i>	13.7	Rif100/Gent a15/Kan50	pSPYNE:35s-GW-derivative containing the CDS of <i>MtTf124</i> (Medtr8g442410) without the Stop-codon (1608 bp) fused to the N-terminal YFP-fragment; cloned via LR-recombination	This work

BH: BSc Thesis of Benedikt Hellwinkel (2018)

HP: Practical course of Henrik Permann (LUH, unpublished)

LH: PhD Thesis of Lisa Hartung (2021)

SK: PhD Thesis of Steven Krüger (LUH, unpublished)

SM: MSc Thesis of Stephanie Müller (2012)

RH: PhD Thesis of Rico Hartmann (2018)

## 3.2 Primers used

Table 3 – Primers used during this work

Primer Name	Primer Sequence	Description	By
Gateway-Screen 1	CACATTATACGAGCCGGAAG CAT	Sequencing primer, binds in the Gateway-cassette of compatible vectors like pSPYCE/pSPYNE-35s-GW.	AP
GUS-INT-Bsal-for	GGTCTCAGTTCATGTTACGTC CTGTAGAAAC	Amplifies the entire <i>gusA</i> Int-cassette from the pGUS-INT plasmid and adds a <i>Bsal</i> -site producing a GTTC-overhang that can be used to directly ligate a promoter-region	AP
GUS-INT-Bsal-rev	GGTCTCAAGCTTTTGGTTTTA GGAATTAGAA	Amplifies the entire <i>gusA</i> Int-cassette from the pGUS-INT plasmid and adds a <i>Bsal</i> -site producing a <i>HindIII</i> -compatible AGCT-overhang that can be used to clone into binary vector pRedRoot	AP
Medtr5g014400_ RT_for	CTACAGATATTGGCCTTCTTT	Primer for sqRT-PCR amplification of a 159 bp fragment starting at position 5 of the <i>MtPalm1</i> -CDS (Medtr5g014400); A17 and R108	RH
Medtr5g014400_ RT_rev	CTTGTCTTGGTGTGTTTAG	Primer for sqRT-PCR amplification of a 159 bp fragment starting at position 5 of the <i>MtPalm1</i> -CDS (Medtr5g014400); A17 and R108	RH
MtArf3-Smal-for	AAACCCGGGGATGGGGTTAA TCGATCTCAACT	Used for amplification of the entire 2049 bp CDS of <i>MtArf3</i> (Medtr2g014770) from cDNA; adds <i>SmaI</i> -site to facilitate cloning into Y2H bait and prey vectors	AP
MtArf3-Smal-rev	AAACCCGGGTCAACCGCCGC CAATGTG	Used for amplification of the entire 2049 bp CDS of <i>MtArf3</i> (Medtr2g014770) from cDNA; adds <i>SmaI</i> -site to facilitate cloning into Y2H bait and prey vectors	AP
MtArf7-Seq	GGATGAATCTCCAGAAAG	Sequencing primer, bridges the gaps in sequencing any plasmids containing the <i>MtArf7</i> -CDS	AP
MtArf7-Smal-for	AAACCCGGGGATGGAAATTG ATCTGAATGA	Used for amplification of the entire 2433 bp CDS of <i>MtArf7</i> (Medtr2g093740) from cDNA; adds <i>SmaI</i> -site to facilitate cloning into Y2H bait and prey vectors	AP
MtArf7-Smal-rev	AAACCCGGGCTAGATTCTAA CTACTGTTGTA	Used for amplification of the entire 2433 bp CDS of <i>MtArf7</i> (Medtr2g093740) from cDNA; adds <i>SmaI</i> -site to facilitate cloning into Y2H bait and prey vectors	AP
MtArf12-Seq	AGCATCAAGAATCCAATG	Sequencing primer, bridges the gaps in sequencing any plasmids containing the <i>MtArf12</i> -CDS	AP
MtArf12-Smal-for	AAACCCGGGGATGGAAATTG ATCTAAACAATGA	Used for amplification of the entire 2379 bp CDS of <i>MtArf12</i> (Medtr4g060460) from cDNA; adds <i>SmaI</i> -site to facilitate cloning into Y2H bait and prey vectors	AP
MtArf12-Smal-rev	AAACCCGGGTTAGACTCTTAC TACTGTTGG	Used for amplification of the entire 2379 bp CDS of <i>MtArf12</i> (Medtr4g060460) from cDNA; adds <i>SmaI</i> -site to facilitate cloning into Y2H bait and prey vectors	AP
MtArf25-XhoI-for	AAACTCGAGGAATGATGGGT TTGATTGATCTCA	Used for amplification of the entire 2106 bp CDS of <i>MtArf25</i> (Medtr4g088210) from cDNA; adds <i>XhoI</i> -site to facilitate cloning into Y2H bait and prey vectors	AP
MtArf25-XhoI-rev	AAACTCGAGTCAATACTGCA GCACACCT	Used for amplification of the entire 2106 bp CDS of <i>MtArf25</i> (Medtr4g088210) from cDNA; adds <i>XhoI</i> -site to facilitate cloning into Y2H bait and prey vectors	AP
MtArf25-Seq	GGAGATGCAGTTCTGTTC	Sequencing primer, bridges the gaps in sequencing any plasmids containing the <i>MtArf25</i> -CDS	AP
MtDella1-GW-for	GGGGACAAGTTTGTACAAAA AAGCAGGCTACATGTGGAGA GAAGAAAAAGA	Amplifies the complete CDS of <i>MtDella1</i> without the stop-codon (Medtr3g065980, 1641 bp) from cDNA or from pGBKT7: <i>MtDella1</i> and adds attB-Sites for Gateway-cloning	AP
MtDella1-GW-rev	GGGGACCACTTTGTACAAGA AAGCTGGGTACTTGGACTCA TTTTGTGGA	Amplifies the complete CDS of <i>MtDella1</i> without the stop-codon (Medtr3g065980, 1641 bp) from cDNA or from pGBKT7: <i>MtDella1</i> and adds attB-Sites for Gateway-cloning	AP



MtDella2-GW-for	GGGGACAAGTTTGTACAAAA AAGCAGGCTACATGAAGAGA GAGCATAAGCTTGA	Amplifies the complete CDS of <i>MtDella2</i> without the stop-codon (contig_52215, 1599 bp) from cDNA or from pGBKT7: <i>MtDella2</i> and adds attB-Sites for Gateway-cloning	AP
MtDella2-GW-rev	GGGGACCACTTTGTACAAGA AAGCTGGGTAGTGCAGAAACC ACCACTGAG	Amplifies the complete CDS of <i>MtDella2</i> without the stop-codon (contig_52215, 1599 bp) from cDNA or from pGBKT7: <i>MtDella2</i> and adds attB-Sites for Gateway-cloning	AP
MtDella3-GW-for	GGGGACAAGTTTGTACAAAA AAGCAGGCTACATGGAAATA GTTTCAGATTCTTCT	Amplifies the complete CDS of <i>MtDella3</i> without the stop-codon (contig_55897, 1503 bp) from cDNA or from pGADT7: <i>MtDella3</i> and adds attB-Sites for Gateway-cloning	AP
MtDella3-GW-rev	GGGGACCACTTTGTACAAGA AAGCTGGGTAACAATCAAAA CGCAGTGTT	Amplifies the complete CDS of <i>MtDella3</i> without the stop-codon (contig_55897, 1503 bp) from cDNA or from pGADT7: <i>MtDella3</i> and adds attB-Sites for Gateway-cloning	AP
MtGras1-GW-for	GGGGACAAGTTTGTACAAA AAAGCAGGCTACATGGATT CAGTTTCGCCATA	Amplifies the complete CDS of <i>MtGras1</i> without the stop-codon (Medtr3g022830, 1314 bp) from cDNA or from pGADT7: <i>MtGras1</i> and adds attB-Sites for Gateway-cloning	BH
MtGras1-GW-rev	GGGGACCACTTTGTACAAG AAAGCTGGGTATCACCTAA ATTTCCAGGCCG	Amplifies the complete CDS of <i>MtGras1</i> without the stop-codon (Medtr3g022830, 1314 bp) from cDNA or from pGADT7: <i>MtGras1</i> and adds attB-Sites for Gateway-cloning	BH
MtGras4-GW-for	GGGGACAAGTTTGTACAAA AAAGCAGGCTACATGGAAA TTGACCATTTTTCTTC	Amplifies the complete CDS of <i>MtGras4</i> without the stop-codon (Medtr7g109580, 1668 bp) from cDNA or from pGADT7: <i>MtGras4</i> and adds attB-Sites for Gateway-cloning	BH
MtGras4-GW-rev	GGGGACCACTTTGTACAAG AAAGCTGGGTATCAAAGAA ACCTCCAAGCT	Amplifies the complete CDS of <i>MtGras4</i> without the stop-codon (Medtr7g109580, 1668 bp) from cDNA or from pGADT7: <i>MtGras4</i> and adds attB-Sites for Gateway-cloning	BH
MtGras5-GW-for	GGGGACAAGTTTGTACAAA AAAGCAGGCTACATGATTCA TCCACACATGC	Amplifies the complete CDS of <i>MtGras5</i> without the stop-codon (Medtr1g069725, 1404 bp) from cDNA or genomic DNA and adds attB-Sites for Gateway-cloning	AP
MtGras5-GW-rev	GGGGACCACTTTGTACAAGA AAGCTGGGTACCTAGAAGTT CTACAAGTCCA	Amplifies the complete CDS of <i>MtGras5</i> without the stop-codon (Medtr1g069725, 1404 bp) from cDNA or genomic DNA and adds attB-Sites for Gateway-cloning	AP
MtGras6-GW-for	GGGGACAAGTTTGTACAAAA AAGCAGGCTACATGCACGTC CACATGAAAGC	Amplifies the complete CDS of <i>MtGras6</i> without the stop-codon (Medtr2g099100, 1374 bp) from cDNA or from pGBKT7: <i>MtGras6</i> and adds attB-Sites for Gateway-cloning	AP
MtGras6-GW-rev	GGGGACCACTTTGTACAAGA AAGCTGGGTACGACACATGT GCATCCATACC	Amplifies the complete CDS of <i>MtGras6</i> without the stop-codon (Medtr2g099100, 1374 bp) from cDNA or from pGBKT7: <i>MtGras6</i> and adds attB-Sites for Gateway-cloning	AP
MtGras7-GW-for	GGGGACAAGTTTGTACAAAA AAGCAGGCTACATGGAGCAA GAAAATCAAGC	Amplifies the complete CDS of <i>MtGras7</i> without the stop-codon (Medtr1g086970, 1441 bp) from cDNA or from pGBKT7: <i>MtGras7</i> and adds attB-Sites for Gateway-cloning	AP
MtGras7-GW-rev	GGGGACCACTTTGTACAAGA AAGCTGGGTAAAGAACTTC CAAGCTGAGA	Amplifies the complete CDS of <i>MtGras7</i> without the stop-codon (Medtr1g086970, 1441 bp) from cDNA or from pGBKT7: <i>MtGras7</i> and adds attB-Sites for Gateway-cloning	AP
MtGrasX-GW-for	GGGGACAAGTTTGTACAAAA AAGCAGGCTACATGAGTCAG CAAGAGATT	Amplifies the complete CDS of <i>MtGrasX</i> without the stop-codon (Medtr7g069740, 1758 bp) from cDNA or genomic DNA and adds attB-Sites for Gateway-cloning	AP
MtGrasX-GW-rev	GGGGACCACTTTGTACAAGA AAGCTGGGTAATTTTTCCAAA TAGAAAATCTTAAT	Amplifies the complete CDS of <i>MtGrasX</i> without the stop-codon (Medtr7g069740, 1758 bp) from cDNA or genomic DNA and adds attB-Sites for Gateway-cloning	AP

MtNsp1-GW-for	GGGGACAAGTTTGTACAAAA AAGCAGGCTACATGACTATG GAACCAAATCC	Amplifies the complete CDS of <i>MtNsp1</i> without the stop-codon (Medtr8g020840, 1662 bp) from cDNA or from pGBKT7: <i>MtNsp1</i> and adds attB-Sites for Gateway-cloning	AP
MtNsp1-GW-rev	GGGGACCACTTTGTACAAGA AAGCTGGGTACTCTGGTTGT TTATCCAGTT	Amplifies the complete CDS of <i>MtNsp1</i> without the stop-codon (Medtr8g020840, 1662 bp) from cDNA or from pGBKT7: <i>MtNsp1</i> and adds attB-Sites for Gateway-cloning	AP
MtNsp2-GW-for	GGGGACAAGTTTGTACAAAA AAGCAGGCTACATGGATTTG ATGGACATGG	Amplifies the complete CDS of <i>MtNsp2</i> without the stop-codon (Medtr3g072710, 1524 bp) from cDNA or from pGADT7: <i>MtNsp2</i> and adds attB-Sites for Gateway-cloning	AP
MtNsp2-GW-rev	GGGGACCACTTTGTACAAGA AAGCTGGGTATAAATCAGAA TCTGAAGAAGAAC	Amplifies the complete CDS of <i>MtNsp2</i> without the stop-codon (Medtr3g072710, 1524 bp) from cDNA or from pGADT7: <i>MtNsp2</i> and adds attB-Sites for Gateway-cloning	AP
MtPalm1-RNAi-1-for	GGGGACAAGTTTGTACAAAA AAGCAGGCTCATCAAACCCA ACCACCGTT	Primer for an RNAi-Knockdown construct targeting <i>MtPalm1</i> (Medtr5g014400). Produces a 100 bp fragment starting at position 334 of the CDS with added attB-Sites for Gateway-cloning	AP
MtPalm1-RNAi-1-rev	GGGGACCACTTTGTACAAGA AAGCTGGGTAAAGAAGGCAC AATCCAGCA	Primer for an RNAi-Knockdown construct targeting <i>MtPalm1</i> (Medtr5g014400). Produces a 100 bp fragment starting at position 334 of the CDS with added attB-Sites for Gateway-cloning	AP
MtPalm1-RNAi-2-for	GGGGACAAGTTTGTACAAAA AAGCAGGCTTGCAAGCTTGT TCTCCATCT	Primer for an RNAi-Knockdown construct targeting <i>MtPalm1</i> (Medtr5g014400). Produces a 188 bp fragment starting at position 566 of the CDS with added attB-Sites for Gateway-cloning	AP
MtPalm1-RNAi-2-rev	GGGGACCACTTTGTACAAGA AAGCTGGGTAGTTGGTGTG GCTTGTCC	Primer for an RNAi-Knockdown construct targeting <i>MtPalm1</i> (Medtr5g014400). Produces a 188 bp fragment starting at position 566 of the CDS with added attB-Sites for Gateway-cloning	AP
MtPalm1-RT-3'-for	CATCCTTCATCACCATTGATA	Primer for sqRT-PCR amplification of a 184 bp fragment starting at position 381 of the <i>MtPalm1</i> -CDS (Medtr5g014400) in R108	AP
MtPalm1-RT-3'-rev	TTGGAGGATAAGATGTTGAT G	Primer for sqRT-PCR amplification of a 184 bp fragment starting at position 381 of the <i>MtPalm1</i> -CDS (Medtr5g014400) in R108	AP
MtPalm1-RT-F-for	CTAAACAACACCAAGAACA A G	Primer for sqRT-PCR amplification of a 242 bp fragment starting at position 160 of the <i>MtPalm1</i> -CDS (Medtr5g014400) in R108 flanking the Tnt1-insertion	AP
MtPalm1-RT-F-rev	TATGAATGGTGATGAAGGAT G	Primer for sqRT-PCR amplification of a 242 bp fragment starting at position 160 of the <i>MtPalm1</i> -CDS (Medtr5g014400) in R108 flanking the Tnt1-insertion	AP
MtPalm1-Smal-for	AAACCCGGGGATGGCTACAG ATATTGGCCT	Used for amplification of the entire 756 bp CDS of <i>MtPalm1</i> (Medtr5g014400) from genomic DNA; adds <i>SmaI</i> -site to facilitate cloning into Y2H bait and prey vectors	AP
MtPalm1-Smal-rev	AAACCCGGGTCAAGTTGGTG TTGGCTTG	Used for amplification of the entire 756 bp CDS of <i>MtPalm1</i> (Medtr5g014400) from genomic DNA; adds <i>SmaI</i> -site to facilitate cloning into Y2H bait and prey vectors	AP
MtPalm1-Tnt1-for	CTACAGATATTGGCCTTCTTT	Primer for directPCR amplification of a 581 bp fragment starting at position 22 of the <i>MtPalm1</i> -CDS (Medtr5g014400) in R108 to detect potential Tnt1-insertions	AP
MtPalm1-Tnt1-rev	AGATGGAGAACAAGTTTGCA	Primer for directPCR amplification of a 581 bp fragment starting at position 22 of the <i>MtPalm1</i> -CDS (Medtr5g014400) in R108 to detect potential Tnt1-insertions	AP
MtPt4f	TCGCGGCCATGTTTGTGTTG	Primer for sqRT-PCR amplification of a 215 bp fragment starting at position 1018 of the <i>MtPt4</i> -CDS (Medtr1g028600)	SM

MtPt4r	GCGAAGAAGAATGTTAGCCC	Primer for sqRT-PCR amplification of a 215 bp fragment starting at position 1018 of the <i>MtPt4</i> -CDS (Medtr1g028600)	SM
MtRad1-GW-for	GGGGACAAGTTTGTACAAA AAAGCAGGCTACATGTAC CTGCACCTTATGCT	Amplifies the complete CDS of <i>MtRad1</i> without the stop-codon (Medtr4g104020, 1566 bp) from cDNA or from pGADT7: <i>MtRad1</i> and adds attB-Sites for Gateway-cloning	BH
MtRad1-GW-rev	GGGGACCACTTTGTACAAG AAAGCTGGGTAGCATTCC AGCAAGAACTG	Amplifies the complete CDS of <i>MtRad1</i> without the Stop-codon (Medtr4g104020, 1566 bp) from cDNA or from pGADT7: <i>MtRad1</i> and adds attB-Sites for Gateway-cloning	BH
MtRam1-GW-for	GGGGACAAGTTTGTACAAA AAAGCAGGCTACATGATCA ATTCACCTTTGTGGAAGCT	Amplifies the complete CDS of <i>MtRam1</i> without the stop-codon (Medtr7g027190, 2025 bp) from cDNA or from pGADT7: <i>MtRam1</i> and adds attB-Sites for Gateway-cloning	BH
MtRam1-GW-rev	GGGGACCACTTTGTACAAG AAAGCTGGGTAGCATCGCC ATGCAGAAGCA	Amplifies the complete CDS of <i>MtRam1</i> without the stop-codon (Medtr7g027190, 2025 bp) from cDNA or from pGADT7: <i>MtRam1</i> and adds attB-Sites for Gateway-cloning	BH
MtRam1_RT_for	CATTACTACTCCGCAATTTTC	Primer for sqRT-PCR amplification of a 293 bp fragment starting at position 1681 of the <i>MtRam1</i> -CDS (Medtr7g027190)	RH
MtRam1_RT_rev	CAACAAACAACCTTTATCCTC	Primer for sqRT-PCR amplification of a 293 bp fragment starting at position 1681 of the <i>MtRam1</i> -CDS (Medtr7g027190)	RH
MtRam2_RT_for	GATCACTCCTACCAATGAAAT	Primer for sqRT-PCR amplification of a 167 bp fragment starting at position 791 of the <i>MtRam2</i> -CDS (Medtr1g040500)	RH
MtRam2_RT_rev	TAGGAAGATAGGGTCAAGTA G	Primer for sqRT-PCR amplification of a 167 bp fragment starting at position 791 of the <i>MtRam2</i> -CDS (Medtr1g040500)	RH
MtStr-RT-for	TACGAAGAGTTTGAGATTGA G	Primer for sqRT-PCR amplification of a 169 bp fragment starting at position 1501 of the <i>MtStr</i> -CDS (MtrunA17_Chr8g0393191)	AP
MtStr-RT-rev	TGAAAATGGTGGATAAGACA A	Primer for sqRT-PCR amplification of a 169 bp fragment starting at position 1501 of the <i>MtStr</i> -CDS (MtrunA17_Chr8g0393191)	AP
MtStr2-RT-for	CTCTTACATACACAGTGACAA	Primer for sqRT-PCR amplification of a 245 bp fragment starting at position 86 of the <i>MtStr2</i> -CDS (Medtr5g030910)	AP
MtStr2-RT-rev	AGTTCTTTAATCAAGCTTGC	Primer for sqRT-PCR amplification of a 245 bp fragment starting at position 86 of the <i>MtStr2</i> -CDS (Medtr5g030910)	AP
MtTef $\alpha$ _f	AAGCTAGGAGGTATTGACAA G	Primer for sqRT-PCR amplification of a 179 bp fragment starting at position 88 of the <i>MtTef<math>\alpha</math></i> -CDS (Medtr6g021805)	NH
MtTef $\alpha$ _r	ACTGTGCAGTAGTACTTGGT G	Primer for sqRT-PCR amplification of a 179 bp fragment starting at position 88 of the <i>MtTef<math>\alpha</math></i> -CDS (Medtr6g021805)	NH
MtTf124-GW-for	GGGGACAAGTTTGTACAAA AAAGCAGGCTACATGTGGC TTTCCTTCTATAT	Amplifies the complete CDS of <i>MtTf124</i> without the stop-codon (Medtr8g442410, 1.608 bp) from cDNA or genomic DNA and adds attB-Sites for Gateway-cloning	AP
MtTf124-GW-rev	GGGGACCACTTTGTACAAGA AAGCTGGGTAAGAAGCTCTG TCAGTATATG	Amplifies the complete CDS of <i>MtTf124</i> without the stop-codon (Medtr8g442410, 1.608 bp) from cDNA or genomic DNA and adds attB-Sites for Gateway-cloning	AP
MtZf1-RNAi-1-for	GGGGACAAGTTTGTACAAAA AAGCAGGCTTGGTTCCACTT GCTATCATGC	Primer for an RNAi-Knockdown construct targeting <i>MtZf1</i> (Medtr5g026730). Produces a 44 bp fragment starting at position 484 of the CDS with added attB-Sites for Gateway-cloning	AP
MtZf1-RNAi-1-rev	GGGGACCACTTTGTACAAGA AAGCTGGGTTCCACCATCTCA CAAGTCCACT	Primer for an RNAi-Knockdown construct targeting <i>MtZf1</i> (Medtr5g026730). Produces a 44 bp fragment	AP

		starting at position 484 of the CDS with added attB-Sites for Gateway-cloning	
MtZf1-RNAi-2-for	GGGGACAAGTTTGTACAAAA AAGCAGGCTACCACATGAAA TTCGCTCACA	Primer for an RNAi-Knockdown construct targeting <i>MtZf1</i> (Medtr5g026730). Produces a 120 bp fragment starting at position 34 of the 3'-UTR with added attB-Sites for Gateway-cloning	AP
MtZf1-RNAi-2-rev	GGGGACCACTTTGTACAAGA AAGCTGGGTTTCAATTGCAA TGAACATGT	Primer for an RNAi-Knockdown construct targeting <i>MtZf1</i> (Medtr5g026730). Produces a 120 bp fragment starting at position 34 of the 3'-UTR with added attB-Sites for Gateway-cloning	AP
MtZf2-RNAi1-for	GGGGACAAGTTTGTACAAAA AAGCAGGCTACCATGCCTCTA AAACCTGTT	Primer for an RNAi-Knockdown construct targeting MtrunA17_Chr7g0268961 ( <i>MtZf2</i> ). Produces a 202 bp fragment located at the 5'-end of Exon 3 with added attB-Sites for Gateway-cloning.	AP
MtZf2-RNAi1-rev	GGGGACCACTTTGTACAAGA AAGCTGGGTGGGTTGAAGAA GATGGAGGC	Primer for an RNAi-Knockdown construct targeting MtrunA17_Chr7g0268961 ( <i>MtZf2</i> ). Produces a 202 bp fragment located at the 5'-end of Exon 3 with added attB-Sites for Gateway-cloning.	AP
MtZf2-RNAi2-for	GGGGACAAGTTTGTACAAAA AAGCAGGCTACCAACCCTCTT ATGAACACT	Primer for an RNAi-Knockdown construct targeting MtrunA17_Chr7g0268961 ( <i>MtZf2</i> ). Produces a 120 bp fragment located on Exon 3 with added attB-Sites for Gateway-cloning.	AP
MtZf2-RNAi2-rev	GGGGACCACTTTGTACAAGA AAGCTGGGTATGAAATTTCTT GTTGTTCTTTT	Primer for an RNAi-Knockdown construct targeting MtrunA17_Chr7g0268961 ( <i>MtZf2</i> ). Produces a 120 bp fragment located on Exon 3 with added attB-Sites for Gateway-cloning.	AP
MtZf3-RNAi-1-for	GGGGACAAGTTTGTACAAAA AAGCAGGCTAGCTAGCTACA CGAGTCACA	Primer for an RNAi-Knockdown construct targeting <i>MtZf3</i> (Medtr3g103960). Produces a 247 bp fragment ending at position 169 of the CDS with added attB-Sites for Gateway-cloning	AP
MtZf3-RNAi-1-rev	GGGGACCACTTTGTACAAGA AAGCTGGGTACATTCGGAAT TGGTCAGTTGA	Primer for an RNAi-Knockdown construct targeting <i>MtZf3</i> (Medtr3g103960). Produces a 247 bp fragment ending at position 169 of the CDS with added attB-Sites for Gateway-cloning	AP
MtZf3-RNAi-2-for	GGGGACAAGTTTGTACAAAA AAGCAGGCTATCTCGATACG GTGTCCCAC	Primer for an RNAi-Knockdown construct targeting <i>MtZf3</i> (Medtr3g103960). Produces a 178 bp fragment starting at position 540 of the CDS with added attB-Sites for Gateway-cloning	AP
MtZf3-RNAi-2-rev	GGGGACCACTTTGTACAAGA AAGCTGGGTCAACCCTCCA TACCAACCC	Primer for an RNAi-Knockdown construct targeting <i>MtZf3</i> (Medtr3g103960). Produces a 178 bp fragment starting at position 540 of the CDS with added attB-Sites for Gateway-cloning	AP
MtZf1-RT-for	TTGTTTCAATGTATCATGTGCG	Primer for sqRT-PCR amplification of a 182 bp fragment starting at position 80 of the <i>MtZf1</i> -CDS (Medtr5g02673)	AP
MtZf1-RT-rev	TGGAACAGCATCATCTTTATT	Primer for sqRT-PCR amplification of a 182 bp fragment starting at position 80 of the <i>MtZf1</i> -CDS (Medtr5g02673)	AP
MtZf1-Smal-for	AAACCCGGGGATGGACGGTG ATCATGGTGA	Used for amplification of the entire 528 bp CDS of <i>MtZf1</i> (Medtr5g026730) from genomic DNA; adds <i>Smal</i> -site to facilitate cloning into Y2H bait and prey vectors	AP
MtZf1-Smal-rev	AAACCCGGGTCACCATCTCAC AAGTCCACT	Used for amplification of the entire 528 bp CDS of <i>MtZf1</i> (Medtr5g026730) from genomic DNA; adds <i>Smal</i> -site to facilitate cloning into Y2H bait and prey vectors	AP
MtZf1-Tnt1-for	GTCTTAGGCCGGCTTTTGTC	Primer for directPCR amplification of a 539 bp fragment starting at position 199 of the <i>MtZf1</i> -CDS (Medtr5g026730) in R108 to detect potential Tnt1-insertions	AP
MtZf1-Tnt1-rev	GGAACGACAAACAGGGCAAT	Primer for directPCR amplification of a 539 bp fragment starting at position 718 of the <i>MtZf1</i> -CDS (Medtr5g026730) in R108 to detect potential Tnt1-insertions	AP

MtZf2-Intron-for	AATAGCAATGGTCCACTAAT	Primer for sqRT-PCR amplification of a 155 bp fragment starting at position 124 of the <i>MtZf2</i> -CDS (MtrunA17_Chr7g0268961) spanning exons 1 and 2 to demonstrate their connection; inefficient for quantification	AP
MtZf2-Intron-rev	TAATGCTCGAGATGGATTATG	Primer for sqRT-PCR amplification of a 155 bp fragment starting at position 124 of the <i>MtZf2</i> -CDS (MtrunA17_Chr7g0268961) spanning exons 1 and 2 to demonstrate their connection; inefficient for quantification	AP
MtZf2-RT-for	AGTTCATGATTTCTTGGAAT	Primer for sqRT-PCR amplification of a 155 bp fragment starting at position 817 of the <i>MtZf2</i> -CDS (MtrunA17_Chr7g0268961)	AP
MtZf2-RT-rev	AAATTGATTTCTCCATTGCTG	Primer for sqRT-PCR amplification of a 155 bp fragment starting at position 817 of the <i>MtZf2</i> -CDS (MtrunA17_Chr7g0268961)	AP
MtZf2-RT-5'-for	ATGTCAAATATTTCAAGGTGATG	Primer for sqRT-PCR amplification of a 156 bp fragment starting at position 0 of the <i>MtZf2</i> -CDS (MtrunA17_Chr7g0268961), not annotated as part of the CDS according to the v5 genome	AP
MtZf2-RT-5'-rev	ATTTTGCTGTTGATTAGTGGA	Primer for sqRT-PCR amplification of a 156 bp fragment starting at position 0 of the <i>MtZf2</i> -CDS (MtrunA17_Chr7g0268961), not annotated as part of the CDS according to the v5 genome	AP
MtZf2-RT-F-for	CATAATCCATCTCGAGCATT	Primer for sqRT-PCR amplification of a 218 bp fragment starting at position 210 of exon 2 of <i>MtZf2</i> (MtrunA17_Chr7g0268961) in R108 flanking the Tnt1-insertion	AP
MtZf2-RT-F-rev	AATGCTCTGTGGGTATAAAA	Primer for sqRT-PCR amplification of a 218 bp fragment ending at position 30 of exon 3 of <i>MtZf2</i> (MtrunA17_Chr7g0268961) in R108 flanking the Tnt1-insertion	AP
MtZf2-Smal-for	AAACCCGGGGATGTCAAATA TTTCAGGTGATGA	Used for amplification of the entire 1566 bp CDS of <i>MtZf2</i> (MtrunA17_Chr7g0268961) from cDNA; adds <i>SmaI</i> -site to facilitate cloning into Y2H bait and prey	AP
MtZf2-Smal-rev	AAACCCGGGTCAAACATCCC AAATTGATTTTC	Used for amplification of the entire 1566 bp CDS of <i>MtZf2</i> (MtrunA17_Chr7g0268961) from cDNA; adds <i>SmaI</i> -site to facilitate cloning into Y2H bait and prey	AP
MtZf2-Tnt1-for	GCAAAAGCACTCTATTAATG	Primer for directPCR amplification of a 573 bp fragment surrounding Exon 2 of <i>MtZf2</i> (MtrunA17_Chr7g0268961) in R108 to detect potential Tnt1-insertions	AP
MtZf2-Tnt1-rev	TCATGGACTTGAAAATAGAA ACA	Primer for directPCR amplification of a 573 bp fragment surrounding Exon 2 of <i>MtZf2</i> (MtrunA17_Chr7g0268961) in R108 to detect potential Tnt1-insertions	AP
MtZf3-RT-for	ATTCTGTCTCCATTTTCTGT	Primer for sqRT-PCR amplification of a 214 bp fragment starting at position 230 of the <i>MtZf3</i> -5'-UTR (Medtr3g103960)	AP
MtZf3-RT-rev	ATGTGCTTATGTGACTAATGT	Primer for sqRT-PCR amplification of a 214 bp fragment starting at position 230 of the <i>MtZf3</i> -5'-UTR (Medtr3g103960)	AP
MtZf3-Smal-for	AAACCCGGGGATGATCAAAA TTCAAACCTTA	Used for amplification of the entire 873 bp CDS of <i>MtZf3</i> (Medtr3g103960) from cDNA; adds <i>SmaI</i> -site to facilitate cloning into Y2H bait and prey vectors	AP
MtZf3-Smal-rev	AAACCCGGGTCAAGTTAACAA GTTCCGC	Used for amplification of the entire 873 bp CDS of <i>MtZf3</i> (Medtr3g103960) from cDNA; adds <i>SmaI</i> -site to facilitate cloning into Y2H bait and prey vectors	AP
Palm1-Complete-Smal-for	AAACCCGGGTAGGTACAATG CAAGCAACT	Used for amplification of a 3768 bp <i>MtPalm1</i> (Medtr5g014400) fragment consisting of the promoter, coding region and terminator from genomic DNA; adds <i>SmaI</i> -site	AP

Palm1-Complete-Smal-rev	AAACCCGGGTCCAAAGGCCA GCGTACTTA	Used for amplification of a 3768 bp <i>MtPalm1</i> (Medtr5g014400) fragment consisting of the promoter, coding region and terminator from genomic DNA; adds <i>SmaI</i> -site	AP
pGolm-Term-rev	AACGTGCACAACAGAATTGA A	Sequencing primer used to read into genes cloned into the pGolm-based overexpression constructs	RH
pgusint	GATTTACGGGTTGGGGTTT CT	Sequencing primer used for promoters cloned upstream of <i>gusAint</i> reporter gene, binds starting at position 15 in the CDS	NH
pMtPalm1-attB-for	GGGGACAAGTTTGTACAAAA AAGCAGGCTTAGGTACAATG CAAGCAACT	Amplifies the promoter-region of Medtr5g014400 ( <i>MtPalm1</i> ) (1980 bp; -1981/-1) and adds attachment sites for a Gateway-BP-reaction.	AP
pMtPalm1-attB-rev	GGGGACCACTTTGTACAAGA AAGCTGGGTGGTACTGTCAC TGACATTTAAG	Amplifies the promoter-region of Medtr5g014400 ( <i>MtPalm1</i> ) (1980 bp; -1981/-1) and adds attachment sites for a Gateway-BP-reaction.	AP
pMtPalm1-EcoRI-for	AAAGAATTCTAGGTACAATG CAAGCAACT	Amplifies the promoter-region of Medtr5g014400 ( <i>MtPalm1</i> ) (1980 bp; -1981/-1) and adds an <i>EcoRI</i> -site used for directional cloning.	AP
pMtPalm1-HindIII-rev	AAAAAGCTTGGTACTGTCAC TGACATTTAAG	Amplifies the promoter-region of Medtr5g014400 ( <i>MtPalm1</i> ) (1980 bp; -1981/-1) and adds a <i>HindIII</i> -site used for directional cloning.	AP
pMtPalm1-HindIII-rev_ver2	GGTCTCAGAAGTCTAGAA AGAAATGGTTGCAG	Amplifies the promoter-region of Medtr5g014400 ( <i>MtPalm1</i> ) (1942 bp; -1981/-38) and adds a <i>HindIII</i> -site used for directional cloning.	AP
pMtZf1-attB-for	GGGGACAAGTTTGTACAAAA AAGCAGGCTACCACAAGAGA AACAAAGGT	Amplifies the promoter-region of Medtr5g026730 ( <i>MtZf1</i> ) (1454 bp; -1455/-1) and adds attachment sites for a Gateway-BP-reaction.	AP
pMtZf1-attB-rev	GGGGACCACTTTGTACAAGA AAGCTGGGTAATCAATGATC ATGTATGTGA	Amplifies the promoter-region of Medtr5g026730 ( <i>MtZf1</i> ) (1454 bp; -1455/-1) and adds attachment sites for a Gateway-BP-reaction.	AP
pMtZf2-attB-for	GGGGACAAGTTTGTACAAAA AAGCAGGCTAGGACCACAAG AGAGACACG	Amplifies the promoter-region of MtrunA17_Chr7g0268961 ( <i>MtZf2</i> ) (1876 bp; -2060/-184) and adds attachment sites for a Gateway-BP-reaction.	AP
pMtZf2-attB-rev	GGGGACCACTTTGTACAAGA AAGCTGGGTATGGTACCAAT ATTGGAAGCAGG	Amplifies the promoter-region of MtrunA17_Chr7g0268961 ( <i>MtZf2</i> ) (1876 bp; -2060/-184) and adds attachment sites for a Gateway-BP-reaction.	AP
pMtZf3-attB-for	GGGGACAAGTTTGTACAAAA AAGCAGGCTCTCCAACACAA ATTGCTTGT	Amplifies the promoter-region of Medtr3g103960 ( <i>MtZf3</i> ) (1013 bp; -1014/-1) and adds attachment sites for a Gateway-BP-reaction.	AP
pMtZf3-attB-rev	GGGGACCACTTTGTACAAGA AAGCTGGGTGGTTTCGGATG GATTAAGGA	Amplifies the promoter-region of Medtr3g103960 ( <i>MtZf3</i> ) (1.013 bp; -1.014/-1) and adds attachment sites for a Gateway-BP-reaction.	AP
pMtZf1-Bsal-for	GGTCTCACCGGACCACAAGA GAAACAAAGGT	Amplifies the promoter-region of Medtr5g026730 ( <i>MtZf1</i> ) (1454 bp; -1455/-1) and adds <i>Bsal</i> -sites producing a <i>XmaI</i> -compatible CCGG-overhang used for cloning into pRedRoot.	AP
pMtZf1-Bsal-rev	GGTCTCAGAACAGAACAATC AATGATCATGTATGTGA	Amplifies the promoter-region of Medtr5g026730 ( <i>MtZf1</i> ) (1454 bp; -1455/-1) and adds <i>Bsal</i> -sites producing a CAAG-overhang. This can be used to add the <i>gusAint</i> -fragment via Golden-Gate-Cloning.	AP
pMtZf2-Bsal-for	GGTCTCACGGAAATAAAT TTGAGTTTATT	Amplifies the promoter-region of MtrunA17_Chr7g0268961 ( <i>MtZf2</i> ) (1569 bp; -1572/-3) and adds <i>Bsal</i> -sites producing a <i>XmaI</i> -compatible CCGG-overhang used for cloning into pRedRoot.	AP
pMtZf2-Bsal-rev	GGTCTCAGAACCAATACAA ATAAATTGAAGTA	Amplifies the promoter-region of MtrunA17_Chr7g0268961 ( <i>MtZf2</i> ) (1569 bp; -1572/-3) and adds <i>Bsal</i> -sites producing a CAAG-overhang. This can be used to add the <i>gusAint</i> -fragment via Golden-Gate-Cloning.	AP

pMtZf2-Sph1_for neu	AAAGCATGCAGGACCACAAG AGAGACACG	Amplifies the promoter-region of MtrunA17_Chr7g 0268961 ( <i>MtZf2</i> ) (1876 bp; -2060/-184) and adds a <i>SphI</i> -site used for directional cloning.	HP
pMtZf2-HindIII- rev	AAAAAGCTTATGGTACCAAT ATTGGAAGCAGG	Amplifies the promoter-region of MtrunA17_Chr7g 0268961 ( <i>MtZf2</i> ) (1876 bp; -2060/-184) and adds a <i>HindIII</i> -site used for directional cloning.	HP
pMtZf2-Bsal-for	GGTCTCACCGGAAATAAATTT GAGTTTATT	Amplifies the promoter-region of MtrunA17_Chr7g 0268961 ( <i>MtZf2</i> ) (1569 bp; -1572/-3) and adds <i>Bsal</i> -sites producing a <i>XmaI</i> -compatible CCGG-overhang used for cloning into pRedRoot.	AP
pMtZf2-Bsal-rev	GGTCTCAGAACCAATACAAA TAAATTGAAGTA	Amplifies the promoter-region of MtrunA17_Chr7g 0268961 ( <i>MtZf2</i> ) (1569 bp; -1572/-3) and adds <i>Bsal</i> -sites producing a CAAG-overhang. This can be used to add the <i>gusA</i> Int-fragment via Golden-Gate-Cloning.	AP
pMtZf3-EcoRI-for	AAAGAATTCCTCCAACACAA ATTGCTTGT	Amplifies the promoter-region of Medtr3g103960 ( <i>MtZf3</i> ) (1013 bp; -1014/-1) and adds an <i>EcoRI</i> -site used for directional cloning.	AP
pMtZf3-HindIII- rev	AAAAAGCTTGGTTTCGGATG GATTAAGGA	Amplifies the promoter-region of Medtr3g103960 ( <i>MtZf3</i> ) (1013 bp; -1014/-1) and adds a <i>HindIII</i> -site used for directional cloning.	AP
pRedRoot-Screen- rev	AGTGGATTAGAAGGAAAG	Sequencing primer, binds 50 bp downstream of mcs1 in pRedRoot to read into promoter- <i>gus</i> fusion	BH
pSPYNE-Screen- rev	TGAACTTGTGGCCGTTTA	Sequencing primer, binds the N-terminal YFP-fragment of pSPYNE to read into the fused CDS	AP
pSPYCE-Screen- rev	TTCTGCTGGTAGTGGTCG	Sequencing primer, binds the C-terminal YFP-fragment of pSPYCE to read into the fused CDS	AP
pUbi-for	AAGAGCTCTTTGGGTATTGT	Used to amplify a 1101 bp fragment of the Ubi3-promoter to construct a complementation construct with native expression, has endogenous <i>SacI</i> -site	AP
pUbi-SpeI-rev	AAAAGTAGTGTGCTTTCCTTA CATTCTGA	Used to amplify a 1101 bp fragment of the Ubi3-promoter to construct a complementation construct with native expression, Adds <i>SpeI</i> -site	AP
Ri_α-Tub_for	TGTCCAACCGGTTTTAAAGT	Primer for sqRT-PCR amplification of the <i>Rhizophagus irregularis</i> α-tubulin housekeeping-gene	NP
Ri_α-Tub_rev	AAAGCACGTTTGGCGTACAT	Primer for sqRT-PCR amplification of the <i>Rhizophagus irregularis</i> α-tubulin housekeeping-gene	NP
Tnt1-F	gcattcaaactagaagacagtgtac c	Used for multiplex-direct PCR detection of Tnt1-insertions, binds 669 bp from the 3'-end of the Tnt1-retrotransposon	MT
Zf1-Complete- Smal-for	AAACCCGGGAAAACCTCCA CAACCACCG	Used for amplification of a 3075 bp <i>MtZf1</i> (Medtr5g026730) fragment consisting of promoter, coding region and terminator from genomic DNA; adds <i>Smal</i> -site	AP
Zf1-Complete- Smal-rev	AAACCCGGGACATTTGAAAG ACGGTGTGACA	Used for amplification of a 3075 bp <i>MtZf1</i> (Medtr5g026730) fragment consisting of promoter, coding region and terminator from genomic DNA; adds <i>Smal</i> -site	AP
Zf2-Complete- Smal-for	AAACCCGGGAGGACCACAAG AGAGACACG	Used for amplification of a 6145 bp <i>MtZf2</i> (MtrunA17_Chr7g0268961) fragment consisting of the promoter, coding region and terminator from genomic DNA; adds <i>Smal</i> -site	AP
Zf2-Complete- Smal-rev	AAACCCGGGCCTGTTACCCG GAGAACCTT	Used for amplification of a 6145 bp <i>MtZf2</i> (MtrunA17_Chr7g0268961) fragment consisting of the promoter, coding region and terminator from genomic DNA; adds <i>Smal</i> -site	AP

AP: This work

BH: BSc Thesis of Benedikt Hellwinkel (2018)

MT: Tadege *et. al* (2008)

NH: Hohnjec *et. al.* (2003)

NP: Pumplin *et. al* (2010)

RH: Hartmann *et. al.* (2019)

SM: MSc Thesis of Stephanie Müller (2012)

### 3.3 Other materials used

Table 4 – Buffers used

Buffer	Component	Concentration
dNTP-mix	dATP	10 mM
	dCTP	10 mM
	dGTP	10 mM
	dTTP	10 mM
Ethidium bromide nucleic acid staining solution	Ethidium bromide	1:2,500 (v/v)
GUS-staining buffer	Tris-HCl, pH 7.6	100 mM
	NaCl	50 mM
	K <sub>3</sub> [Fe(CN) <sub>6</sub> ]	2 mM
	K <sub>4</sub> [Fe(CN) <sub>6</sub> ]	2 mM
	X-Gluc	1 mg/ml
Infiltration Buffer	MES, pH 5.6	10 mM
	MgCl <sub>2</sub>	10 mM
	Acetosyringone	150 µM
10x Ligation buffer	Tris-HCl, pH 7.6	500 mM
	MgCl <sub>2</sub>	100 mM
	DTT	10 mM
	PEG 8000	50% (w/v)
Loading dye	Glycerin	0.08 l
	TA buffer (10x)	0.02 l
	Bromophenol blue	0.25 g/l
P1 buffer	Tris-HCl, pH 7.6	50 mM
	EDTA	10 mM
	• Adjusted to pH 8.0 w/ HCl	
P2 buffer	NaOH	200 mM
	SDS	1% (w/v)
P3 buffer	K-Ac	2.55 M
	• Adjusted to pH 4.8 w/ Acetic acid	
PS buffer	Na <sub>2</sub> HPO <sub>4</sub>	49.31 mM
	NaCl	85.56 mM
	KHPO <sub>4</sub>	22.05 mM
PBS	NaCl	140 mM
	KCl	2.7 mM
	KH <sub>2</sub> PO <sub>4</sub>	1.8 mM
	Na <sub>2</sub> HPO <sub>4</sub> x H <sub>2</sub> O	1 mM
	• Adjusted to pH 7.3 w/ KOH	
RNase buffer	Tris-HCl, pH 7.6	50 mM
	EDTA	10 mM
½ strength Hoagland's solution	Ca(NO <sub>3</sub> ) <sub>3</sub> x 4H <sub>2</sub> O	2.5 mM
	KNO <sub>3</sub>	2.5 mM
	MgSO <sub>4</sub> x 7H <sub>2</sub> O	1 mM
	NaFe-EDTA	50 µM
	KH <sub>2</sub> PO <sub>4</sub>	20 µM / 75 µM



	H <sub>3</sub> BO <sub>3</sub>	10 µM
	MnCl <sub>2</sub> x 2H <sub>2</sub> O	2 µM
	ZnSO <sub>4</sub> x 7H <sub>2</sub> O	1 µM
	CuSO <sub>4</sub> x 5H <sub>2</sub> O	0.5 µM
	CoCl <sub>2</sub> x 6H <sub>2</sub> O	0.2 µM
	Na <sub>2</sub> MoO <sub>4</sub> x 2H <sub>2</sub> O	0.2 µM
	NiCl <sub>2</sub> x 6H <sub>2</sub> O	0.2 µM
	• Adjusted to pH 6.3-6.5 w/ KOH	
10x TA buffer	K-Ac	660 mM
	Tris-HCl, pH 7.6	330 mM
	MgCl <sub>2</sub> x 6H <sub>2</sub> O	100 mM
	DTT	5 mM
	BSA	1 mg/ml
	• Adjusted to pH 7.5 w/ Acetic acid	
TAE buffer	Tris-HCl, pH 7.6	40 mM
	NaO-Ac	10 mM
	EDTA	1 mM
	• Adjusted to pH 7.8 w/ Acetic acid	
Tbf1 buffer	RbCl	100 mM
	MnCl <sub>2</sub> x 2H <sub>2</sub> O	50 mM
	MES	10 mM
	CaCl <sub>2</sub> x 2H <sub>2</sub> O	10 mM
	• Adjusted to pH 6	
Tbf2 buffer	CaCl <sub>2</sub> x 2H <sub>2</sub> O	75 mM
	Glycerin (87%)	50 mM
	MOPS	10 mM
	RbCl	10 mM
	• Adjusted to pH 6.5	
TCM buffer	CaCl <sub>2</sub> x 2H <sub>2</sub> O	10 mM
	MgCl <sub>2</sub> x 6H <sub>2</sub> O	10 mM
	Tris-HCl, pH 7.6	10 mM
	• Adjusted to pH 7.5 w/ HCl	

Table 5 – Chemicals used

Substance	Manufacturer
Acetic acid (Ac)	Carl Roth, Karlsruhe, Germany
Agarose (for solid media)	Invitrogen, Carlsbad, California, USA (Thermo Fisher Scientific, Waltham, Massachusetts, USA)
Agarose (pure)	PEQLAB Biotechnologie, Erlangen, Germany
Alexa488-WGA	Invitrogen, Carlsbad, California, USA (Thermo Fisher Scientific, Waltham, Massachusetts, USA)
3-Aminotriazole	Sigma-Aldrich, St. Louis, Missouri, USA
Antibiotic Medium No. 3	Oxoid, Wesel, Germany (Thermo Fisher Scientific, Waltham, Massachusetts, USA)
Bromophenol blue	Merck, Darmstadt, Germany
Bovine serum albumin (BSA)	SERVA Electrophoresis, Heidelberg, Germany
Ca(NO <sub>3</sub> ) <sub>2</sub> x 4H <sub>2</sub> O	Carl Roth, Karlsruhe, Germany
CaCl <sub>2</sub> x 2H <sub>2</sub> O	Merck, Darmstadt, Germany
CF488-WGA	Biotium, San Francisco, USA
CoCl <sub>2</sub> x 6H <sub>2</sub> O	Sigma-Aldrich, St. Louis, Missouri, USA
CuSO <sub>4</sub> x 5H <sub>2</sub> O	Sigma-Aldrich, St. Louis, Missouri, USA

ddH <sub>2</sub> O	Carl Roth, Karlsruhe, Germany
Dimethylsulfoxide (DMSO)	Carl Roth, Karlsruhe, Germany
dNTPs	Invitrogen, Carlsbad, California, USA (Thermo Fisher Scientific, Waltham, Massachusetts, USA)
Dithiothreitol (DTT)	Sigma-Aldrich, St. Louis, Missouri, USA
Ethanol	Carl Roth, Karlsruhe, Germany
Ethylenediaminetetraacetic acid (EDTA)	Merck, Darmstadt, Germany
Ethidium bromide	Carl Roth, Karlsruhe, Germany
GeneRuler (50 bp, 100 bp and 1 kb)	Thermo Fisher Scientific, Waltham, Massachusetts, USA
Glycerin	AppliChem, Darmstadt, Germany (Illinois Tool Works, Glenview, Illinois, USA)
H <sub>3</sub> BO <sub>3</sub>	Sigma-Aldrich, St. Louis, Missouri, USA
HCl (Hydrochloric Acid) 37%	Carl Roth, Karlsruhe, Germany
H <sub>2</sub> SO <sub>4</sub> (Sulfuric Acid) (concentrated)	Carl Roth, Karlsruhe, Germany
Ink	Sheaffer, Shelton, Connecticut, USA
Isopropyl alcohol	Carl Roth, Karlsruhe, Germany
Isopropyl β-D-1-thiogalactopyranoside (IPTG)	Carl Roth, Karlsruhe, Germany
K-Ac (Potassium acetate)	Merck, Darmstadt, Germany
K <sub>3</sub> [Fe(CN) <sub>6</sub> ] (K-Ferricyanide)	Merck, Darmstadt, Germany
K <sub>4</sub> [Fe(CN) <sub>6</sub> ] (K-Ferrocyanide)	Merck, Darmstadt, Germany
KH <sub>2</sub> PO <sub>4</sub>	Carl Roth, Karlsruhe, Germany
KNO <sub>3</sub>	Carl Roth, Karlsruhe, Germany
KOH	Carl Roth, Karlsruhe, Germany
KCl	Merck, Darmstadt, Germany
β-Mercaptoethanol	Sigma-Aldrich, St. Louis, Missouri, USA
2-Morpholin-4-ylethanesulfonic acid (MES)	SERVA Electrophoresis, Heidelberg, Germany
MgCl <sub>2</sub> x 6H <sub>2</sub> O	Merck, Darmstadt, Germany
MgSO <sub>4</sub> x 7H <sub>2</sub> O	Sigma-Aldrich, St. Louis, Missouri, USA
MnCl <sub>2</sub> x 2H <sub>2</sub> O	Merck, Darmstadt, Germany
3-Morpholinopropane-1-sulfonic acid (MOPS)	AppliChem, Darmstadt, Germany (Illinois Tool Works, Glenview, Illinois, USA)
N <sub>2</sub> (liquid)	Linde, Munich, Germany
N,N-Dimethylformamide	Merck, Darmstadt, Germany
NaCl	Merck, Darmstadt, Germany
NaClO	Carl Roth, Karlsruhe, Germany
NaFe-EDTA	Sigma-Aldrich, St. Louis, Missouri, USA
Na <sub>2</sub> HPO <sub>4</sub> x H <sub>2</sub> O	Merck, Darmstadt, Germany
Na <sub>2</sub> MoO <sub>4</sub> x 2H <sub>2</sub> O	Sigma-Aldrich, St. Louis, Missouri, USA
NaOH	Carl Roth, Karlsruhe, Germany
NaO-Ac (Sodium acetate)	Merck, Darmstadt, Germany
NiCl <sub>2</sub> x 6H <sub>2</sub> O	Carl Roth, Karlsruhe, Germany
Phytoagar	Duchefa Biochemie, Haarlem, Netherlands
Polyethylene glycol (PEG)	SERVA Electrophoresis, Heidelberg, Germany
RbCl	Merck, Darmstadt, Germany
RNase-free water (DEPC-treated)	Carl Roth, Karlsruhe, Germany
Salmon-Sperm carrier DNA	Invitrogen, Carlsbad, California, USA (Thermo Fisher Scientific, Waltham, Massachusetts, USA)
SD-(Agar)-base	TaKaRa Bio, Mountain View, USA
SD-supplements	TaKaRa Bio, Mountain View, USA
Sodiumdodecylsulfate (SDS)	SERVA Electrophoresis, Heidelberg, Germany
Tris(hydroxymethyl)aminomethane (Tris)	MP Biomedicals, Santa Ana, California, USA
Tryptone	Oxoid, Wesel, Germany (Thermo Fisher Scientific, Waltham, Massachusetts, USA)
Tween20	Merck, Darmstadt, Germany
Yeast extract	Oxoid, Wesel, Germany (Thermo Fisher Scientific, Waltham, Massachusetts, USA)
X-α-Gal	TaKaRa Bio, Mountain View, USA
X-Gal (5-bromo-4-chloro-3-indolyl-β-D-galactopyranoside)	Carl Roth, Karlsruhe, Germany
X-Gluc (5-Bromo-4-chloro-1H-indol-3-yl β-D-glucopyranosiduronic acid)	PEQLAB Biotechnologie, Erlangen, Germany
ZnSO <sub>4</sub> x 7H <sub>2</sub> O	Merck, Darmstadt, Germany

Table 6 – Enzymes used

Enzyme	Manufacturer
BP-Clonase	Thermo Fisher Scientific, Waltham, Massachusetts, USA
<i>Apa</i> I	Thermo Fisher Scientific, Waltham, Massachusetts, USA
<i>Bpi</i> I	Thermo Fisher Scientific, Waltham, Massachusetts, USA
<i>Bsa</i> I	Thermo Fisher Scientific, Waltham, Massachusetts, USA
<i>Eco</i> RI	Thermo Fisher Scientific, Waltham, Massachusetts, USA
<i>Hind</i> III	Thermo Fisher Scientific, Waltham, Massachusetts, USA
Klenow-Fragment (10 U/ $\mu$ l) (incl. buffer)	Thermo Fisher Scientific, Waltham, Massachusetts, USA
LR-Clonase	Thermo Fisher Scientific, Waltham, Massachusetts, USA
Phire Hot-Start Polymerase (incl. buffer)	Thermo Fisher Scientific, Waltham, Massachusetts, USA
Phusion HF Polymerase (incl. buffer)	Thermo Fisher Scientific, Waltham, Massachusetts, USA
<i>Pst</i> I	Thermo Fisher Scientific, Waltham, Massachusetts, USA
RNase A	SERVA Electrophoresis, Heidelberg, Germany
RNase-free DNase	Thermo Fisher Scientific, Waltham, Massachusetts, USA
<i>Sac</i> I	Thermo Fisher Scientific, Waltham, Massachusetts, USA
<i>Sal</i> I	Thermo Fisher Scientific, Waltham, Massachusetts, USA
Shrimp Alkaline Phosphatase (1 U/ $\mu$ l) (incl. buffer)	Invitrogen, Carlsbad, California, USA (Thermo Fisher Scientific, Waltham, Massachusetts, USA)
<i>Sma</i> I	Thermo Fisher Scientific, Waltham, Massachusetts, USA
<i>Spe</i> I	Thermo Fisher Scientific, Waltham, Massachusetts, USA
<i>Sph</i> I	Thermo Fisher Scientific, Waltham, Massachusetts, USA
SuperscriptIII reverse transcriptase	Invitrogen, Carlsbad, California, USA (Thermo Fisher Scientific, Waltham, Massachusetts, USA)
T4-Ligase (1 U/ $\mu$ l)	Thermo Fisher Scientific, Waltham, Massachusetts, USA
<i>Xba</i> I	Thermo Fisher Scientific, Waltham, Massachusetts, USA
<i>Xho</i> I	Thermo Fisher Scientific, Waltham, Massachusetts, USA
<i>Xma</i> I	Thermo Fisher Scientific, Waltham, Massachusetts, USA

Table 7 – Commercial kits used

Kit	Manufacturer
Bioanalyzer RNA 6000 Nano Kit	Agilent Technologies, Santa Clara, USA
DNaseI (on column digestion)	QIAGEN, Venlo, Netherlands
DNeasy Plant Mini Kit	QIAGEN, Venlo, Netherlands
Matchmaker Gold yeast Two Hybrid System	TaKaRa Bio, Mountain View, USA
Matchmaker Insert Check PCR Mix	TaKaRa Bio, Mountain View, USA
Nucleospin DNA purification Kit	Macherey-Nagel, Düren, Germany
Peggold Plasmid MiniPrep Kit	Peqlab Biotechnology, Erlangen, Germany
Phire Plant Direct PCR Kit	Thermo Fisher Scientific, Waltham, Massachusetts, USA
QIAPrep Spin Miniprep Kit	QIAGEN, Venlo, Netherlands
RNeasy Plant Mini Kit	QIAGEN, Venlo, Netherlands
SensiFAST SYBR No-ROX One-Step Kit	Bioline, Luckenwalde, Germany
Superscript III reverse transcription Kit	Invitrogen, Carlsbad, California, USA (Thermo Fisher Scientific, Waltham, Massachusetts, USA)

Table 8 – Materials used

Material	Manufacturer
1.5 ml Reaction tubes	Sarstedt, Nümbrecht, Germany
1.5/2 ml Reaction tubes (safe lock)	Eppendorf, Hamburg, Germany
1.5 ml Reaction tubes (RNase-free)	Carl Roth, Karlsruhe, Germany
5 ml Pipette tips	Eppendorf, Hamburg, Germany
6/96-well plates	Greiner, Kremsmünster, Austria
13 ml tubes (round base with push cap)	Greiner, Kremsmünster, Austria
Centrifugation tubes (15/50 ml)	Greiner, Kremsmünster, Austria
Cover slips	Carl Roth, Karlsruhe, Germany
Cuvettes	Sarstedt, Nümbrecht, Germany
Electroporation cuvettes	PEQLAB Biotechnologie, Erlangen, Germany
FastPrep-Tubes with 1.4 mm ceramic spheres	MP Biomedicals, Santa Ana, Canada
Filters	Sarstedt, Nümbrecht, Germany
Glass Beakers	Schott, Mainz, Germany
Glass Bottles	Schott, Mainz, Germany
Glass Bottles (Simax)	Kavalierglass, Křižová, Czech Republic
Glass Pipettes	Brand, Wertheim/Main, Germany
Gloves	Ansell, Richmond, Australia
Gloves (ethidium bromide)	StarLab, Hamburg, Germany
Insulin syringes	BD Medical, Franklin Lakes, New Jersey, USA
Laboratory Film (Parafilm)	Bemis NA, Neenah, Wisconsin, USA
Microscope slides	Thermo Fisher Scientific, Waltham, Massachusetts, USA
Pasteur pipettes (glass)	Brand, Wertheim/Main, Germany
Pasteur pipettes (one way)	Carl Roth, Karlsruhe, Germany
PCR-tubes	Sarstedt, Nümbrecht, Germany
Petri dish (12 cm)	Greiner, Kremsmünster, Austria
Petri dish (small)	Greiner, Kremsmünster, Austria
Pipette tips	StarLab, Hamburg, Germany
Pipette tips (with filter)	StarLab, Hamburg, Germany
Razor blades	ScienceServices, Munich, Germany
RT-PCR Plates	BioRad, Hercules, California, USA
Scalpels	B. Braun, Melsungen, Germany
Seramis	Seramis, Mogendorf, Germany
Serological pipettes	Carl Roth, Karlsruhe, Germany
Syringes	B. Braun, Melsungen, Germany
Wipes	Kimberly-Clark, Irving, Texas, USA

Table 9 – Machines and devices

Device	Manufacturer
Agarose gel documentation "UV-Solo"	Biometra, Göttingen, Germany
Autoclave "WX150"	Systec, Linden, Germany
Binocular microscope "EL6000"	Leica, Wetzlar, Germany
Bioanalyzer 2100	Agilent Technologies, Santa Clara, USA
Camera (microscope mount) "XC50"	Olympus, Tokyo, Japan
Centrifuge "5810R" with rotors "HL030" and "A-4-62"	Eppendorf, Hamburg, Germany
Cleanbench "HERASafe K518"	Thermo Fisher Scientific, Waltham, Massachusetts, USA
Confocal Microscope "TCS SP8 MP"	Leica, Wetzlar, Germany
Electroporator "Cellject Uno"	Thermo Fisher Scientific, Waltham, Massachusetts, USA
Heating Block "Thriller"	Peqlab, Erlangen, Germany
Heat Sterilizer "T 6420"	Thermo Fisher Scientific, Waltham, Massachusetts, USA
Homogenizer "FastPrep-24"	MP Biomedicals, Santa Ana, Canada
Incubator "B6"	Thermo Fisher Scientific, Waltham, Massachusetts, USA
Incubator "B20"	Thermo Fisher Scientific, Waltham, Massachusetts, USA
Light (for microscopy) KL200	Leica, Wetzlar, Germany
LMPC "Axio Observer Z1"	Carl Zeiss, Oberkochen, Germany

Microscope “BH 2”	Olympus, Tokyo, Japan
Micropipettes “Research Plus”	Eppendorf, Hamburg, Germany
Millipore arium 611	Sartorius, Göttingen, Germany
Nanodrop 1000	Thermo Fisher Scientific, Waltham, Massachusetts, USA
pH-Meter “pH 7110”	Inolab, Mexico City, Mexico
Photometer “BioPhotometer plus”	Eppendorf, Hamburg, Germany
Phytochamber “JC-ESC 300”	Johnson Controls, Milwaukee, Wisconsin, USA
Power supply “Consort EV2310”	Carl Roth, Karlsruhe, Germany
Scales “Extend ED22025-0CE”	Sartorius, Göttingen, Germany
Scales “Extend ED1245”	Sartorius, Göttingen, Germany
Shaker “Gyrotory G2	New Brunswick Scientific, Edison, New Jersey, USA
Tabletop Centrifuge “5415 D”	Eppendorf, Hamburg, Germany
Thermal Cycler “Mastercycler pro S”	Eppendorf, Hamburg, Germany
Thermal Cycler (qPCR) “Mastercycler realplex”	Eppendorf, Hamburg, Germany
Vent “TA 1200”	Bense, Hardegsen, Germany
Vortex “M53 basic”	IKA, Staufen, Germany
Water bath “1002, 1003”	GFL, Burgwedel, Germany

Table 10 – Software used

Name	Developer/Reference
Adobe Photoshop CS4 (Version 11.0)	Adobe Systems, 1990-2008
AnalySIS getIT 5.0	Olympus Soft Imaging Solutions
AxioVision 4.9.1	Carl Zeiss Microvision, 2003-2008
Citavi 6	Swiss Academic Software, 2001-2022
CLC Main Workbench 8.1.3	CLC bio (QIAGEN), 2008-2013
Inkscape 1.1.2	Inkscape Development Team, 2004-2021
Integrative Genomics Viewer 2.12.2	Robinson <i>et. al</i> (2011)
Fiji (ImageJ)	Schindelin <i>et. al</i> (2012)
Leica Application Suite X 3.7.1	Leica Microsystems, 2019
<i>Medicago truncatula</i> Gene Expression Atlas V3	Benedito <i>et. al</i> , (2008)
<i>Medicago truncatula</i> Genome Database v4.0	Tang <i>et. al</i> (2014)
<i>Medicago truncatula</i> Genome Database v5.0	Pecrix <i>et. al</i> (2018)
Microsoft Office 2016	Microsoft, 2016
MtSSPdb	Boschiero <i>et. al</i> (2020)
Nanodrop 2000	Thermo Fisher Scientific, 2009-2014
PANTHER DB 16.0	Mi <i>et. al</i> (2013)
Pathview Web	Luo <i>et. al</i> (2017)
Primer3web version 4.0	Untergasser <i>et. al</i> (2012)
Realplex 2.2	Eppendorf, 2005-2008
Venny 1.11	Inkscape Project, 2003-2022

## 3.4 Nucleic acid extraction from plants and quantification

### 3.4.1 Extraction of genomic DNA from *M. truncatula*

Genomic DNA of *M. truncatula* was regularly required as a template for PCR-amplifications. To isolate it, five young leaves or approx. 100 mg of plant material were transferred into a bead-filled microtube (Lysing Matrix D with 1.4 mm beads, MP Biomedical, see Table 8). The leaves were subsequently treated with five to eight 20 s bursts of rapid shaking (6 m/s) in a FastPrep24 bead-beating machine (MP Biomedical, see Table 9) to fully rupture the material. Column-based DNA-purification was then performed with the QIAGEN DNeasy Plant Kit (Table 7) according to manufacturer instructions. After final elution (typically 30-40  $\mu$ l), DNA was visualized on a 1% Agarose gel and quantified via photometric Nanodrop measurement (see 3.4.3).

### 3.4.2 Extraction of RNA from *M. truncatula*

To obtain RNA-samples for further applications such as cDNA-production and sqRT-PCR, root-, or other material from *M. truncatula* plants was flash-frozen in liquid nitrogen ( $\text{LN}_2$ ). Then,  $\sim$ 150 mg of tissue material was transferred into bead-filled microtube (Lysing Matrix D with 1.4 mm beads, MP Biomedical, see Table 8) along with 500  $\mu$ l of buffer RLT containing 5  $\mu$ l of  $\beta$ -mercaptoethanol. The samples were then subjected to six 30 s bursts of rapid shaking (6 m/s) in a FastPrep24 bead-beating machine (MP Biomedical, see Table 9). Afterwards, tubes were spun down to reduce foaming in order to be able to recover as much of the resulting suspension as possible. The material was transferred onto a Qias shredder-column with collecting tube as part of the QIAGEN RNeasy Plant Kit (Table 7) and centrifuged at 16,100  $\times g$  for 2 min. Further steps were performed in accordance with the provided manual. In between washing steps for the bound RNA, an on-column DNase-digestion was performed. To that end, the RNeasy column was equilibrated with 80  $\mu$ l of DNase-mix, consisting of 10  $\mu$ l of DNase in 70  $\mu$ l of buffer RDD (RNase free DNase Set, QIAGEN, Table 6) and incubated for 15 min at RT.

The final RNA-sample obtained was checked on a 1% agarose gel for integrity using characteristic 18s and 28s ribosomal RNA bands alongside Nanodrop measurements (3.4.3) for quantification. Samples could additionally be examined via capillary electrophoresis using the Bioanalyzer (Agilent Technologies, Table 9).

To ensure no DNA was left in the isolate that would falsify expression data obtained, another DNase-digestion was performed (DNaseI, QIAGEN, Table 6). Each 1  $\mu$ g of RNA were mixed with 1  $\mu$ l of 10x reaction buffer and 1  $\mu$ l of DNaseI (filled up to 10  $\mu$ l with RNase-free water) and incubated at 37°C for 30 min. To terminate the reaction, 1  $\mu$ l of EDTA (50 mM) was added before incubating another 10 min at 65°C. Afterwards, RNA samples were checked again on agarose gels and via the Nanodrop (3.4.3).

### 3.4.3 Quantification of nucleic acids via the Nanodrop spectrophotometer

To determine the concentration and relative purity of DNA- or RNA-extractions, photometric measurements were performed via the Nanodrop spectrophotometer (Thermo Fisher Scientific, Table 9): Nucleic acids have a characteristic absorption maximum at a wavelength of 260 nm. By measuring the absorbance of a nucleic-acid containing solution over a defined optical path length the concentration in ng/ $\mu$ l can be estimated. Additionally, by comparing absorbance to characteristic maxima of other substances, relative purity can be determined as well: 280 nm absorbance for proteins and 230 nm for phenolic compounds and chaotropic salts, where ratios 260/230 and 260/280 of  $\sim$ 2 are considered relatively pure.

### 3.4.4 Estimation of RNA quality via Bioanalyzer capillary electrophoresis

RNA-samples for RNASeq were checked via capillary electrophoresis on the Bioanalyzer (2100, Agilent Technologies, Table 9). Samples were prepared as to the instructions of the Bioanalyzer RNA 6000 Nano Kit (Table 7). Based on the detection of the characteristic 28s and 18s ribosomal RNAs present in relation to a predefined marker, an RNA integrity number (RIN) between 1 and 10 is calculated (higher is better) based on the estimated degradation of the sample. Only samples with a RIN  $\geq$ 8 were used for the RNASeq-approach.

## 3.5 PCR-based methods

### 3.5.1 Standard PCR protocol

Polymerase Chain Reactions (PCRs) were used to amplify specific DNA-fragments from plasmids or genomic DNA. When the amplicons were to be used for further cloning steps, the Phusion HF polymerase (Thermo Fisher Scientific, Table 6) with proofreading activity was used in order to avoid induced mutations due to replications errors.

Table 11 – Standard PCR setup

Component	Amount	Final concentration
5x Phusion HF buffer	10 $\mu$ l	1x
10 mM dNTP-mix	1 $\mu$ l	200 $\mu$ M each
10 $\mu$ M forward-Primer	2.5 $\mu$ l	0.5 $\mu$ M
10 $\mu$ M reverse-Primer	2.5 $\mu$ l	0.5 $\mu$ M
Genomic DNA	1 $\mu$ l	2 ng/ $\mu$ l
Phusion HF polymerase	0.5 $\mu$ l	0.02 U/ $\mu$ l
Ultrapure water	32.5 $\mu$ l	-
Total	50 $\mu$ l	

Component	Amount	Final concentration
5x Phusion HF buffer	10 µl	1x
10 mM dNTP-mix	1 µl	200 µM each
10 µM forward-Primer	2.5 µl	0.5 µM
10 µM reverse-Primer	2.5 µl	0.5 µM
Template plasmid	1 µl	20 pg/µl
Phusion HF polymerase	0.5 µl	0.02 U/µl
Ultrapure water	32.5 µl	-
<b>Total</b>	<b>50 µl</b>	

Cycle step	Temperature	Time	Cycles
Initial denaturation	98°C	3 min	1
Denaturation	98°C	10 s	
Annealing	XX°C*	30 s	35
Extension	72°C	30 s per kb	
Final extension	72°C	5 min	1
Hold	4°C	∞	1

\*Dependent on the specific primers used

### 3.5.2 Reverse Transcriptase (RT)-PCR

In order to obtain the complete CDS-region excluding introns from genes with intron-exon structure, cDNA was generated from mRNA isolated from mycorrhized *M. truncatula* roots via the SuperscriptIII (Thermo Fisher Scientific, Table 6) first-strand cDNA-synthesis protocol using oligo-dT primers. The cDNA was then used in a 1:10 dilution as the template in a subsequent PCR:

Table 12 – RT-PCR setup

Component	Amount	Final concentration
5x Phusion HF buffer	10 µl	1x
10 mM dNTP-mix	1 µl	200 µM each
10 µM forward-Primer	2.5 µl	0.5 µM
10 µM reverse-Primer	2.5 µl	0.5 µM
Template cDNA	1 µl	2 ng/µl
Phusion HF polymerase	0.5 µl	0.02 U/µl
Ultrapure water	32.5 µl	-
<b>Total</b>	<b>50 µl</b>	

Cycle step	Temperature	Time	Cycles
Initial denaturation	98°C	2 min	1
Denaturation	98°C	10 s	
Annealing	XX°C	20 s	35
Extension	72°C	30 s per kb	
Final Extension	72°C	5 min	1
Hold	4°C	∞	1



### 3.5.3 Detection of mutants via direct PCR screening

In order to detect *Tnt1*-insertions in certain regions of interest, the Phire Plant Direct PCR Kit (Thermo Fisher Scientific, Table 7) was used. For detecting full transgenic plants, small discs were punched into the leaves via a 1000  $\mu$ l pipette tip and subsequently transferred into 20  $\mu$ l of the Dilution Buffer included with the kit. The material was then ruptured and treated in a 70°C water bath for 3 min. 1  $\mu$ l of the supernatant was used in the 20  $\mu$ l PCR reaction volume.

Table 13 – Direct PCR setup

Component	Amount	Final concentration
2x Phire Plant PCR buffer	10 $\mu$ l	1x
10 $\mu$ M forward primer	1 $\mu$ l	0.5 $\mu$ M
10 $\mu$ M reverse primer	1 $\mu$ l	0.5 $\mu$ M
(10 $\mu$ M additional Primer)	1 $\mu$ l	0.5 $\mu$ M
Plant extract	1 $\mu$ l	-
Phire Hot-start polymerase	0.4 $\mu$ l	-
Ultrapure water	Ad 20 $\mu$ l	-

Cycle step	Temperature	Time	Cycles
Initial denaturation	98°C	5 min	1
Denaturation	98°C	5 s	
Annealing	XX°C	10 s	40
Extension	72°C	20 s per kb	
Final extension	72°C	1 min	1
Hold	4°C	$\infty$	1

### 3.5.4 Semi-quantitative real-time RT-PCR

In order to quantify mRNA amounts and thereby make assertions about the expression of individual genes, the method of semi-quantitative real-time RT-PCR was employed. More specifically, a one-step protocol as part of the SensiFAST™ SYBR® No-ROX Kit (Bioline, Table 7) was used. Here, the present mRNA is first transcribed into copyDNA by reverse transcriptase in the reaction volume as the initial step. This cDNA then serves as a template in the subsequent PCR-amplification using primers specific to a fragment of 150 – 250 bp of the respective target gene. Also present in the reaction volume is the fluorophore SYBR-Green able to specifically bind to double stranded DNA. By optically detecting this fluorescent signal after each amplification cycle, the increase of PCR-product can be observed. Based on the number of cycles at which the signal reaches a “threshold” above background fluorescence (Cycle threshold, Ct), the initial transcript amount can be determined based on the assumption that the amount of dsDNA doubles during each cycle. However, RNA-concentrations can vary between

individual samples, which has to be excluded as a potential influence. To do this, all other genes measured are related to the measurements of a constitutively expressed gene (Translation elongation factor  $\alpha$ , *MtTef $\alpha$*  during this work) by calculating the  $\Delta Ct$  ( $2^{-\Delta Ct} = 2^{-(Ct^{Gene\ of\ interest} - Ct^{Tef\alpha})}$ ). As such, the expression is determined relative to that of the *MtTef $\alpha$*  gene, not the absolute transcript amount. In addition to the sample volume indicated below, -RT controls were run, lacking reverse transcriptase to make exclude the possibility of genomic DNA-contamination altering the quantification results. Additionally, after the finished PCR run, a melting curve analysis was performed by default during this protocol. To that end, samples were continually heated from 40-95°C while constantly monitoring fluorescence intensity. At a temperature specific to the relative PCR amplicon, the dsDNA is denatured, which can be observed as a rapid reduction in fluorescence intensity. This was done to ensure only the specific target fragment was produced, as additional undesired PCR products would be detectable as aberrant or additional peaks in the melting curve's first derivative. After completing the reactions in a Realplex thermal cycler (Eppendorf, see Table 9), computational analyses were performed via the supplied Realplex software (see Table 10).

Table 14 – sqRT-PCR setup

Component	Amount	Final concentration
2x SensiFast OneStep SYBR	10 $\mu$ l	1x
Primer-mix (2.5 $\mu$ M each)	4 $\mu$ l	0.5 $\mu$ M
RNA (1 ng/ $\mu$ l)	5 $\mu$ l	0.25 ng/ $\mu$ l
RNase inhibitor	0.4 $\mu$ l	0.5 $\mu$ M
Reverse transcriptase	0.2 $\mu$ l	-
RNase free water	0.4 $\mu$ l	-
Total	20 $\mu$ l	

Cycle step	Temperature	Time	Cycles
Reverse transcription	45°C	10 min	1
Initial denaturation	95°C	5 min	1
Denaturation	95°C	5 s	
Annealing	55°C	10 s	40
Extension	72°C	8 s	
Denaturation	95°C	15 s	1
Melting curve analysis	40-95°C	1°C/15 s	1
Hold	10°C	$\infty$	1

### 3.5.5 Purification of PCR- and Klenow-reaction volumes

Following a successful PCR-amplification, the reaction volume was loaded and run on a preparative agarose gel to cut out only the target fragment.

The agarose gel fragment with the target was subsequently used in the Nucleospin DNA purification kit (Macherey-Nagel, Table 7). Here, 100 mg of 1%-agarose were mixed with 200 µl of guanidinium thiocyanate containing buffer NTI (more with denser agarose gels as per manufacturer instructions) and incubated at 50°C while shaking until the gel had completely dissolved. The denatured DNA was then bound to a silica column via centrifugation. Further steps were performed as per manufacturer instructions.

The same general protocol was used for clean-up of Klenow or Golden-Gate-reactions: for every 100 µl of the appropriate reaction volume, 200 µl of buffer NTI were added. The mixture was then transferred to the silica column directly.

## 3.6 Bacterial cultures

### 3.6.1 Growth conditions for bacterial cultures

*Escherichia coli* strains used for cloning approaches were generally grown overnight at 37°C either on solid LB/PA media containing an appropriate antibiotic for selection or as LB-based liquid cultures.

Soil bacteria such as *Rhizobium radiobacter* or *Rhizobium rhizogenes* used in this work were grown on TY/LB-A-based solid media for 2 d at 30°C. Liquid cultures were grown for approximately 24 h.

Table 15 – Strains of bacteria and corresponding media

Bacteria	Media	Antibiotics	Plasmids
<i>E. coli</i>	LB	Kan50, Spec50, Chloro15	pK18, pRedRoot, pDONR221, pMWR, pK7GW, pSPYCE/pSPYNE, p9RFP-D35s-Expr, pGBKT7
<i>E. coli</i>	PA	Amp100	pGUS-int, pGADT7
<i>R. rhizogenes</i>	TY	Strep600/Spec100, Strep600/Kan100	pRedRoot, pK7GW, p9RFP-D35s-Expr
<i>R. radiobacter</i>	LB-A	Rif100/Genta15/Kan50	pSPYCE/pSPYNE

Table 16 – Standard media for bacterial cultures

Medium	Component	Amount
LB-medium (Luria-Bertani Broth, Evans, 1990)	Tryptone	10 g/l
	Yeast extract	5 g/l
	NaCl	5 g/l
• Adjusted to pH 7.4		
TY-medium (Beringer, 1974)	Tryptone	5 g/l
	Yeast extract	3 g/l
	CaCl <sub>2</sub> x 2H <sub>2</sub> O	0.7g/l
• Adjusted to pH 7.2		
PA-medium	Antibiotic Medium No. 3 (Oxoid)	17.5 g/l
LB-A-medium	Tryptone	10 g/l
	Yeast extract	5 g/l
	NaCl	10 g/l
• Adjusted to pH 7.2		

Table 17 – Antibiotic solutions

Antibiotic	Stock concentration	Solvent	Final concentration
Ampicillin (Amp)	100 mg/ml	Ultrapure water	100 µg/ml
Chloramphenicol (Chloro)	15 mg/ml	Ethanol	15 µg/ml
Gentamycin (Genta)	15 mg/ml	Ultrapure water	15 µg/ml
Kanamycin (Kan)	50 mg/ml	Ultrapure water	50/100 µg/ml
Nalidixic acid (Ndx)	25 mg/ml	Ultrapure water	25 µg/ml
Rifampicin (Rif)	100 mg/ml	DMSO	100 µg/ml
Spectinomycin (Spec)	50 mg/ml	Ultrapure water	50/100 µg/ml
Streptomycin (Strep)	300 mg/ml	Ultrapure water	600 µl/ml

### 3.6.2 Production of chemically competent *E. coli* for heat-shock transformation

*E. coli* DH5α *mcr'* were treated with Rubidium Chloride (RbCl) to produce cells capable of taking up plasmid DNA: 10 ml of LB medium (see Table 16) containing Nalidixic acid (Ndx, 25 µg/ml) were inoculated with 10 µl of Gly-stock and incubated over night at 37°C while shaking. 2 ml of the overnight culture were then used to inoculate 200 ml of LB medium which was incubated at 37°C while shaking until reaching an OD<sub>600</sub> of 0.6-0.8. The total volume was distributed to 50 ml centrifuge tubes before pelleting the cells at 805 xg for 15 min at 4°C. The supernatant was removed and the cells were subsequently resuspended in 30 ml of Tbf1-buffer (see Table 4) while on ice. After centrifugation at the same conditions again, Tbf1-buffer was removed and the cells were carefully resuspended on ice in 4 ml of pre-cooled Tbf2-buffer. The resulting cell suspension was frozen at -80°C in aliquots of 100 µl. Chemically competent *E. coli* were kept under these conditions until use.

### 3.6.3 Heat-shock transformation of chemically competent *E. coli*

Previously treated competent *E. coli* DH5 $\alpha$  mcr' were thawed out on ice. 50  $\mu$ l of TCM-buffer (Table 4) and 10  $\mu$ l ligated plasmid or 1-2  $\mu$ l of diluted purified plasmid were then added. After carefully mixing the cells were then incubated on ice for 30 min before performing the heat-shock for 1:15 min in a 42°C water bath. Immediately afterwards, the bacteria were cooled on ice and rested for 5 min. Then, 1 ml of liquid LB-medium was added and cells were grown shaking at 37°C for 1 h. Finally, dilution series were plated on LB/PA-media containing the appropriate antibiotics. Transformed colonies were generally observed following incubation overnight at 37°C.

### 3.6.4 Electroporation for transformation of *Rhizobium*-strains

*Rhizobium radiobacter* (old: *Agrobacterium tumefaciens*) and *R. rhizogenes* strains were transformed using electroporation. To prepare for this procedure, cells of empty strains were freshly grown in an overnight 10 ml liquid culture at 30°C while shaking. Then, a 200 ml main culture was inoculated with 2 ml of the overnight culture and grown shaking at 200 rpm at 30°C up to an OD<sub>600</sub> of 0.6 – 0.8. The entire culture was subsequently split into four 50 ml centrifuge tubes and spun down at 805 xg for 10 min at 4°C. The supernatant was discarded and the pellets resuspended in 50 ml of a pre-chilled 10% solution of glycerol in water. These washing steps were repeated three times to remove any electrolytes present in the solution. Finally, the cells were resuspended in 4x4 ml 10% glycerol, aliquoted into 1.5 ml tubes and flash-frozen in IN<sub>2</sub>. The cells were stored at -80°C until use.

To perform the transformation, the prepared aliquots were thawed on ice before adding 1-3  $\mu$ l of pure plasmid DNA (depending on the concentration as estimated via Nanodrop-measurements, see 3.4.2). The cell suspension was then transferred into a pre-chilled electroporation cuvette. The subsequent treatment with a pulse of 1,800 V induced lesions into the bacterial cell wall for plasmid DNA to enter. Immediately following the electric shock, 1 ml of liquid medium (TY- or LB-A, see Table 16) was added to the cuvette. The entire suspension was then transferred to a 1.5 ml tube for subsequent shaking incubation at 30°C. Afterwards, a serial dilution of the cells was spread on appropriate solid media and grown for 2 d at 30°C.

### 3.6.5 Long-term storage of bacterial strains using glycerol

For long-term storage of any bacterial strains produced, a confluent plate was grown overnight at 37°C for *E. coli* (slower growing *Rhizobia* were grown for 2 d at 30°C). The bacteria were then scraped off and resuspended in 500 µl of LB/TY medium. To that mixture 600 µl of sterile 87% Glycerol were added before vortexing to mix. The resulting cell suspension was then stored at -20°C.

### 3.6.6 Quick plasmid-isolation for testing purposes

Manual HB-Lysis (Becker *et. al*, 1993) was used to quickly obtain non-pure DNA to check the uptake of the desired plasmid by competent *E. coli*. For that purpose, *E. coli* freshly grown on appropriate solid medium were scraped off using a glass pipette and resuspended in 200 µl P1-buffer (buffers listed in Table 4). Then, 200 µl of P2-buffer containing NaOH and SDS were added to lyse the cells. Following inversion to mix, 200 µl of P3-buffer were added before inverting again to neutralize the previously alkaline conditions. Cell debris was subsequently pelleted via centrifugation for 10 min at 16,100 xg. The resulting supernatant was transferred into a new 1.5 ml tube containing 500 µl of Isopropyl-alcohol to precipitate the DNA, which was in turn pelleted via centrifugation at 16,100 xg for 20 min. The supernatant was removed using a pipette before washing the pellet with 500 µl of Ethanol. Following centrifugation at 16,100 xg for 2 min, the ethanol was removed. The pellet was then dried completely before recovering the DNA by dissolving in 40 µl of TE-buffer.

This procedure results in a high amount of total isolated DNA. Since, however, this protocol does not employ a silica-column to specifically enrich plasmid DNA, genomic DNA is still present. Additionally, because of the missing digestion with RNase, large amounts of RNA also contaminate the isolate. Therefore, the DNA recovered via this method was only used for testing purposes.

### 3.6.7 Plasmid purification from *E. coli*

Silica-column-based isolations of plasmid DNA were performed to obtain pure samples for further cloning-, sequencing- and transformation procedures. Fresh *E. coli* strains were prepared for plasmid isolation via cultivation over night at 37°C on solid medium containing the appropriate antibiotic. The plasmid isolation was performed using the kits “QIAPrep Spin Mini” or “PeqGold” (see Table 7 for both) using approximately 1/3 of the confluent bacteria on the plate as material. All subsequent steps were performed as per the manufacturer’s manual.

Resulting plasmid DNA was observed via agarose gelelectrophoresis and quantified using nanodrop-measurements. In case of newly constructed plasmids, inserts were verified via Sanger-sequencing performed by service provider Seqlab-Microsynth (Göttingen, Germany) as per their instructions.

### 3.6.8 Plasmid isolation from *Rhizobium* strains

For verification purposes of transformed *R. radiobacter* or *R. rhizogenes* strains, plasmids were isolated and checked via sequencing prior to use in plant transformation experiments. To that end, the respective strains were grown overnight in appropriate TY- or LB-A medium (for specifics see Table 16) at 30°C while shaking.

The resulting overnight culture was then transferred to a 50 ml tube and centrifuged at 3,220 xg for 10 min. The supernatant was discarded and bacteria were subsequently resuspended in 2 ml of P1-buffer (Table 4). Then, 2 ml of P2-buffer were added to initiate cell lysis. After mixing by inverting, 2 ml of P3-buffer were quickly added before inverting again. The following centrifugation at 3,220 xg for 10 min pelleted the proteins and cell debris. Afterwards, the supernatant was carefully transferred to a new tube containing 5 ml of isopropyl alcohol. The solution was mixed and then centrifuged at 3,220 xg for 20 min to precipitate the DNA. This pellet was subsequently washed using 2 ml of ethanol and another centrifugation at 3,220 xg for 2 min. The alcohol was fully removed with any residue being left to dry completely. Finally, the pellet was resuspended in buffer P1 of a plasmid purification kit (Table 7) to isolate the plasmid from this crude DNA-extraction. The remainder of the steps performed were identical to the protocol for isolation of pure plasmid DNA (see prior section 3.6.7).

## 3.7 Cloning methods

### 3.7.1 Classical cloning via Type-II restriction endonucleases

TypeII restriction endonucleases are able to cut dsDNA at an enzyme-specific palindromic recognition site. This can lead to fragments with either 3'- or 5'-overhangs ("sticky ends") to facilitate specific and directional cloning of cleaved fragments or blunt ends without any single-stranded overhangs. A typical reaction volume consisted of a variable amount of DNA substrate, 2 µl 10x TA-buffer (self-made, see Table 4) or enzyme-specific buffer if required and 1-2 µl of each enzyme (restriction endonucleases used are listed in Table 6) in a total volume of 20 µl ultrapure water. DNA-digestion reactions were performed for 3 h at the respective enzyme's optimum temperature followed by heat inactivation for 10 min.

In order to facilitate cloning of different inserts into the previously cleaved vectors by preventing religation, phosphate-groups at the 5'-ends were removed using Shrimp Alkaline Phosphatase (SAP, Thermo Fisher Scientific, Table 6). To perform these reactions, varying amounts of linearized plasmid were added to a 1.5 ml tube alongside 1 µl of SAP and 2 µl of 10x SAP buffer in a total volume of 20 µl. Dephosphorylation was performed at 37°C for 15 min for sticky ends or up to 1 h for blunt ends before heat inactivation at 70°C for 15 min.

Following this treatment, the inserts were ligated to the dephosphorylated linear vector. This was done in a reaction volume of 20 µl using 1-3 ml of T4-Ligase enzyme (see Table 6), 2 µl of 10x concentrated Ligation buffer and a ratio insert:vector of approximately 3:1 at varying amounts. The ligation was run over night in a thermos-jug with the initial water temperature adjusted to a temperature between 18°C and 21°C depending on the size of the insert. By placing the jug at 4°C, it was ensured that the temperature would fall over time, facilitating reaction at its respective optimum temperature.

### 3.7.2 Fill-in of single-stranded 5'-overhangs using the Klenow-Fragment

The large fragment of DNA-Polymerase I, also known as the Klenow-Fragment (Table 6), is able to fill in 5'-overhangs on the ends of DNA molecules with its 5'-3'-polymerase-activity. This enables the generation of blunt-end fragments from sticky-end cleavage products. This, in turn, makes it possible to ligate a fragment cut with a blunt-end-restriction-enzyme with otherwise incompatible overhangs.

The reaction following reaction components were mixed in a 1.5 ml tube: A variable amount of DNA, 2 µl of Klenow-Buffer, 1 µl of Klenow-Polymerase, 2 µl of dNTP-mix (10 µM of each, Table 5) in a total volume of 20 µl of ultrapure water. The reaction was incubated at 37°C for 15 min before adding 1 µl of 200 mM EDTA, followed by thermal inactivation at 75°C for 10 min.

### 3.7.3 Golden-Gate cloning via Type-IIs restriction endonucleases

In cases of promoter-*gus* fusions that could not be constructed via subcloning into pGUS-int, the promoter was fused directly to the *gusA*int fragment using Type-IIs restriction enzymes. As opposed to the Type-II restriction endonucleases, Type-IIs enzymes such as *Bsa*I have a separate recognition site at a defined distance from the cleavage site. As such, the overhang created by the restriction can be any four nucleotides. Therefore, these endonucleases allow for directional cloning without restriction residues, as the sticky ends can be part of the target sequence itself while the recognition sites are not included in the final cloning product.



This reaction was done using T4-Ligase as well as the *Bsa*I restriction enzyme (see Table 6) in the same 20 µl reaction volume. By using a thermal cycler to switch between optimal temperatures of the endonuclease and the ligase, overhangs created during the digestion step are quickly ligated with a compatible overhang. If religation occurs, the fragment would be cleaved again during the next cycle. Once ligated correctly, however, the process is irreversible and over time, the assembled product is enriched. The resulting product could be used for further subcloning either directly or amplified in a PCR before proceeding. In the specific case of fusions of promoter-*gus*-fusions, a CAAG-overhang compatible at the 3'-end of the promoter was ligated to a compatible with a GTTC on the 5'-end of a *gusA*int-fragment.

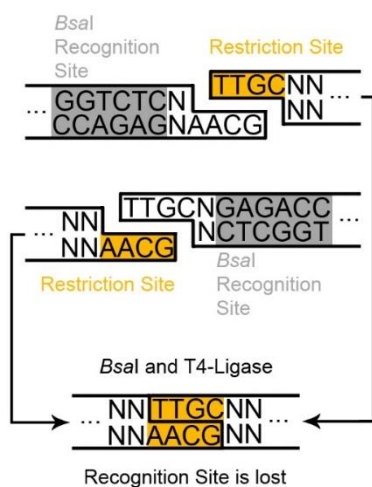


**Figure 8 – Principle of Golden-Gate cloning via Type-II's restriction endonucleases**

Type-II's restriction enzymes such as *Bsa*I have separate recognition- (gray) and restriction-sites (yellow) a defined distance apart. By adding a non-native recognition site to the end of any DNA-fragment, compatible overhangs that are part of the sequence itself can be created. For Golden-Gate-cloning, T4-Ligase is added to the same reaction volume so that compatible overhangs created by restriction can immediately be ligated. Since the recognition site is no longer part of resulting fragment, this reaction is irreversible.

**Table 18 – Golden-gate cloning reaction setup**

Component	Volume
Promoter-fragment	50 ng
<i>gusA</i> int-fragment	50 ng
10x Ligase buffer	2 µl
BSA (1 µg/µl)	2 µl
T4-Ligase	1 µl
<i>Bsa</i> I	0.5 µl
Ultrapure water	Ad 20 µl

Cycle step	Temperature	Time	Cycles
Digestion	37°C	5 min	50
Ligation	20°C	10 min	
Final Ligation	20°C	1 h	1
Hold	4°C	∞	1

### 3.7.4 Gateway-cloning

Some plasmids produced in this work such as those based on the pK7GWIWG2- and pMWR-backbones were cloned using the Gateway-system for site-specific recombination. This strategy is based on attachment-sites (*att*-sites) recognized by the λ-Phage recombinase. To use this system for cloning, target fragments were PCR-amplified using primers with added *attB*-sites. These could then be used in

an initial recombination reaction with the attP-sites present in the pDONR™221 (Thermo Fischer Scientific) entry vector (BP-recombination, BP-clonase listed in Table 6). The target fragment now flanked by attL-sites could subsequently be transferred into a destination vector containing attR-sites to finally produce the desired plasmid (LR-recombination, LR-clonase listed in Table 6). These reactions were performed according to the manual provided with the system.

### 3.8 Plant treatment and cultivation

#### 3.8.1 Seed sterilization and germination

To ensure simultaneous germination of seeds, the seed coat (“testa”) needed to be made permeable. This was done chemically using sulphuric acid during the scarification process: isolated *M. truncatula* seeds in a 50 ml tube were immersed in concentrated H<sub>2</sub>SO<sub>4</sub> for 10 – 15 min while moving constantly. Afterwards, the acid was removed completely and the seeds were washed with an excess of sterile water, which was immediately removed to prevent excessive heating. Three more washing steps with sterile water were subsequently done while inverting for 1 min. In order to sterilize the seeds, they were then treated with 2% (w/v) sodium-hypochlorite (NaClO) for 1 – 2 min. Following removal of the NaClO, four 2 min washing steps were performed using sterile water under a laminar flow hood (see Table 9). The seeds were then left to soak in sterile water for 4 h in an illuminated growth cabinet. Following this incubation, the seeds were placed on moist phytoagar (Table 5) and left to germinate in the dark at 4°C for 4 d. This was followed by incubation in the dark at RT for 1 d and finally 4-8 hours at RT in the light. At this stage, the germlings were ready for the induction of transgenic hairy roots and/or potting.

#### 3.8.2 Plant growth conditions

The plants were kept in a growth chamber (JC-ESC 300, Johnson Controls, Table 9) under the following conditions: 16 h of light at 22°C followed by 8 h of dark at 18°C (Further information on the light regime is provided in Hartmann *et. al*, 2019). Relative humidity was kept constant at 60%. Plants were watered and fertilized with ½-strength Hoagland’s solution as necessary.

#### 3.8.3 Induction of transgenic roots

*R. rhizogenes* is able to induce the growth of transgenic roots in a wild-type background. This is accomplished via two distinct plasmids carried by the *R. rhizogenes* Arqua1 strain: A binary plasmid with the target transgenes flanked by a left- and a right-border sequence and a Root-inducing (Ri)

plasmid containing a Transfer-DNA (T-DNA) with genes necessary for the induction of root growth alongside virulence (*vir*) genes. In response to the perception of an injured nearby plant as a target for infection, the *vir* genes are activated by the bacterium. They are responsible for the translocation of any sequences flanked by border-sequences into the plant cell nucleus and the subsequent genomic integration. In the event of successful transformation of a plant cell, the genes on the T-DNA will promote auxin biosynthesis and, in turn, induce the growth of a transgenic root from that initial cell.

In order to utilize this system for the expression of arbitrary genes in roots, a transformed *R. rhizogenes* strain carrying the desired plasmid was freshly grown for 2 d at 30°C on TY-solid medium with the appropriate antibiotics (Table 16). To subsequently prepare for inoculation of germlings, bacteria on the plate were scraped off and resuspended in 6 – 10 ml of PS buffer (Table 4). The cell suspension was then drawn up into a syringe.

Using the syringe, two longitudinal cuts (approximately 5 mm) were made into the thickened hypocotyl of a prepared germling. Additionally, some suspension was injected directly into the lesion. Following this procedure, the plants were potted into multi-pot plates filled with moistened Seramis while leaving the injection site uncovered. Finally, any bacterial suspension remaining after all desired plants were inoculated was added to the injection sites to maximize the potential for successful transformation. Plants were incubated overnight at 18°C in the dark and subsequently transferred to the growth chamber for further cultivation.

#### 3.8.4 Detection and screening of transgenic roots using the *dsRed* reporter

The binary vectors used in this work for the induction of transgenic roots all contain a fluorescent marker gene as part of their T-DNA, such that successfully transformed roots express a tetrameric red fluorescent protein from *Discosoma sp.* (*DsRed*) with an excitation wavelength of 556 nm and an emission wavelength of 583 nm. Visual inspection under a binocular microscope with the appropriate filter set allowed transgenic roots to be visually distinguished. Any roots not visibly transgenic were cut off. Plants without any detectable fluorescence were discarded entirely. This screening was performed both prior to mycorrhization after approximately 4 weeks after inoculation with *R. rhizogenes* and prior to sample collection (freezing/staining).

#### 3.8.5 Mycorrhization by inoculation with *R. irregularis* spores

Mycorrhization of root systems was performed via co-incubation with *Rhizophagus irregularis*: roots of four week old *M. truncatula* plants (usually directly following screening) were placed in pairs in

1 ml spore suspension (4000 spores per ml, Premier Tec, Canada) and incubated for 3-4 h. During this incubation period, the roots were covered to reduce light-exposure. Any non-mycorrhized controls were left covered in moist Seramis in the meantime. Afterwards, the plants were potted in pairs in Seramis moistened with ½ Hoagland’s solution with 75 µM Phosphate (Table 4). Any remaining spores were added to the pots as well.

### 3.8.6 Histochemical detection of β-Glucuronidase activity

To obtain information on gene activity in *M. truncatula* roots, promoter-regions of target genes were fused to a *gusAint* reporter via restriction-based cloning (indicated in Table 19 below). This gene encodes for the *E. coli* enzyme β-glucuronidase, responsible for hydrolysis of β-D-glucuronic-acid residues from mucopolysaccharide-ends. When using X-Gluc (5-bromo-4-chloro-3-indolyl glucuronide) as a substrate, cleavage results in a stable blue precipitate. When performing this histochemical stain in fresh tissue samples, spatiotemporal promoter-activity can be estimated.

To do this, roots systems were screened for transgenicity and quickly immersed in GUS staining buffer (Table 4). Samples were incubated at 37°C for 6 – 24 h depending on the condition and the promoter examined. Note that non-mycorrhized controls were often stained for longer as the genes examined were AM-induced. When visible, but no overly intense staining was achieved, samples were washed three times with sterile water and stored at 4°C until microscopy or further stains.

Table 19 – Cloning and staining procedures for promoter-gus constructs

Promoter	Construct and cloning strategy	Typical staining duration	Maximum staining duration
<i>pMtPalm1_ver1</i>	pRR: <i>pMtPalm1-gus_ver1</i> ; <i>gusAint</i> fusion via <i>HindIII</i> , blunt insertion into pRedroot with Klenow-filled <i>EcoRI/XbaI</i> -sites	8 – 14 h	24 h
<i>pMtPalm1_ver2</i>	pRR: <i>pMtPalm1-gus_ver2</i> ; <i>gusAint</i> fusion via <i>HindIII</i> , blunt insertion into pRedroot with Klenow-filled <i>EcoRI/XbaI</i> -sites	7 – 8 h	14 h
<i>pMtZf1</i>	pRR: <i>pMtZf1-gus</i> ; <i>gusAint</i> fusion via <i>BsaI</i> (Golden-Gate), inserted into pRedroot via <i>XmaI/HindIII</i> -sites	6 – 8 h	24 h
<i>pMtZf2_ver1</i>	pRR: <i>pMtZf2-gus_ver1</i> ; <i>gusAint</i> fusion via <i>BsaI</i> (Golden-Gate), inserted into pRedroot via <i>XmaI/HindIII</i> -sites	14 h	24 h
<i>pMtZf2_ver2</i>	pRR: <i>pMtZf2-gus_ver2</i> ; <i>gusAint</i> fusion via <i>HindIII</i> , blunt insertion pRedroot with Klenow-filled <i>SpeI</i> -sites	8 – 14 h	14 h
<i>pMtZf3</i>	pRR: <i>pMtZf3-gus</i> ; <i>gusAint</i> fusion via <i>HindIII</i> , inserted into pRedroot with Klenow-filled <i>EcoRI/XbaI</i> -sites	6 – 8 h	24 h

### 3.8.7 Staining of fungal structures

For microscopic analyses, AMF structures within the roots needed to be visualized. This was accomplished either using ink or wheat germ agglutinin with (WGA) the capacity to specifically bind chitin in the fungal cell walls conjugated with a fluorophore. For both procedures, roots first had to be made permeable. To that end, root samples were immersed in 10% (w/v) KOH and incubated at 95°C for 3 – 10 min (depending on the total mass of the sample and general condition i.e. previously frozen roots were already subject to some disruption). The samples were then washed three times with sterile water.

For ink staining, the staining solution consisting of 5% black ink (v/v) in 8% acetic acid (v/v) was subsequently added. Roots were then incubated at 95°C for 3 min before performing three washing steps with 0.8% (v/v) acetic acid. Following the final washing step, the root samples were left in the destaining solution for 20 min to remove more excess ink from the plant cells. The fungal hyphae retained the black ink and could now be visualized microscopically. Samples could be stored in sterile water at 4°C if necessary.

For fluorescent WGA staining, prepared root samples were immersed in staining solution consisting of 200 µg of fluorophore-conjugated WGA (Alexa488-/CF-488-WGA, see Table 5) in 10 ml PBS (Table 4). Incubation was performed over-night in the dark. Afterwards, the staining solution was removed and roots were washed three times with sterile water to remove any unbound lectins. The stained roots could then be stored at 4°C or analyzed via fluorescence microscopy.

### 3.8.8 Randomized quantification of intraradical AMF structures via the Gridline Intersection method

To observe any possible quantitative effects on the amount of AM fungus present in roots of plants carrying RNAi- or overexpression-constructs as well as KO-mutations, present hyphae, arbuscules and vesicles were quantified using the Gridline-Intersection method (Giovanetti and Mosse, 1980). Here, stained roots (outlined under 3.8.7) of a sample pool were cut into ~0.5 cm fragments and immersed in Glycerol in a petri dish (Greiner Bio, Table 8) with a grid of 8x8 squares. All root segments intersecting with a horizontal or vertical line were inspected for AMF structures until 300 such root sections were examined. For this purpose, observed structures were categorized as Arb (root sections containing arbuscules, hyphae and no visible vesicles), Arb+Ves (root sections containing arbuscules, hyphae and visible vesicles), Hyp (root sections containing intraradical hyphae and no other structures) and Ves (root sections containing hyphae and visible vesicles and no other structures). These counting procedures were always performed blindly to avoid biases.

### 3.8.9 Arbuscule size measurements

To obtain insights into whether a knockdown or overexpression of target genes has an impact on arbuscule health or integrity, arbuscule sizes were estimated. To do this, random mycorrhized regions of blind root samples were pre-selected. Then, 10 – 20 microscopic images (CLSM or LMPC, see also Table 9) were taken at random from each sample pool and subsequently analyzed with the imaging software Fiji (ImageJ, Table 10) by measuring the longitudinal expansion of any arbuscules present, previously marked with the linear drawing tool. Measurements obtained could then be binned into different size categories to obtain arbuscule size distributions for each sample.

### 3.8.10 Cloning and application of RNAi-based knockdown constructs

To study potential effects that loss of functionality for the respective candidate genes in this work might induce, targeted transcript reductions (“knockdowns”) were performed using RNA-interference or RNAi. This method hijacks a highly conserved gene regulation mechanism of the host plant in which dsRNA-molecules are recognized by Dicer-like enzymes and cleaved into small 21-23 bp fragments. These “short interfering RNAs” or siRNAs are subsequently integrated into a protein-complex called RISC (RNA-induced silencing complex), removing one of the complementary strands in the process. This ssRNA can now bind to complementary mRNAs for inactivation and cleavage. To employ this system for targeting of arbitrary transcripts, dsRNAs of unique regions from the target genes are overexpressed under control of a constitutively active CMV 35s-promoter to be processed by Dicer and integrated into the RISC.

To that end, unique regions of the respective candidate genes *MtPalm1*, *MtZf1*, *MtZf2* and *MtZf3* were identified via BLAST search. These were then amplified from *M. truncatula* A17 genomic DNA using primers with added attB-sites to facilitate recombination into a pDONR221 entry vector (see 3.7.4). From there, two copies of the respective fragment were integrated flanking an intron into the binary RNAi expression vector pK7GW-dsRed via an LR-recombination. With one of the fragments in reverse complementary orientation, the resulting RNA can form a stem-loop-structure *in vivo* that to be processed into the target dsRNA molecule. Two such constructs were created targeting each of the genes of interest to increase the chances of a successful knockdown. As depicted in Figure 9, pK7GW:*MtPalm1*-RNAi-1 contains a fragment of 100 bp starting at position 334 of the CDS, whereas the second construct comprises a 188 bp fragment starting at position 566. *MtZf1*-RNAi1 targets a very small fragment of 44 bp at 484 bp in the CDS, as many regions within the gene are highly conserved. The pK7GW:*MtZf1*-RNAi-2 construct contains a 120 bp fragment in the 3'-UTR of the mRNA. *MtZf2*-RNAi1 uses a 202 bp long unique region starting at position 128 of the second annotated exon of *MtZf2*.

RNAi construct 2 targets a 120 bp region beginning at position 561 of the same Exon 2. *MtZf3* is targeted using RNAi fragments of 247 bp beginning in the 5'-UTR and with a 178 bp fragment starting at position 540 of the CDS.

Analogous to the promoter-*gus* studies, these pK7GW-based binary vectors were transformed into *R. rhizogenes* and could then be used to induce transgenic roots in otherwise wild-type *M. truncatula* plants (illustrated under 3.8.3). Successfully transformed roots could be identified using *dsRed*-expression as a marker (3.8.4). The transgenic root systems were then inoculated with *R. irregularis* spores and grown for 49 dpi (assay 1), 54 dpi (assay 2) or 42 dpi (assay 3). During sample collection, the root systems were split and flash frozen in  $\text{IN}_2$  to facilitate both RNA-isolation and phenotypic analysis. For two additional knockdown trials, three root systems were pooled together into one sample, as with this method more material would remain for microscopy after RNA-isolation. As controls, roots simultaneously mycorrhized expressing a pK7GW-based RNAi-construct targeting a *gus*-gene nonexistent on the *M. truncatula* A17 genome were used. During the first and third trials, the experiment was split into two separate setups with their own control groups while for trial 2, all conditions were compared to the same set of *gus*-controls.

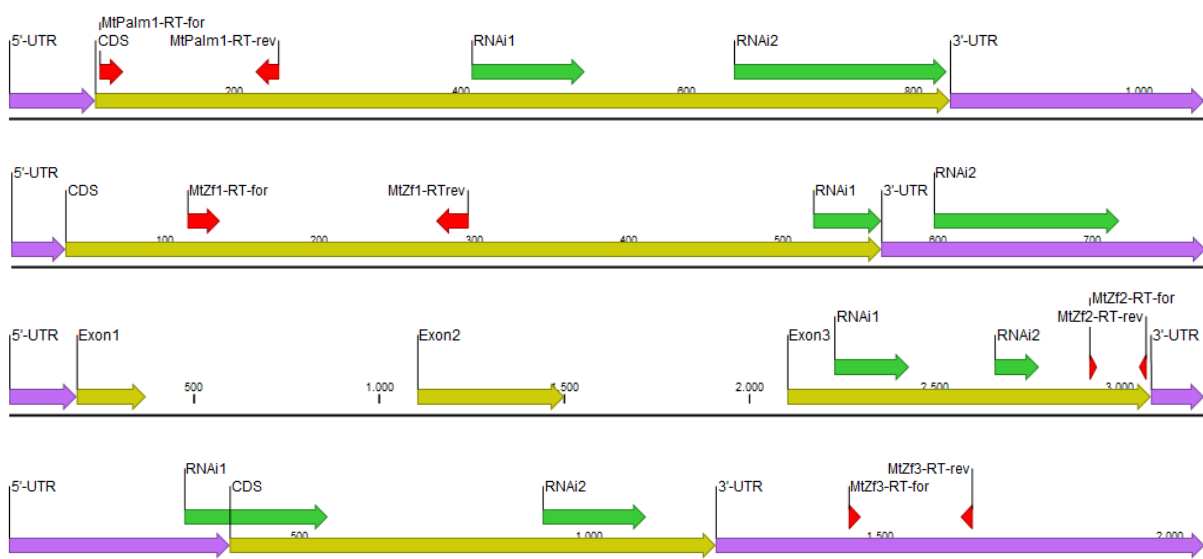


**Figure 9 – Overview of the RNAi-knockdown target regions**

Schematic overview of the target genes *MtPalm1*, *MtZf1*, *MtZf2* and *MtZf3* for the RNAi-based knockdown approach during this work. Two regions were targeted by separate constructs for each gene. These respective target regions are labeled with green arrows. Standard primers used for mRNA quantification during sqRT-PCR are marked in red. Coding regions are marked in yellow, respective untranslated parts of the transcripts are shown in purple.

### 3.8.11 *Tnt1*-lines and complementation

*M. truncatula* R108 mutant plants were obtained from the *Tnt1*-insertion database (Tadege *et. al*, 2008). Putative lines carrying mutations in the target genes *MtPalm1*, *MtZf1* and *MtZf2* were identified via BLAST search on the *M. truncatula* mutant database website (<https://medicagomutant.dasnr.okstate.edu/mutant/index.php>), where flanking sequence tags (FSTs) around *Tnt1*-insertions sites are available. One such insertion line carrying a mutation in the CDS of the target genes was selected and ordered. Plants were grown from the obtained seeds and subjected to direct PCR tests to verify the presence of mutations (see 3.5.3). As part of these tests, the mutations in the *MtPalm1* (line NF18424) and *MtZf2* (line NF6681) could be verified in the PCR and subsequent sequencing analyses. No insertion in *MtZf1* could be detected in the NF0154 line. Positive mutants were self-propagated to obtain homozygous plants for further analyses.

To verify any potential effects of the mutations present in the target genes on the AM symbiosis, complementation constructs were generated to compensate for the non-functional gene copy. To that end, the entire genes as obtained from the A17 cultivar were cloned into the binary pGolm-true-empty vector. For *MtPalm1*, the 1979 bp promoter, 756 bp CDS and 1033 bp terminator region were used. In the case of *MtZf2*, the fragment consisted of 1867 bp promoter, the coding region comprising 3093 bp and 1185 bp terminator region. The resulting constructs (pGolm:*MtPalm1*-Comp / pGolm:*MtZf2*-Comp) could then be expressed in transgenic roots of the mutant lines as an additional test condition.

### 3.8.12 RNASeq transcriptome analyses

For quantification of all mRNA and identification of differentially regulated genes, transcriptome analyses were performed via RNAseq. To that end, three RNA samples were selected from the first *MtPalm1*-RNAi knockdown approach in addition to three corresponding gus-controls. RINs higher than 8 as determined via the Bioanalyzer as well as a representative expression profile as measured during sqRT-PCR were used as criteria. All six samples selected were adjusted to 50 ng/μl total RNA in a volume of 20 μl. Further sample preparation, Illumina sequencing, read mapping to the Mtv4 genome, Novogene Europe (Cambridge, UK) provided quantification services and statistical analyses of differential expression.



### 3.8.13 Enrichment analyses

For further insight into the transcriptome data, lists of differentially expressed genes were subjected to additional enrichment analyses: Gene Ontology (GO) enrichment analyses were performed via the PANTHER 16.0 classification system (Mi *et. al*, 2013) via the <http://geneontology.org/> online tool. Here, relative abundance of specific gene annotations can be compared to all 49,634 annotated genes in the Mtv4 genome as well as all genes included in the analysis. Annotations consisting of multiple genes that are more abundant in the differentially regulated genes than in the reference set (FDR-corrected  $p < 0.05$ ) are reported as specifically enriched. Similarly, underrepresented clusters of genes are reported as well.

Further, pathway analyses were performed using the differential expression data as well via Pathview (Luo and Brouwer, 2013; Luo *et. al*, 2017) to visualize the differentially regulated genes in the data as part of metabolic- and signaling pathways. To that end, gene annotations from the Kyoto Encyclopedia of Genes and Genomes (KEGG) are used.

## 3.9 Yeast cultivation and applications

### 3.9.1 Yeast 1-Hybrid

Yeast 1-Hybrid (Y1H) screens were used to identify TFs potentially able to bind to certain regions of DNA on the promoters of *MtPalm1*, *MtZf1*, *MtZf2* and *MtZf3*. This method, in principle works by combining two *S. cerevisiae* strains: One “Bait” containing the DNA-regions of interest putatively containing cis-regulatory elements upstream of a reporter gene and another “Prey” expressing the putative TF fused to a GAL4 trans-activation domain that, in case of a Protein-DNA-interaction, would facilitate transcription of the reporter gene.

To perform this assay, the same promoter regions of *MtPalm1*, *MtZf1*, *MtZf2* and *MtZf3* used in the histochemical GUS-stains were PCR-amplified with attB-sites for Gateway-recombination into the pDONR221 entry vector (see 3.7.4). From there, the DNA-fragments were integrated into the pMWR-vectors #2 and #3 via Gateway LR-reactions: In the pMWR#2-derivates, the target promoter is cloned in front a *HIS3*-gene encoding the enzyme Imidazoleglycerol-phosphate dehydratase, which catalyzes a crucial step in the Histidine-biosynthesis in yeast and can be exploited as a marker gene when transformed into an *S. cerevisiae* background otherwise incapable in performing this step (YM4271). For pMWR#3, the promoter is placed in front of a *LacZ*-reporter gene encoding  $\beta$ -Galactosidase capable of catalyzing the production of a blue-colored precipitate from the X-Gal (5-bromo-4-chloro-

3-indolyl- $\beta$ -D-galactopyranoside) substrate. Additionally, pMWR#3 also contains a copy of the URA3-gene conferring auxotrophy for media lacking Uracil. Both vectors were then co-integrated into the yeast nuclear genome via homologous recombination as described by (Fuxman Bass *et. al*, 2016b). Such co-integrands could be identified by their ability to grow on defined SD-HIS/-URA media lacking these auxotrophy markers. In addition, the prey-strains were generated via classical cloning of several TF's CDS-regions downstream of and in frame with the GAL4-activation domain present in the pGADT7-AD plasmid and subsequent transformation into the Y187 background.

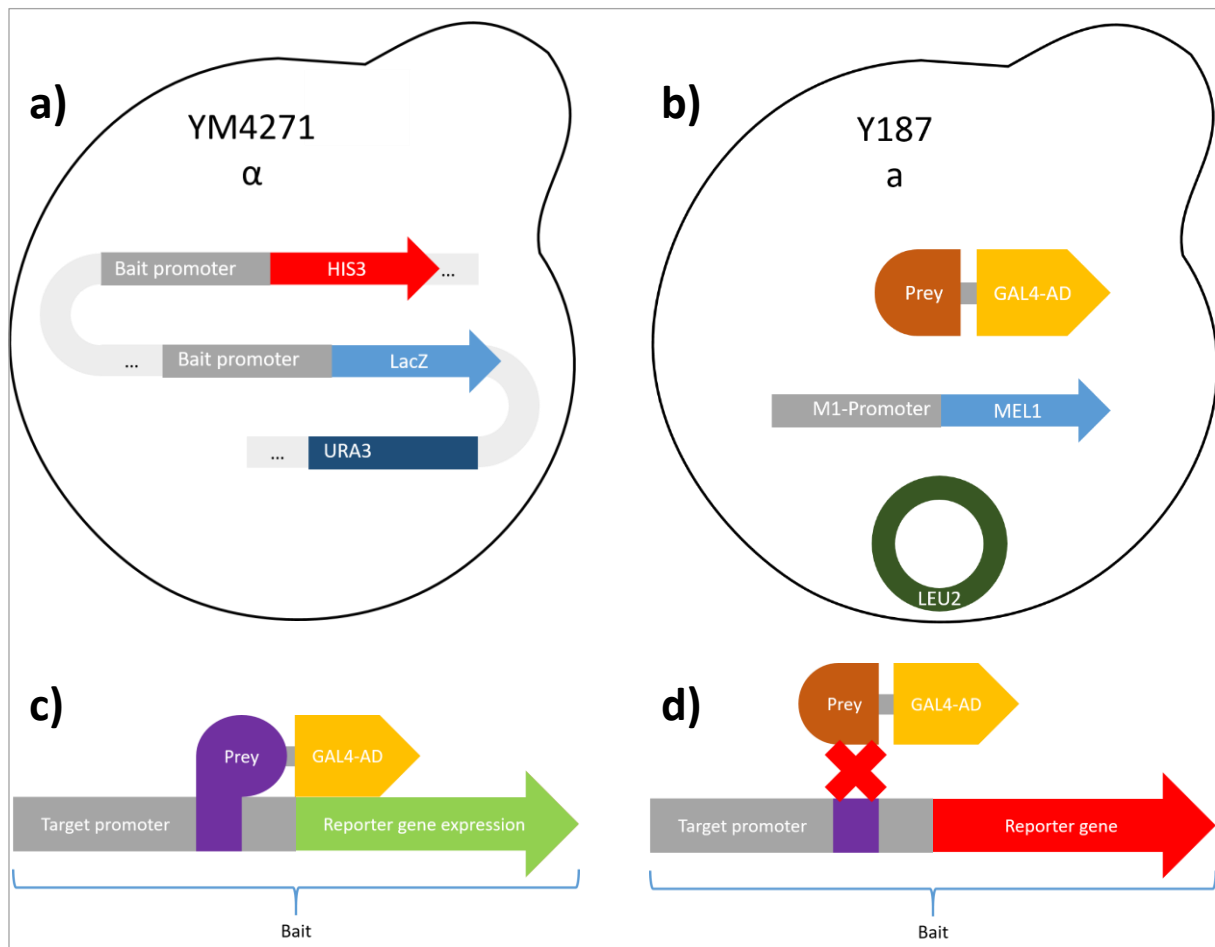


**Figure 10 – Principle of the Yeast 1-Hybrid system employed**

The Y187-strain of the mating-type  $\alpha$  co-integrates pMWR#2 and pMWR#3-derivates carrying genes for Histidine (HIS3) and Uracil (URA3) auxotrophy, respectively. The Bait-DNA-promoter is placed upstream of the HIS3 and LacZ-reporter genes to form the Bait-strain in the Y1H-system (a). The Y187 strain depicted under b) of the mating-type a is transformed with a pGADT7-derivate conferring a Leucine-auxotrophy (LEU2) to form the Prey. Additionally, the plasmid contains the gene encoding the protein-of-interest fused to a GAL4-*trans*-activation domain. The MEL1 gene, encoding an  $\alpha$ -Galactosidase is unused in the Y1H-system. Diploid strains produced by mating the Bait- and Prey-yeasts produce the Prey-protein fused to the GAL4-AD. In case of an interaction between the proteins-of-interest and the target DNA, the GAL4-AD is able to facilitate reporter gene expression as depicted in c). As a result, media containing the Histidine-biosynthesis inhibitor 3-Aminotriazole (3-AT) present in the medium can be overcome. Likewise, the LacZ facilitates colorimetric distinction of positives. In cases of no protein-DNA-interaction as shown in d), the reporter genes are not activated and yeast cells are unable to grow on media containing 3-AT.

As some promoters might be activated endogenously by the yeast, autoactivity assays were performed prior to these matings by replica plating the unmated yeast colonies onto SD-HIS/-URA-plates containing 0 mM – 80 mM 3-AT as described by (Fuxman Bass *et. al*, 2016c). Additionally, the  $\beta$ -galactosidase assays were performed. Clones exhibiting the least autoactivity were used for subsequent matings.

By co-incubating (mating) the generated Bait- and Prey-strains overnight, as described under 3.9.5, offspring of both genetic backgrounds are produced to assay. These mated cultures could then be plated on SD-HIS/-URA/-LEU media containing different 3-Aminotriazole (3-AT, 0 mM – 80 mM+), a competitive inhibitor for the HIS3-enzyme to ascertain the relative strength of the induction by promoter-activation. Yeasts on the control plates with 0 mM 3-AT were typically grown for 3d, while 6 – 10 d were required for growth on 3-AT. The colorimetric  $\beta$ -Galactosidase assay as performed as described by Fuxman Bass *et. al* (2016a).

### 3.9.2 Replica plating for yeast autoactivity tests

In order to inoculate filter paper plates used for the colorimetric assays, yeasts were replica plated from the mating-control plates containing no 3-AT. This was done to ensure exact replication of the plate layout and to avoid transferring highly variable amounts of yeasts to inoculate the new plate.

This procedure was done by affixing a sterile velvet cloth on a round stamper the size of a petri dish. Then, the plate to be replicated was placed on the cloth (yeast side down) and firmly pressed down. The cloth was then cleaned by placing two clean agar media to remove excess yeast before placing a YPDA plate with a filter paper on the replica plating apparatus. The yeasts were then grown overnight at 30°C directly on the filter paper to be removed and used for the colorimetric assay.

### 3.9.3 Yeast 2-Hybrid

Yeast 2-Hybrid assays in this work were based on the Matchmaker Gold Yeast Two-Hybrid system. Bait and Prey constructs were generated via restriction endonuclease-based cloning of the target gene CDS-region in frame (see also Table 2) with the respective reporter genes present in the pGBKT7-BD- and pGADT7-AD-vectors compatible with the system.

Transformation of *S. cerevisiae* strains for Y2H with the respective pGBKT7-BD- and pGADT7-AD-derivates was performed via a method adapted from the Yeastmaker Yeast Transformation System 2: One fresh colony of Y2HGold or Y187 was incubated shaking at 200 rpm in 10 ml liquid YPDA-medium overnight at 30°C. Afterwards, the cells were pelleted by centrifugation for 5 min at 1,000 xg and the

supernatant was discarded. Cells were then washed with 10 ml of ddH<sub>2</sub>O. This washing step was repeated once before dividing the cell suspension into 1 ml aliquots in 1.5 ml microcentrifuge tubes.

Cells were then prepared for transformation: After spinning the cells down at 3,500 xg for 5 min they were resuspended in 100 µl freshly prepared LiAc-buffer (see Table 4). In the meantime, Salmon-Sperm carrier DNA (Thermo Fisher Scientific, see Table 5) was prepared by heating to 99°C for 5 min then immediately cooling on ice. 6 µl of this carrier DNA and 100 ng of plasmid DNA were then mixed with the cell suspension. A heat-shock transformation was then performed via incubation in a 45°C water bath for 30 min. During this incubation, the suspensions were mixed every 10 min, after which 40 µl were spread on appropriate selective media (SD-Trp for pGBKT7-BD or SD-Leu for pGADT7-AD). The transformed yeasts were then grown for 3-5 d at 30°C.

#### 3.9.4 Bait-autoactivation test

Bait autoactivation can occur when the Bait protein is able to activate any reporter genes in the absence of a mated Prey protein. This was assayed by plating the unmated pGBKT7-based Bait strains on SD-media (single dropout) containing no additional selection marker or Aureobasidin A (AbA). X-α-Gal (X) was also supplied to ascertain staining activity. Further information is provided in the user manual of the system.

#### 3.9.5 Yeast direct mating

Direct matings for both Y1H and Y2H assays were performed as follows: a single freshly grown colony of every strains assayed was suspended in 700 µl of YPDA liquid medium. Then, 20 µl of Bait- and 20 µl of Prey-suspension were combined with 160 µl of YPDA in a well of a 96-well plate. The resulting liquid cultures were incubated overnight at 30°C shaking at 200 rpm. For Y2H, 20 µl were dropped onto double dropout (DDO)/DDO+X+AbA/quadruple dropout (QDO)+X+AbA, which were subsequently grown at 30°C for 3-5 d. In Y1H-approaches, cells were pelleted by centrifugation at 1.000xg for 3 min, resuspended in ddH<sub>2</sub>O, of which 15 µl were then dropped on the appropriate media.

#### 3.9.6 Yeast library mating

Library screening was performed using a pGBKT7-Bait strain and a yeast-library consisting of pGADT7-derivates containing cDNA transcribed from *M. truncatula* mRNA from the following sources: 50% mycorrhized roots, 16.6% root nodules, 16.6% roots in contact with Nod-factors and 16,6% sterile roots (Hartmann, 2018). The mating itself was done according to the “Matchmaker GoldYeast-Two-Hybrid

System User Manual” by Clontech (Table 7). Resulting positive clones were checked via the “Matchmaker Insert-Check PCR” and subsequent sequencing and BLAST-search against the *M. truncatula* A17 genome.

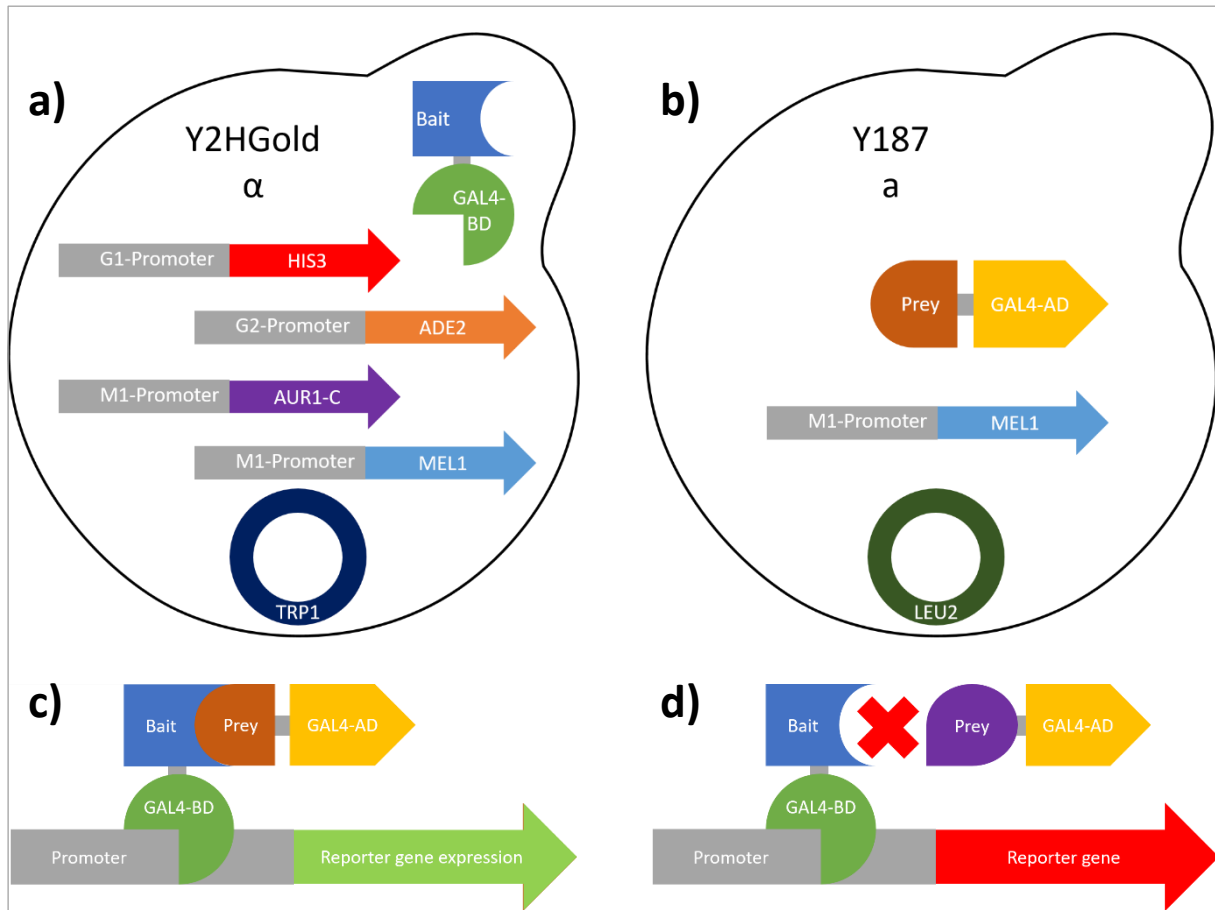


**Figure 11 – Principle of the Yeast 2-Hybrid system employed**

The Y2HGold-strain of the mating-type  $\alpha$  is transformed with pGBKT7-derivates conferring a Tryptophan-auxotrophy (TRP1-gene) to form a Y2H Bait-strain producing the protein-of-interest fused to a GAL4-DNA-binding-domain (a). This GAL4-BD is able to bind to specific regions in the G1-, G2- and M2-promoters upstream of the respective reporter genes: HIS3, if active allows Histidine biosynthesis, while ADE2-expression allows Adenine-auxotrophy. AUR1-C encodes the enzyme inositol phosphoryl ceramide synthase and confers resistance to the toxic compound Aureobasidin A. Finally, MEL1 encodes  $\alpha$ -Galactosidase, which forms a blue compound when reacting with X- $\alpha$ -Gal present in the growth medium. The Y187 strain depicted under b) of the mating-type a is transformed with a pGADT7-derivate conferring a Leucine-auxotrophy (LEU2). Additionally, the plasmid contains the gene encoding the protein-of-interest fused to a GAL4-*trans*-activation domain. The MEL1 gene is encoded in this strain as well. Diploid strains produced by mating the Bait- and Prey-yeasts produce both the Bait-protein fusion with the GAL4-BD able to bind the promoters upstream of the various reporter genes and the Prey-protein fused to the GAL4-AD. In case of an interaction between both proteins-of-interest, the GAL4-AD is able to facilitate reporter gene expression as depicted in c). If no protein-dimer is formed (d) the reporter genes are not activated and yeast cells are unable to grow on media lacking Histidine and Adenine and/or containing Aureobasidin A.

## 3.10 Protein binding-assays via Bimolecular Fluorescence Complementation

### 3.10.1 Principle of BiFC

Previously obtained potential protein-protein interaction results were to be confirmed as well as new potential interactions observed using another method: Bimolecular fluorescence complementation (BiFC) involves the translational fusion of the CDS of a protein of interest to a DNA fragment encoding for the carboxy (C)- or amino (N)-terminal half of a yellow fluorescent protein (YFP). By co-transforming one putative interactor fused to one YFP-fragment and its possible interacting partner to the other, binding between them can be microscopically detected as yellow fluorescence. This is based on the fact that a true interaction between the proteins of interest, both halves of the split YFP are brought into close proximity allowing the full, functional fluorophore to be restored. This method has a few advantages over protein interaction studies in Yeast 2-Hybrid assays: On a base level, it allows the interactions to take place *in planta*, where general physiology and specifically features of protein expression such as codon usage and glycosylation patterns are similar. Furthermore, certain proteins and especially TFs are able to induce yeast reporter genes without an interaction partner. This autoactivation problem leading to some candidates not being evaluable can be avoided here.

BiFC-approaches, however, also present some problems and challenges: The strong overexpression of the fusion proteins may lead to false positives due to the sheer number of proteins produced. (Horstman *et. al*, 2014). To exclude any such false positives, YFP fluorescence had to be detected strongly above the background level and be verified using  $\lambda$ -scans (outlined below). Additionally, the matrix of structurally related GRAS-proteins itself acts as a control, as detection of strong signal in some combinations but not in others likely stems from actually specific protein features. Moreover, an interaction was only fully accepted as a positive in the case of both orientations yielding a signal.

### 3.10.2 Cloning of BiFC constructs

To perform the BiFC-assay, a system based on the binary vectors pSPYCE/pSPYNE-35s-GW was chosen (Walter *et. al*, 2004). These *R. radiobacter* compatible vectors contain the respective C- or N-terminal YFP-fragment downstream of a CMV 35s-promoter for overexpression. Cloning of the respective gene of interest in frame with the YFP-reporter is facilitated via a Gateway-cassette located upstream (see 3.7.4). To that end, the CDS of each of the candidates was amplified without the stop-codon with compatible attachment-sites for integration into a pDONR-backbone. From there, LR-recombination was possible to both pSPYCE- and pSPYNE-destination vectors. Due to the pDONR and both destination vectors having the same selection marker, the pDONR had to be cleaved prior to the LR-reaction.

### 3.10.3 Infiltration of *A. tumefaciens* into *N. benthamiana* leaves

In order to perform the BiFC-assays, *N. benthamiana* leaves had to be infiltrated using *Rhizobium radiobacter* GV3101::pMP90 to facilitate transformation of epidermal cells. To prepare for this infiltration, the *R. radiobacter* strains carrying the desired binary vectors were incubated overnight at 30°C in liquid LB-A medium containing 100 µg/ml rifampicin and 15 µg/ml gentamycin alongside the appropriate marker for selection of the desired plasmid (50 µg/ml kanamycin for pSPYCE/pSPYNE-derivatives). Additionally, a GV3101 strain containing the viral silencing inhibitor p19 also had to be prepared (Lakatos *et. al*, 2004). To perform the assay itself, the overnight cultures were centrifuged in a swing-out rotor at 3,220 xg. After removing the supernatant, the *Agrobacterium* pellet was resuspended in Infiltration Buffer (Table 4), containing freshly added Acetosyringone (0.1 mM). The suspension was then adjusted to an OD<sub>600</sub> of approximately 0.6 for the expression strains and ~0.3 for the p19 strain. To activate the *vir* genes, the *Agrobacteria* were generally incubated in this buffer for 1-3 h. After mixing the strains appropriately (for BiFC interaction studies the ratio used was pSPYCE:pSPYNE:p19 1:1:0.5). This suspension could then be drawn up into a sterile syringe without a needle and pressed into young leaves of 4-5 wk old *N. benthamiana* plants. After 1d further growth, leaves were shaded using a tin foil cover to reduce light exposure and prevent bleaching of the fluorophores that are potentially formed.

For sample collection, leaf disks were taken from *N. benthamiana* plants 2 d after inoculation by punching holes into the infiltrated portions of the leaves with the lid of a 1.5 ml tube. Such disks were kept in Infiltration Buffer for up to 1 h before microscopy. Transport took place in the dark to protect potentially weak YFP fluorescence from bleaching due to light exposure.

### 3.10.4 YFP signal detection via confocal laser scanning microscopy

Microscopy slides with the leaf discs immersed in Infiltration Buffer were observed under a Leica DM6000 CS confocal laser scanning microscope. Overview images for quantitative analyses were taken at 20x optical magnification. 40x in addition to digital zoom were occasionally used for closeup images.

The fluorophores were excited via a 514 nm laser. Putative YFP-fluorescence was detected in the range of 523 nm – 542 nm with the theoretical peak emission at 528 nm as a “yellow” channel (false colors). Additionally, chlorophyll autofluorescence was captured at 670 nm – 695 nm and is shown in red. Finally, an artificial bright-field image was also taken in grayscale.

In order to verify the signals detected in the YFP-channel,  $\lambda$ -scans were performed: Here, a series of images are captured covering the spectrum from 523 nm to 553 nm in steps of 3 nm with a detection range of 3 nm for each step. This way, an emission spectrum of the putative YFP signal could be reconstructed and compared to the theoretical eYFP spectrum with a 528 nm expected peak and subsequent gradual reduction in signal. The presence of an additional background peak around 538 nm was typically observed as part of the background and did not affect the acceptance of emission spectra as true YFP.

To exclude potential false positives, any interactions pairs exhibiting signals were re-evaluated in at least one other independent experiment. Additionally, at least five random overview images (usually >10) were taken and evaluated for present signals. At least half of all such images had to contain such signals for a candidate pair to be accepted as a potential positive.

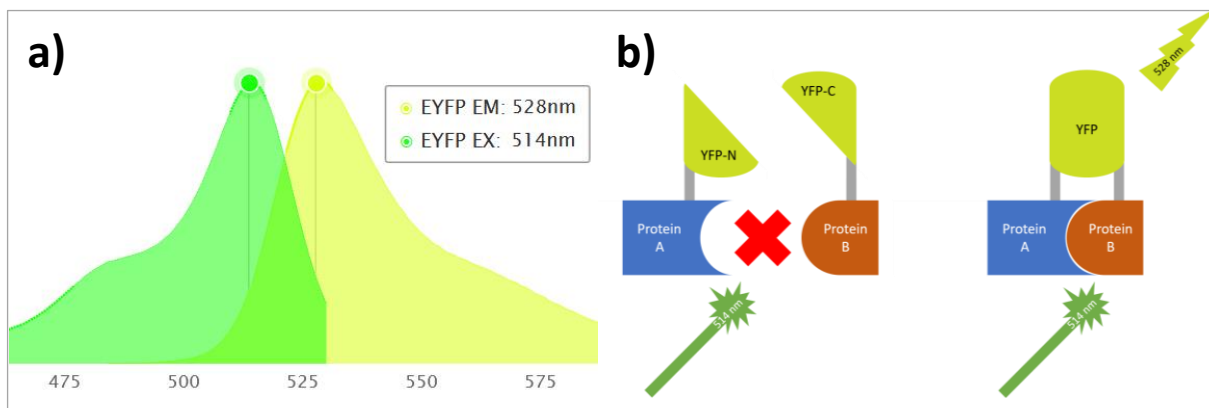


**Figure 12 – Bimolecular fluorescence complementation assay**

a) Excitation (green) and emission (yellow) spectra for YFP. Dots mark the approximate excitation and emission peaks and 514 nm and 528 nm, respectively. (Modified from: <https://www.fpbases.org/protein/eypf/>) The principle for BiFC is illustrated under b): two proteins of interest A and B are fused to N- and C-terminal YFP fragments. Without interactions between the target proteins, no fluorescent signal is produced when excited using a 514 nm laser. If both proteins of interest interact, the YFP-fragments are brought into close proximity, allowing the detection of YFP-fluorescence when excited.



## 4 Results

### 4.1 The Zinc finger genes *MtPalm1*, *MtZf1*, *MtZf2* and *MtZf3* are upregulated during the AM-symbiosis of *M. truncatula*

In this thesis, the *M. truncatula* Zinc finger genes of *MtPalm1*, *MtZf1*, *MtZf2* and *MtZf3* were to be examined. The expression data presented in Figure 6 served as initial indication for the induction of these genes under conditions involving AM-symbiosis. To confirm these results and to obtain a higher sensitivity level for the detection of potentially weakly expressed transcripts, sqRT-PCR measurements were performed on RNA-samples from an *M. truncatula* A17 mycorrhization time course. The material for this analysis was obtained as follows: Plants were inoculated with *R. irregularis* spores for 4 h, after which two root systems were directly flash frozen. Then, samples were taken from two pots containing two plants every week for a total of 7 weeks.

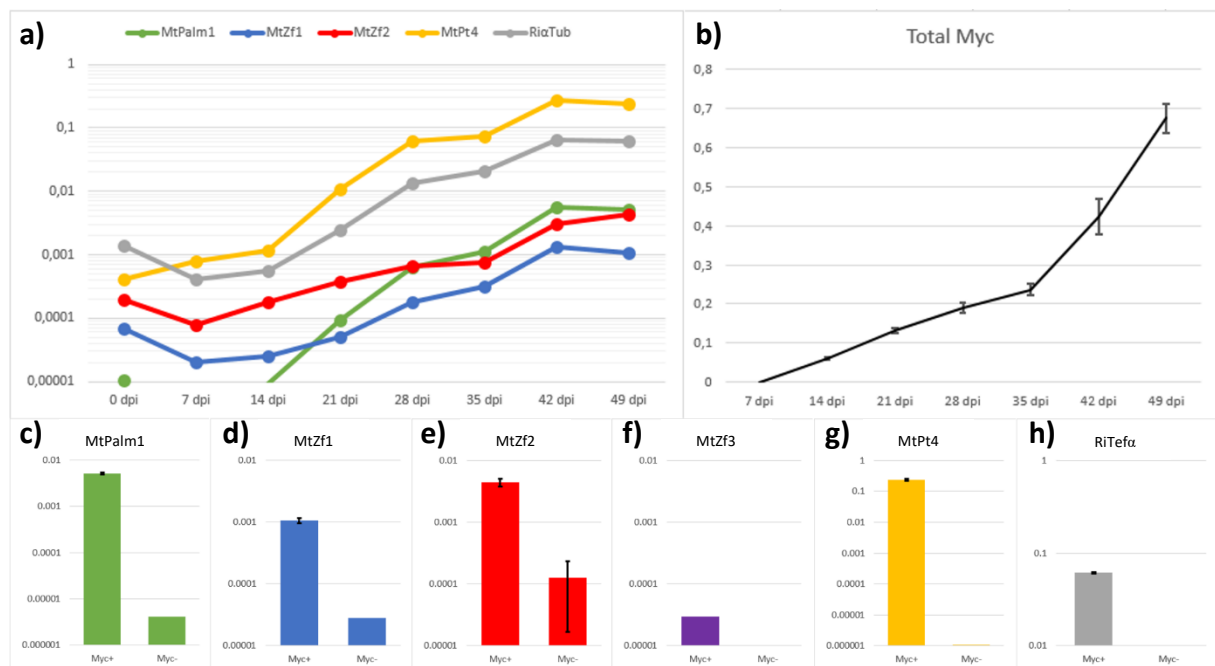


**Figure 13 – Measurements of AM-induced Zinc finger genes in a *M. truncatula* mycorrhization time course via sqRT-PCR**

For this time course experiment, *M. truncatula* plants were inoculated with *R. irregularis* spores and grown for up to seven weeks. Directly after contact with the spores and subsequently every week, roots were frozen in  $\text{LN}_2$  and used for RNA-extraction. The transcripts of *MtPalm1*, *MtZf1* and *MtZf2* were measured via sqRT-PCR as were the arbuscule marker *MtPt4* and the fungal gene *RiαTub* normalized to the housekeeping gene *MtTefα*. Results of these measurements are represented by the line chart under a). Fungal progression was subsequently confirmed in the remaining root material via counting of stained fungal structures with the Gridline-Intersection method. Line chart b) shows total mycorrhization as a ratio compared to all root sections observed. Non-mycorrhized plants were grown in parallel for 7 weeks, after which the same sqRT-PCR measurements were performed on the same set of genes. These transcript measurement results in comparison to the relative expression in mycorrhized roots after 49 dpi are represented by the bar charts under c)-h). Error bars represent standard deviation between samples.

To confirm progression of AM-symbiosis, expression of the arbuscule marker gene *MtPt4* was measured, which consistently rose up until 42 days post inoculation (dpi) then fell slightly at 49 dpi, likely due to the increased abundance of old and degenerated arbuscules (Figure 13a, yellow). The *R. irregularis* alpha-tubulin housekeeping-gene (*RiaTub*) was strongly measurable on the roots in direct contact with the spores (0 dpi). Subsequent obtained expression values were lower during the first two weeks as mycorrhization was establishing, after which a steady increase was measured, overall confirming steady intraradical growth of the symbiotic fungus. This continuous increase in overall AMF-colonization was also validated by quantifying ink-stained fungal structures in the remaining root material (Figure 13b).

Results for the new Zinc finger candidate genes were as follows: At 0 dpi, *MtPalm1* expression was measurable, suggesting that the gene responds directly to contact with spores. Conversely, *MtPalm1* transcripts were not detectable at 7 dpi and then exhibited a continual rise from 14-42 dpi (Figure 13a, green). At 49 dpi, like *MtPt4*, a slight decrease was observed, indicating a response to functional arbuscules. The pattern was similar for *MtZf1* (Figure 13a, green), though with more basal expression at the earlier timepoints and less strong induction overall compared to *MtPalm1*. *MtZf2* (Figure 13a, red) was the only candidate gene that exhibited a continually rising expression level all the way from 7 dpi until 49 dpi, possibly indicating a role up until the very late stages of the arbuscular life cycle. Transcript measurements were not directly performed for *MtZf3*. However, time course data from a prior GeneChip transcriptomics experiment (Hartmann, LUH, unpublished) revealed a high level of basal expression as well as an induction during early contact with the spores (Supplementary Figure S1). The expression fell in comparison at the subsequent timepoints and only exhibited another rise at the latest stages examined.

Additionally, non-mycorrhized roots were grown in parallel and harvested after 7 weeks to serve as a direct reference point to compare induction of these candidate genes. In these measurements, *MtPt4* and *RiaTub* were not detectable as expected (Figure 13g and h). For *MtPalm1*, a measurement was obtained that suggested an approximate induction of 1275-fold under mycorrhized conditions compared to non-mycorrhized roots (Figure 13c). Still, *MtPalm1* transcripts were barely detectable under non-mycorrhized conditions. The less strongly expressed *MtZf1* showed an increase of 37-fold compared to non-mycorrhized root systems (Figure 13d) which was very similar to the result for *MtZf2* at 35-fold induction (Figure 13e). *MtZf3* expression was measured to be comparatively low both in the non-mycorrhized roots and the 49 dpi Myc+ roots. As part of this experiment, the *MtZf3* transcript was only measurable under mycorrhized conditions, supporting its status as an AM-induced gene (Figure 13f).

## 4.2 Functional analysis of *MtPalm1* under AM-conditions

### 4.2.1 Exclusion of a putative oORF from the *MtPalm1* promoter increases the intensity of histochemical stains

To ascertain the correlation between the AM symbiosis and *MtPalm1* and to gain an understanding of the pattern of *MtPalm1* expression on the cellular level, the promoter region -1980/-1 relative to the start-codon was fused to the *gusAint* reporter gene and integrated into the pRedRoot binary vector. During this initial examination of the *MtPalm1* promoter-region, a peculiar feature was identified within its putative 5'-UTR in the form of an additional start codon 17 bp upstream of the ATG of the CDS region (Figure 14a, orange). This potential overlapping open reading frame (oORF), when translated, would lead to a short 16 aa peptide, before running into a stop codon. This oORF could therefore interfere with the correct translation of either the MtPALM1 protein in the natural system or the GUS-protein in the promoter reporter gene study, which could lead to comparatively low staining intensities. To test this, a version of the promoter truncated at position -38 relative to the canonical ATG ("ver2", -1980/-38, see also Figure 14a, purple) was cloned and used for transgenic root induction, as well as mycorrhization in order to perform histochemical stainings in direct comparison to the complete -1980/-1 "ver1".

Induced transgenic root systems were grown in contact with AM fungus as well as under non-mycorrhized conditions and analyzed via histochemical staining. For the *pMtPalm1-gus\_ver1* construct, clearly visible coloration was typically obtained after at least 8 h of incubation, though more typically overnight staining (~14 h) was required to obtain strong signals. After such incubation periods, background activity was also visible to some extent, particularly in the vasculature.

When related to Alexa488-stained fungal structures, activity in the root cortex was observed exclusively in the presence of arbuscular mycorrhiza. This promoter activation could specifically be related to arbuscule containing cells, though after shorter incubation only some were clearly stained, while occasionally even entire infected regions exhibited weak activity in comparison to others (Figure 14b, c). Incubation overnight led to a very clear match between staining and arbuscocytes but also to likely nonspecific coloration of the vasculature (Figure 14f, g).

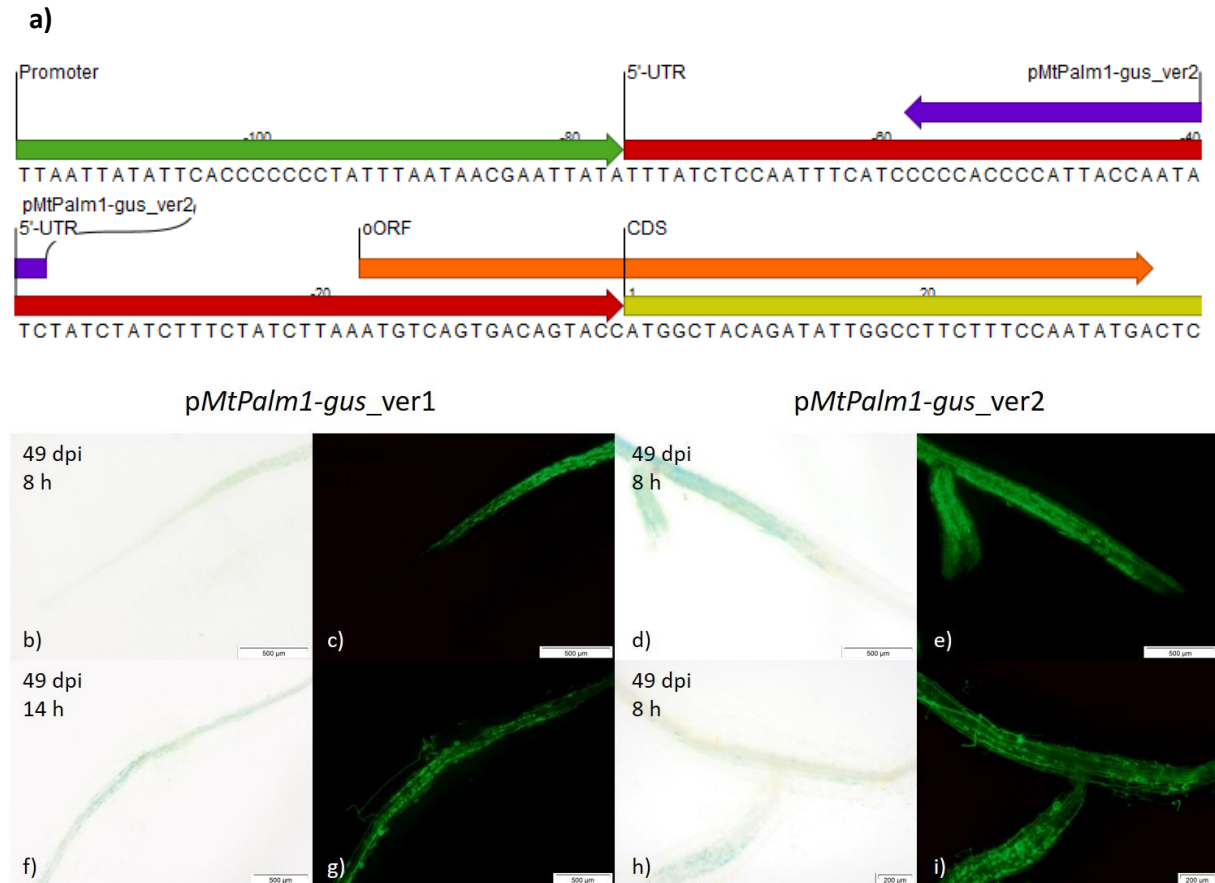


**Figure 14 – Comparative analysis of AM-induced *MtPalm1*-promoter activity in a full and a 3'-truncated version**

During initial cloning of the *pMtPalm1-gus\_ver1* construct the entire putative 5'-UTR (a, red) up to the start-codon was included. Since the oORF (orange, ends in a stop-codon) might lead to a lack of GUS-expression, another version of this promoter-reporter gene fusion was constructed excluding this region. The new reverse primer marking the 3'-end of the *MtPalm1\_ver2* promoter is shown in purple. The sequence information depicted was taken from the *M. truncatula* A17 reference Genome v4. The promoter-*gus* fusion constructs were expressed in transgenic root systems in the *M. truncatula* A17 WT background inoculated with *R. irregularis* spores in parallel with non-mycorrhized controls. Images were taken after GUS staining of transgenic root systems for the stated time periods (bright field images) and subsequent counter-staining of fungal chitin via Alexa488-WGA. The images b),c),f),g) depict the full *pMtPalm1-gus\_ver1* construct (-1980/-1). Staining generally corresponds to regions containing AM. Strong, complete staining of arbuscocytes required 14 h of staining. In comparison, the truncated *pMtPalm1-gus\_ver2* lacking a putative oORF (d,e,h,i) is fully stained after 8 h. The pattern of only reacting to the presence of arbuscules is retained.

In comparison, the *ver2* lacking the putative oORF consistently exhibited strong blue staining of mycorrhized regions after 8 h (Figure 14d, e). Observing less strongly colonized regions revealed that the specificity towards arbuscule containing cells remained the same as in the full *ver1* promoter (Figure 14h, i), as the presence of hyphae alone did not elicit a response in either. Similarly, staining of the *ver2* appeared to be complete after the same 8 h incubation period with all AM-containing root sections exhibiting clear activity. Overall, the response of the *pMtPalm1-gus* construct appears significantly stronger without the oORF, suggesting a role in the regulation of *MtPALM1*. In further *MtPalm1*-promoter-*gus* analyses the *ver2* was used.

#### 4.2.2 Activity of the *MtPalm1* promoter is strongly correlated with arbuscule containing cells of mycorrhized roots

Subsequent to the prior comparative analysis, detailed observation of the *pMtPalm1-gus* assays revealed a clear correlation between regions of the roots containing active arbuscular mycorrhiza and GUS-activity (Figure 15a, b and k, l). The non-mycorrhized controls generally did not yield visible staining or only typical background in the vasculature, particularly when staining for longer periods (Figure 15m-p). Furthermore, it appears that only arbuscule containing cells exhibited any visually detectable activity after 8 h staining. As illustrated by Figure 15c) and d), very young infection units containing recently established arbuscules were sufficient to elicit this response.

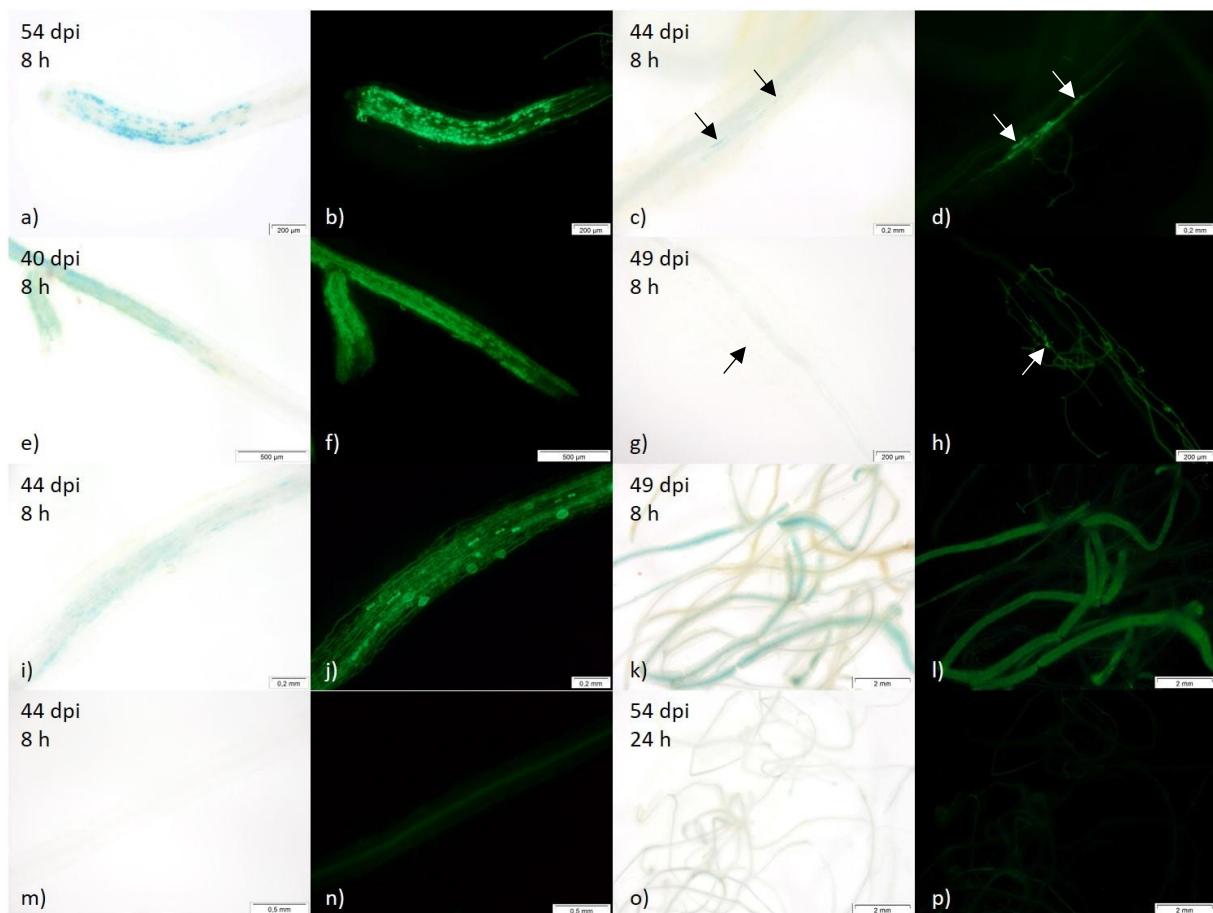


**Figure 15 – Histochemical localization of *MtPalm1* promoter activity in wild-type mycorrhized roots**

The *pRR:pMtPalm1-gus* construct was expressed in transgenic root systems in the *M. truncatula* A17 WT background. Roots (a-l) were mycorrhized via inoculation with *R. irregularis* spores. Myc- roots (m-p) were grown in parallel. Images were taken after GUS staining of transgenic root systems for the stated time periods (bright field images) and subsequent counter-staining of fungal chitin via Alexa-/CF488-WGA. *MtPalm1* promoter activity is strongly associated with arbuscules within the root cortex (a,b,k,l). Young arbuscules from newly established infection units suffice to activate this response (c,d), while the sole presence of hyphae (e,f) or appressoria (g,h) does not. Old AM with degenerated arbuscules still yields some activity, though weaker than in active arbuscocytes. Non-mycorrhized roots exhibit no *pMtPalm1* activity even after long staining periods (m,n,o,p).

The presence of internal hyphal growth in contrast did not activate the *MtPalm1* promoter and neither did the presence of appressoria initiating the entrance of the AM symbiotic partner into the roots (Figure 15e, f, g, h). Sections containing seemingly older and degenerated arbuscules still exhibited some weaker, possibly residual staining, whereas active arbuscules showed a much stronger response (Figure 15i, j). Thus, based on these results, it appears that *pMtPalm1* is activated specifically in cortical cells harboring active arbuscules. This fits well to the findings of Hogekamp *et. al* (2011), where *MtPalm1* appeared as part of a set of transcription factor genes specifically upregulated in the presence of arbuscules.

#### 4.2.3 *MtPalm1* promoter activity is strongly diminished in the *ram1-1* and *pt4-2* mutants

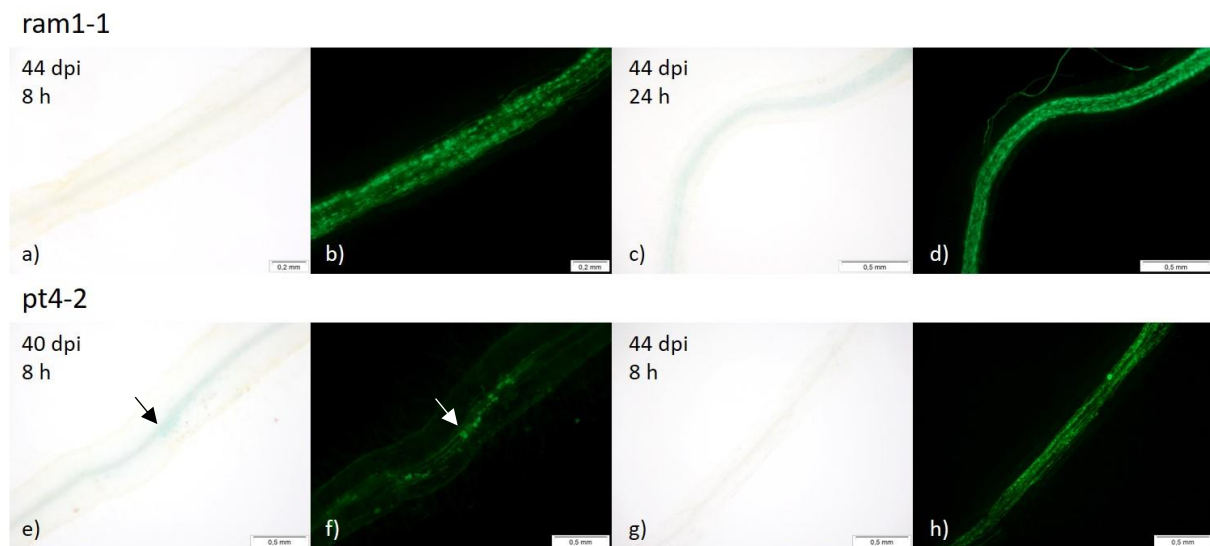


**Figure 16 – Histochemical localization of *MtPalm1* promoter activity in mycorrhizal roots of *ram1-1* and *pt4-2* mutants**

The *pRR:pMtPalm1-gus* construct was expressed in transgenic root systems in the *M. truncatula ram1-1* and *pt4-2* mutant backgrounds. All roots depicted were mycorrhized via inoculation with *R. irregularis* spores. Images were taken after GUS staining of transgenic root systems for the stated time periods (bright field images) and subsequent counter-staining of fungal chitin via Alexa/CF488-WGA. The activity of *pMtPalm1* in *RAM1*-deficient mycorrhized roots as depicted in a)-d) is strongly diminished and generally only detectable in overnight staining. *MtPalm1* promoter activity in the *pt4-2* mutant background depends on the presence of prematurely degenerated arbuscules: In a normal phenotype (e,f), *pMtPalm1* activity is retained, whereas it is abolished in cells with degenerated arbuscules (g,h).

In the mutant background deficient in the key AM-regulator MtRAM1, *MtPalm1*-promoter activity was strongly diminished and not detectable during otherwise typical 8 h staining periods (Figure 16a, b). However, longer incubation times as shown in Figure 16c) and d) revealed some slight induction in the presence of arbuscules. MtPALM1 therefore appears to not be fully dependent on regulation by MtRAM1. Activity of p*MtPalm1* was also assayed in the *pt4-2* mutants. Deficiencies in PT4 often, but not always lead to premature arbuscules degeneration (PAD; Breuillin-Sessoms *et. al*, 2015). In the presence of arbuscules without this visible PAD-phenotype, p*MtPalm1* activity was detected as normal (Figure 16e, f). Degenerated arbuscules like in Figure 16g) and h), however yielded no such activity, indicating that the role of *MtPalm1* is likely earlier than during the senescence phase of the arbuscular lifecycle.

#### 4.2.4 Overexpression of *MtPalm1* had no significant effect on the AM symbiosis

After this initial analysis of its arbuscule-induced native expression, an overexpression experiment was performed for *MtPalm1* to determine whether an increase in overall abundance might be sufficient to drive increased AM-colonization or potentially have a suppressive effect indicating a negative regulatory role. To that end, the *MtPalm1*-CDS was overexpressed under control of a constitutive CMV-35s-promoter using induced transgenic root systems in the *M. truncatula* A17 WT background. Transformed roots were mycorrhized via *R. irregularis* spores and grown for 6 weeks before flash freezing in pools of three, after which RNA was extracted and sqRT-PCR measurements were performed (n = 3 x 8).

In comparison to the mycorrhized empty vector control roots grown in parallel, *MtPalm1* was successfully overexpressed 87-fold over the entire root system (Figure 17a). Measurements of arbuscule marker gene *MtPt4* showed no significant differences in expression between the different sample pools (Figure 17b). Blind counting of stained AMF structures in the remaining root material showed likewise no significant differences, though like *MtPt4* transcripts, the *MtPalm1*-OE roots trended lower in every category (Figure 17c). Arbuscule sizes were measured in pictures taken from the different sample pools likewise exhibiting no significant differences compared to the controls (Figure 17e).

Based on these results, no clear effects on the AM-symbiosis were observed by an increase of *MtPalm1* expression alone, indicating that MtPALM1 alone does not have a negative regulatory effect while also not itself being sufficient to drive an increase in overall colonization. Interestingly, during harvesting, the length of the remaining shoots of the plants were measured which revealed that *MtPalm1*-OE plants were on average 2.5 cm shorter (P = 0.0007, Figure 17d, see also supplementary Figure S2), serving as an indication of some level of stress suffered by the plants due to the overexpression.



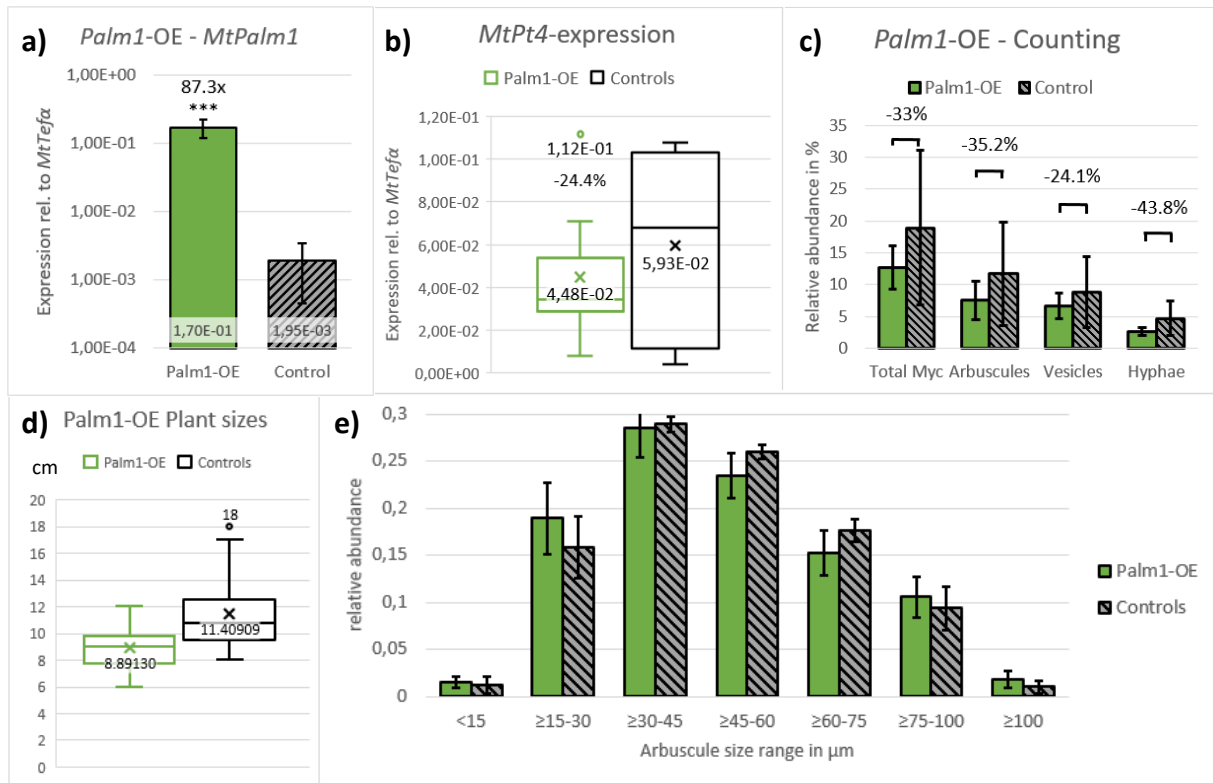


**Figure 17 – Effects of *MtPalm1*-overexpression on AM-colonization and arbuscule sizes**

*MtPalm1* was constitutively overexpressed in transgenic root systems of the *M. truncatula* A17 cultivar under control of a CMV-35s-promoter. Resulting positively transformed roots were mycorrhized via inoculation with *R. irregularis* spores. Plants grown with transgenic roots carrying the empty vector were used as controls under the same conditions. At 42 dpi, roots were flash frozen ( $n = 3 \times 8$  for each group) for subsequent RNA-isolation and sq-RT-PCR measurements. The bar charts in a) represent mean *MtPalm1* expression levels of the overexpression roots compared to the controls. Measurements of the AM-marker gene *MtPt4* are represented in b) as box plots. Remaining root material of both OE- and control-roots was used for quantification (percentage of 300 root sections per sample) of internal AMF colonization shown as bars in c). During harvesting, shoot length of both groups was recorded and is depicted under d) in cm. Finally, arbuscule size distribution was determined from 20 blind images of colonized root sections (e). Error bars on the bar charts represent 95% confidence intervals, asterisks mark statistical significance of differences between experimental conditions at 95% (\*), 99% (\*\*), and 99.9% (\*\*\*) confidence as determined by Student's t-Test. Numbers shown on the box plots represent the respective arithmetic means also marked by the x as well as outlier measurements outside 1.5 x IQR.



#### 4.2.5 An RNAi-mediated knockdown of *MtPalm1* leads to a reduction in overall AM colonization and in the rate of arbuscules

In order to study the role of *MtPalm1* during the establishment and maintenance of AM symbiosis further, two separate constructs consisting of double-stranded fragments from unique regions of the CDS were designed to perform an RNAi-based-knockdown (*MtPalm1*-RNAi-1 and *MtPalm1*-RNAi-2, outlined in Figure 9). Using both constructs, three separate gene silencing experiments were independently performed via inductions of transgenic root systems in an *M. truncatula* A17 wild-type background.

Transcript amounts from the extracted RNA of mycorrhized root systems were measured via sqRT-PCR. Across the three separate experiments performed, *MtPalm1* was significantly reduced in mycorrhized roots expressing the *MtPalm1*-RNAi-1 construct by an average of 84.3% compared to the controls containing a knockdown construct targeting a *gus*-gene. For *MtPalm1*-RNAi-2, an average reduction of *MtPalm1* by 66.5% was measured on average which represents a statistically significant knockdown-effect in 2/3 experiments. In each case, a significant knockdown of *MtPalm1* correlated with significantly lower transcript amounts of the AM-specific phosphate transporter gene *MtPt4* at an average of 78.3% and 47% compared to the expression levels in the controls, respectively. Taken together, these results indicate the presence of fewer arbuscules due to an overall reduction in AM-colonization in roots with diminished *MtPalm1*-expression.

In detail, the first of these independent experiments showed that 49 dpi mycorrhized roots expressing *MtPalm1*-RNAi-1 (Figure 18a, red) had reduced target transcript amounts by an average 82.4% ( $p = 0.0001$ ,  $n = 12$ ) compared to the respective *gus*-controls. These results were subject to some variation between individual samples, but the knockdown was clearly observed in the entire sample pool with the highest *MtPalm1*-measurements from the RNAi-set being comparable to the lowest controls (Supplementary Figure S3). The *MtPalm1*-RNAi-2 (Figure 18a, blue) sample pool averaged 83.2% ( $p = 0.007$ ) less *MtPalm1*-mRNA compared to *gus*-control set two. For this construct, half of the samples tested showed no remaining clearly detectable presence of *MtPalm1*-transcripts. However, overall, the results were more varied across the entire set leading to a less significant average result in spite of a stronger knockdown effect. The arbuscule-marker gene *MtPt4* was likewise significantly downregulated to 28.6% in the RNAi-1 set ( $p = 0.001$ ) and 27.6% for RNAi-2 ( $p = 0.001$ ) compared to its respective average expression level in the controls (Figure 18d).

In the second *MtPalm1*-knockdown experiment, average target transcript amounts were significantly reduced by 83.3% ( $p = 0.001$ ) for *MtPalm1*-RNAi-1 and 90.3% ( $p = 0.0005$ ) for *MtPalm1*-RNAi-2 ( $n = 8$ , Figure 18b). As a result, *MtPt4*-expression fell to an average 20.4% ( $p = 0.002$ ) in the RNAi-1-roots and to 11.8% ( $p = 0.0009$ ) for RNAi-2 compared to the *gus*-controls (Figure 18e). Other measured AM

marker genes such as *MtRam1*, (22.7% and 13.4%) *MtRam2* (24.4% and 16.9%) exhibited similarly proportional reductions in transcript amounts, indicating that none of these genes are specifically differentially regulated in the absence of MtPALM1 (Supplementary Figure S4). Total fungal mass was also reduced as measured by the constitutively expressed fungal *RiaTub* gene at a residual 13% and 10%, respectively. The observed reductions were generally stronger but less consistent across all samples in *MtPalm1*-RNAi-2, which had also been the case in the previous experiment.

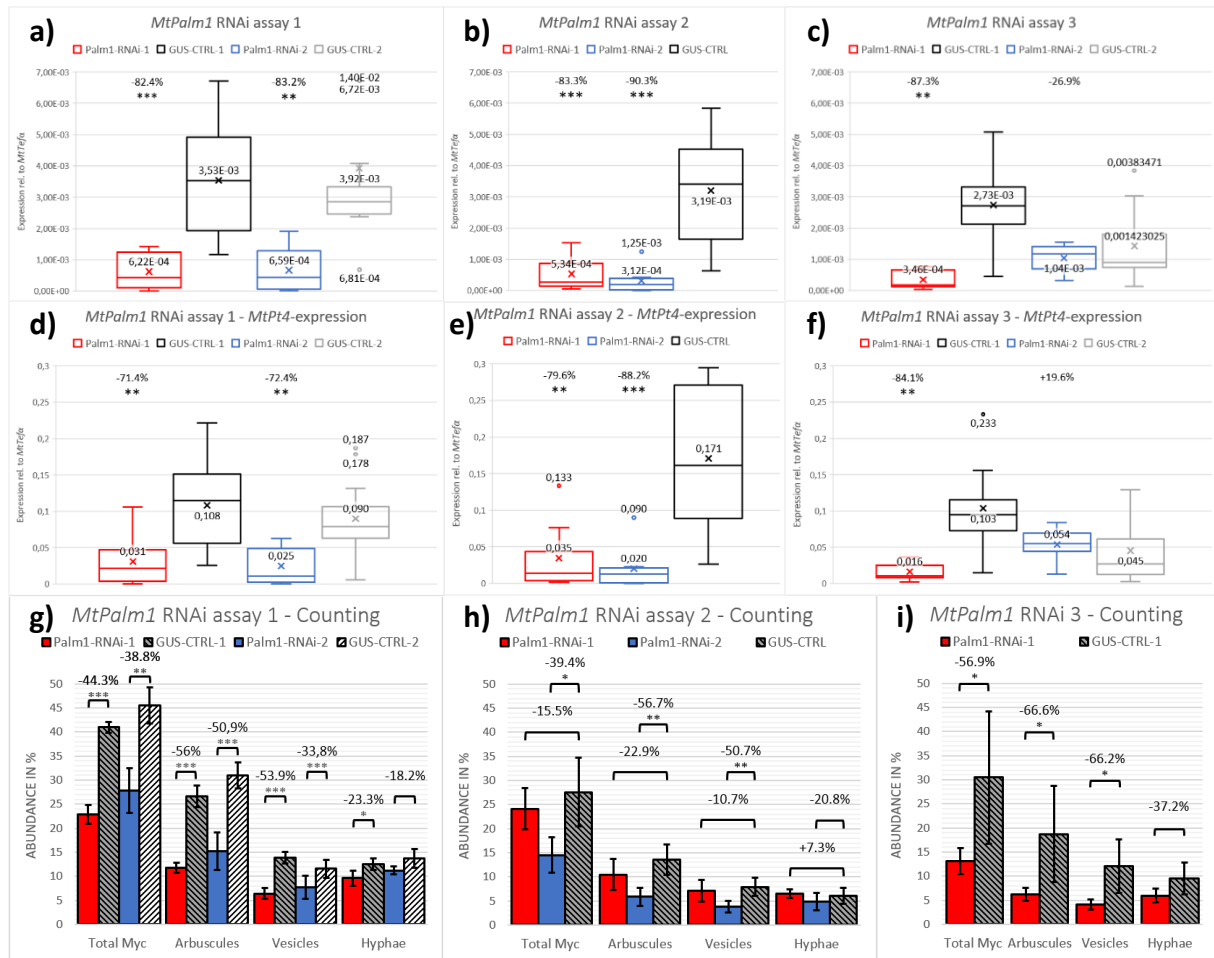


**Figure 18 – Effects of an *MtPalm1*-RNAi-knockdown on the expression of AM marker gene *MtPt4* and overall AM-colonization**

Two RNAi constructs targeting *MtPalm1* were expressed in transgenic root systems in WT *M. truncatula* A17 plants as part of three separate knockdown experiments ( $n_1 = 12$ ,  $n_2/n_3 = 3 \times 8$ ). Transgenic roots containing a knockdown construct targeting a *gus*-gene were used as controls. Roots were grown for 49, 54 and 42 dpi with *R. irregularis* spores, respectively, after which RNA samples were extracted and used for sq-RT-PCR measurements. Box plots a-c) show *MtPalm1* transcript reductions in the RNAi-roots compared to the controls in the three separate experiments. Plots d-f) underneath depict reductions in the *MtPt4* arbuscule marker gene due to the *MtPalm1*-RNAi-effects. Numbers shown represent the respective arithmetic means also marked by the x as well as outlier measurements outside 1.5 x IQR. Remaining root material was used for quantification (percentage of 300 root sections per sample) of fungal structures within the roots represented as arithmetic mean by the bar charts g-i). Error bars represent 95% confidence intervals, asterisks mark statistical significance of differences between experimental conditions at 95% (\*), 99% (\*\*), and 99.9% (\*\*\*) confidence as determined by Student's T-Test.

During a third replication, the second of the *gus*-control sets (comparison to *MtPalm1*-RNAi-2) exhibited uncharacteristically low levels of *MtPt4*-expression in half of the eight samples measured, likely due to poor mycorrhization. This, in addition to a seemingly weaker knockdown compared to the previous measurements, led to only a weak, statistically insignificant 26.9% reduction in *MtPalm1*-transcripts (Figure18c, blue). *Gus*-control set one yielded expression levels similar to the first two experiments. The *MtPalm1*-RNAi-1 roots in comparison had 87.3% ( $p = 0.002$ ) less *MtPalm1*-transcripts (Figure18c, red) and 84.1% less *MtPt4*-expression ( $p = 0.007$ ) in strong agreement with the prior trials (Figure18f).

For each of the successful knockdown experiments, remaining root material was used for further microscopic analyses after staining of the present fungal structures. For the first knockdown experiment, the small amounts of material for each group were pooled so it should be noted that difference between individual roots could not be measured. The resulting samples were then counted blindly as described under 3.8.8. In the initial experiment, both control pools yielded very similar results with an overall mycorrhization rate of an average 41% for the *gus*-control 1 set and 45.5% for *gus*-control 2 as well as similar arbuscule abundance at 26.6% and 30.9%, respectively (Figure18g). By comparison, *MtPalm1*-RNAi-1 root fragments were approximately 22.8% mycorrhized with only 11.7% of all sections counted containing arbuscules, which represents reductions by about 45% and 54% compared to the corresponding *gus*-control 1 set. *MtPalm1*-RNAi2 yielded a similar reduction in mycorrhization by 39% compared to the *gus*-controls 2 with 27.8% of observed root sections containing AMF colonization. Arbuscule frequency similarly was halved to 15.2%. These results represent a significant reduction in both mycorrhization overall and arbuscules specifically due to the knockdown of *MtPalm1*. Arbuscule sizes were measured in these samples as well, but no significant differences in comparison to the *gus*-controls were observed (Supplementary Figure S5). These results are generally in agreement with the preceding *MtPt4* transcript measurements. However, the reduction in arbuscular mycorrhiza observed phenotypically was much less severe than the more than 80% reduction of the AM marker gene transcript levels.

In further repetitions, the same samples used for sqRT-PCR-measurements were used for microscopic analysis. The root material from the second knockdown assay exhibited a significant reduction in arbuscules by 56.5% ( $P = 0.001$ ) only in the *MtPalm1*-RNAi-2 set. In these samples, total fungal colonization was likewise reduced by 47.4% ( $P = 0.018$ ) compared to the *gus*-controls. The total number of observed vesicles was reduced as well. Surprisingly, in spite of a similar level of downregulation of AM marker genes measured in the sqRT-PCR, roots expressing *MtPalm1*-RNAi-1 showed no significant reductions in intraradical AMF compared to the controls (Figure 18h). The reason

for this discrepancy is unclear, but such an instability has been observed before in RNAi-knockdown studies using this system (Hartung, 2021).

During the third trial, *MtPalm1*-RNAi-2 yielded no significant downregulation of its target. It was therefore determined to be unlikely that an effect would be observed and only the successful RNAi-1 knockdown was used for counting. This analysis revealed a significant 56.1% ( $P = 0.04$ ) reduction in overall fungal colonization at only 13.1% of root sections counted. Arbuscules and fungal vesicles were also significantly reduced by 66.6% ( $P = 0.04$ ) and 66.2% ( $P = 0.02$ ), respectively (Figure 18i).

The results from this knockdown show that a reduction of around 80% in *MtPalm1* transcript levels repeatedly led to significant reductions in fungal marker genes, as well as total AM colonization, pointing to an important regulatory role of *MtPALM1* in the arbuscular mycorrhiza symbiosis.

#### 4.2.6 Negative effects of a *MtPALM1*-KO on the arbuscule rate and overall AM colonization were partially rescued via the introduction of a functional gene copy

As further proof of the role of *MtPALM1* in AM-symbiosis, plants containing an insertion mutation in the *MtPalm1* gene were used in another mycorrhization experiment. This was done in direct comparison to transgenic roots of the wild-type background as well as the insertion containing mutants with an added functional *MtPalm1* copy. To that end, the *Tnt1*-insertion line NF18424 of the *M. truncatula* R108 cultivar was identified to contain an insertion at position 355 in the CDS of *MtPalm1* (see Figure 19a). Homozygous offspring exhibiting the expected pentafoliate phenotype were confirmed via PCR and sequence analyses and could then be used for this assay: *MtPalm1-Tnt1* mutant plants were inoculated with *R. rhizogenes* containing either the empty vector (*MtPalm1-Tnt1*-EV) to provide fully *MtPALM1*-deficient plants or a complementation construct (*MtPalm1-Tnt1*-Comp) consisting of the entire 1,979 bp native A17 *MtPalm1* promoter region, followed by the coding region (756 bp) and an additional 1,033 bp region containing the terminator. For an overall reference of the mycorrhization levels, roots of wild-type *M. truncatula* R108 plants were also transformed with the empty vector (WT-EV). All plants with transgenic root systems were mycorrhized using *R. irregularis* spores and subsequently grown for six weeks before harvesting the root material of three plants as one sample into  $LN_2$  ( $n = 3 \times 6$ ).

Transcriptional measurements via sqRT-PCR performed with RNA extracted from seven *MtPalm1-Tnt1*-EV samples revealed no complete abolishing of *MtPalm1*-mRNA due to nonsense-mediated decay (Figure 19b). This was somewhat expected, as the primer pair normally used for sqRT-measurements of *MtPalm1* bind upstream of the *Tnt1*-insertion site. When using primers flanking the

retrotransposon-insertion, no amplicons corresponding to *MtPalm1* were produced, as confirmed via sequencing. This additional scrutiny confirmed the complete knockout (Supplementary Figure S6). The residual expression quantified stems from erroneous PCR-products as marked by the red X in Figure 19c). Roots expressing the *MtPalm1* complementation construct in the mutant background exhibited significantly elevated *MtPalm1*-expression levels (2.93-fold,  $p = 0.005$ ) as compared to the WT-EV control set using the standard primers (Figure 19b, red). This is likely an effect of the addition of another gene copy to the non-functional transcripts as measurements using the *Tnt1*-flanking primers did not corroborate these findings (Figure 19c).

Expression levels of arbuscule marker gene *MtPt4* were significantly reduced ( $p = 0.041$ ) by an average 63.4% in the *MtPalm1-Tnt1*-EV group compared to the WT-EV controls in agreement with the RNAi-knockdown results, as indicated in Figure 19d). In the mutants with the complementation construct, *MtPt4* transcript levels were not significantly reduced ( $p = 0.091$ ), though on average the measurements were still lower compared to the controls (-48.6%).

As with the RNAi approach, AMF structures in the remaining root material were counted as depicted in Figure 19e, confirming the results of the *MtPt4* measurements: In the MtPALM1-deficient roots, overall mycorrhization was reduced significantly ( $p = 0.034$ ) by 34.5% compared to the WT-EV controls. As was the case during the RNAi-knockdown trials, root sections containing arbuscules were even more strongly diminished at 54.4% ( $p = 0.044$ ) compared to the controls. The frequency of vesicles observed was similarly down to 57.8% ( $p = 0.03$ ). Solely the average occurrence of internal hyphae did not change between sample sets. In *MtPalm1-Tnt1*-Comp roots, observed frequencies of all AMF-structures were in between the measurements for the other two experimental groups and not significantly different from either one, showing the same trend as the sqRT-measurements, together indicating an incomplete rescue of the MtPALM1-deficiency.

A repetition of this experiment could not be fully completed. However, counting of fungal structures overall revealed the same trend towards a reduction in overall mycorrhization and arbuscules due to the deficiency in *MtPalm1* (Supplementary Figure S13). These experiments, together with the RNAi-based knockdowns serve as strong evidence for MtPALM1 acting as an important positive regulator for the AM-symbiosis in general and arbuscule-formation in particular.

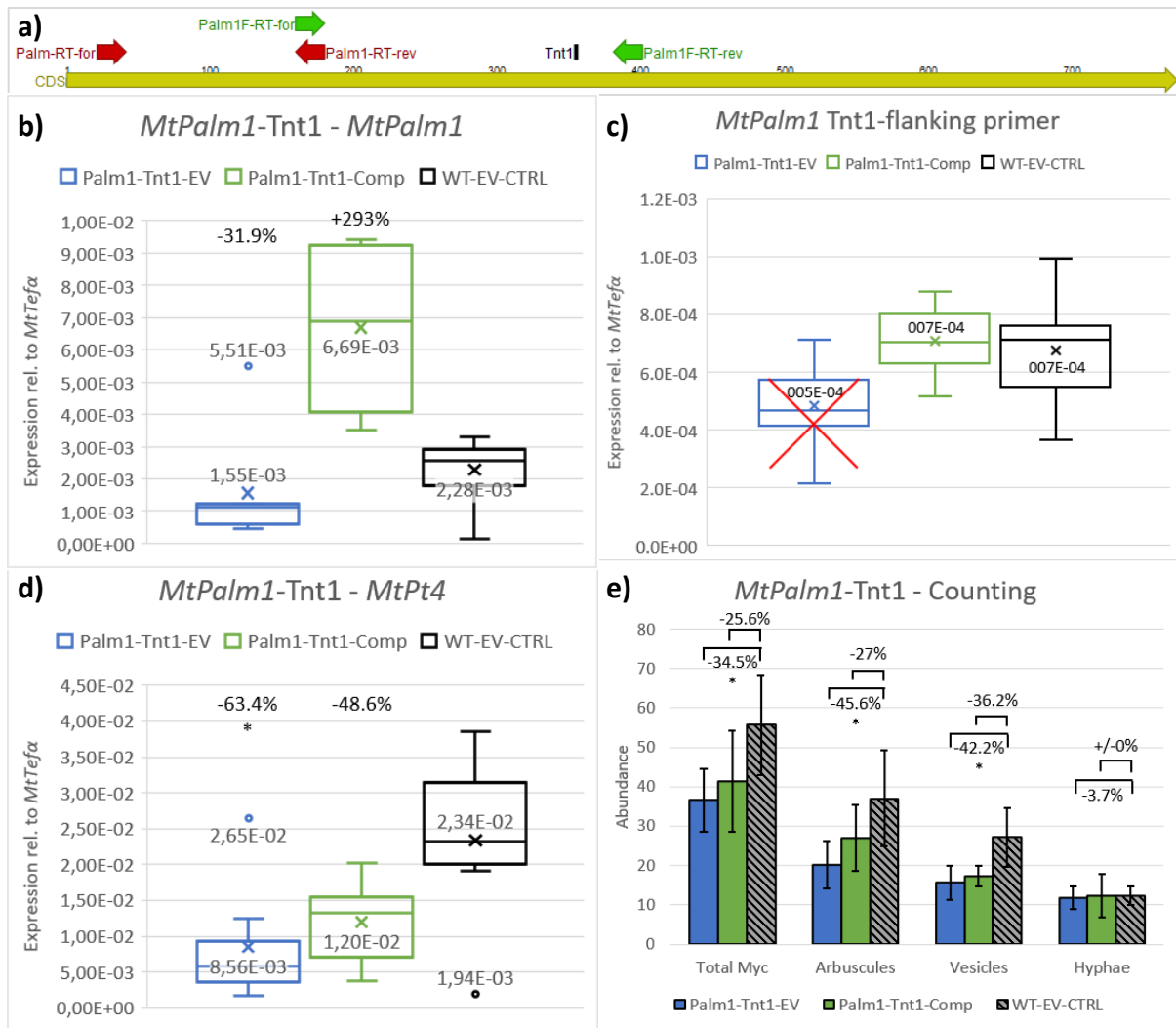


**Figure 19 – Effects of a *MtPalm1-Tnt1*-knockout and -complementation on the expression of AM-marker *MtPt4* and overall AM-colonization**

The *M. truncatula* R108 *Tnt1*-retrotransposon insertion line NF18424 was determined to contain an insertion in the CDS of *MtPalm1* as depicted in black under a). Arrows indicate binding sites of primers pairs used for sqRT-PCR measurements: red was the standard primer pair used in previous experiments; the primers flanking the *Tnt1*-insertion site are marked in green and blue indicates an additional downstream primer pair. Transgenic roots containing either a secondary gene copy of *MtPalm1* (*MtPalm1-Tnt1-Comp*) or the empty vector (*MtPalm1-Tnt1-EV*) were induced in the homozygous *Tnt1*-mutant background. Additionally, wild-type plants with the empty vector served as controls (WT-EV-CTRL). These plants were mycorrhized using *R. irregularis* spores and harvested for RNA-isolation after 42 dpi (n = 3 x 6). SqRT-PCR measurements were performed using the standard primers (b) and the *Tnt1*-flanking primers (c). Box plots under d) depict the transcript amounts measured for *MtPt4*. The (X) indicates measured transcripts determined to be erroneous as confirmed via sequencing. Numbers shown represent the respective arithmetic means also marked by the x as well as outlier measurements outside 1.5 x IQR. Remaining root material was used for quantification (total numbers observed in 300 root sections per sample) of fungal structures within the roots represented as arithmetic mean by bar chart e). Error bars represent 95% confidence intervals, asterisks mark statistical significance of differences between experimental conditions at 95% (\*), 99% (\*\*), and 99.9% (\*\*\*) confidence as determined by Student's T-Test.

#### 4.2.7 Transcriptome analysis of *MtPalm1*-knockdown roots via RNASeq reveals a potential involvement in hormonal signaling networks

The prior experiments involving the C2H2-ZF-TF MtPALM1 demonstrated strong induction of the *MtPalm1* gene in and around arbuscocytes and a significant quantitative effect on the AM-symbiosis overall. In order to gain initial indications for concrete functions of MtPALM1 in the context of mycorrhized roots, an RNASeq approach was utilized to obtain transcriptome data. To that end, three 49 dpi mycorrhized RNA-samples from roots expressing *MtPalm1*-RNAi-2 were compared to three of their respective *gus*-controls (attributions to the sqRT-PCR measurements are shown in Figure 20). As a result, out of a total of 52,407 annotated *M. truncatula* genes, transcripts mapping to a total of 31,949 genes were obtained from at least one of the six samples. The initial analysis of this data revealed 3,341 genes out of this entire pool of data to be differentially regulated based on at least a 2-fold induction or reduction of transcript amounts at an FDR-corrected statistical significance of  $p < 0.05$ . When considered separately, 1,633 genes were found to be co-downregulated with *MtPalm1*, whereas 1,708 genes were expressed significantly more highly in the knockdown roots than in the controls (see also Figure 21a).

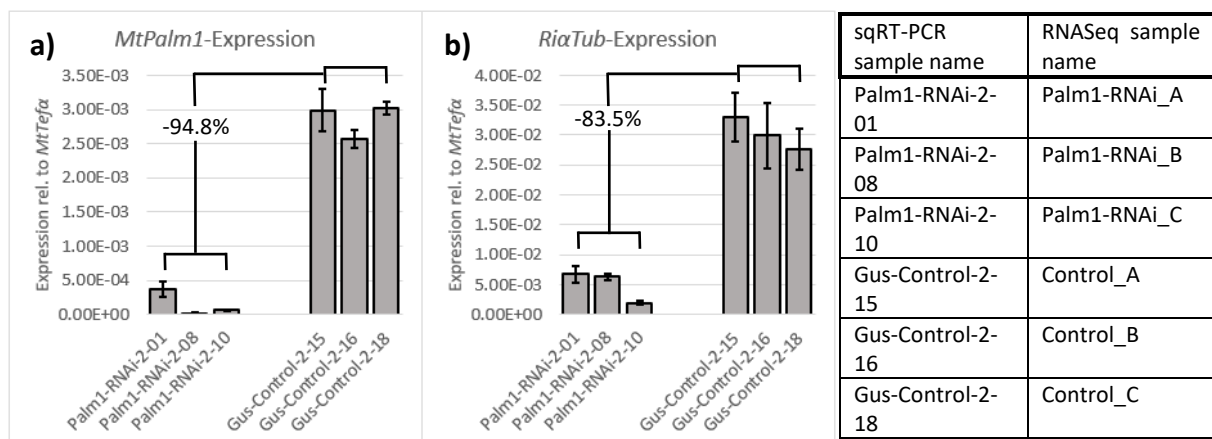


**Figure 20 – Expression of *MtPalm1* and *RiaTub* in the RNA-samples used for the RNASeq analysis**

Quantification via sqRT-PCR of mRNAs extracted from single *M. truncatula* 49 dpi mycorrhized roots expressing the *MtPalm1*-RNAi-2 construct in comparison to the respective *gus*-controls. The six samples depicted were used for RNASeq analyses to obtain transcriptome data under conditions of substantially reduced *MtPalm1* expression. Transcript amounts of *MtPalm1* are depicted under a). Based on these measurements, transcripts were barely detectable in the *MtPalm1*-RNAi-2 sample 8. AMF marker gene *RiaTub* (shown in b) was significantly reduced by an average 83.5% in the *MtPalm1*-RNAi samples compared to the controls. The Table to the right contains the attributions of sample names used during sqRT-PCR analysis to the sample names used in the RNASeq study.

Clustering analyses performed on the six conditions (shown in Figure 21b) revealed the expected strong co-induction or -reduction of the differentially expressed genes under RNAi-knockdown or control-conditions, though differences are highlighted as well: A number of strongly upregulated genes in sample *MtPalm1*\_RNAi\_B were not as strongly up- or even slightly downregulated in the other two RNAi-samples. Such differences in the downregulation intensity are also present in the upregulated genes presented in green. This was somewhat expected due to the probable heterogeneity of RNAi-knockdown effects compounding with divergent mycorrhization levels between repetitions. The overall smaller impact of the latter effects is also the likely cause of the less severe differences between the three control-samples.

The reads from 78 differentially regulated genes did not map to any of the gene models from the *M. truncatula* genome version 4 (Mtv4). As such, a number of differentially regulated genes were included as novel genes, despite being annotated in genome version 5 (Mtv5). Further analyses against the updated Mtv5 annotation data allowed the identification of 62 of these genes, most crucially including *MtZf2* (see also Supplementary Figure S7). As such, transcripts from 16 novel genes were obtained as part of this analysis (highlighted in Figure 21a).

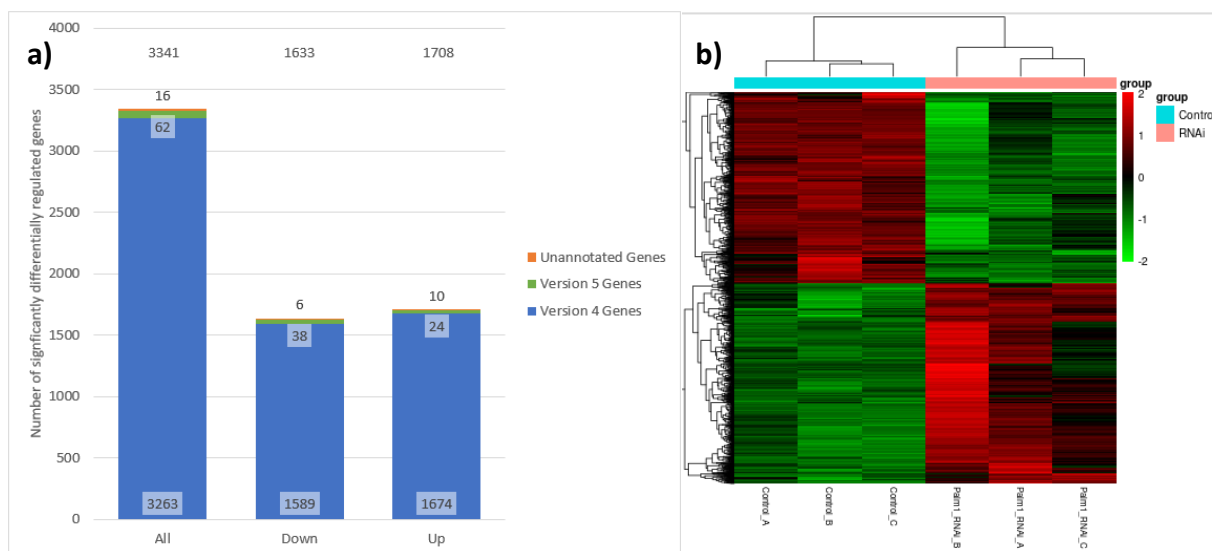


**Figure 21 – Overview of differentially regulated genes in mycorrhized roots expressing an *MtPalm1*-RNAi construct**

Three RNA-samples of mycorrhized roots expressing *MtPalm1*-RNAi-2 were used for RNASeq transcriptome analyses (performed by Novogene, Cambridge, UK) in comparison to three controls containing the GUS-control construct. As a result, 3,341 genes in total were found to be significantly differentially regulated (at least 2-fold increase or decrease in transcript reads, FDR-corrected  $p < 0.05$ ) under *MtPALM1*-deficient conditions. Reads were mapped to the *M. truncatula* genome Mtv4 gene models, which included annotations for 3,263 of these genes (a, in blue). Another 62 genes could be identified as annotated in the newer Mtv5 genome (green). 16 unannotated genes remained (orange). Of these differentially regulated genes, 1,633 were downregulated with *MtPalm1*, while 1,708 were upregulated. Clustering analyses performed as part of routine data analyses of Novogene shown under b) revealed stronger overlap in co-up- and downregulated genes between the control-samples than the samples treated with the *MtPalm1*-RNAi construct.



As expected, based on the strong reduction of AM marker gene expression during prior sqRT-PCR analyses and the reduction in overall colonization observed as part of the morphological analyses, a number of genes with AM-dependent expression could be identified in the significantly downregulated part of the dataset. Outlined in Figure 22a) in blue are a number of known and potential TFs related to AM-conditions and their relative average transcript abundance under knockdown conditions compared to the controls. This set includes a number of AM-induced AP2/ERF-TF genes including the *MtWri5*-likes *a*, *b* and *c* largely responsible for controlling the AM-dependent FA-biosynthesis (Luginbuehl *et. al*, 2017), crucial GRAS-TFs such as *MtRam1*, *MtRad1* and the *MtNsp*-genes (Delaux *et. al*, 2013; Gobbato *et. al*, 2013; Park *et. al*, 2015), some strongly AM-induced CCAAT-box binding factors (Cbf) of as of yet unknown function (Hogekamp *et. al*, 2011; Steven Krüger, LUH, unpublished) as well a variety of other genes including CYCLOPS, *Myb1* (Yano *et. al*, 2008; Floss *et. al*, 2017) and all ZF-candidate genes that are subject of this work. In this context, the downregulation of AM-dependently expressed GRAS-TF gene *MtGras7* (Hartmann *et. al*, 2019) was especially severe, with only small remaining detectable transcripts in one of the three samples.

In addition, a number of known AM-functional genes were also found in the *MtPalm1*-RNAi co-downregulated data, such as those encoding the MtLYR and MtLYK4 receptor-kinases, arbuscule structural proteins like MtBCP1 and MtSbtM1, AM-specific transporters such as MtSTR/STR2 responsible for FA-export, the ammonium-transporters MtAMT2;3/4 and metabolic enzymes like the MtSucS1, the SL-biosynthesis gene *MtDwarf27* as well as MtFatM and MtRAM2 involved in lipid-synthesis.

It should be noted that the expression of *MtPalm1* itself was quantified incorrectly as part of these analyses, due to the presence of transcripts from the RNAi-knockdown constructs, which map specifically to the 3'-region of the CDS. When not correcting for this, an average 15.6% residual transcripts were still present. However, visualization of reads mapped to *MtPalm1* reveals residual transcripts only in one out of the three samples examined (*MtPalm1*-RNAi\_A, see also supplementary Figure S8). This is in agreement with sqRT-PCR measurements performed with these three samples as outlined under Figure 20), demonstrating almost complete abolishment of *MtPalm1* transcripts in the samples used for the RNASeq study.

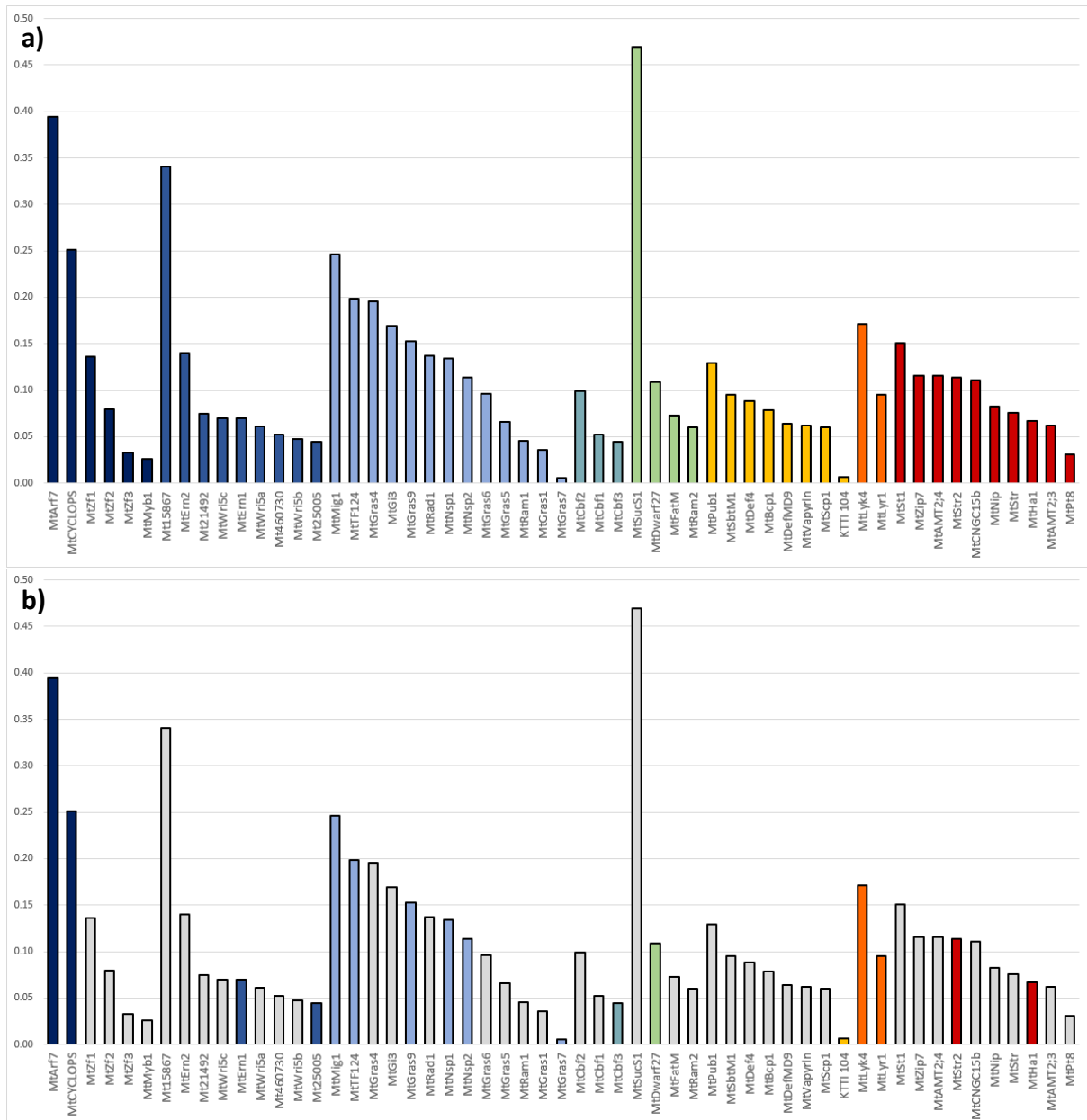


**Figure 22 – Known or putative AM-related genes downregulated in mycorrhizal roots expressing *MtPalm1*-RNAi**

RNAseq transcriptome analyses were performed on three samples from 49 dpi mycorrhizal *M. truncatula* roots expressing *MtPalm1*-RNAi-2 in comparison to three *gus*-controls. Relative transcript abundance of a number of known AM-related genes exhibiting significant downregulation in the MtPALM1-deficient conditions (FDR-corrected  $p < 0.05$ ,  $\geq 2$ -fold change) are depicted. The above set of bar charts under a) includes various (putative) TFs in blue, including the *MtZf* genes subject to this work *MtZf1*, 2 and 3, as well as those encoding TFs from the AP2/ERF-, GRAS-, and CBF-families. In addition, genes corresponding to known enzymes important for AM-symbiosis are shown in green, structural proteins in yellow, receptors in orange and transporters in red. The lower graphic b) only shows colored bars for genes more strongly downregulated in the absence of MtPALM1 than observed in Myc- conditions.

In general, this analysis further demonstrates the reduction of overall AM in *MtPalm1*-deficient root systems. However, a number of genes observed to be less strongly expressed under RNAi-conditions will be due to this generalized reduction of mycorrhization and not any specific regulation by MtPALM1. To account for this, the differentially regulated genes obtained from this RNASeq-experiment were compared to transcriptome data obtained from two prior experiments: mycorrhized roots deficient in *MtRam1* in comparison to wild-type roots (Hartmann, 2018) and expression profiles from *M. truncatula* roots inoculated with the AM fungi *R. irregularis* and *Glomus mossae* in comparison to non-mycorrhized conditions (Hohnjec, LUH, unpublished data). Specifically, stronger up- or downregulation in the MtPALM1-deficient data than in these two datasets was defined as the criterion to accept potential targets of direct or indirect regulation through *MtPalm1*.

When applying this additional scrutiny, 1,094 significantly downregulated and 854 significantly upregulated annotated Mtv4 genes remain. When including the additional Mtv5 genes, the numbers increase to 1,109 and 890, respectively (see Figure 23). In detail, this comparison reveals a number of 382 core genes with AM-dependent expression downregulated in all three conditions. 180 AM-related genes common to both RAM1-deficiency and Myc- conditions were not significantly downregulated in the *MtPalm1*-RNAi dataset, while 140 and 274 genes were found exclusively downregulated in *MtRam1*-mutants and non-mycorrhized conditions, respectively. This relatively small number compared to the 1109 downregulated genes in the absence of *MtPalm1* highlight the likelihood that MtPALM1 regulates a number of basic processes outside the scope of the regular AM program.

Co-upregulation exhibits significantly less overlap between these conditions: Only 107 genes comprise the overlap between those upregulated under all three conditions with a much larger 395 genes at the intersection between RAM1-dependence and non-mycorrhized conditions and 650 more abundant genes common to MtPALM1-deficiency and Myc-. This comparison, again, shows the partial independence of the transcriptional reprogramming performed by MtPALM1 compared to other AM-regulatory processes.

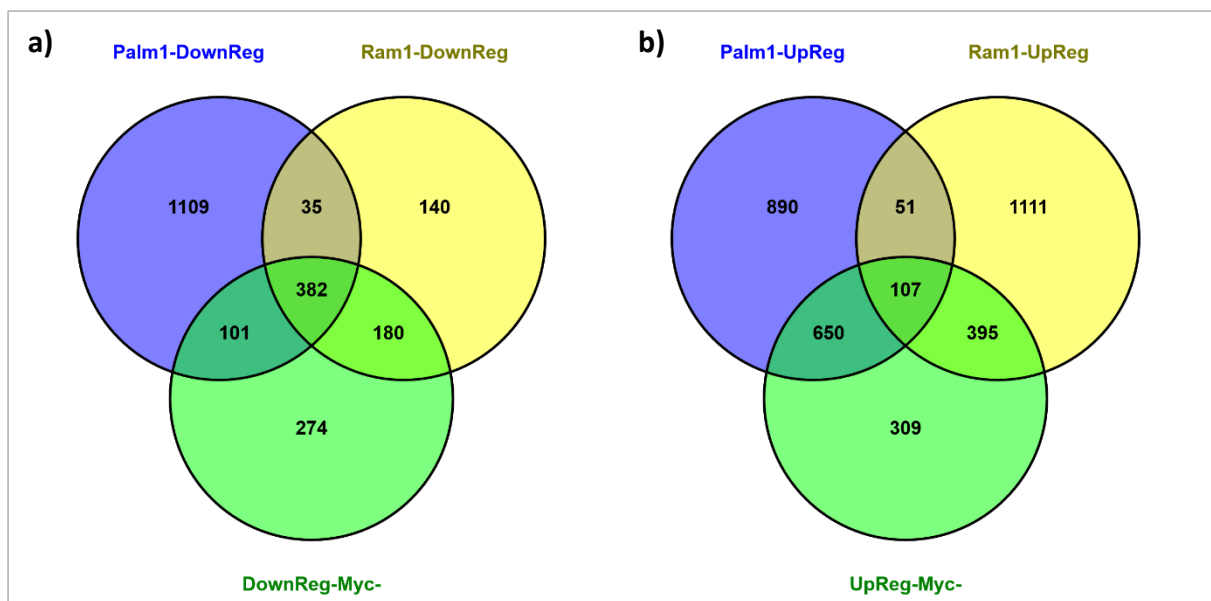


**Figure 23 – Overlap between *MtPalm1*-downregulation and the general AM transcriptional program**

Venn diagrams outlining Co-up- and -downregulation between the RNASeq data obtained from *MtPalm1*-RNAi samples and GeneChip transcriptional profiles from mycorrhized roots of *ram1-1* KO-mutant plants and non-mycorrhized (Myc-) roots. Of all 1,627 annotated (Mtv4 and Mtv5 genome) downregulated genes, 1,109 are more strongly or uniquely downregulated in the roots expressing an *MtPalm1*-RNAi construct. 382 genes central to the AM-symbiosis program are downregulated in all three datasets. 1,698 annotated genes were upregulated under MtPALM1-deficient conditions in mycorrhized roots. When compared to the set of upregulated genes under conditions of reduced (*ram1-1*) or absent mycorrhization, 890 genes remain specifically upregulated in *MtPalm1*-RNAi. Here, only 107 genes are co-upregulated across the datasets, with a larger overlap specifically between Myc- and *MtPalm1*-RNAi (650) as well as Myc- and *ram1-1* (395). (Oliveros, J.C.; 2007-2015; <https://bioinfo.cnb.csic.es/tools/venny/index.html>)

Out of 1,999 potential MtPALM1-targets identified, expression of 54 genes in total was abolished uniquely in all *MtPalm1*-RNAi samples (Supplementary Tables S1 and S2). Conversely, transcripts mapping to 34 genes were only expressed in the absence of *MtPalm1*. When taking into account the potentially complete abolition of functional MtPALM1 from RNAi-samples B and C compared to the few residual transcripts in sample A, 26 additional potential direct regulation targets emerge due to only being detected in *MtPalm1*-RNAi\_A, including already characterized AM-related genes *MtGras7* and AMT2;3 (see also Figure 22b).

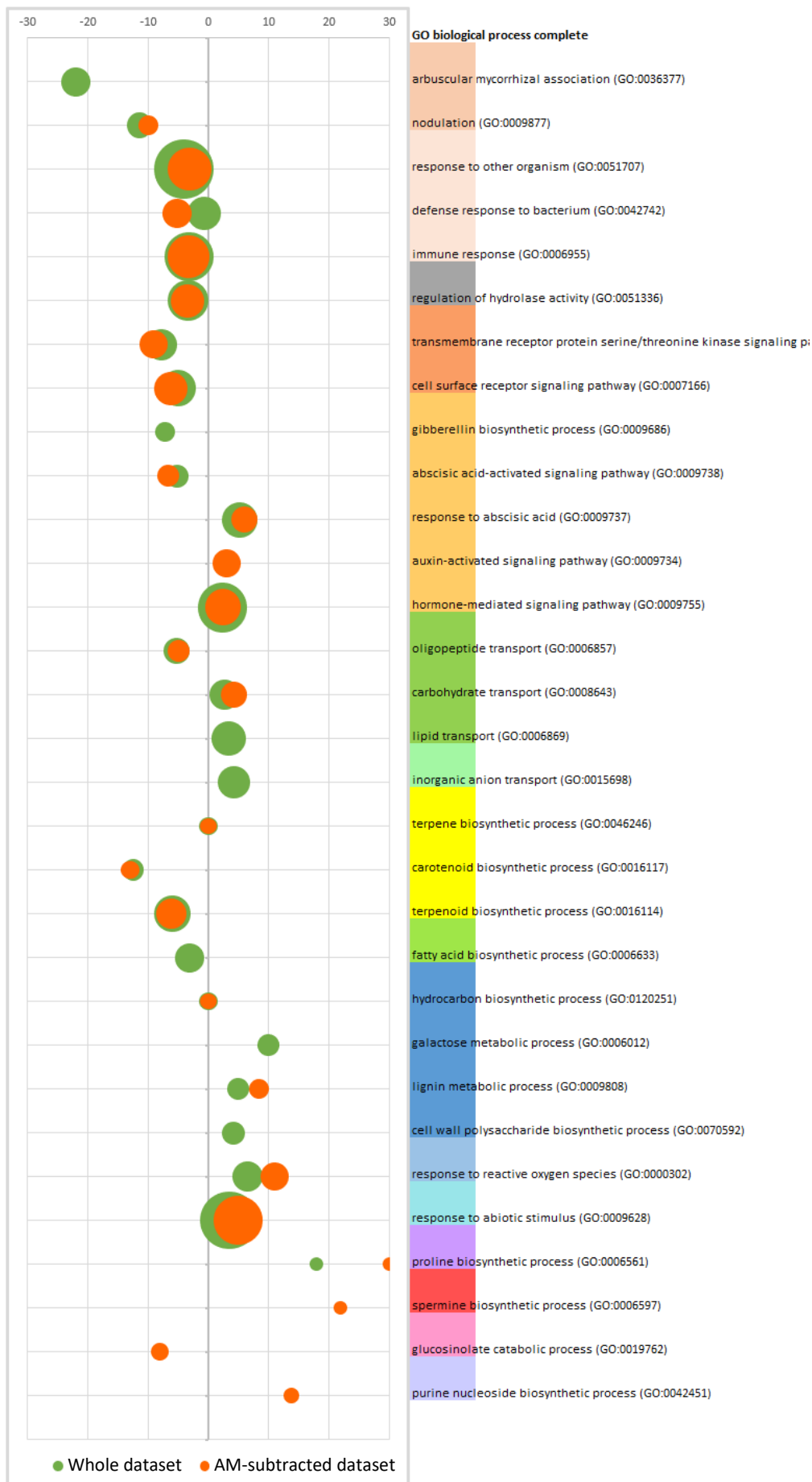




**Figure 24 – GO-enrichment analyses of groups of genes differentially regulation in the absence of MtPALM1**

Depicted are a selection of significantly enriched GO-categories (FDR-corrected  $p < 0.05$ ) among the genes significantly up- or downregulated in the absence of *MtPalm1* compared to the controls. Green bubbles represent the results for entire dataset of 3,341 differentially regulated *Mtv4* annotated genes. Shown in orange is the enrichment for the 1,999 genes remaining after subtracting the influence of overall AM-reduction. Relative sizes of the bubbles represent the number of genes associated with the respective GO-category present in the respective dataset. The position on the X-axis is determined by the intensity of enrichment of categories in the datasets compared to their proportions of all 49,634 *M. truncatula* genes used as reference. Enrichment in the downregulated datasets is shown by placing the bubbles at negative values, while positive values represent enrichment of upregulated genes. GO-categories exhibiting enrichment in both up- and downregulated datasets are placed at 0. Analyses of GO terms (Biological Process, Molecular Function and Cellular Component) were done using the PANTHER 16.0 classification system (Carbon and Mungall, 2018) via <http://geneontology.org/> online.

In order to gain further insight into processes and functions impacted by the *MtPalm1* knockdown, Gene Ontology enrichment analyses were performed. As inputs, both the whole set of 3,341 up- and downregulated *M. truncatula* Genome version4 and the 1,999 differentially regulated genes remaining after accounting for differences due to less overall mycorrhization (“AM-subtracted dataset”, outlined in prior section and in Figure 23) were used.

As a result, a number of GO-classifications were significantly overrepresented ( $p < 0.05$ ) under MtPALM1-deficient conditions, as compared to their relative proportion of all annotated *M. truncatula* genes: In total, 475 different categories and sub-categories were enriched across all three major GO-terms with 256 belonging to “Biological Process”, 194 being associated with “Molecular Function” and 25 belonging to “Cellular Component”. A number of representative GO-classifications and their relative enrichment in both full and AM-subtracted datasets is visualized in Figure 24.

Unsurprisingly, genes associated with the process of AM symbiosis were heavily overrepresented in the group of *MtPalm1* co-downregulated genes, probably due to the observed significantly reduced overall mycorrhization (top of Figure 24, green). This influence was successfully removed by the employed strategy of subtracting genes generally downregulated under RAM1-deficient and Myc-conditions, as indicated by the absence of any datapoint from the AM-subtracted dataset for the GO-category “arbuscular mycorrhiza association”. Similarly, other processes related to AM-symbiosis are only enriched in the whole dataset, such as FA-biosynthesis as required for the lipid supply of the fungus (“fatty acid biosynthetic process”) and genes involved in the synthesis of gibberellins for regulation of mycorrhization.

In contrast to these categories appearing as downregulated, genes associated with galactose-metabolism and cell-wall biogenesis are more upregulated under reduced AM-conditions, likely due to requiring less supply of sugars to the symbiotic fungus. “Lipid transport” and “inorganic ion transport” are likewise increased in less strongly mycorrhized, MtPALM1-deficient roots. This is supported further by significant differential regulation observed for the “Molecular Function” of various ion-transporters, especially ammonium-transporters involved with AM. Lastly, downregulated genes involved with the periarbuscular membrane (under GO-term Cellular Component) only appear enriched in the dataset without subtracted AM-influences, providing further evidence for the validity of this strategy.

Interestingly, some sets of AM-associated genes were not eliminated via the subtraction strategy and are therefore more likely candidates for a direct or indirect regulation by MtPALM1 (compare orange and green bubbles overlapping in Figure 24): These include some organic transporters such as for sugars and amides as well as a number of TFs, including CYCLOPS, MtNSP1/2, ERN1 and various CCAAT-box binding factors, which appear as their own category under the GO-term “Cellular Component”.

Furthermore, various defense-response related groups of genes remain enriched among those downregulated in the *MtPalm1*-RNAi roots, despite the subtraction of AM-influences, including an apparent reduced activity of hydrolases. In addition, a number of other potentially stress- or defense-related genes appear as specifically regulated in the AM-subtracted dataset. These include proline-biosynthetic processes that can be related to a variety of stresses, including oxidative stress responses that also appear induced in the absence of MtPALM1. Similarly, genes associated with the synthesis of spermine, a polyamine involved in stress responses as well as AM-symbiosis are more upregulated while catabolism of likewise stress-related glucosinolates appears as reduced. Other processes and functions differentially regulated with lower *MtPalm1* expression level include nucleotide-metabolism and metal-ion binding proteins.

The processes outlined above are likely candidates for a regulation by MtPALM1, though it is unclear whether this is due to direct regulation or might be a consequence of several differentially regulated signaling components inducing broader effects. Such a potential explanation is reflected by a number of proteins annotated as part of transmembrane signaling pathways being significantly downregulated in both the full and AM-reduced datasets, with serine/threonine-kinases standing out specifically.

Even more specific effects can be gleaned from hormonal signaling, where besides gibberellin-biosynthesis, also genes associated with abscisic acid (ABA) and auxin responses are differentially regulated. Interestingly, in the “biological process” enrichment analysis, genes associated with ABA signaling appear overrepresented in downregulated datasets, while ABA-responsive genes are more prevalent amongst the upregulated section, perhaps indicating a negative regulation of these genes by ABA. Interestingly, auxin signaling pathway components appear overrepresented among the upregulated genes only in the AM-subtracted dataset (indicated by the sole presence of a green bubble in Figure 24), suggesting a strong regulatory influence of MtPALM1 on these hormonal signals.

Finally, genes involved in terpenoid biosynthetic processes that, among other metabolites, lead to the production of carotenoid-derived phytohormones such as the gibberellic acids (GA) and abscisic acid, as well as AM-promoting strigolactones (SL) appear differentially regulated as well, possibly suggesting a mechanism by which *MtPalm1* might act on these pathways.



**Table 20 – Differentially regulated genes annotated as part of biosynthetic and signaling pathways**

This table shows all annotated differentially regulated genes involved in the pathways shown in Figures 25 and 26. Information includes the associated Mtv4-IDs, a short description of the annotation according to the KEGG-database, the associated BRITE-IDs, the process the gene product is putatively involved in, whether it appears in the full or AM-subtracted data and up- or downregulation under MtPALM1-deficient conditions.

Mtv4 ID	KEGG Orthology	BRITE ID	Process	Dataset	Regulation
Medtr7g011663	ent-copalyl diphosphate synthase	5.5.1.13	GA-Syn	Subtracted	-
Medtr3g058160	ent-kaurene synthase	4.2.3.19	GA-Syn	Subtracted	-
Medtr2g105360	ent-kaurene oxidase	1.14.14.86	GA-Syn	Full	-
Medtr2g031930	ent-kaurenoic acid monooxygenase	1.14.14.107	GA-Syn	Subtracted	-
Medtr4g005230	beta-amyrin 11-oxidase	1.14.14.152	GA-Syn	Full	-
Medtr1g102070	gibberellin-44 dioxygenase	1.14.11.12	GA-Syn	Full	-
Medtr1g011580	gibberellin 3-beta-dioxygenase	1.14.11.15	GA-Syn	Subtracted	-
Medtr4g074130	gibberellin 2-beta-dioxygenase	1.14.11.13	GA-Cat	Full	-
Medtr2g070870	gibberellin 2-beta-dioxygenase	1.14.11.13	GA-Cat	Subtracted	+
Medtr4g123020	gibberellin 2-beta-dioxygenase	1.14.11.13	GA-Cat	Subtracted	+
Medtr5g076620	15-cis-phytoene synthase	2.5.1.32	Carotene	Subtracted	+
Medtr3g083630	15-cis-phytoene synthase	2.5.1.32	Carotene	Full	-
Medtr3g084830	15-cis-phytoene desaturase	1.3.5.5	Carotene	Subtracted	-
Medtr1g081290	zeta-carotene desaturase	1.3.5.6	Carotene	Subtracted	-
Medtr1g054965	prolycopene isomerase	5.2.1.13	Carotene	Subtracted	-
Medtr1g471050	beta-carotene isomerase DWARF27	5.2.1.14	SL	Subtracted	-
Medtr6g048440	beta-carotene 3-hydroxylase	1.14.15.24	Aba-Syn	Subtracted	+
Medtr7g079440	beta-ring hydroxylase	1.14.-.-	Aba-Syn	Full	-
Medtr4g022850	zeaxanthin epoxidase	1.14.15.21	Aba-Syn	Subtracted	+
Medtr7g116630	violaxanthin de-epoxidase	1.23.5.1	Aba-Syn	Subtracted	+
Medtr2g086730	capsanthin/capsorubin synthase	5.3.99.8	Aba-Syn	Subtracted	-
Medtr2g070460	9-cis-epoxycarotenoid dioxygenase	1.13.11.51	Aba-Syn	Subtracted	+
Medtr5g025270	9-cis-epoxycarotenoid dioxygenase	1.13.11.51	Aba-Syn	Full	+
Medtr1g019410	(+)-abscisic acid 8'-hydroxylase	1.14.14.137	Aba-Syn	Subtracted	+
Medtr8g072260	(+)-abscisic acid 8'-hydroxylase	1.14.14.137	Aba-Syn	Subtracted	-
Medtr2g040060	lycopene epsilon-cyclase	5.5.1.18	Lutein	Subtracted	+
Medtr7g079440	beta-ring hydroxylase	1.14.-.-	Lutein	Full	-
Medtr6g048440	beta-carotene 3-hydroxylase	1.14.15.24	Lutein	Subtracted	+
Medtr1g062190	carotenoid epsilon hydroxylase	1.14.14.158	Lutein	Subtracted	+
Medtr3g078170	NAD-dependent aldehyde dehydrogenase family protein	1.2.1.3	Auxin-Syn	Subtracted	+
Medtr3g088150	NAD-dependent aldehyde dehydrogenase family protein	1.2.1.3	Auxin-Syn	Subtracted	+
Medtr2g042330	NAD-dependent aldehyde dehydrogenase family protein	1.2.1.3	Auxin-Syn	Subtracted	+
Medtr7g107710	indole-3-pyruvate monooxygenase	1.14.13.168	Auxin-Syn	Subtracted	+
Medtr1g069275	indole-3-pyruvate monooxygenase	1.14.13.168	Auxin-Syn	Subtracted	+
Medtr7g107690	indole-3-pyruvate monooxygenase	1.14.13.168	Auxin-Syn	Full	+
Medtr4g415390	auxin influx carrier	-	Auxin	Subtracted	-
Medtr3g072870	auxin influx carrier	-	Auxin	Subtracted	+
Medtr5g024640	Auxin efflux carrier	-	Auxin	Subtracted	+
Medtr7g096090	auxin-responsive protein IAA	-	Auxin	Full	+
Medtr8g014520	auxin-responsive protein IAA	-	Auxin	Subtracted	+
Medtr1g070520	auxin-responsive protein IAA	-	Auxin	Subtracted	+
Medtr2g093740	auxin response factor-like protein	-	Auxin	Subtracted	-
Medtr4g124900	auxin response factor 2 gene	-	Auxin	Subtracted	+
Medtr8g014520	auxin response factor gene	-	Auxin	Full	+
Medtr7g094190	auxin responsive GH3 gene family	-	Auxin	Subtracted	-
Medtr5g016320	auxin responsive GH3 gene family	-	Auxin	Full	+
Medtr1g063950	SAUR family protein	-	Auxin	Subtracted	-
Medtr7g405740	SAUR family protein	-	Auxin	Full	-
Medtr4g072910	SAUR family protein	-	Auxin	Subtracted	-
Medtr7g101740	SAUR family protein	-	Auxin	Subtracted	-
Medtr1g089310	gibberellin receptor GID1	3.-.-.-	GA	Full	+

Medtr4g114640	EIN3-binding F-box-like protein	-	GA	Subtracted	+
Medtr7g110810	helix loop helix DNA-binding domain protein	-	GA	Subtracted	+
Medtr5g083270	abscisic acid receptor PYR/PYL	-	Aba	Subtracted	-
Medtr7g070050	abscisic acid receptor PYR/PYL	-	Aba	Subtracted	-
Medtr3g071740	abscisic acid receptor PYR/PYL	-	Aba	Subtracted	-
Medtr4g014460	abscisic acid receptor PYR/PYL	-	Aba	Subtracted	-
Medtr5g030500	abscisic acid receptor PYR/PYL	-	Aba	Subtracted	-
Medtr5g009370	protein phosphatase 2C	3.1.3.16	Aba	Subtracted	+
Medtr8g102550	protein phosphatase 2C	3.1.3.16	Aba	Subtracted	+
Medtr3g068200	protein phosphatase 2C	3.1.3.16	Aba	Subtracted	+
Medtr1g028300	protein phosphatase 2C	3.1.3.16	Aba	Subtracted	+
Medtr5g080680	protein phosphatase 2C	3.1.3.16	Aba	Subtracted	+
Medtr3g086940	serine/threonine-protein kinase SRK2	2.7.11.1	Aba	Subtracted	-
Medtr5g064540	serine/threonine-protein kinase SRK2	2.7.11.1	Aba	Full	+
Medtr4g099240	serine/threonine-protein kinase SRK2	2.7.11.1	Aba	Full	-
Medtr3g101780	ABA responsive element binding factor	-	Aba	Subtracted	+
Medtr1g098590	ABA responsive element binding factor	-	Aba	Subtracted	+
Medtr2g086390	ABA responsive element binding factor	-	Aba	Subtracted	-

To further investigate any systematic changes in metabolic and signaling pathways, genes differentially regulated under MtPALM1-deficient conditions were mapped to these networks according to their annotation in the “Kyoto Encyclopedia of Genes and Genomes” (KEGG) database. For this purpose and subsequent visualization, including relative induction or repression of the genes involved, the Pathview online tool was used (<https://pathview.uncc.edu/>; Luo and Brouwer, 2013; Luo *et al.*, 2017).

As a result, specific downregulation of genes involved in the production of GAs from terpenoid backbones could be observed in the absence of MtPALM1 as outlined in Figure 25a. This set comprises seven downregulated genes outlined in Table 20 (GA-Syn). Furthermore, several genes potentially involved in the catabolism of the bioactive gibberellic acids GA1, GA3, GA4 and GA7 were upregulated in the *MtPalm1*-RNAi condition (three “GA-Cat” genes in total, see Table 20), suggesting a possible GA reduction in mycorrhized *MtPalm1*-RNAi roots. This analysis therefore proposes a potential role of MtPALM1 in the regulation of AM-colonization through the differential expression of genes involved in GA-biosynthesis and -catabolism.

Similar systematic changes could be observed for the biosynthetic pathways leading to ABA and strigolactones derived from longer carotenoids: Here, four genes contributing to the elongation of carotenes appear downregulated with *MtPalm1* in the AM-subtracted dataset (Figure 25b and Table 20) leading to lycopene. This compound is then further metabolized to SLs in a pathway involving the  $\beta$ -carotene isomerase encoded by the *MtDwarf27* gene, which appears downregulated in the MtPALM1-deficient roots. This might suggest an overall reduction in SLs in the absence of MtPALM1. Likewise, biosynthetic pathways leading away from this synthesis towards abscisic acid and lutein appear as systematically upregulated, suggesting negative regulation by MtPALM1. For the ABA-synthesis pathway, this comprises ten differentially regulated genes (eight in the AM-reduced dataset) and four leading to lutein (three with AM-influence removed, see Table 20).

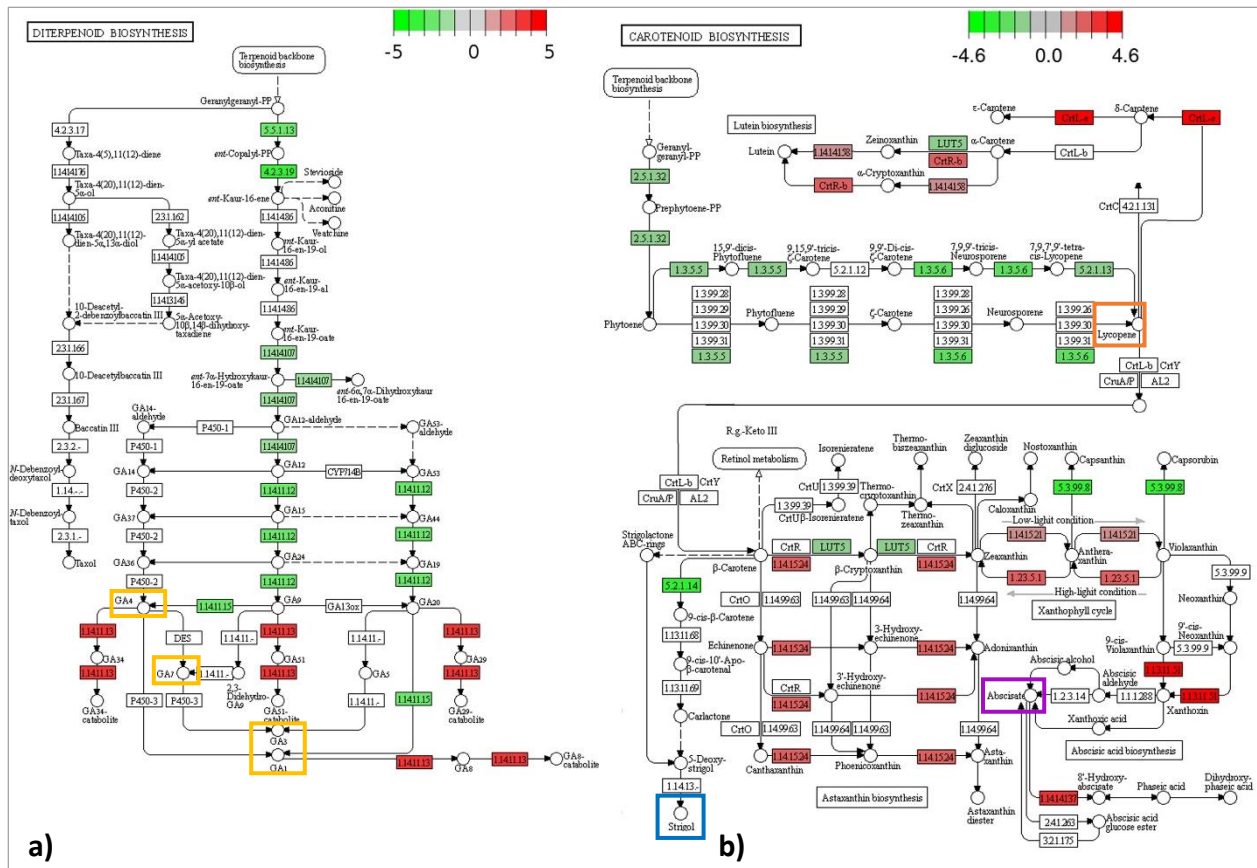
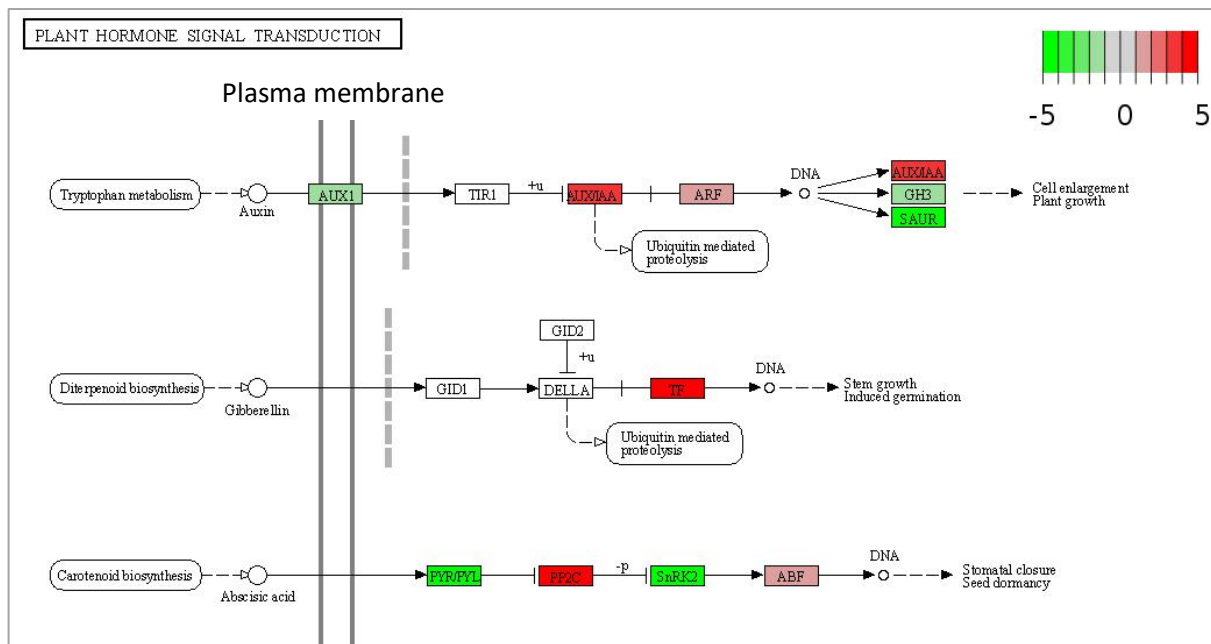


Figure 25 – Terpenoid and carotenoid biosynthetic pathways exhibiting differential regulation in MtPALM1-deficient mycorrhizal roots

Excerpts of metabolic pathway graphs rendered in Pathview. Enzymes encoded by genes downregulated under MtPALM1-deficient conditions are shown in green, while those upregulated in the absence of MtPALM1 are depicted in red. Unaffected genes are shown in white. The diterpenoid biosynthesis pathway under a) leads to the bioactive gibberellic acids GA1, GA3, GA4 and GA7 highlighted by the yellow boxes. The carotenoid metabolism shown under b) includes lycopene (orange), strigolactones (blue) as well as abscisic acid (purple, (Luo and Brouwer, 2013; Luo *et al.*, 2017).

Interestingly, either as a result of a production of less abscisic acid or due to differential regulation by MtPALM1, components of ABA signaling as shown in Figure 26 are also differentially regulated: Genes annotated as ABA receptors are universally downregulated, while the phosphatases they inhibit show increased expression in the absence of MtPALM1 (five genes each, see Table 20). Differential regulation of the further downstream components appears more complex, with the majority (2/3), but not all SRK2-kinases exhibiting lowered expression. Similarly, only two of the three ABA responsive element binding factors in the RNAseq-dataset are upregulated. Still, this pathway analysis provides some evidence towards regulation of ABA homeostasis through MtPALM1. In contrast, responses to gibberellic acid (and other phytohormone-pathways not included in Figure 26) are only minor, with only some downstream TFs responding by upregulation (see Table 20).



**Figure 26 – Selection of phytohormone signaling pathways exhibiting differential regulation in mycorrhized *MtPalm1*-RNAi roots**

Excerpt of a signaling pathway graph rendered in Pathview. Each rectangle represents a component of the respective cascade and can stand for multiple genes. Average induction or reduction of expression of these genes in mycorrhized *MtPalm1*-RNAi roots compared to their respective *gus*-controls is shown in red/green (between 5-fold increase/reduction). Signaling components past the grey dotted lines signify processes in the nucleus (Luo and Brouwer, 2013; Luo *et. al.*, 2017).

Finally, the signaling pathway for the phytohormone auxin appears strongly regulated: Two genes encoding the auxin influx carrier *AUX1* are differentially regulated in *MtPALM1*-deficient mycorrhized, with a tendency for downregulation (see Table 20). In turn, downstream *AUX/IAA* proteins, undergoing negative regulation by upstream components of the signaling cascade, are more strongly expressed under *MtPALM1*-deficient conditions. Regulation of *ARF*-proteins previously shown to negatively regulate *MtPalm1* itself appear less consistent, with some up- and downregulated members (see Table 20). The downstream expression of auxin-responsive genes encoding Gretchen Hagen 3 (*GH3*) as well as *SAUR*-family proteins is downregulated together with *MtPalm1*. Finally, several components of the tryptophan biosynthetic pathway involved in indole-3-acetic acid-biosynthesis (Supplementary Figure S9) are also upregulated in *MtPALM1*-deficient roots, suggesting a role for the TF encoded by *MtPalm1* in the stimulation of auxin production. Overall, this pattern might suggest that the compound-leaf determining factor *MtPALM1* is also an autoregulatory component of the auxin-signaling pathway and could integrate these hormonal stimuli with the transcriptional program regulating AM overall and arbuscule-formation in particular.

### 4.3 Functional analysis of *MtZf1* under AM-conditions

#### 4.3.1 Promoter activity of *MtZf1* is stimulated in the presence of fungal structures and during early AM infection

Based on the existing expression data (Figure 6), induction in the presence of AMF was expected for the *MtZf1* gene. This could already be confirmed through the sqRT-PCR measurements shown in Figure 13. To further determine the spatiotemporal pattern of *MtZf1* activity during the process of mycorrhization, the -1455/-1 region relative to the translational start was cloned upstream of the *gusAint* reporter gene encoding the enzyme  $\beta$ -Glucuronidase. The resulting promoter-*gus* fusion was expressed in *M. truncatula* A17 transgenic roots. Following mycorrhization via inoculation with *R. irregularis* spores, roots were typically stained for 6-8 h, thereby allowing for the visualization of the p*MtZf1* induction. Non-mycorrhized roots grown under the same conditions served as controls.

In these experiments, GUS-activity was strongly associated with the presence of AMF structures. Non-mycorrhized regions of mycorrhized root systems exhibited strongly diminished staining, while completely roots completely devoid of AMF showed no such activity following typical incubation periods of 6-8 h (Figure 27m-p). However, as compared to p*MtPalm1*, *MtZf1* promoter activity did not appear to be specifically focused on arbuscocytes but instead in and around all cortical cells harboring AM structures. This is illustrated by Figure 27a and b, where blue staining is visible around the infected root sections but does not always allow arbuscule-containing cells to be clearly identified. Similarly, the presence intraradical hyphae of *R. irregularis* alone stimulated p*MtZf1* activity in the surrounding cells (Figure 27c, d). This pattern holds true in very young infection units and even for the sole presence of appressoria initiating the infection of the root as indicated by Figure 27g, h). Furthermore, results like the ones shown in Figure 27e) and f) even suggest that *MtZf1* activity occurred in cortical cells in preparation of fungal infection as the staining is visible in parts of the root where the intraradical hyphae are not yet present. Root sections with older infection units still exhibited promoter activity, although staining in the parts with the most degenerated arbuscules appears to be less strong and is possibly only residual (Figure 27i, j). Overall, these results indicate that the activation of *MtZf1* occurs likely in preparation to or at least during the very early stages of fungal colonization of roots or root sections.

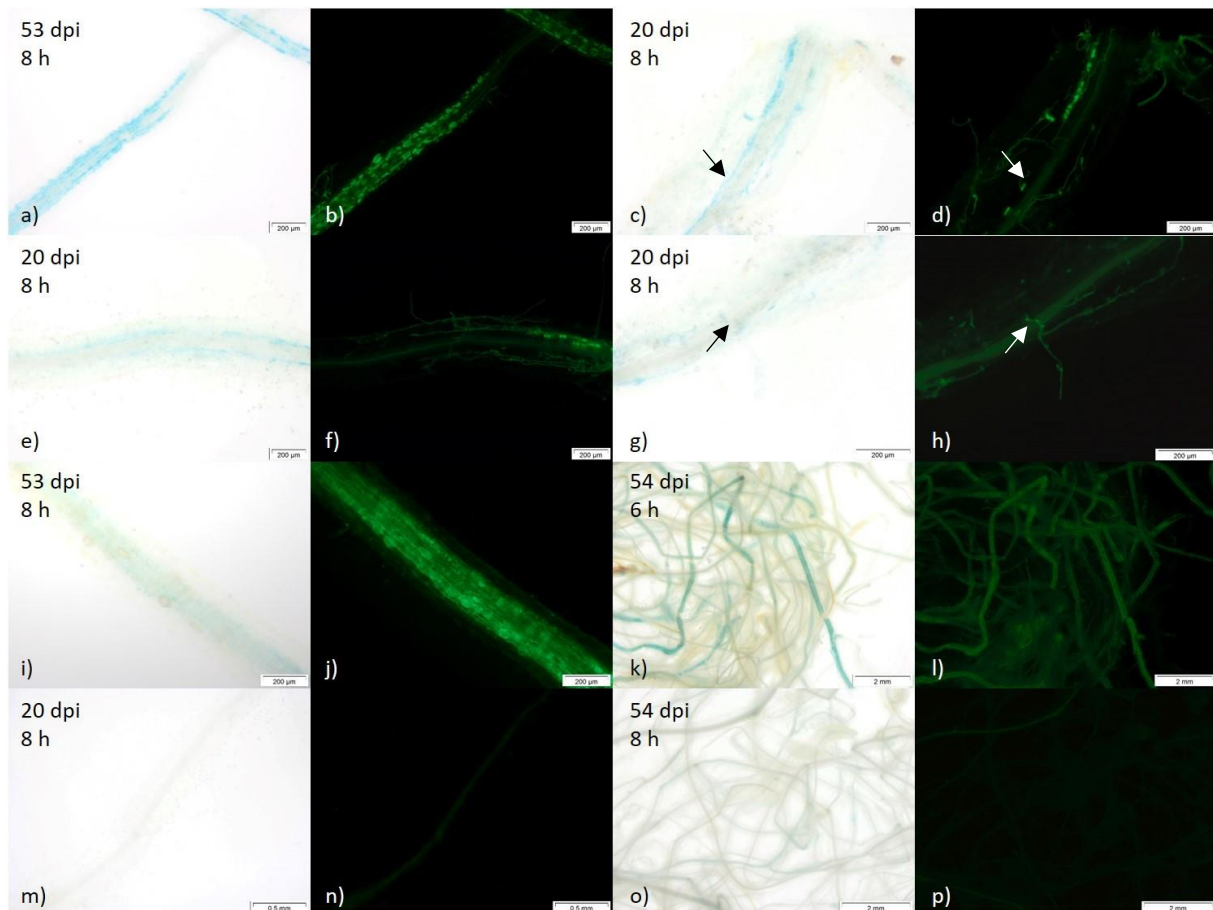


**Figure 27 – Histochemical localization of *MtZf1* promoter activity in wild-type mycorrhized roots**

The pRR:*pMtZf1-gus* construct was expressed in transgenic root systems in the *M. truncatula* A17 WT background. Roots (a-l) were mycorrhized via inoculation with *R. irregularis* spores. Myc- roots (m-p) were grown in parallel. Images were taken after GUS staining of transgenic root systems for the stated time periods (bright field images) and subsequent counter-staining of fungal chitin via Alexa488-WGA. Activation of the *MtZf1* promoter is strongly associated with mycorrhized root sections (a,b,k,l). Very young infection units including appressoria (c,d,g,h) already provoke this response as does the presence of hyphae in the roots (e,f). Root sections containing partially degenerated arbuscules still exhibited *pMtZf1* activation. Non-mycorrhized (Myc-, m-p) exhibit little to no activity.

#### 4.3.2 *MtZf1* promoter activity is not impaired in *ram1-1* and *pt4-2* mutant backgrounds

When testing the *pMtZf1-gus* construct in the *ram1-1* and *pt4-2* mutant backgrounds, no clear differences in comparison to the wild-type GUS-activity could be observed: After 8 h staining, blue coloration could still be seen clearly localized in mycorrhized regions of the roots, suggesting that *MtZf1* acts independently of the key regulator *MtRam1* (Figure 28a-d). The full symbiotic functionality of the arbuscule disrupted in the *pt4-2* mutant line likewise had no negative effect on *pMtZf1* activation (Figure 28e-h). The intensity also appeared unaffected in cells containing clearly truncated or prematurely degenerated arbuscules in either mutant. These results serve as additional evidence that *MtZf1* might serve an early function in the progression of the AMF and thereby prior to establishment of the arbuscules within the root's cells.

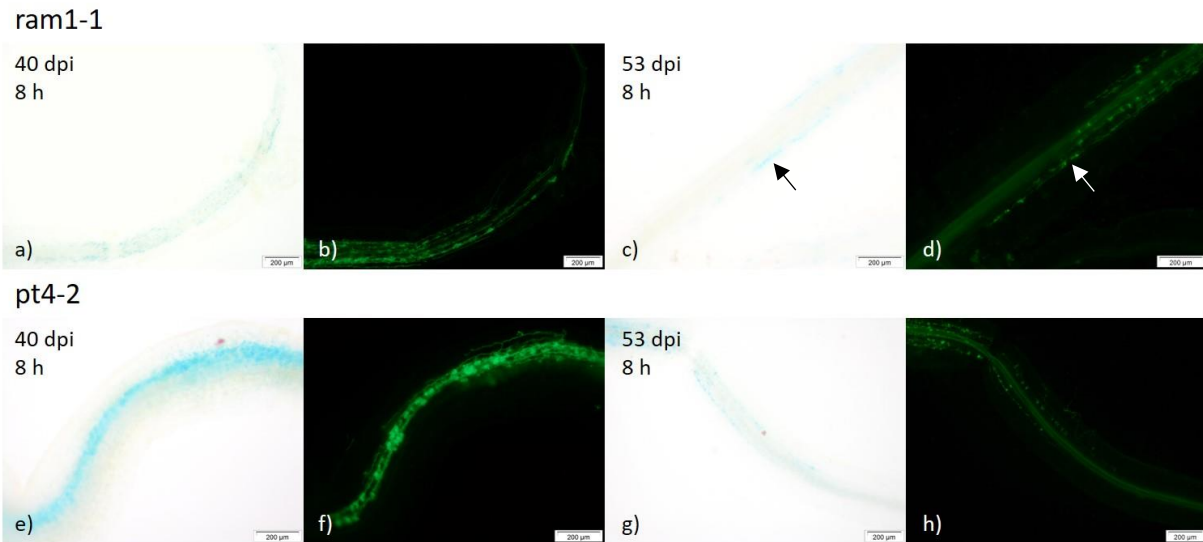


**Figure 28 – Histochemical localization of *MtZf1* promoter activity in mycorrhized roots of *ram1-1* and *pt4-2* mutants**

The pRR:p*MtZf1-gus* construct was expressed in transgenic root systems in the *M. truncatula ram1-1* and *pt4-2* mutant backgrounds. All roots depicted were mycorrhized via inoculation with *R. irregularis* spores. Images were taken after GUS staining of transgenic root systems for the stated time periods (bright field images) and subsequent counter-staining of fungal chitin via CF488-WGA. Images a-d depict the activity of p*MtZf1* in RAM1-deficient mycorrhized roots, which is fully retained. *MtZf1* promoter activity in roots deficient in nutrient exchange (*pt4-2*) likewise is not reduced, neither in the presence of arbuscules with a wild-type-like phenotype (e,f) nor around degenerated arbuscules (g,h).

#### 4.3.3 Overexpression of *MtZf1* had no significant effect on the AM symbiosis

As the initial transcriptional and promoter analysis suggested an induction of *MtZf1* in the presence of early AMF structures, an *MtZf1*-overexpression experiment might lead to increased infections or a higher number of arbuscules. To that end, the *MtZf1*-CDS was placed under control of a constitutive CMV-35s-promoter and ectopically overexpressed in transgenic roots induced via *R. rhizogenes* in the *M. truncatula* A17 background. These roots, as well as a set of controls carrying an empty vector, were mycorrhized via inoculation with *R. irregularis* spores. At 42 dpi, roots samples consisting of three root systems each were frozen in IN<sub>2</sub> for subsequent RNA-extraction.



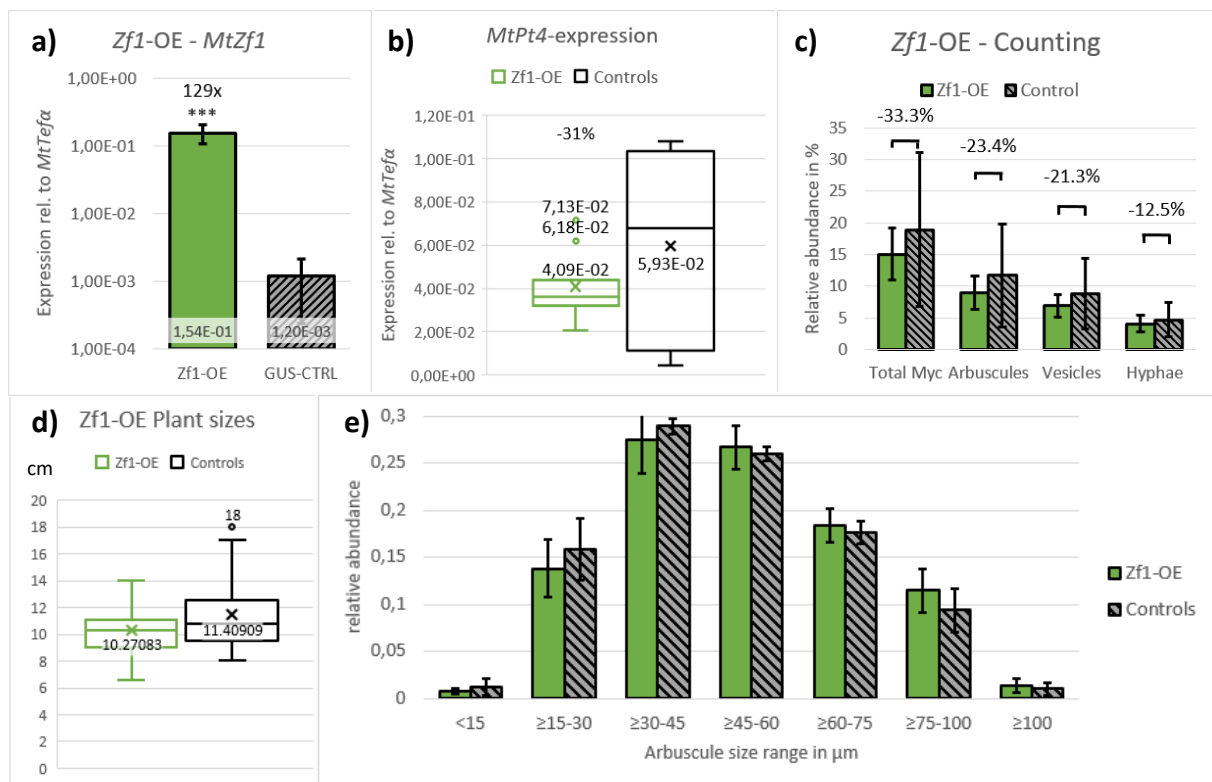


**Figure 29 – Effects of *MtZf1*-overexpression on AM-colonization and arbuscule sizes**

*MtZf1* was constitutively overexpressed in transgenic root systems of the *M. truncatula* A17 cultivar under control of a CMV-35s-promoter. Transformed roots were mycorrhized via inoculation with *R. irregularis* spores. Plants grown with transgenic roots carrying the empty vector were used as controls under the same conditions. At 42 dpi, roots were flash frozen ( $n = 8$  for each group) for subsequent RNA-isolation and sq-RT-PCR measurements. The bar charts under a) represent mean expression levels of the overexpression roots compared to the controls. Measurements of the AM-marker gene *MtPt4* are represented in b) as box plots. Remaining root material of both OE- and control-roots was used for quantification (percentage of 300 root sections per sample) of internal AMF colonization shown as bars in c). During harvesting, shoot length of both groups was recorded and is depicted under d) in cm. Finally, arbuscule size distribution was determined from 20 blind images of colonized root sections (e). Error bars on the bar charts represent 95% confidence intervals, asterisks mark statistical significance of differences between experimental conditions at 95% (\*), 99% (\*\*), and 99.9% (\*\*\*) confidence as determined by Student's T-Test. Numbers shown on the box plots represent the respective arithmetic means also marked by the x as well as outlier measurements outside 1.5 x IQR.

Transcript measurements via sqRT-PCR revealed a successful 129-fold overexpression of *MtZf1* on average in the *MtZf1*-OE group (Figure 29a). The AM-marker gene *MtPt4*, however, did not significantly change in transcript abundance as a result (Figure 29b). Likewise, subsequent counting of AM-structures within the roots showed no significant differences compared to the controls and neither did the size distribution of arbuscules (Figure 29c and e). Shoot sizes, as recorded during harvesting (Figure 29d), also showed no differences to the controls (see also Supplementary Figure S2).



#### 4.3.4 An RNAi-mediated knockdown of *MtZf1* led to decreased AM-colonization only in roots exhibiting substantially reduced target gene expression

In order to study the effect of the absence of *MtZf1* on AM colonization as another aspect in its functional analysis, two RNAi knockdown constructs were cloned and used to induce transgenic roots in an *M. truncatula* A17 background. Three separate such experiments were performed.

During the first attempt (n = 12), sqRT-PCR measurements of RNA extracted from the mycorrhized RNAi roots showed no significant effect of *MtZf1*-RNAi-1 in comparison to the *gus*-controls (Figure 30a). For *MtZf1*-RNAi-2, interpretation of the knockdown results was more complex: although the overall average *MtZf1* transcript amounts were only reduced by not significant (p = 0.168) 31.1% compared to the *gus*-controls, five out of the twelve RNAi samples, as indicated in Figure 30d exhibited a very strong reduction. These samples also had comparatively low *MtPt4*-expression (Figure S10), suggesting that the observed near abolishing of *MtZf1* transcripts in the five individual root samples might be due to the RNAi-knockdown. Still, overall *MtPt4* transcript levels were only down by 23.6% (p = 0.426) and thus not significantly reduced compared to the controls across the entire sample pool.

During replications of the knockdown-experiments, use of the *MtZf1*-RNAi-1-construct was not repeated due to its apparent ineffectiveness. For these subsequent second and third experiments, eight sample pools of three root systems were made. Still, the high level of variability in the knockdown yielded by *MtZf1*-RNAi-2 was observed again with only 5/8 individual samples exhibiting a clear reduction (Figure 30e). Overall, however, the apparent knockdown result was stronger at an average 58.7% less *MtZf1* transcript amounts than of the *gus*-controls (p = 0.021, Figure 30b). This reduction in the target gene also had a significant negative effect on *MtPt4*-expression, which was down by 64.4% on average (p = 0.012, Figure 30h). Other measured AM-marker genes *MtRam1* and *MtRam2* yielded similar results with reductions by 59% and 65%, respectively. Total fungal mass, as illustrated by measurement of the *R. irregularis*  $\alpha$ -Tubulin transcript, was reduced by an average 73.7% compared to the control roots (Supplementary Figure S4).

For the third assay, *MtZf1* transcripts were again strongly reduced in only five out of eight sample pools, even compared to the only weakly mycorrhized *gus*-control 2 set (Figure 30f). Over the entire pool of samples, this average reduction by 56.5% *MtZf1*-transcripts was still just outside the 95% confidence range for statistical significance at p = 0.054 (Figure 30c). Measurement of *MtPt4*-expression likewise yielded no significant reduction, though mean transcript amounts throughout the entire sample pool still trended 25.8% lower and individual samples with low *MtZf1* values also exhibited low *MtPt4* levels (Figure 30i, see also Figure S10).

In total, *MtZf1*-RNAi-2 was partially successful in decreasing the target gene expression with an overall average reduction across all experiments by 47.3%. Throughout three separate experimental setups, the effect of successful knockdowns only occurring in around half of the samples was consistently and uniquely observed for *MtZf1*. In samples with reduced target transcript amounts, AM marker genes were likewise reduced, suggesting a causal link to the RNAi-effect. However, due to the inconsistent success rate throughout the entire sample pools, only the 58.7% *MtZf1* reduction and correlated AM-marker reductions observed in the second round of experiments were fully statistically relevant. Still, the unique instability of the *MtZf1* knockdown suggests that this might be a real part of *MtZf1*-RNAi-2's effect.

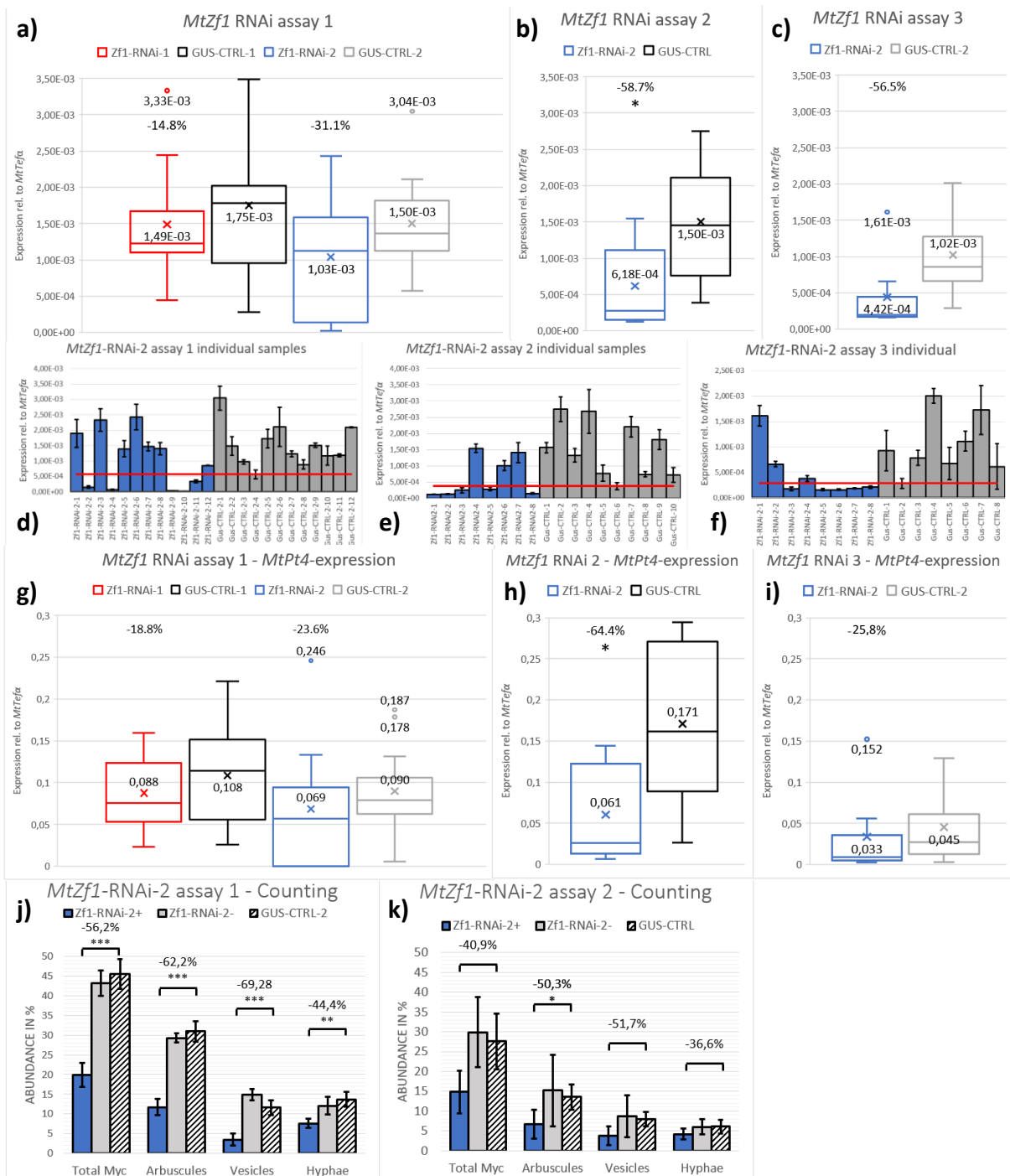


**Figure 30 – Effects of an *MtZf1*-RNAi-knockdown on the expression of AM marker gene *MtPt4* and overall AM-colonization**

Two RNAi constructs targeting *MtZf1* were expressed in transgenic root systems in WT *M. truncatula* A17 plants in three separate knockdown experiments ( $n_1 = 12$ ,  $n_2/n_3 = 8$ ). Transgenic roots containing a knockdown construct targeting a *gus*-gene were used as controls. Roots were grown with *R. irregularis* spores (49, 54 and 42 dpi) after which RNA samples were extracted and used for sq-RT-PCR measurements. Numbers shown in the box plots represent the respective arithmetic means also marked by the x as well as outlier measurements outside 1.5 x IQR. Box plots in a) show no *MtZf1* transcript reductions in the RNAi-roots compared to the controls in this initial experiment. Bar chart d) depicts the *MtZf1*-RNAi-2 samples individually, showing strong effects in 5/12 samples. In this context, the red lines depict the lowest measured *MtZf1* expression in the controls. The RNAi-knockdown experiment was repeated twice with the RNAi-2 construct. Plots b) and c) depict the reduction of *MtZf1*-transcripts in these subsequent knockdown assays. Bar charts e) and f) show the variability of knockdown success of *MtZf1*-RNAi-2 to be similar in the second and third attempts. Box plots g)-i) contain the measured *MtPt4* transcript amounts in the RNAi-roots compared to the respective *gus*-controls. Bar charts j) and k) show the results of counting AMF structures within residual root material from knockdown experiments 1 and 2 (% of 300 root sections), respectively. When counting roots with exhibiting *MtZf1* knockdown effects separately (*MtZf1*-RNAi-2+), strong reductions are observed compared to the controls. However, across the whole sample set (*MtZf1*-RNAi-2-), no such reductions can be measured.

For further evidence as to whether the effect of the *MtZf1*-RNAi-2 knockdown on the AM symbiosis was true or not, the remaining root material was stained and used for blind counting of fungal structures. During the initial RNAi trial, the small amounts of residual material were pooled into two categories depending on the measured efficacy of the knockdown. The *MtZf1*-RNAi-2+ set of root samples, consisting of samples exhibiting a strong reduction, unsurprisingly contained significantly fewer arbuscules, which were present in 11.7% of sections counted compared to the control set's 30.9% (Figure 30j). The overall mycorrhization rate of these roots was also just 19.9%, representing a 56.2% reduction compared to the corresponding set of controls at 45.5%. The remaining 7/12 samples representing the sqRT-measurements for *MtZf1*-RNAi-2-roots that did not show any effect were counted as the pool "*MtZf1*-RNAi-2-" and as expected showed no significant difference to the *gus*-controls for any of the mycorrhizal structures quantified. Observing the size distribution of individual arbuscules revealed no significant differences (supplementary Figure S5).

For the repetition of this experiment, individual root samples were counted as illustrated in Figure 30k). As an average across all samples, no significant reductions in any quantified fungal structures were detected. When considering roots with a substantial *MtZf1*-knockdown in isolation as was done in the first trial, similarly strong reductions by 40.9% in overall fungal colonization can be observed. In these *MtZf1*-RNAi-2+ roots, the rate of arbuscules (6.75%) was also significantly reduced by 50.3% ( $p = 0.043$ ) compared to the *gus*-controls' 13.6%.

In total, the half of samples nearly devoid of *MtZf1* transcripts exhibited very strong reductions of AM-marker gene expression as well as significant negative effects on overall AM-colonization. Due to the unavailability of viable *MtZf1*-*Tnt1*-insertion mutant, these results could not yet be confirmed further.

## 4.4 Functional analysis of *MtZf2* under AM-conditions

### 4.4.1 A partially truncated *MtZf2* promoter exhibits activity around strongly AM colonized areas of the roots

As with *MtPalm1* and *MtZf1*, data from available transcriptome datasets and sqRT-PCR measurements demonstrated *MtZf2* to be transcriptionally induced in roots under conditions involving AM-symbiosis (Figure 6 and 13). In order to further elucidate the spatiotemporal pattern of activation, the promoter-region of *MtZf2* was to be fused to a *gusAint* reporter gene. However, confounding this strategy was the ambiguous gene annotation for *MtZf2*: Based on the most current *Mtv5* genome, the encoded C2H2 ZF-TF (identifier *MtrunA17\_Chr7g0268961*) consists of two exons. However, RNASeq- and EST-data available suggests the existence an exon further upstream (Supplementary Figure S7). The promoter-region to be fused *gusAint* reporter gene (-1572/-3) was thus picked in relation to this first, unannotated exon. When testing the activity of this construct in mycorrhized, transgenic roots no staining was detected (Figure 31a-d). The parallel non-mycorrhized controls shown in Figure 31e-h) likewise exhibited no activity.

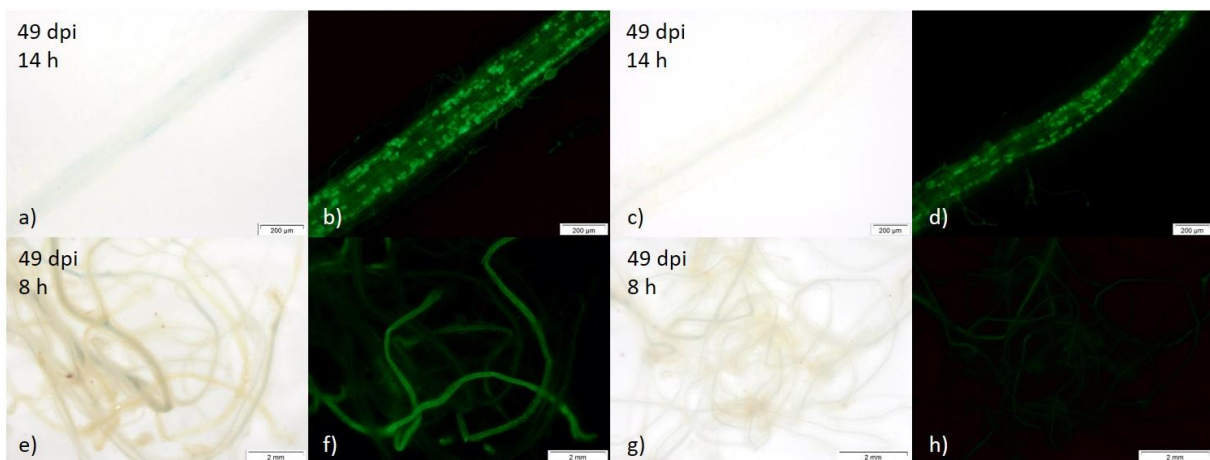


**Figure 31 – A *gus*-fusion construct of the -1,572/-3 *MtZf2* promoter region shows no activity in wild-type mycorrhized roots**

The pRR:p*MtZf2-gus\_ver1* construct (promoter region -1,572/-3 in relation to start-ATG) was expressed in transgenic root systems in the *M. truncatula* A17 WT background. Roots a-f) were mycorrhized via inoculation with *R. irregularis* spores. Non-mycorrhized roots (g, h) were grown in parallel. Images were taken after GUS staining of transgenic root systems for the stated time periods (bright field images) and subsequent counter-staining of fungal chitin via CF488-WGA. Activity of the complete *MtZf2* promoter up to the start-ATG was not detected even when staining overnight (c, d). Only slight activity was sporadically observed in some cells in the epidermal layer of older roots (a, b). No differences were observed between mycorrhized (e, f) or non-mycorrhized root systems (g-h).

Similar to *MtPalm1*, a potential upstream translational start was also found in the 5'-UTR of the *MtZf2* transcript at position -183, which was excluded from a subsequent “ver2” promoter-*gus* construct (-2059/-184, see Figure 32a).

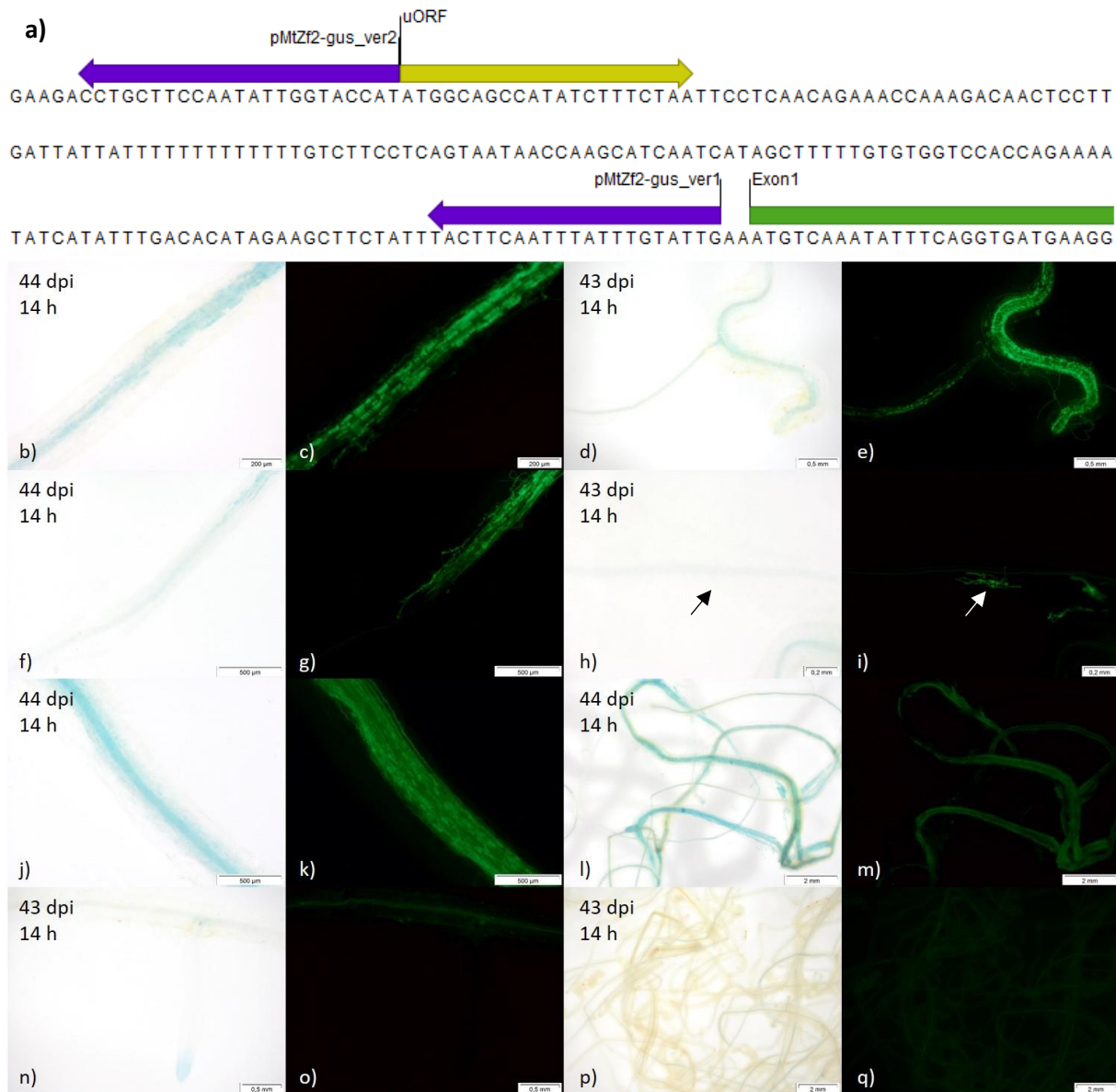


**Figure 32 – Histochemical localization of *MtZf2* promoter (-2,059/-184) activity in wild-type mycorrhized roots**

The pRR:p*MtZf2-gus\_ver2* construct (promoter region -2,059/-184 in relation to start-ATG) was expressed in transgenic root systems in the *M. truncatula* A17 WT background. The sequence leading up to the first exon (green) is illustrated under a). The rev primers defining the 3'-end of the ver1 and ver2 promoters are shown in purple, the 21 bp uORF is depicted in yellow. Roots b-m) were mycorrhized via inoculation with *R. irregularis* spores. Myc- roots (n-q) were grown in parallel. Images were taken after GUS staining of transgenic root systems for the stated time periods (bright field images) and subsequent counter-staining of fungal chitin via CF488-WGA. *MtZf2* promoter activity is associated with AMF (b-l). Single arbuscocytes are stained (b,c), but not exclusively so, as activity in the vicinity of hyphae can also be observed (f,g). Newly establishing infection units (d,e,h,i) do not appear to activate p*MtZf2*. In contrast, staining is retained in older infection units (l,j). Non-mycorrhized roots exhibit some activity in the vasculature as well as strong staining of root tips (m-o).

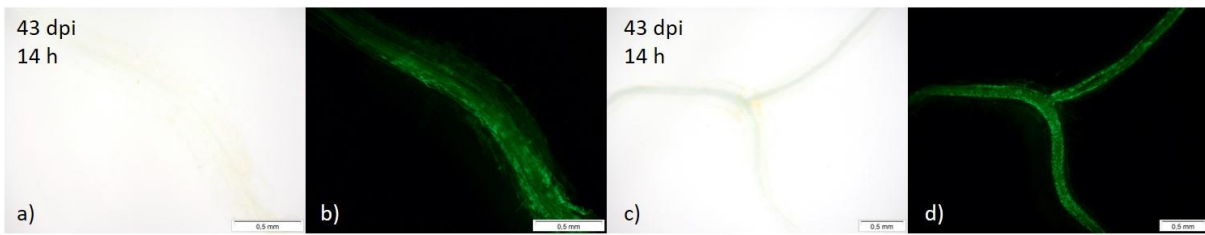
Initial tests with the revised *pMtZf2-gus\_ver2* construct revealed a much higher degree of activity, both in the presence and without any AMF after typical overnight staining for 14 h (Figure 32). Further examination, as indicated in Figure 32b) and c), showed increased coloration in root sections containing a large number symbiotically active arbuscule containing cells. Compared to the present background in the vascular tissue (Figure 32p, q), a visible shift in staining towards the root cortex was also observed in the presence of AMF. Regions harboring only hyphae or only a small number of arbuscocytes exhibited very limited activity (Figure 32d, e). Still, in the presence of arbuscules, all surrounding cortical cells appeared to respond, which is well in agreement with the measurements of Hogekamp *et. al* (2011). Young infection units without present arbuscules likewise did not provoke an *MtZf2* promoter response (Figure 32h, i). Conversely, older infection units containing degenerated arbuscules appeared to be strongly stained, indicating some activity in the later stages of the arbuscule's lifecycle (Figure 32j, k). This observation would also be in agreement with the continuous increase of *MtZf2*-expression over the time course. Still, the relatively weak signal that was observed overall indicates that the promoter region, as it was used for this analysis, is likely still incomplete.

#### 4.4.2 AM-related promoter activity of *MtZf2* is abolished in *ram1-1* but not in *pt4-2* mutant backgrounds

In the *MtRam1*-deficient mutant background incapable of forming properly branched, mature arbuscules, no cortical promoter activity around AM colonization could be observed, though staining of the vasculature or of the root tips was retained (Figure 33a-d). It is unclear whether this results from direct regulation by the key factor RAM1 or if arbuscules in this background do not reach the stage where *MtZf2* might be active. In the *pt4-2* mutants shown in Figure 33 e)-h), normal levels of induction provoked by mycorrhized regions were observed, despite the expected disruption of the nutrient exchange. Like in the wild-type, increased *pMtZf2* activity appeared to correlate well with relatively highly AMF colonized regions of the roots, while infection units with few arbuscules provoked little such activity. The apparent morphology of arbuscules had no discernible effect, as degenerated arbuscules (Figure 33g, h) could be stained while less densely packed, wild-type looking arbuscules were not (Figure 33e, f). These results further hint at the role of *MtZf2* during the later stages of the AM, possibly even during the degeneration of arbuscules.



### ram1-1



### pt4-2

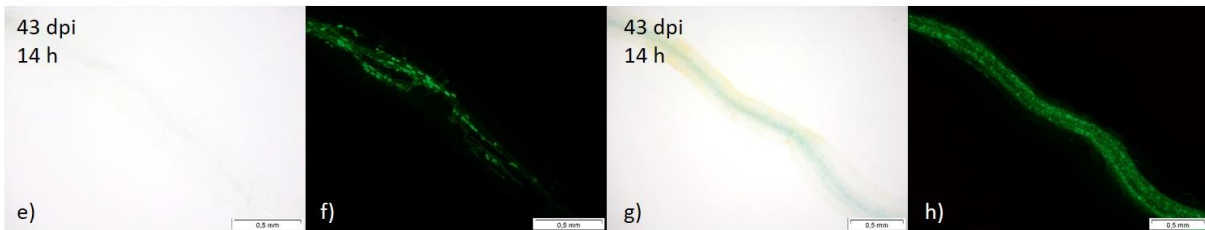


**Figure 33 – Histochemical localization of *MtZf2* promoter activity in mycorrhized roots of *ram1-1* and *pt4-2* mutants**

The pRR:*pMtZf2-gus* construct was expressed in transgenic root systems in the *M. truncatula ram1-1* and *pt4-2* mutant backgrounds. All roots depicted were mycorrhized via with inoculation with *R. irregularis* spores. Images were taken after GUS staining of transgenic root systems for the stated time periods (bright field images) and subsequent counter-staining of fungal chitin via CF488-WGA. In the *ram1-1* mutants, no AM-related promoter response was detected, although some staining in the vasculature was still present (a-d). In the *pt4-2* mutant background only a slight response was observed due to low mycorrhization (e,f) while rare, densely mycorrhized regions could still exhibit staining (g,h).

#### 4.4.3 Overexpression of *MtZf2* led to a significant reduction in AM marker gene expression as well as in the sizes of arbuscules

Previous experiments showed that *MtZf2* is measurably upregulated during arbuscular mycorrhiza on the transcript level and exhibits some correlation with colonized regions in the promoter-*gus* experiments. To ascertain whether the gene can act as a transcriptional regulator and potentially enhance or suppress AMF infection, an overexpression experiment was performed with *MtZf2*. This was done by placing the CDS under control of a CMV-35s-promoter to drive consistently high expression throughout the entire transgenic root system. Roots transformed with an empty vector served as controls. Transgenic roots in the *M. truncatula* A17 WT background were then mycorrhized by incubation with *R. irregularis* spores and grown for 42 days. During harvesting, shoot sizes were recorded and measured to be on average 2.84 cm shorter in the *MtZf2*-OE plants than the control set ( $p = 0.0001$ , Figure 34d, see also Supplementary Figure S2). The root material was split for RNA-isolation and sqRT-PCR measurements and subsequent microscopic analyses.

As compared to the normal AM-induced expression in the control roots, *MtZf2* was successfully overexpressed 16.5-fold (Figure 34a). Measurements of *MtPt4* as a marker gene for the presence of arbuscules revealed a reduction by 70.5% ( $p = 0.042$ ) in the *MtZf2*-OE samples (Figure 34b).

Furthermore, AMF structures in the remaining roots were stained and counted, revealing no significant changes (Figure 34c). In contrast, measurements of the arbuscules sizes in the *MtZf2*-OE roots revealed a significant increase in smaller arbuscules (+38.5% in 15-30  $\mu\text{m}$ ,  $p = 0.05$ ) compared to the controls (Figure 34e). This was accompanied by decreases in the proportion of medium arbuscules between 45 and 75  $\mu\text{m}$ , suggesting a shift in size distribution.

Based on these results, it would appear that *MtZf2* could be a negative regulator for certain conditions of the AM-symbiosis. Specifically, its late activity detected in the transcript measurements and promoter-*gus* studies could place its activity in the senescence phase of the arbuscule life cycle.

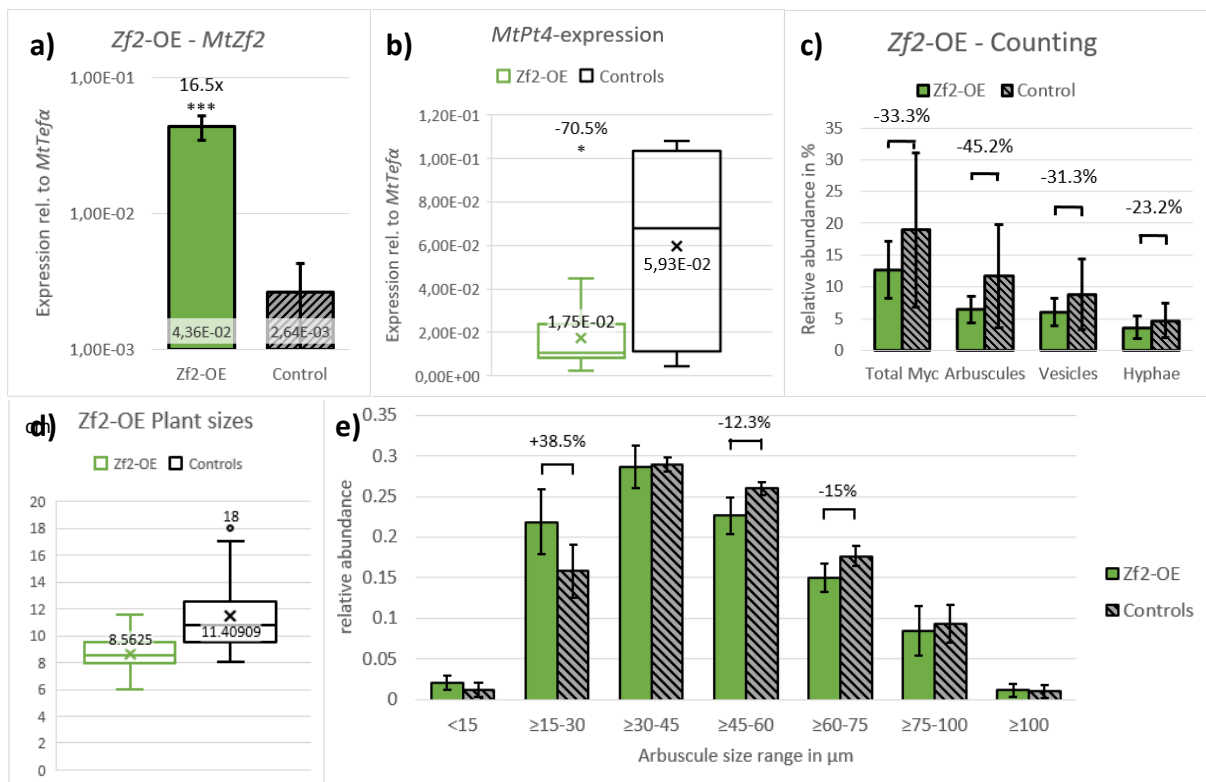


**Figure 34 – Effects of *MtZf2*-overexpression on AM-colonization and arbuscule sizes**

*MtZf2* was constitutively overexpressed in transgenic root systems of the *M. truncatula* A17 cultivar under control of a CMV-35s-promoter. Resulting positively transformed roots were mycorrhized via inoculation with *R. irregularis* spores. Plants grown with transgenic roots carrying the empty vector were used as controls under the same conditions. At 42 dpi, roots were flash frozen ( $n = 8$  for each group) for subsequent RNA-isolation and sq-RT-PCR measurements. The bar charts under a) represent mean expression levels of the overexpression roots compared to the controls. Measurements of the AM-marker gene *MtPt4* are represented in b) as box plots. Remaining root material of both OE- and control-roots was used for quantification (percentage of 300 root sections per sample) of internal AMF colonization shown as bars in c). During harvesting, shoot length of both groups was recorded and is depicted under d) in cm. Finally, arbuscule size distribution was determined from 20 blind images of colonized root sections. Shifts in size distribution indicated were determined to be statistically significant with 95% confidence. (e). Error bars on the bar charts represent 95% confidence intervals, asterisks mark statistical significance of differences between experimental conditions at 95% (\*), 99% (\*\*), and 99.9% (\*\*\*) confidence as determined by Student's T-Test. Numbers shown on the box plots represent the respective arithmetic means also marked by the x as well as outlier measurements outside 1.5 x IQR.



#### 4.4.4 Successful RNAi-mediated knockdowns of *MtZf2* negatively affected AM-symbiosis

Prior results showed *MtZf2* activity to be increased in the presence of AM as well as slight negative effects due to constitutive overexpression. To further study its potential role during symbiotic interaction via a knockdown, two RNAi-constructs targeting the second annotated exon of *MtZf2* were used in mycorrhized transgenic root systems (see also Figure 9). Two such experiments (n = 3 x 8) were performed independently, both of which were successful: *MtZf2*-RNAi-1 yielded an average reduction of target gene transcript amounts by 75.5% across the two separate assays (average between reduction shown under Figure 35a and b in red). The measured knockdown-effect from *MtZf2*-RNAi-2 was slightly stronger and more consistent with an average 87% *MtZf2* mRNA reduction (Figure 35b and c, blue). In the case of both constructs, this knockdown of the target gene could also have a significant negative impact on the transcript amounts of AM marker genes such as *MtPt4*.

In detail, the sqRT-PCR measurements of RNA from *MtZf2*-RNAi-1 root material revealed an average 70.6% reduction in target gene transcript abundance compared to parallel *gus*-controls (Figure 35a). Though statistically significant overall (p = 0.006), this RNAi effect was not as stable as knockdowns of *MtPalm1* also performed during this work (Supplementary Figure S11). The arbuscular marker *MtPt4* was reduced by an average 57.5% (p = 0.05) compared to the control set (Figure 35d). Similar observations were made for *MtZf2*-RNAi-2: Target gene transcript amounts were down consistently across samples by an average 87.4% (p = 0.001). This more severe reduction also led to a stronger negative effect on *MtPt4*, which was significantly reduced by an average 84.1% (p = 0.001, see Figure 35d). Measurements of the transcripts from other AM marker genes yielded similar results with *MtRam1* being down by 82.9% and *MtRam2* by 82.1%. The fungal marker *RiaTub* saw a reduction by an average 89.2% (Supplementary Figure S4). These results indicate an overall reduction in AM colonization due to *MtZf2* knockdown.

Similar results were obtained in a repetition of this experiment: *MtZf2*-RNAi-1 yielded a significant reduction of its target gene by 80.4% (p = 0.0036) compared to the *gus*-control set 1 (Figure 35b). In turn, 92.9% fewer transcripts were measured for the arbuscule marker gene *MtPt4* during this trial (p = 0.0045), indicating strongly diminished mycorrhization (Figure 35e). The second RNAi construct targeting *MtZf2* led to a significant reduction as well with a decrease by 86.7% (p = 0.0053) compared to the respective set of controls, as shown in Figure 35c). This was in spite of the fact that the mycorrhization rate as indicated by the *MtPt4* measurements in the control set 2 was uniquely low. Therefore, it is not too surprising that the 74% reduction of *MtPt4* expression observed in the *MtZf2*-RNAi-2 set was not significant in this experiment (Figure 35f, p = 0.094).

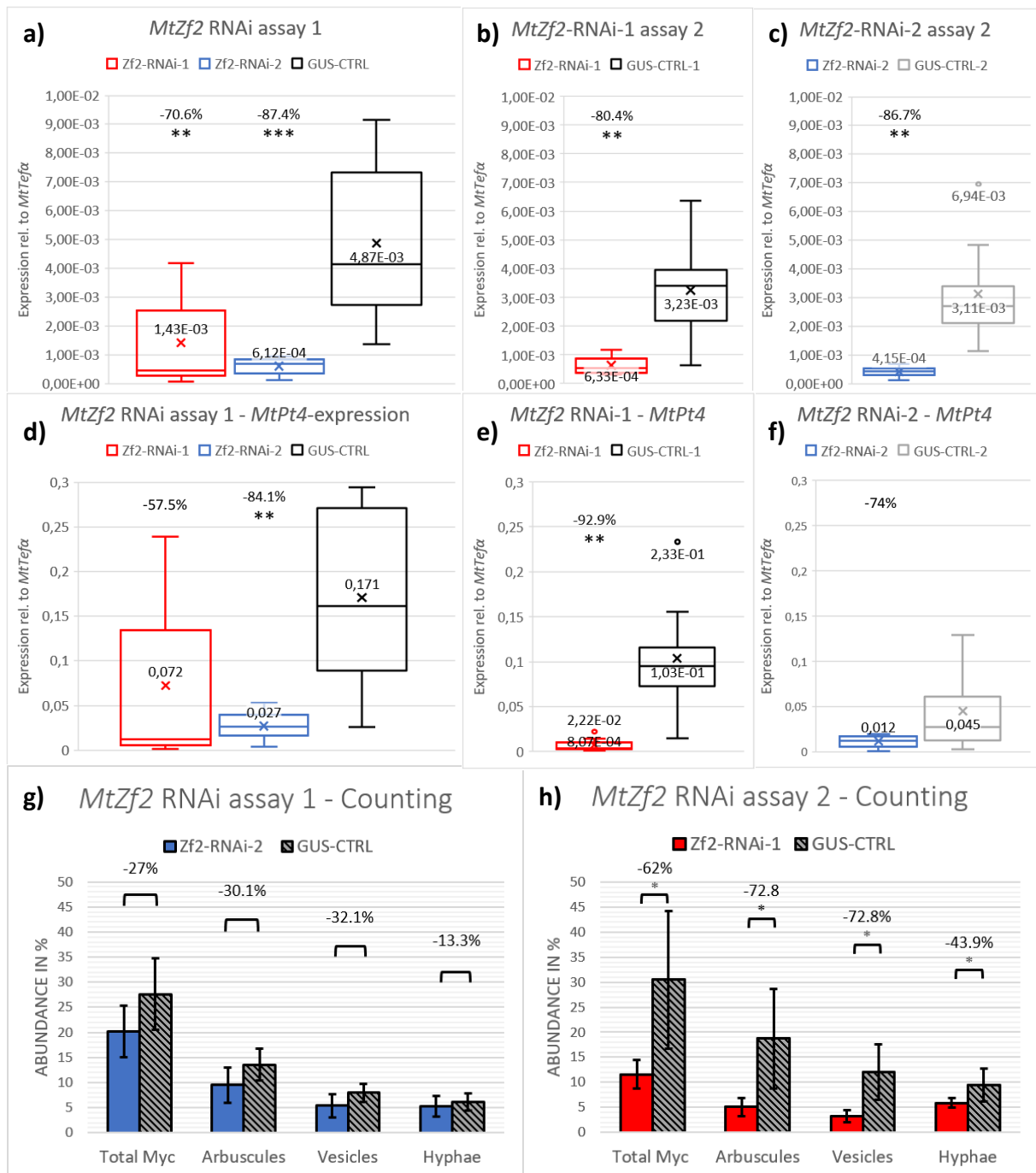


**Figure 35 – Effects of an *MtZf2*-RNAi-knockdown on the expression of AM marker gene *MtPt4* and overall AM-colonization**

Two RNAi constructs targeting *MtZf2* were expressed in transgenic root systems in WT *M. truncatula* A17 plants as part of two separate knockdown experiments (n = 8). Transgenic roots containing a knockdown construct targeting a *gus*-gene were used as controls. Roots were grown for 54 and 42 dpi with *R. irregularis* spores, after which RNA samples were extracted and used for sqRT-PCR measurements. Box plots a)-c) show *MtZf2* transcript reductions in the RNAi-roots compared to the controls. Plot a) depicts both RNAi-treatments with a common set of controls, while b) and c) contain samples from the second experiment with separate controls. Plots d)-f) underneath depict reductions in the *MtPt4* arbuscule marker gene due to the *MtZf2*-RNAi-effects. Numbers shown represent the respective arithmetic means also marked by the x as well as outlier measurements outside 1.5 x IQR. Remaining root material from the more effective RNAi sets was used for quantification (percentage of 300 root sections each) of fungal structures within the roots represented as arithmetic mean by the bar charts g)-i). Error bars represent 95% confidence intervals, asterisks mark statistical significance of differences between experimental conditions at 95% (\*), 99% (\*\*), and 99.9% (\*\*\*) confidence as determined by Student's T-Test.

The remaining RNAi root samples from the more successful knockdowns were stained with CF488-WGA to quantify individual AM structures. For the initial experiment, no significant reductions ( $p = 0.093$ ) in AMF structures were detected throughout the *MtZf2*-RNAi-2 set compared to the *gus*-controls, though as a trend, overall mycorrhization was decreased by 27.1% (Figure 35g). The rate of arbuscules or of other structures was likewise seemingly unaffected. This was unexpected, as transcript measurements of AM marker genes suggested reductions by ~80% compared to the controls.

In the repetition, overall mycorrhization in the *MtZf2*-RNAi-1 roots exhibiting over 90% reduction in *MtPt4* expression was down by an average of 62% (Figure 35h,  $p = 0.028$ ). All other AMF structures within the roots were likewise significantly reduced in abundance: Arbuscule containing sections were reduced by 72.8% ( $p = 0.028$ ) compared to the *gus*-controls and fungal vesicles were down by 72.8% ( $p = 0.013$ ).

These results seem to suggest that a lack of *MtZF2* negatively affects the arbuscular mycorrhiza symbiosis. However, the RNAi-based knockdown might not be strong enough to clearly and consistently evoke these resulting effects. In addition, the role of *MtZf2* might be a minor one, so that its absence might only lead to stable and substantial effects on AM under specific external conditions.

#### 4.4.5 Negative effects of an *MtZF2*-KO on the overall mycorrhization rate were partially rescued via the introduction of a functional gene copy

As further evidence for the relevance of *MtZf2* during AM-symbiosis, a study using full mutants was conducted. To that end, the *M. truncatula* R108 *Tnt1*-line NF6681 was identified to contain a retrotransposon-insertion at position 361 in Exon2 of *MtZf2*, leading to a nonfunctional gene (Figure 36a).

Plants using this background could then be used for induction of transgenic roots containing another gene copy of *MtZf2* including the entire native promoter- (1867 bp) coding- (3093 bp) and terminator-regions (1185 bp) to complement the knockout-mutation (*MtZf2*-*Tnt1*-Comp). These mycorrhized root systems were directly compared to the *MtZf2*-*Tnt1*-mutants containing the empty vector (*MtZf2*-*Tnt1*-EV) as well as the R108 WT also transformed with the empty vector (WT-EV). At 42 dpi, six samples consisting of three root systems were flash frozen and used for RNA-isolation and subsequent phenotypic analyses.

*MtZf2*-transcript measurements performed via sqRT-PCR revealed an apparent increase in overall expression in the *MtZf2-Tnt1-Comp* samples compared to both the WT and KO-mutant plants, as depicted in Figure 36b). This was surprising, as the amplicon used for *MtZf2*-transcript quantification used throughout this study is a fragment at the very 3'-end of the CDS (outlined in Figure 36a). As such, nonsense-mediated-decay due to the presence of the *Tnt1*-insertion was expected, but was not detectable. By performing the same sqRT-PCR using primers directly flanking the insertion site, however, no remaining transcripts were detected indicating a complete knockout (Figure 36c). With these flanking primers it could also be confirmed that the complementation construct yielded approximately wild-type levels of expression, as there was no significant difference to the WT-EV control set (-32.2%,  $p = 0.5$ ). As a result, the expression of the arbuscule marker gene *MtPt4* shown in Figure 36d) was down significantly by 40.5% in comparison between the full, non-compensated mutants to the controls. The mutants expressing the additional intact *MtZf2* copy still trended lower at 27.7% less *MtPt4* transcripts, but not significantly so ( $p = 0.094$ ). As such, these results indicate a reduction in AM marker gene expression similar to the RNAi-based knockdown approach.

Further phenotypic analysis via randomized counting of AMF structures present in the roots revealed this reduction to indeed be based on a 44% reduction in overall mycorrhization (Figure 36e,  $p = 0.05$ ). The number of arbuscules was reduced by a similar amount, though this difference was just under the confidence level to be accepted as significant ( $p = 0.074$ ). The remaining quantified fungal structures trended lower as well. Similarly, the *MtZf2* mutants carrying the complementation construct exhibited less fungal mass in all categories observed. However, none of the categories were significantly different compared to the WT-EV controls or the full mutants in overall agreement with the sqRT-PCR measurements of AM marker genes.

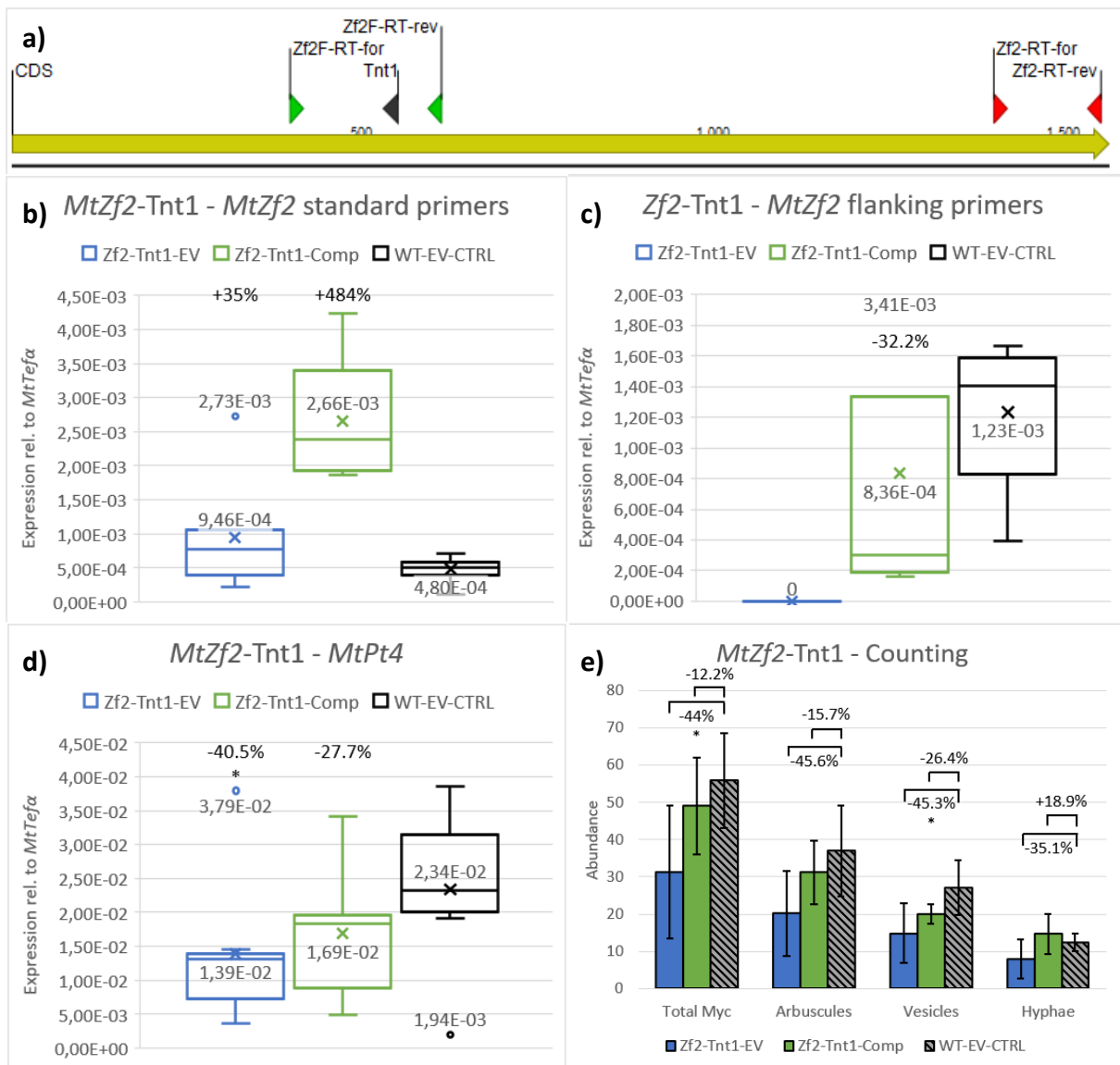


**Figure 36 – Effects of a *MtZf2-Tnt1*-knockout and -complementation on the expression of AM-marker *MtPt4* and overall AM-colonization**

The *M. truncatula* R108 *Tnt1*-retrotransposon insertion line NF6681 was determined to contain an insertion in the CDS of *MtZf2* as depicted in black under a). Arrows indicate binding sites of primers pairs used for sqRT-PCR measurements: red was the standard primer pair used in previous experiments; the primers flanking the *Tnt1*-insertion site are marked in green. Transgenic roots containing either a secondary gene copy of *MtZf2* (*MtZf2-Tnt1-Comp*) or the empty vector (*MtZf2-Tnt1-EV*) were induced in the homozygous *Tnt1*-mutant background. Additionally, wild-type plants with the empty vector served as controls (WT-EV-CTRL). These plants were mycorrhized using *R. irregularis* spores and harvested for RNA-isolation after 42 dpi (n = 3 x 6). SqRT-PCR measurements were performed using the standard primers (b) and the *Tnt1*-flanking primers (c). Box plots under d) depict the transcript amounts measured for *MtPt4*. Numbers shown represent the respective arithmetic means also marked by the x as well as outlier measurements outside 1.5 x IQR. Remaining root material was used for quantification (total numbers observed in 300 root sections per sample) of fungal structures within the roots represented as arithmetic mean by bar chart e). Error bars represent 95% confidence intervals, asterisks mark statistical significance of differences between experimental conditions at 95% (\*), 99% (\*\*), and 99.9% (\*\*\*) confidence as determined by Student's T-Test.

When taking into account additional *MtZf2-Tnt1* plants as well as controls not subject to the sqRT-PCT transcript quantifications (n = 14 for each of the three groups), all intraradical fungal structures were significantly reduced in abundance by approximately 33% ( $p < 0.05$ , Figure S13). In this dataset, this reduction was fully compensated via the introduction of a complementation construct, adding further evidence of a minor effect of *MtZf2*-abolishment is prone to be masked by variation between individual root samples.

These results thereby confirm the reduction of AM-colonization indicated by the *MtPt4* transcript measurements. Arbuscule size analyses that were also performed with these roots, but revealed no consistent differences between the non-compensated mutants and the control group (Figure S14). As such, the observed effect of the knock-out appears to differ from the altered arbuscule size distributions that occurred when *MtZf2* was overexpressed.

As such, the results from this partially rescued knockout largely line up and add compelling evidence to suggest that the negative quantitative effects observed both in this assay and the RNAi knockdown trials were indeed based on the reduction or abolishment of *MtZf2* expression. These effects are likely minor which might contribute to being clearly observable in only some of the experiments.

## 4.5 Functional analysis of *MtZf3* under AM-conditions

### 4.5.1 Activity of the *MtZf3* promoter is increased in the presence of functional arbuscular mycorrhiza

Based on existing data, the C3H-type Zinc finger protein encoded by *Medtr3g103960* (*MtZf3*) is expected to be induced in the presence of AM symbiotic fungi (Figure 13). To ascertain this hypothesis on a cellular level, the promoter region of the gene (-1013/-1) was fused to a *gusAint* reporter gene and integrated into the pRedRoot binary vector. The induced transgenic roots containing this construct were then stained to obtain information on the tissue- and cell-specific promoter activity. This was done both in root systems mycorrhized with *R. irregularis* as well as in sterile roots without fungal contact.

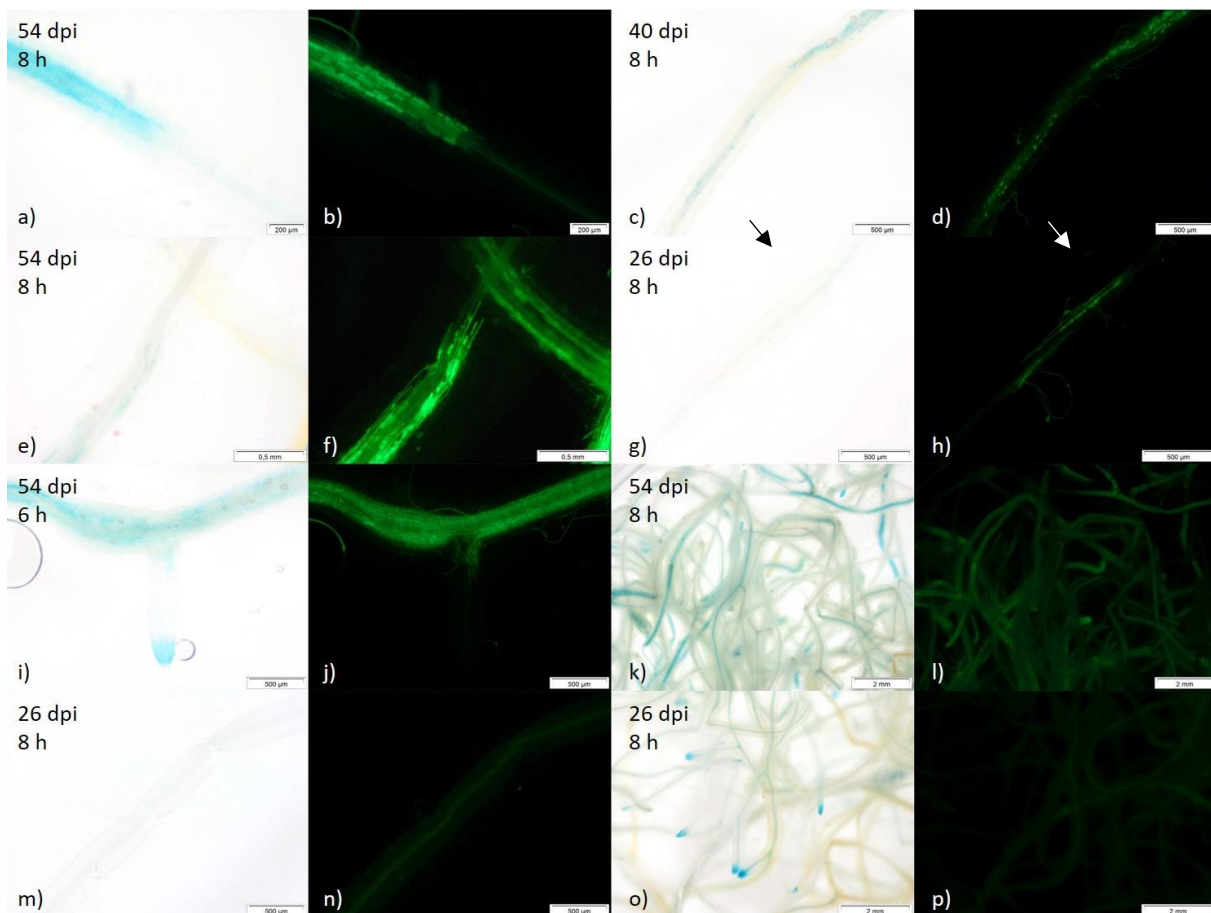


**Figure 37 – Histochemical localization of *MtZf3* promoter activity in wild-type mycorrhized roots**

The pRR:p*MtZf3*-*gus* construct was expressed in transgenic root systems in the *M. truncatula* A17 WT background. Roots a-l were mycorrhized via inoculation with *R. irregularis* spores. Myc- roots (m-p) were grown in parallel. Images were taken after GUS staining of transgenic root systems for the stated time periods (bright field images) and subsequent counter-staining of fungal chitin via Alexa488-WGA. *MtZf3* promoter activity is diffusely correlated with AM colonization, as single arbuscules are barely distinguishable (a-d,k,l). Due to unknown reasons, occasions were observed where the *MtZf3* promoter is not activated in the presence of AMF. Newly establishing infection units (g,h) do not appear to activate p*MtZf3*. In contrast, staining is strongly retained in older infection units (l,j). Non-mycorrhized roots show only weak staining in the vasculature but strong staining of root tips (m-o).

These analyses revealed that the *MtZf3* promoter exhibited stronger basal activity throughout the transgenic root systems compared to the other promoters examined even with relatively shorter incubation times of 6 h. This activity across the whole root was observed to be increased overall in the presence of AMF compared to the non-mycorrhized controls (compare Figure 37m, n, o, p to Figure 37k, l). As for the cell specific pattern of activity, Figure 37a) and b) show a typical staining of a root containing an actively proceeding AM infection that appears to provoke GUS-staining in arbuscule containing cells and likely also the surrounding cortical tissue. Despite this, very young infection units without or with very few or young arbuscules typically did not activate the *MtZf3* promoter (Figure 37g, h). Likewise, the proceeding of hyphae through the root by itself was not correlated with GUS-staining without present arbuscocytes, as can be seen in Figure 37c) and d). Even with the presence of arbuscules, staining intensity was not always stable for *pMtZf3*, as illustrated by Figure 37e) and f). Generally, roots containing old infection units with degenerated arbuscules still yielded promoter activity that appeared to be of similar intensity to the staining of cells containing mature arbuscules (Figure 37i, j). This, together with the tendency to be inactive in fresh infection units, suggests a role in the later stages of arbuscule life.

To summarize, these results further demonstrate that *MtZf3* activity is not specific to AM-conditions, even if the presence of a symbiotic partner seems to increase its activity. This was expected, as available expression data already suggests more generalized activity in roots. Nevertheless, cell-type specific expression data predicts stronger activity in arbuscule containing cortical cells compared to such cells only surrounded by hyphae, which could be confirmed here.

#### 4.5.2 *MtZf3* promoter activity depends on the presence of functional arbuscules

To clarify the specificity of AM-induced activity of *pMtZf3* due to the potential regulation by key regulator MtRAM1 or functional AM nutrient exchange, the promoter-*gus* construct was tested in the *ram1-1* and *pt4-2* mutant lines. In both backgrounds, *MtZf3* activity was almost entirely abolished for typical staining times of 6 to 8 h, even including unspecific activity observed in the vasculature of wild-type plants (Figure 38). There also appeared to be no difference between arbuscules in the mutants exhibiting wild-type-like morphology and truncated or degenerated arbuscules. This suggests that *MtZf3* activity depends on functional symbiotic nutrient exchange in the arbuscules and potentially regulation by RAM1.



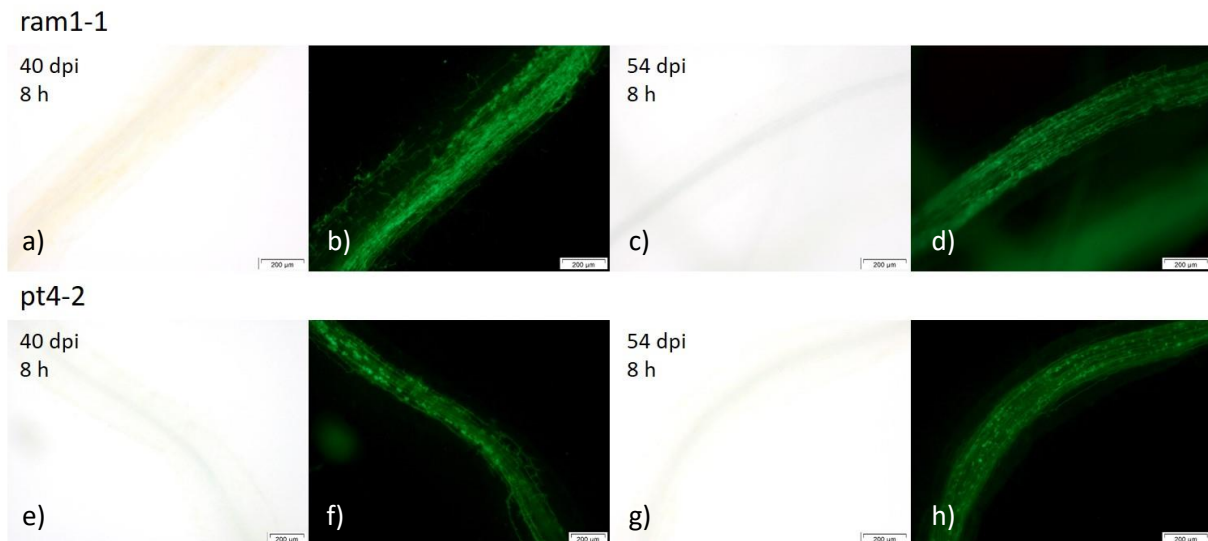


**Figure 38 – Histochemical localization of *MtZf3* promoter activity in mycorrhized roots of *ram1-1* and *pt4-2* mutants**

The pRR:*pMtZf3-gus* construct was expressed in transgenic root systems in the *M. truncatula ram1-1* and *pt4-2* mutant backgrounds. All roots depicted were mycorrhized via inoculation with *R. irregularis* spores. Images were taken after GUS staining of transgenic root systems for the stated time periods (bright field images) and subsequent counter-staining of fungal chitin via CF488-WGA. The AM-dependent response of *pMtZf3* was entirely abolished in the *ram1-1* (a-d) mutant background. The same goes for the *pt4-2* mutant irrespective of arbuscules exhibiting a normal phenotype (e,f) or prematurely degenerated arbuscules (g,h).

#### 4.5.3 An RNAi-mediated knockdown of *MtZf3* had slightly negative effects on overall AM colonization

Based on the promoter-reporter gene fusion and expression data it remains unclear if *MtZf3* has a supporting role during the AM symbiosis. To determine whether the gene's absence might affect some aspect of the AM symbiosis or overall colonization, an RNAi-knockdown study was performed using two separate dsRNA-constructs targeting different regions of the transcript (see Figure 9). Three separate such experiments were performed on mycorrhized transgenic root systems in an *M. truncatula* A17 wild-type background.

To determine the efficacy of these knockdowns, *MtZf3* transcripts were measured via sqRT-PCR in RNA-samples isolated from twelve roots for each sample group. *MtZf3*-RNAi-1 yielded a significant 69.7% reduction ( $p = 0.018$ ) of *MtZf3* transcripts compared to the *gus*-controls (Figure 39a). The *MtZf3*-RNAi-2 construct was entirely unsuccessful with the average target transcript amounts approximately 7% higher than the controls, although not statistically significantly so ( $p = 0.812$ ). For both knockdown-constructs and the controls, the measurements of individual samples are spread more strongly compared to the other target genes (Supplementary Figure S12). This was somewhat expected with its

expression pattern also appearing to only weakly correlate with *MtPt4* transcript levels which fits to the weakly AM-induced expression profile of *MtZf3* and lower specificity in the promoter-*gus*-study. As such, it is not too surprising that neither RNAi-construct targeting *MtZf3* had a measurable effect on *MtPt4*-expression shown in Figure 39d) ( $p = 0.714/0.056$ ).

For the subsequent repetitions of this experiment, only the initially effective *MtZf3*-RNAi-1 construct was used. The first such repeat trial, depicted in Figure 39b), yielded an average knockdown of 73.3% compared to the *gus*-control samples ( $p = 0.028$ ,  $n = 3 \times 8$ ). In this *MtZf3*-RNAi-1 set *MtPt4* transcript amounts were also significantly reduced by 72.8% (Figure 39e,  $P = 0.003$ ), indicating a reduction in active arbuscules (Figure 39e). Other AM marker genes saw even higher reductions such as *MtRam1* at 86.9% and *MtRam2* at 79.9%. The marker for total AMF present *RiaTub* was reduced by 89.7% on average (Supplemental Figure S4) leading to the conclusion that during this experiment, AM colonization was impaired in roots deficient for *MtZF3*.

The third trial, however, did not corroborate these findings across the eight sample pools: Though an average knockdown effect of 48.2% ( $p = 0.016$ ) was achieved, as shown in Figure 39c), no difference in *MtPt4* expression between the RNAi samples and the *gus*-controls was measured (Figure 39f). As such, only one out of three successful knockdown experiments for *MtZf3* led a reduction of AM marker genes.

Using the residual root material from the RNAi-knockdowns, fungal structures were microscopically quantified to potentially observe any phenotypic effects on the AM symbiosis. It should be noted that during the first knockdown experiment, root material was pooled to obtain large enough samples sizes for quantification. In this assay, total mycorrhization was down to 34.3% in *MtZf3*-RNAi-1 compared to the 41% of the *gus*-controls, which would only represent a very minor effect (Figure 39g). Likewise, the arbuscule-rate was not reduced, which appears as consistent with the sqRT-measurements not showing a reduction in *MtPt4*-transcript amounts. Arbuscules size distributions were also recorded and showed no significant differences with to the controls.

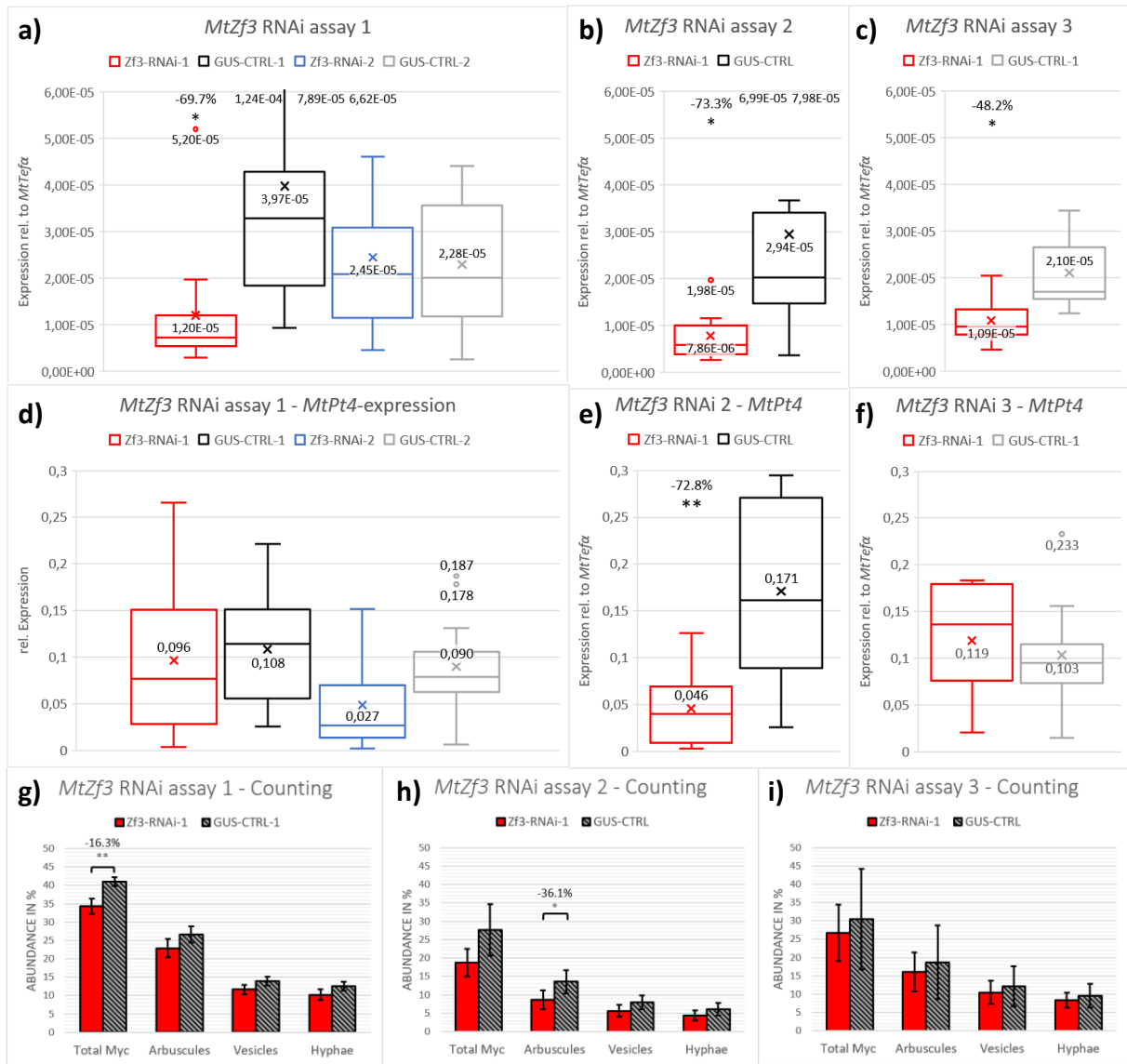


**Figure 39 – Effects of an *MtZf3*-RNAi-knockdown on the expression of AM marker gene *MtPt4* and overall AM-colonization**

Two RNAi constructs targeting *MtZf3* were expressed in transgenic root systems in WT *M. truncatula* A17 plants as part of three separate knockdown experiments. Transgenic roots containing a knockdown construct targeting a *gus*-gene were used as controls. Roots were grown for 49, 54 and 42 dpi with *R. irregularis* spores, respectively, after which RNA samples were extracted and used for sq-RT-PCR measurements. Numbers shown represent the respective arithmetic means also marked by the x as well as outlier measurements outside 1.5 x IQR. Box plots a)-d) show *MtZf3* transcript reductions in the RNAi-roots compared to the controls. As only *MtZf3*-RNAi-1 was initially successful in reducing target transcript amounts, *MtZf3*-RNAi-2 was not used further. Plots e)-h) depict reductions in the *MtPt4* arbuscule marker gene due to the *MtZf3*-RNAi-effects. Remaining root material was used for quantification of fungal structures within the roots. Bar charts i)-k) summarize the resulting observed reduction in fungal structures, which were only partially significant.

For subsequent gridline counting analyses, the same individual samples as in the sqRT-PCR measurements. In the second trial, the observed rate of arbuscules in the *MtZf3*-RNAi-1 roots was reduced by 36.1% compared to the controls (Figure 39h,  $p = 0.045$ ). The overall observed rate of AMF structures was not significantly reduced ( $p = 0.055$ ). This result is largely in agreement with the transcript measurements that exhibited significant reduction in arbuscule marker genes.

In the final repetition, again fitting the sqRT-PCR measurements, no significant differences between the *MtZf3* knockdown samples and the controls were observed (Figure 39i).

In total, only minor and sporadic negative effects on AM symbiosis were correlated to the *MtZf3*-knockdown. Together with the expression profile, some relation to mycorrhization is likely for this candidate, though it is very likely minor role was not conducive to strong and repeatable phenotypic effects.

#### 4.6 Yeast 2-Hybrid interaction analyses involving MtPALM1, MtZF1 and MtZF2 as well as MtARF-proteins

After examining the effects of loss-of-function of the AM-induced *MtZf* genes on mycorrhization, it still remains unclear if and how the resulting proteins could interact with the wider network of TFs and signaling components involved with AM-symbiosis. To elucidate this, protein-interaction studies were performed with yeast strains expressing *MtPalm1*, *MtZf1*, *MtZf2* and *MZf3* as part of Yeast 2-Hybrid assays (principle and strategy are explained further under 3.9.3 and 3.9.5). Additionally, the MtARF proteins were examined for their potential involvement in the regulation of *MtPalm1*. This was done both in targeted direct matings with a number of AM-related TFs that were previously analyzed (see Table 21 for a short overview) as well as with an existing CDS-library constructed from an *M. truncatula* transcriptome (Hartmann, 2018), where possible.

**Table 21 – Information on AM-related candidate genes selected for the protein-interaction studies**

For better understanding of potential functional relationships revealed by the Y1H and Y2H approaches used in this work, this table gives a short summary of known information on the function these AM-related factors. In addition to the trivial names used in the subsequent text, the Mtv4-IDs are given, alongside the TF-family and whether the respective gene's expression is specifically induced under conditions involving AM, according to existing transcriptome data. The final column provides sources for the functions described.

Trivial Name	Gene ID	TF-Family	AM-induced	Description	Citation
Mt15867	Medtr4g130270	AP2/ERF	Yes	RAM1-dependent; regulated by WRI5B/WRI5C; might enhance expression of AM-dependent FA-enzyme KASII	Hartung, 2021
Mt25005	Medtr7g011630	AP2/ERF	Yes	Potential interactor of AM-dependent NF-Y TFs; might enhance expression of AM-dependent FA-enzyme KASII	Hartung, 2021
Mt460730	Medtr2g460730	AP2/ERF	Yes	RAM1-dependent; might enhance expression of AM-dependent FA-enzyme KASII	Hartung, 2021
MtArf3	Medtr2g014770	ARF3	No	Negative regulator of MtPALM1 in leaves; one of four <i>MtArf3</i> -like genes expressed in roots	Peng <i>et. al</i> , 2017; Shen <i>et. al</i> , 2015
MtArf7	Medtr2g093740	ARF3	No	One of four <i>MtArf3</i> -like genes expressed in roots	Shen <i>et. al</i> , 2015
MtArf25	Medtr4g088210	ARF3	No	One of four <i>MtArf3</i> -like genes expressed in roots	Shen <i>et. al</i> , 2015
MtCbf1	Medtr2g081600	NF-YC	Yes	Strongly arbuscule induced; a double-knockdown with <i>MtCbf2</i> led to a stark reduction in AM colonization; interacts with MtCBF3 and likely NF-YA-proteins	Hogekamp <i>et. al</i> , 2013; Dissertation SK
MtCbf2	Medtr2g081630	NF-YC	Yes	Strongly arbuscule induced; a double-knockdown with <i>MtCbf1</i> led to a stark reduction in AM colonization; interacts with MtCBF3 and likely NF-YA-proteins	Hogekamp <i>et. al</i> , 2013; Dissertation SK
MtCbf3	Medtr8g091720	NF-YB	Yes	Strongly arbuscule induced; interacts with MtCBF1/2, NF-YA- and potentially MtWRI5-proteins	Hogekamp <i>et. al</i> , 2013; Dissertation SK; Hartung, 2021
MtDella1	Medtr3g065980	GRAS	No	Influences AM through GA signaling by enhancing <i>MtRam1</i> expression; interacts	Floss <i>et. al</i> 2013; 2016; 2017;

				with NSP2, RAD1 and IPD3; less colonization in <i>MtDella1/2</i> -KO	Pimprikar <i>et. al</i> 2016
MtDella2	contig_52215	GRAS	No	Influences AM through GA signaling by enhancing <i>MtRam1</i> expression; interacts with NSP2, RAD1 and MYB1 as well as IPD3; less colonization in <i>MtDella1/2</i> -KO	Floss <i>et. al</i> , 2013; 2016; 2017; Pimprikar <i>et. al</i> 2016
MtDella3	contig_55897	GRAS	No	Another MtDELLA protein; likely function in AM-signaling but no known interactions	Floss <i>et. al</i> , 2013; Hartmann, 2018
MtGras1 (MtTF80)	Medtr3g022830	GRAS	Yes	RAM1-dependent; putative enhancer for other GRAS-TFs; potential interactor with RAM1; knockdown might lead to smaller arbuscules	Park <i>et. al</i> , 2015; Hartmann <i>et. al</i> , 2019
MtGras4	Medtr7g109580	GRAS	Yes	Active independently of RAM1; potentially regulates <i>MtGras7</i>	Hartmann <i>et. al</i> , 2019
MtGras5 (MtSym SCL1)	Medtr1g069725	GRAS	Yes	Knockdown strongly reduces nodulation; no effect on AM; weak dependence on RAM1	Kim and Nam, 2013; MSc JV
MtGras6	Medtr2g089100	GRAS	Yes	Active independently of RAM1; putative enhancer for other GRAS-TFs; Knockout might lead to smaller arbuscules	Hartmann <i>et. al</i> , 2019; MSc AP
MtGras7	Medtr1g086970	GRAS	Yes	RAM1-dependent; potentially regulated by GRAS4	Hartmann <i>et. al</i> , 2019
MtGrasX	Medtr7g069740	GRAS	No	Possible orthologue of OsDIP1, a DELLA interacting protein with an enhancing function in AM	Yu <i>et. al</i> , 2014; This work
MtNF-YA1	Medtr1g056530	NF-YA	No	Possible candidate for interaction with AM-induced NF-YB/C proteins	Laporte <i>et. al</i> , 2014; Dissertation SK
MtNF-YA2	Medtr7g106450	NF-YA	Yes	Potentially interacts with CBF1/3- and CBF2/3-complexes to facilitate DNA-binding	Dissertation SK
MtNF-YA3	Medtr2g041090	NF-YA	No	Potentially interacts with CBF1/3- and CBF2/3-complexes to facilitate DNA-binding	Dissertation SK
MtNF-YA4	Medtr2g099490	NF-YA	No	Possible candidate for interaction with AM-induced NF-YB/C proteins	Dissertation SK
MtNF-YA7	Medtr8g037270	NF-YA	No	Potentially interacts with CBF1/3- and CBF2/3-complexes to facilitate DNA-binding	Dissertation SK
MtNsp1	Medtr8g020840	GRAS	No	Interacts with NSP2 and MYB1; involved in early signaling of nodulation and AM symbiosis; KO-mutation leads to decreased response to Myc-LCOs, SL-synthesis and reduced colonization	Hirsch <i>et. al</i> , 2009; Delaux <i>et. al</i> , 2013; Floss <i>et. al</i> , 2017
MtNsp2	Medtr3g072710	GRAS	No	Interacts with NSP1, RAM1, RAD1 as well as DELLA proteins (among others); involved in early signaling of nodulation and AM symbiosis including response to LCOs and SL-synthesis, but also regulation of entire arbuscule lifecycle; KO-mutation leads to less AM-colonization overall	Hirsch <i>et. al</i> , 2009; Gobbato <i>et. al</i> , 2012; Laouressergues <i>et. al</i> , 2012; Park <i>et. al</i> , 2015; Xue <i>et. al</i> , 2015; Heck <i>et. al</i> , 2016; Fonouni-Farde <i>et. al</i> , 2016
MtPalm1 (MtIrg1)	Medtr5g014400	C2H2 ZF	Yes	Controls compound leaf patterning and abaxial wax deposition; negatively regulated by ARF5 in leaves; shows strong induction in arbuscocytes	Chen <i>et al.</i> , 2010; Uppalapati, <i>et. al</i> , 2012; Peng <i>et. al</i> , 2017
MtRad1	Medtr4g104020	GRAS	Yes	Regulator of AM-colonization and arbuscule development; known interactor of DELLA1 and 2, RAM1 and NSP2	Park <i>et. al</i> , 2015; Floss <i>et. al</i> , 2016
MtRam1	Medtr7g027190	GRAS	Yes	Key regulator necessary for AM-colonization higher order branching of arbuscules; known interactor of RAD1, NSP2 and GRAS1; induced by DELLA-complex	Gobbato <i>et. al</i> , 2012; Park <i>et. al</i> , 2015

MtWri5a	Medtr8g468920	AP2/ERF	Yes	RAM1-dependent; Potential direct activator of AM-based FA-biosynthesis genes <i>MtStr</i> and <i>MtKasII</i> as well as <i>MtPt4</i> ; knockdown leads to fewer and truncated arbuscules	Luginbuehl <i>et. al</i> , 2017; Hartung, 2021
MtWri5b (MtErf1)	Medtr7g009410	AP2/ERF	Yes	RAM1-induced; Activator of AM-based FA-biosynthesis genes; potential direct regulator of other AP2/ERF-TFs <i>Mt15867</i> and <i>Mt21492</i> and FA-synthesis gene <i>MtStr</i> ; knockdown leads to deformed arbuscules	Devers <i>et. al</i> , 2013; Luginbuehl <i>et. al</i> , 2017; Hartung, 2021
MtWri5c	Medtr6g011490	AP2/ERF	Yes	RAM1-induced; Activator of AM-based FA-biosynthesis genes; potential direct regulator of other AP2/ERF-TFs <i>Mt15867</i> and <i>Mt21492</i> and FA-synthesis gene <i>MtStr</i>	Luginbuehl <i>et. al</i> , 2017; Hartung, 2021
MtZf1	Medtr5g026730	C3HC4 ZF	Yes	RAM1-independent: active during early infection and around hyphae; infection hampered in knockdown	This work
MtZf2	MtrunA17_Chr7g0268961	C2H2 ZF	Yes	Active in and around arbuscules in strongly colonized root sections; OE might lead to stunted arbuscules	This work

#### 4.6.1 Y2H bait strains expressing *MtPalm1*, *MtZf2* and *MtArf12* exhibit some level of autoactivity

When expressing proteins fused to a yeast binding-domain, autoactivity can occur when the TF itself possesses an activation domain or might recruit components of the yeast transcription initiation machinery. Therefore, to distinguish such endogenous activity resulting from the specific protein expressed and true protein-protein interactions, bait-constructs were initially observed in isolation by plating the target-protein expressing yeast strains on SD-Trp media containing X- $\alpha$ -Gal for a colorimetric measure of activity and with the growth inhibitor Aureobasidin A (AbA).

For the bait strains produced as part of this work, *MtZf2* and *MtArf12* produced the strongest blue staining, indicating considerable autoactivation (Figure 40). For the yeast expressing *MtArf12*, this was even enough to become partially resistant to AbA, making this particular bait strain unsuitable for further analyses. *MtPalm1*, *MtZf1* and *MtArf25* displayed weak to moderate staining activity and were all unable to grow on AbA containing media.

Further experiments with bait strains expressing *MtPalm1* and *MtZf2* showed that autoactivation in yeast matings was so severe that no meaningful results could be obtained. As such, mating experiments with a CDS-library were likewise not performed. In addition, *MtPalm1*- and *MtZf2*- preys revealed no strong candidates for potential interactions in direct matings. For further details, see supplemental chapters S1 and S2.

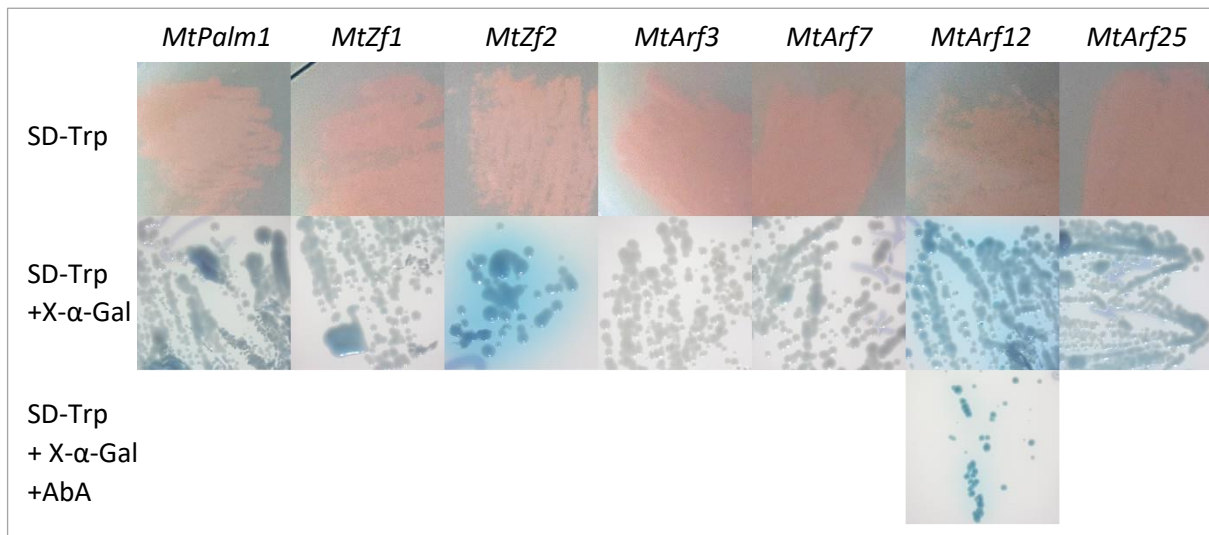


**Figure 40 – Autoactivation-test for Y2H-bait strains produced during this work**

A single colony of transformed Y2H bait strains was streaked onto SD-Trp, SD-Trp+X-α-Gal and SD-Trp+X-α-Gal+Aureobasidin A. All bait strains on their own exhibited normal growth on the SD-Trp control media. Slight blue staining for baits expressing *MtPalm1*, *MtZf1*, *MtArf7* and *MtArf25* indicates weak to moderate autoactivity. Stronger staining was observed for *MtZf2* and *MtArf12*. The yeast strain containing pGBKT7:*MtArf12* was able to overcome the fungicide AbA and was therefore unsuitable for further mating experiments.

Autoactivity for other bait-constructs used as part of direct matings in this work are outlined in Table 22. In general, GRAS-TFs display some autoactivity but do not generally overcome AbA. In contrast, several AP2/ERF-TFs such as *Mt15867*, *Mt21492* and *Mt460730* displayed strong autoactivity such that the corresponding yeast strains could grow on AbA without a mated interaction partner. Thus, despite being interesting potential candidates, they were excluded from further analyses.



**Table 22 – Relative autoactivity of any Y2H bait-strains used in this work**

All transformed Y2H bait-strains bait strains were streaked onto SD-Trp, SD-Trp+X- $\alpha$ -Gal and SD-Trp+X- $\alpha$ -Gal+Aureobasidin A. Relative growth performance on the SD-Trp control media is indicated as +, ++ or +++ in the first column. The same media supplemented with X- $\alpha$ -Gal led to a colorimetric compound indicating autoactivation. Intense blue staining indicates relatively strong autoactivity, while pale blue staining observed in most strains indicates some weak to moderate autoactivation. Bait strains able to grow on media containing Aurebasidin A (AbA) are indicated in the right column and are strongly autoactive. Any strains marked with an asterisk (\*) were generated prior to this work.

Bait-construct	SD-Trp	SD-Trp+X- $\alpha$ -Gal	SD-Trp+X- $\alpha$ -Gal+AbA
pGBKT7: <i>Mt15867</i> *	+++	blue	+
pGBKT7: <i>Mt21492</i> *	++	pale	+
pGBKT7: <i>Mt25005</i> *	+++	pale	-
pGBKT7: <i>Mt460730</i> *	+++	blue	+
pGBKT7: <i>MtArf3</i>	+++	white	-
pGBKT7: <i>MtArf7</i>	+++	pale	-
pGBKT7: <i>MtArf12</i>	+++	blue	+
pGBKT7: <i>MtArf25</i>	+++	blue	-
pGBKT7: <i>MtCbf1</i> *	+++	white	-
pGBKT7: <i>MtCbf2</i> *	+++	white	-
pGBKT7: <i>MtCbf3</i> *	+++	pale	-
pGBKT7: <i>MtGras1</i> *	+++	pale	-
pGBKT7: <i>MtGras4</i> *	+++	pale	-
pGBKT7: <i>MtGras6</i> *	+++	pale	-
pGBKT7: <i>MtGras7</i> *	+++	pale	-
pGBKT7: <i>MtNsp1</i> *	+++	pale	-
pGBKT7: <i>MtPalm1</i>	+++	pale	-
pGBKT7: <i>MtWri5a</i> *	+++	pale	-
pGBKT7: <i>MtWri5b</i> *	+++	white	-
pGBKT7: <i>MtWri5c</i> *	+++	pale	-
pGBKT7: <i>MtZf1</i>	+++	pale	-
pGBKT7: <i>MtZf2</i>	+	blue	-

#### 4.6.2 A Y2H library mating revealed potential interaction candidates for MtZF1

The Yeast 2-Hybrid bait strain expressing *MtZf1* previously shown not to exhibit any considerable autoactivation (Figure 40) was used in a direct mating approach with a variety of TFs relevant for AM symbiosis development or maintenance (Table 23). None of the mated cultures were able to overcome media containing AbA as main criteria for potentially positive interactions. Only some exhibited slight blue staining on the DDO mating control media, thus yielding no potentially positive interaction candidates. The *MtZf1*-preys were likewise mated with a selection of the same TFs as bait-strains, which grew only with strains expressing *MtPalm1* and *MtZf2* – both of which were likely due to autoactivation (see Figure 40 as well as supplementary Tables S2 and S3). Other baits tested produced only minor staining activity and only agreed with the *MtZf1*- bait matings in the case of *Mt25005*. As such, no interaction candidates for MtZF1 were obtained from the Y2H direct mating assays.

**Table 23 – Y2H direct mating results for MtZF1**

Results for prey strains mated with the MtZF1 bait are indicated in the left half of the table. The right half shows mating results for MtZF1 prey mated with a variety of different baits. Growth performance is indicated by the stringency level reached: Growth on the DDO (double dropout) mating control medium needed to be observed to be included as a valid result. Growth on DDO+Aureobasidin A (AbA) indicates potentially weak interactions. The highest stringency quadruple dropout medium (QDO) + AbA indicates strong potential interactions. No growth on higher stringency media than the mating-controls is indicated by a (-). Additionally, observed X- $\alpha$ -Gal staining intensity is indicated as well (blue). Tests not performed are indicated with three dashes and a red color. No potential interaction partners for MtZF1 were identified during this assay.

<b>MtZF1-bait</b>	<b>prey</b>	<b>bait</b>	<b>MtZF1-prey</b>
-	Mt15867	Not tested	---
-	Mt25005	Mt25005	-
-	Mt460730	Not tested	---
-	MtArf3	MtArf3	-
-	MtArf7	MtArf7	-
-	MtArf25	MtArf25	-
-	MtCbf1	MtCbf1	-
-	MtCbf2	MtCbf2	-
-	MtCbf3	MtCbf3	-
-	MtColE	Not tested	---
-	MtDella1	Not tested	---
-	MtDella2	Not tested	---
-	MtDella3	Not tested	---
-	MtGras1	MtGras1	-
-	MtGras4	MtGras4	-
-	MtGras5	Not tested	---
-	MtGras6	MtGras6	-
-	MtGras7	MtGras7	-
-	MtNF-YA1	Not tested	---
-	MtNF-YA2	Not tested	---
-	MtNF-YA3	Not tested	---
-	MtNF-YA4	Not tested	---
-	MtNF-YA5	Not tested	---
-	MtNF-YA6	Not tested	---
-	MtNF-YA7	Not tested	---
-	MtNF-YA8	Not tested	---
-	MtNsp1	MtNsp1	-
-	MtPalm1	MtPalm1	DDO+AbA
-	MtRad1	Not tested	---
-	MtRam1	Not tested	---
-	MtWri5a	MtWri5a	-
-	MtWri5b	MtWri5b	-
-	MtWri5c	MtWri5c	-
-	MtZf1	MtZf1	-
-	MtZf2	MtZf2	DDO+AbA

Since no interaction candidates were identified in direct matings and the *MtZf1*-bait did not exhibit considerable autoactivation, a library screen was performed: Out of an approximate 7.8 million mated clones, 41 colonies were able to grow on DDO+AbA medium. Most of these were also able to grow on the higher stringency QDO+AbA medium and were thus considered potential positive interactors. The inserts of these clones were subsequently checked via PCR and sequencing analyses. BLAST-search results are indicated in Table 24 below.

In total, a number of E2-ubiquitin-conjugating enzymes were identified as potential interactors of MtZF1, pointing at role in targeted protein degradation. Potential targets for such an activity were likewise identified in two cysteine-rich receptor-kinases, three transporters and a putative MADS-box TF. In addition, two potential enzymes were identified as interactors, annotated respectively as a protein disulfide isomerase and a NAD(P)H:quinone oxidoreductase.

In order to confirm these preliminary results, such library mating experiments could be repeated, which was not possible in the scope of this work. Likely interaction candidates could further be confirmed in subsequent direct matings as well as via other targeted methods for investigating protein-protein interactions such as pull-down assays and Bimolecular Fluorescence complementation (BiFC). The latter method was successfully used as part of this work to confirm a number of interactions between GRAS-TFs involved with AM-symbiosis in *N. benthamiana* leaves, the results of which are presented in supplementary chapter S3.

In summary, these Y2H results indicate the role of MtZF1 during AM-symbiosis to be related to ubiquitination-dependent signaling networks.

**Table 24 – Results for the MtZF1 Library mating**

Results compiled from BLAST searches of sequenced fragments obtained from the clones that yielded a potential positive interaction with MtZF1. Annotation data was taken from automated gene annotations from the *M. truncatula* Genome version4/version5. Expression data was obtained from the MtGEA (Benedito *et. al*, 2008; Carrere *et. al*, 2021) as well as a mycorrhization time course (Hartmann, LUH, unpublished). Two genes differentially regulated in the *MtPalm1*-RNAi RNASeq-data are highlighted in green.

Genome v4/v5 ID	Annotation	Expressed in roots	Myc-induced
Medtr3g062450	ubiquitin-conjugating enzyme E2	Yes	No
Medtr5g075580	ubiquitin-conjugating enzyme E2	Yes	No
Medtr7g116940	ubiquitin-conjugating enzyme E2	Yes	No
MtrunA17_Chr7g0275361	ubiquitin-conjugating enzyme 28	Yes	No
Medtr4g073240	ubiquitin-conjugating enzyme E2	Yes	Repressed
Medtr5g075580	ubiquitin-conjugating enzyme E2	Yes	Repressed
Medtr8g071040	ubiquitin-conjugating enzyme E2	Yes	No
Medtr1g021150	ubiquitin-conjugating enzyme E2	Yes	No
MtrunA17_Chr5g0448741	putative transcription factor MADS-type1	Yes	No
Medtr2g088980	cysteine-rich RLK	Yes	Repressed
Medtr2g088930	cysteine-rich RLK	No	No
Medtr4g107530	peptide/nitrate transporter	Yes	No
Medtr5g099280	CMP-sialic acid transporter	Yes	No
Medtr4g094695	heavy metal P-type ATPase Cu-Transporter	Yes	No
Medtr2g035840	heavy metal P-type ATPase Cu-Transporter	Yes	No
MtrunA17_Chr5g0422291	28S ribosomal RNA	Yes	No
Medtr4g091900	NAD(P)H:quinone oxidoreductase	Yes	No
Medtr3g088220	protein disulfide isomerase	Yes	No
Medtr2g007570	PPR containing plant-like protein	Yes	Yes
MtrunA17_Chr8g0347301	Hypothetical protein	Yes	No
MtrunA17_Chr3g0142661	Hypothetical protein	Yes	No
Medtr4g132790	Hypothetical protein	Yes	No
Medtr4g133627	Hypothetical protein	Yes	Repressed
MtrunA17_Chr2g0302191	Hypothetical protein	Yes	No
MtrunA17_Chr7g0219731	Hypothetical protein	Yes	No

#### 4.7 Identification of AM-related TFs interacting with *MtPalm1*, *MtZf1*, *MtZf2* and *MtZf3* promoters via Yeast 1-Hybrid direct mating

During the prior promoter reporter gene studies, all four candidate genes *MtPalm1*, *MtZf1*, *MtZf2* and *MtZf3* exhibited some level of induction under conditions of AMF-colonization. The specific regulation necessary for these responses is likely accomplished via the binding of TFs to cis-acting regulatory elements (CREs) in the genes' respective promoter regions such as the AM-CYC box mentioned under 2.3. or computationally proposed AM-responsive regions (Favre *et. al*, 2014). In order to identify putative transcriptional regulators that might contribute to the specific induction or repression of *MtPalm1*, *MtZf1*, *MtZf2* and *MtZf3* during AM-symbiosis, the respective promoters were analyzed in a Yeast 1-Hybrid direct mating approach with several TFs known or hypothesized for their role during AM as well as the putative ZF-TFs that are subject of this work (see Table 21).

Since it is possible for endogenous Yeast-TFs to bind to the target promoters introduced into their genome and thereby activate the reporter genes allowing for the production of histidine as well as of the enzyme  $\beta$ -Glucuronidase (see also Figure 10), yeast bait-strains initially needed to be tested for autoactivity. To that end, unmated clones were replica plated onto increasing levels (10 mM – 80 mM) of 3-Aminotriazole (3-AT), a competitive inhibitor of histidine-biosynthesis (see also 3.9.1.). Via this test, one bait-strain for each of the promoters was selected for optimal growth on DDO-control-media containing no 3-AT but minimal growth on 3-AT-containing media. The selected clones were used in all mating experiments and are depicted at the bottom of Figures 40 – 43. For *pMtPalm1*, colonies were clearly observed on media with a 3-AT concentration of 10 mM. On 20 mM, only single, very small colonies could grow and no growth was observed at higher concentrations. Therefore, concentrations of 40 mM or higher needed to be overcome for a potential interaction to be accepted (depicted as lines in Figures 41 to 44). Similarly, this test revealed autoactivity for *pMtZf1* up to 10 mM with a single colony sporadically able to overcome higher concentrations, setting the threshold at multiple colonies on 3-AT concentrations of at least 20 mM. Yeast strains for *pMtZf2* and exhibited no visible colonies on any media containing even the minimal 3-AT-concentration of 10 mM. Finally, *pMtZf3* exhibited only a single colony on 10 mM 3-AT indicating likewise very low autoactivity. In addition to these growth tests, colorimetric assays were also performed on these unmated strains as another point of reference for potentially stronger signal due to promoter activation in mated cultures.

Matings of the bait-strains containing the promoters were performed with a total of 30 preys containing *M. truncatula* A17 TFs putatively relevant for AM symbiosis (further information depicted in Table 21), fused to a yeast trans-activation domain to facilitate induction of the reporter genes. This was done in four batches, of which the following results were compiled.

In general, all matings involving the prey-strains producing MtARF5, MtARF7, MtDELLA1, MtNF-YA1, MtNF-YA7 and MtWRI5A consistently grew poorly even on mating-control media, meaning all of the corresponding results involving the 3-AT dilution growth assays need to be evaluated cautiously.

#### 4.7.1 A diverse group of TFs including AP2/ERF, GRAS, and NF-YA potentially bind to the *MtPalm1* promoter

Direct matings involving the promoter of *MtPalm1* revealed an overall stronger ability to overcome 40 mM 3-AT more consistently than the prior autoactivity tests suggested, with most cultures producing at least some very small colonies at this stringency level (Figure 41). At the highest assayed 3-AT concentration of 80 mM, the bait strains expressing the genes *MtNF-YA3*, *MtRad1*, *MtWri5c* and *MtZf1* uniquely exhibited large, clearly visible colonies, making them the strongest candidates for possible further promoter-binding analyses. Overall weaker potential interactions that still exhibited activity above the observable background were recorded for the MtDELLA proteins, all other MtNF-YA-TFs tested, some other GRAS-TFs such as MtRAM1, MtGRAS1, 5 and 7, MtNSP1 and 2 as well as some of the assayed AP2-ERF-TFs such as Mt15867, Mt460730 and MtWRI5B. This breadth of potential interaction was unexpected but perhaps not too surprising given that baits included in this analysis were TFs potentially capable of DNA-binding, some of which may act unspecifically. In order to further distinguish stronger candidates, the colorimetric filter-lift assays were performed as additional evidence for the strength of potential protein-DNA interactions.

In general, agreement between intensity of the staining and ability to overcome 3-AT was good, with most of the strongest bait-candidates, such as those containing *MtNF-YA3*, *MtRad1* and *MtZf1*, also producing increased coloration. Additionally, mating involving Mt25005, Mt460730, MtDELLA2 and 3, MtGRAS5, MtNSP2 as well as WRI5A, B and C produced some of the strongest signals in this assay. The bait strain expressing *MtWri5a* was especially surprising in this context, as it was very weak in its growth assay. This might possibly be demonstrative of overall low fitness even on the control-medium that was observed fairly consistently for matings involving the *MtWri5a*-expressing prey strain.

A similar phenomenon might explain the low growth performance by the previously reported *pMtPalm1*-interactor MtARF5 (Peng *et. al*, 2017), which also exhibited rather poor growth in all mated cultures involving the *MtArf3*-prey construct. The colorimetric  $\beta$ -Galactosidase assay for the *pMtPalm1*-MtARF3 interaction indeed revealed clear induction compared to unmated cultures and was among the strongest signals observed, serving as evidence that the growth assay alone was not a good indicator of true binding activity. However, based on the results of the other *MtArf*-genes tested, no new potential regulators for MtPALM1 from this already known pathway were discovered.

Over the entire heterologous DNA-binding assay a number of new potential regulators of *pMtPalm1* were revealed to be analyzed further: The strongest such candidates are *MtNF-YA3*, *MtRad1* and *MtZf1* due to the observed solid ability to grow on 3-AT as well as clear colorimetric signals. In addition, pre-strains expressing *Mt460730*, *MtDella2* and *3*, *MtGras5*, *MtNsp2* and the *Wri5*-genes *b* and *c* might also make good candidates due to their consistent activity. Finally, further analysis of *Wri5c* might also make sense due to its very strong signal in the colorimetric assay and overall reported conserved activity of all the *MtWri5* genes reported by Luginbuehl *et. al* (2017).

Overall, the diverse group of potential promoter-interactors does not directly provide clear indications for a specific role of *MtPalm1* during AM, though some information can be gathered: potential interactions with AP2/ERF-TFs like the MtWRI5-proteins or *Mt460730* and *Mt25005* are plausible due to the presence of an AP-domain in MtPALM1 (Jiao *et. al*, 2020) and reported reciprocal regulation within this family (Hartung, 2021). A potential regulatory relationship with MtDELLA-proteins would be interesting as it would link regulation of *MtPalm1* to GA-signaling as a reportedly crucial negative early regulator of colonization and arbuscule-establishment. In this context, the other potential positive interactors from the GRAS-family could also be of note as it has been reported for both to interact with each other and with MtDELLA-proteins. Therefore, orchestrated activation of *MtPalm1* by these GRAS-TFs may be a possibility during arbuscule formation. However, the absence of *MtRam1* as a potentially positive candidate as well as the apparent partial independence of *pMtPalm1*-activity from this key regulator would serve as evidence against this hypothesis. Finally, the potential functions of MtZF1 and MtNF-YA3 during AM have not been demonstrated, though DNA-binding is likely due to their activity in all promoter-binding assays. It might be possible that these factors might facilitate DNA-binding for other complexes. Still, these preliminary results would have to be confirmed via additional targeted pull-down assays or ChIP-Seq/ChIP-PCR to be reported as valid.



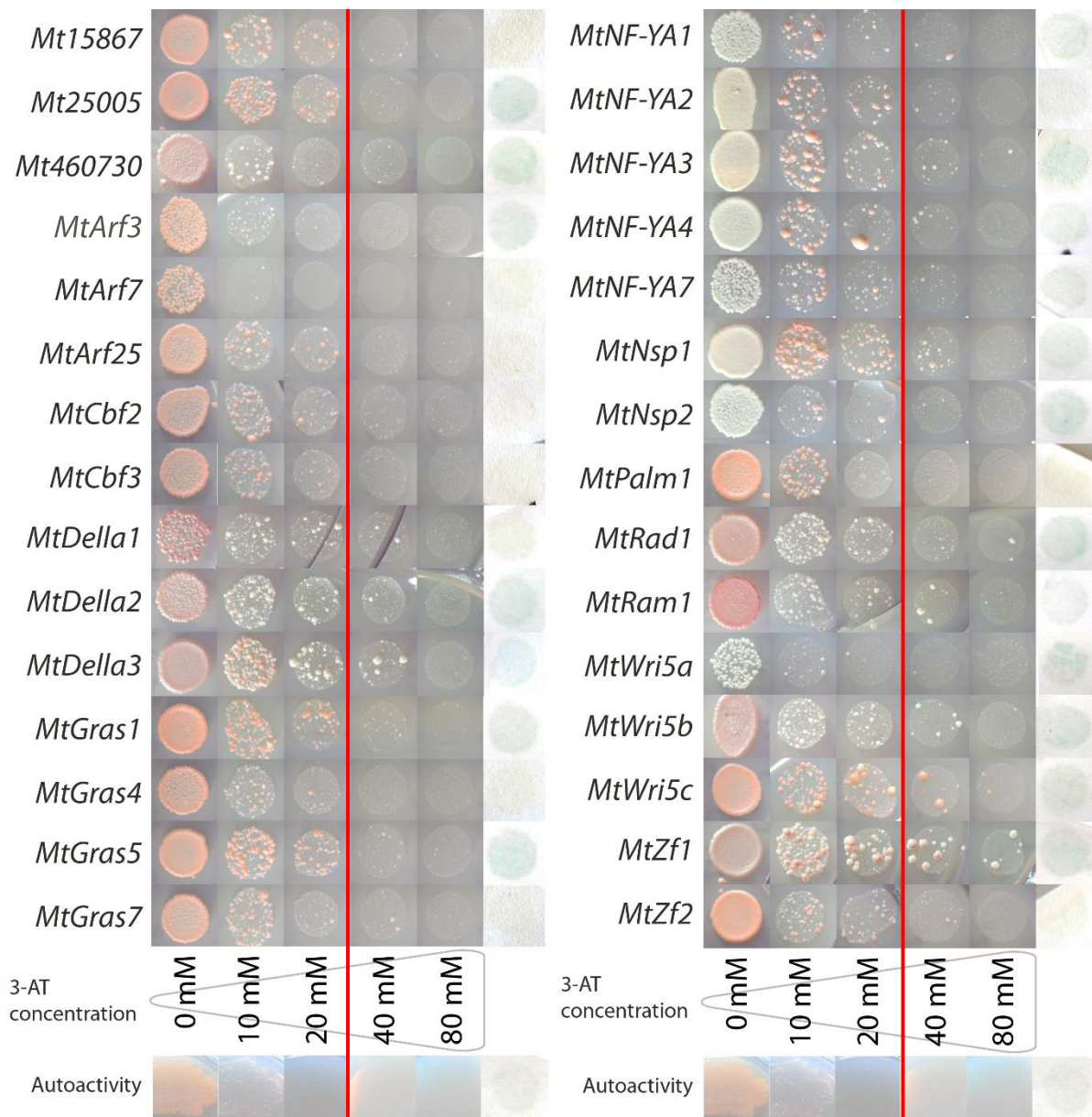


**Figure 41 – Yeast 1-Hybrid assay revealing potential binding of the *MtPalm1* promoter by multiple TFs important during AM**

*S. cerevisiae* YM4271 carrying co-integrated pMWR#2/pMWR#3:p*MtPalm1* were mated overnight with 30 Y187 strains carrying pGADT7-derived plasmids with the CDS-regions of the respective genes and plated onto SD-HIS/-LEU/-URA. For the growth assays, yeasts on 3-AT- concentrations of 10 mM – 80 mM were grown for up to 10 d at 30°C, after which micrographs were captured. For the  $\beta$ -Galactosidase filter-lift assays depicted to the right for each of the matings, colonies grown on the control-plates without 3-AT were replica plated onto YPDA-plates with Whatman-filters and grown overnight at 30°C. Yeasts grown on the filters were then lysed by flash-freezing in  $\text{LN}_2$  and incubated in staining-buffer up to overnight at 37°C before drying and taking photographs. For p*MtPalm1*, the autoactivity baseline, as shown on the bottom, was at 20 mM (also denoted by red line), where small, single colonies were still able to grow. Potential strong interactors such as *MtNF-YA3*, *MtRad1*, *Wri5c* and *MtZf1* were able to grow up to 80 mM 3-AT as multiple single colonies. A number of colorimetric assays show induction strongly above the baseline such as *Mt25005*, *Mt460730*, *MtArf3*, *MtDella2* and 3, *MtGras5*, *MtNF-YA3*, *MtNsp2*, *MtRad1*, *MtWri5a*, *b* and *c* as well as *MtZf1*.



#### 4.7.2 Binding to the *MtZf1* promoter was possible for members of an NF-Y-complex as well as a number of other AM-related TFs

For matings involving bait strains containing *pMtZf1*, generally fewer and larger colonies were observed on 3-AT containing media in comparison to the other promoters assayed. In contrast to the autoactivity level of 10 mM and a single colony at higher concentrations, preys expressing *Mt25005*, *MtGras1* and 5, *MtNF-YA2* and 3, *MtNsp1*, *MtRad1*, *MtWri5c* as well as *MtZf1* and 2 managed to overcome at least a concentration of 40 mM 3-AT with multiple colonies (Figure 42). Other candidates like the yeast strains expressing *MtCbf2* and 3, *MtDella1* and 2 as well as ERF-TF gene *Mt15867* still overcame the 20 mM level in the growth assay.

To further discriminate between this large number of potential interaction candidates, the colorimetric  $\beta$ -Galactosidase assays were also evaluated: Here, the strongest signals were observed for a potential binding by MtCBF2 and 3, MtDELLA2 and 3, MtNF-YA3, MtNSP1 and 2, MtRAD1, MtWRI5C as well as MtZF1. Slight, but visible coloration was also produced by Mt25005, MtGRAS1, MtNF-YA4 and 7, MtRAM1 and MtZF2. In comparison to the other colorimetric assays performed, however, overall activity was low for all *pMtZf1*-matings. When combining these two criteria for a potential positive promoter-protein-interaction, the strongest remaining candidates are MtNF-YA3, MtRAD1 and MtWRI5C, exhibiting both among the strongest growth in the dataset and clear blue coloration. Still, it is clear that for at least this particular *pMtZf1*-bait, overall activity was low, either due to only sporadic interactions or the specific strain possibly exhibiting poor integration of the promoter-reporter gene fusions into the yeast genome. Other remaining candidates for further interaction studies include MtCBF2 and 3, MtDELLA2, MtGRAS1, MtNSP2 as well as MtZF1 and MtZF2, due to clear activity above background in both assays.

The presence of *MtZf1* as a weak positive is interesting and might point to either autoregulation or perhaps nonspecific DNA-binding capabilities. This explanation is supported by the fact that MtZF1 appears as a potential positive interactor in three out of the four promoters tested alongside MtNF-YA3. In this context, MtZF1 and MtNF-YA3 could function as the DNA-binding part of a heteromultimeric complex for example as previously demonstrated with MtCBF2/3, which were also weak positives in this dataset. Potential interactions with GRAS-domain proteins involved in AM-signaling were less here than for example for *pMtPalm1* with only MtRAD1, MtDELLA2, MtGRAS1 and MtNSP2 emerging as good candidates despite being highly represented in the matings. Interactions between these three have only been demonstrated for MtDELLA2 and MtNSP2 with MtRAD1, while the function of MtGRAS1 is as of yet unknown. Additionally, direct regulation by these arbuscule-associated TFs would be unlikely due to the expression of *MtZf1* prior to arbuscule formation, as indicated by the promoter-*gus* data (Figure 27, see also Figure 45).

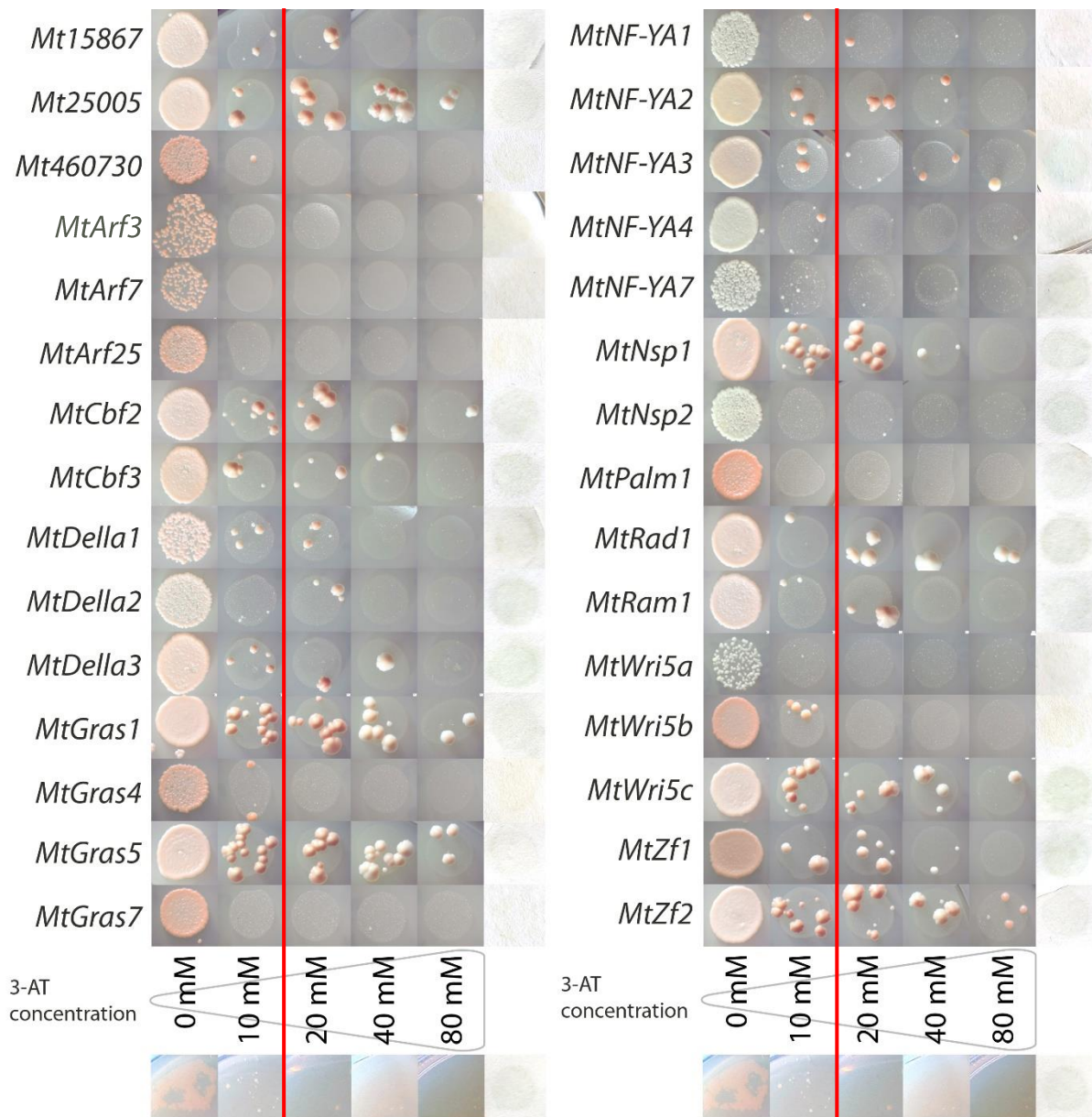


**Figure 42 – Yeast 1-Hybrid assay revealing potential binding of the *MtZf1* promoter by multiple TFs important during AM**

*S. cerevisiae* YM4271 carrying co-integrated pMWR#2/pMWR#3:p*MtZf1* were mated overnight with 30 Y187 strains carrying pGADT7-derived plasmids with the CDS-regions of the respective genes and plated onto SD-HIS/LEU/-URA. For the growth assays, yeasts on 3-AT- concentrations of 10 mM – 80 mM were grown for up to 10 d at 30°C, after which micrographs were captured. For the  $\beta$ -Galactosidase filter-lift assays depicted to the right for each of the matings, colonies grown on the control-plates without 3-AT were replica plated onto YPDA-plates with Whatman-filters and grown overnight at 30°C. Yeasts grown on the filters were then lysed by flash-freezing in  $\text{LN}_2$  and incubated in staining-buffer up to overnight at 37°C before drying and taking photographs. For p*MtZf1*, the autoactivity baseline, as shown on the bottom, was at 10 mM (also denoted by red line), where multiple small colonies were still able to grow. Additionally, higher concentrations still harbored a single colony. Potential strong interactions such as with *Mt25005*, *MtCbf2*, *MtGras1* and 5, *MtNF-YA3*, *MtRad1*, *Wri5c* and *MtZf2* facilitated growth up to at least 40 mM 3-AT as multiple colonies. Stronger colorimetric reactions were recorded for *MtCbf2* and 3, *MtDella2* and 3, *MtNF-YA3*, *MtNsp1* and 2, *MtRad1*, *MtWri5c* as well as *MtZf1* among other weaker reactions above the background.

#### 4.7.3 The *MtZf2* promoter exhibits binding properties in combination with numerous different TFs from various families

For *pMtZf2*-matings with the various TF-bait strains, the background activity level to be overcome was low at 10 mM 3-AT. This stringency level was reached or exceeded by a majority of candidates tested, especially in matings exhibiting strong growth on the control-media (shown in Figure 43). Conversely, some mated cultures that typically grew well across the different assays like for example *MtGras4* or *MtRad1*, were unable to overcome even the background activity level of 10 mM and could clearly be excluded. Cultures like those expressing *MtDella1* or *NF-YA1/7* with a low number of viable mated clones in each of these samples according to the growth on the control media still reached this level, indicating that the growth assay gives reliable results in this instance. When using higher stringency to select for potential interactors, *Mt25005*, *MtGras5*, *MtNsp1* as well as *MtZf1* and 2 stick out with visible to large colonies on the highest 3-AT level of 80 mM.

To obtain further indications for more likely interaction candidates, the colorimetric  $\beta$ -Galactosidase test was also taken into account: Here, activity of *pMtZf2* was observed to be quite high even in the unmated background control. Interestingly, some mated strains were unable to reach even this level of staining like those expressing the *MtArf*-genes or some *MtGras*-genes like 4, 5, 7, *Rad1* and *Ram1*. These typically correlated with low growth in the 3-AT assay as expected. On the other hand, the highest staining activities were recorded in the matings involving preys expressing *MtNF-YA1*, 3 and 7, as well as *MtWri5a* and *b*. Furthermore, strains with *Mt25005*, *MtCbf2* and 3, *MtDella3*, *MtGras1* and 5, *MtNsp2* and *MtZf1* exhibited some activity in the colorimetric test. Still, in contrast to the other promoters tested, none of the strongest indicated candidates from the two activity assays overlapped, leading to a number of potential, weaker candidates for further studies:

The strongest indications could be detected for binding of *Mt25005*, *MtGRAS5* and *MtNF-YA3* to the *MtZf2* promoter due to the relatively strong growth and elevated staining intensities. Some other candidates include *MtCBF2*, *MtDELLA3*, *MtWRI5B* and *MtZF1* due to moderate staining and relatively good growth on at least 40 mM 3-AT. In contrast, low staining but stronger growth was observed for *MtNSP1* and *MtZF2*, whereas *MtNF-YA-7* and *MtWRI5a* could still be interesting for further analyses due to their strong activity in the colorimetric assay.

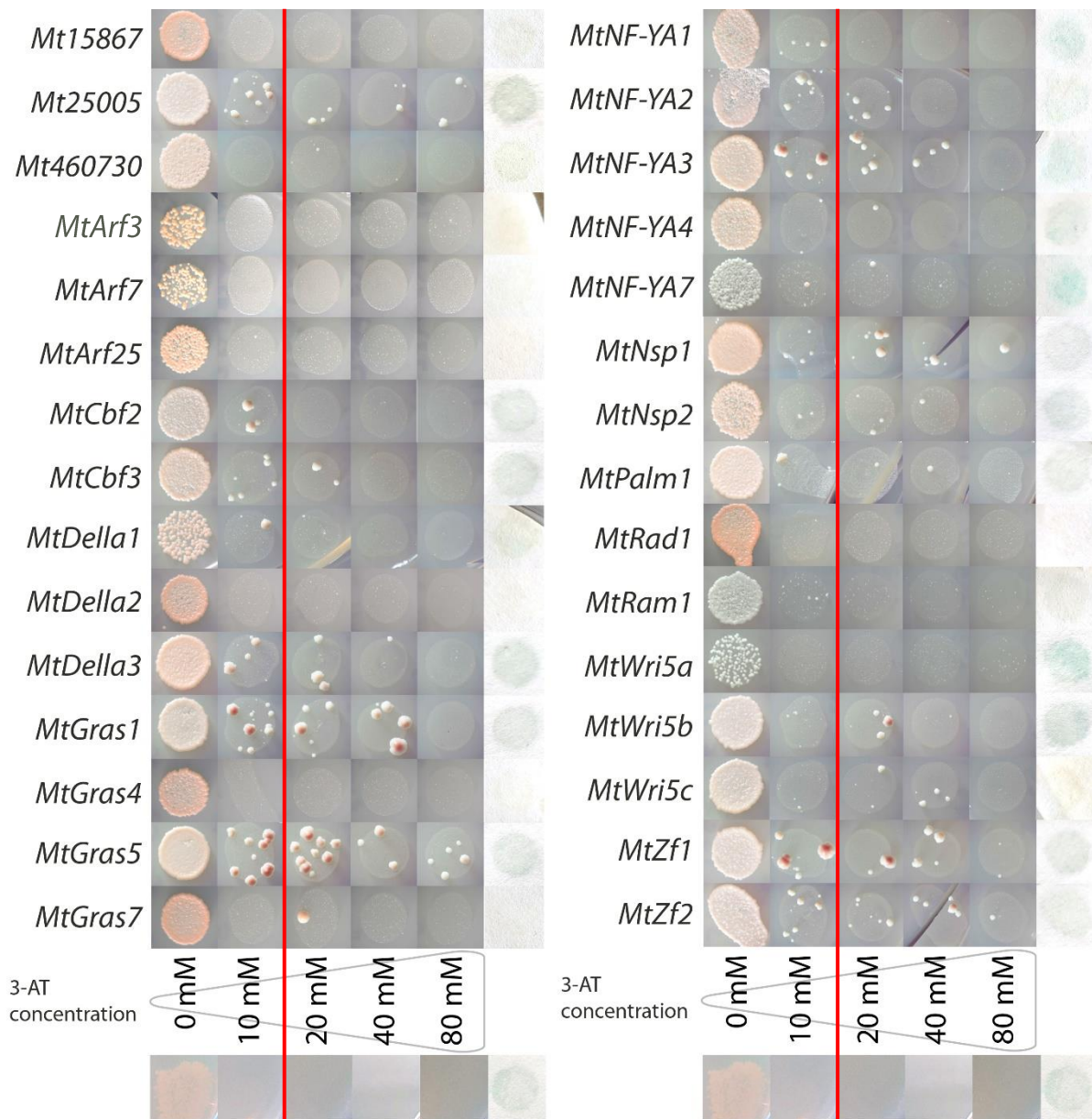


**Figure 43 – Yeast 1-Hybrid assay revealing potential binding of the *MtZf2* promoter by multiple TFs important during AM**

*S. cerevisiae* YM4271 carrying co-integrated pMWR#2/pMWR#3:p*MtZf2* were mated overnight with 30 Y187 strains carrying pGADT7-derived plasmids with the CDS-regions of the respective genes and plated onto SD-HIS/LEU/URA. For the growth assays, yeasts on 3-AT- concentrations of 10 mM – 80 mM were grown for up to 10 d at 30°C, after which micrographs were captured. For the  $\beta$ -Galactosidase filter-lift assays depicted to the right for each of the matings, colonies grown on the control-plates without 3-AT were replica plated onto YPDA-plates with Whatman-filters and grown overnight at 30°C. Yeasts grown on the filters were then lysed by flash-freezing in  $\text{N}_2$  and incubated in staining-buffer up to overnight at 37°C before drying and taking photographs. For p*MtZf2*, the autoactivity baseline, as shown on the bottom, was at 10 mM (also denoted by red line), where some colonies were still able to grow. Potential strong interactions such as with *Mt25005*, *MtGras5*, *MtNsp1*, and *MtZf1*, 2 facilitated growth up to 80 mM 3-AT. A number of mated cultures still exhibited growth above expected background but lower than these top candidates. Clear colorimetric reactions were recorded for *Mt25005*, *MtCbf2* and 3, *MtDella3*, *MtGras1* and 5, *MtNF-YA1*, 3 and 7, *MtNsp2* and 2, *MtWri5a* and *b*; as well as *MtZf1*. It is notable that staining autoactivity was comparatively high for p*MtZf2*.



#### 4.7.4 The *MtZf3* promoter is putatively bound by the AM-related GRAS-TFs MtRAM1, MtNSP1 and MtNSP2

Matings with yeast strains containing the *MtZf3* promoter depicted in Figure 44 exhibited a generally lower ability to overcome 3-AT concentrations compared to the other promoters, as none of the mated cultures were able to grow on the highest assayed level of 80 mM. On the plates containing 40 mM 3-AT, only four candidates exhibited significant growth: *Mt25005*, *MtDella1*, *MtNF-YA3* and *MtNsp1*. In contrast, most matings were able to grow on the next lower stringency level of 20 mM, limiting good indications of potential promoter binding to these four.

In the  $\beta$ -Galactosidase staining, only a small number of candidates overcame the already low background activity with approximately half of all tested prey-strains eliciting no visible response. In quite stark contrast, several matings like those with strains expressing *MtNF-YA3*, *MtNsp1* and *MtWri5a* revealed quite strong activity with a number of others including *Mt460730*, *MtGras1*, *MtNF-YA2*, *MtNsp2* and *MtRam1* at least showing some coloration.

In total, this suggests that overall, only a relatively small number of potential interactions candidates remain for *pMtZf3*, which could be due to lower autoactivity allowing better discrimination of false positives, but might also be an effect of the gene's apparently less AM-dependent expression and therefore less likely connection with this set of TFs implied to have a role in AM-symbiosis. In any case, only *MtNF-YA3* and *MtNSP1* remain as strong potential promoter binding partners, both exhibiting exceptionally strong staining activity and decent growth for this dataset. Medium activity for both tests was recorded for preys expressing *Mt15867*, *MtNF-YA2* and 7, *MtNsp2* in addition to *MtRam1* making these further potential interaction candidates for subsequent studies. These hypothetical connections to regulation by MtRAM1 and associated factors like the MtNSPs might make sense in light of the observed abolition of *pMtZf3*-activity observed in the promoter-gus assay, especially since these TFs activate a large variety of different genes during transcriptional reprogramming for establishment and maintenance of arbuscules.

Finally, ERF-TFs *Mt460730* and *MtWri5a*, while not passing the growth assay, did yield relatively strong results in the colorimetric assay while exhibiting low growth activity even on the control plates, indicating fitness problem that in case of *MtWri5a* were observed in all tests performed.

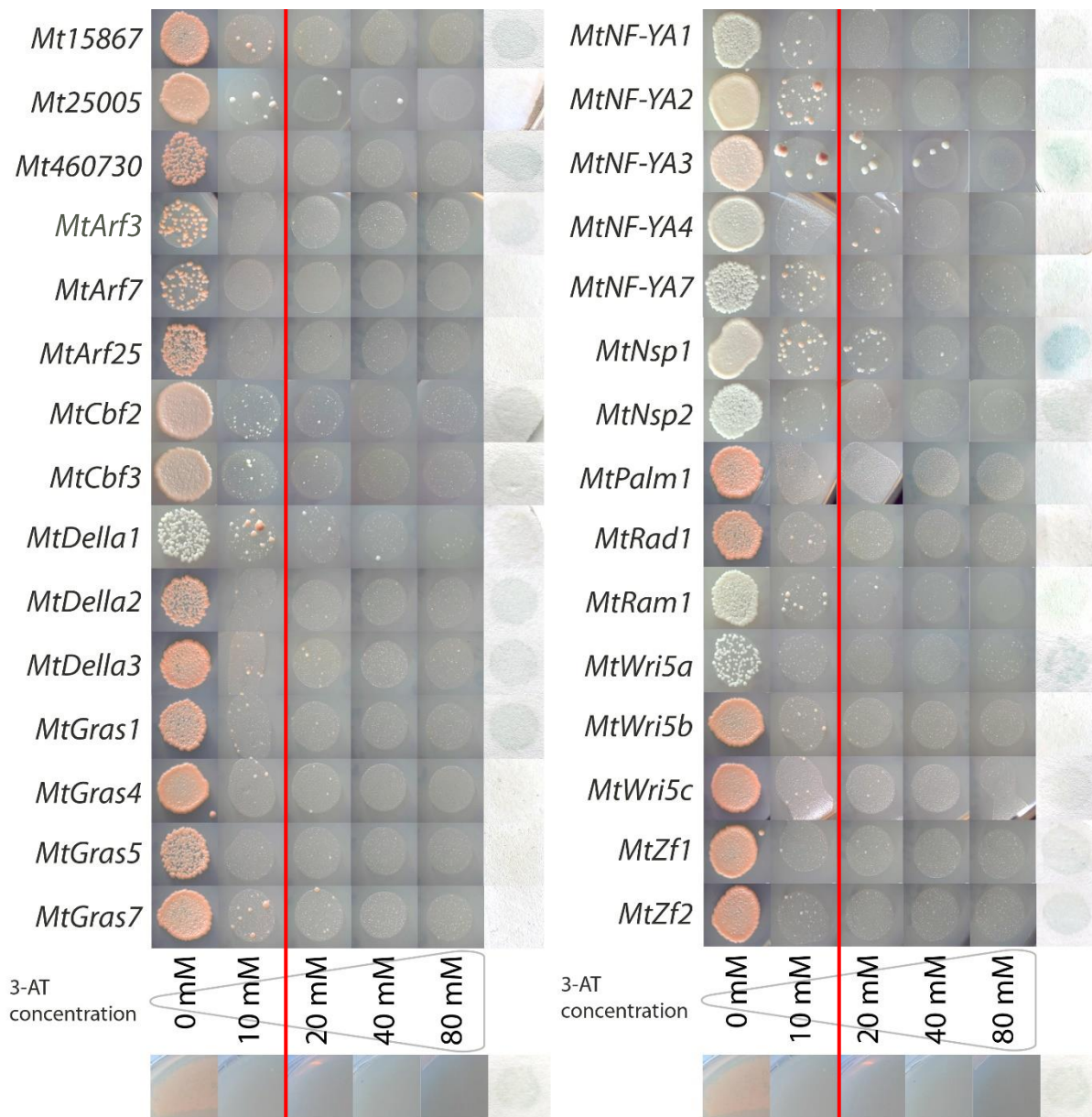


**Figure 44 – Yeast 1-Hybrid assay revealing potential binding of the *MtZf3* promoter by multiple TFs important during AM**

*S. cerevisiae* YM4271 carrying co-integrated pMWR#2/pMWR#3:p*MtZf3* were mated overnight with 30 Y187 strains carrying pGADT7-derived plasmids with the CDS-regions of the respective genes and plated onto SD-HIS/-LEU/-URA. For the growth assays, yeasts on 3-AT- concentrations of 10 mM – 80 mM were grown for up to 10 d at 30°C, after which micrographs were captured. For the  $\beta$ -Galactosidase filter-lift assays depicted to the right for each of the matings, colonies grown on the control-plates without 3-AT were replica plated onto YPDA-plates with Whatman-filters and grown overnight at 30°C. Yeasts grown on the filters were then lysed by flash-freezing in LN<sub>2</sub> and incubated in staining-buffer up to overnight at 37°C before drying and taking photographs. For p*MtZf3*, the autoactivity baseline, as shown on the bottom, was at 10 mM (also denoted by red line), where a single colony was still detected. Potential stronger interactions such as with *Mt25005*, *MtDella1*, and *MtNF-YA3* and *MtNsp1* facilitated growth of clearly visible colonies up to 40 mM 3-AT. A number of mated cultures still exhibited growth above expected background but lower than these top candidates. Clear colorimetric reactions above expected background activity were recorded for *Mt15867*, *Mt460730*, *MtNF-YA2*, and 3, *MtDella3*, *MtNsp1* and 2 as well as *MtWri5a*.

#### 4.7.5 Yeast 1-Hybrid mating results indicate functional regulatory relationships between *MtZf*-gene expression and AM-related TFs

Taking all Y1H direct mating results into account, a number of patterns emerge, as laid out in Table 25: NF-YA3 appears to bind to all MtZF-promoters tested, either indicating a potential nonspecific DNA-binding capacity or a tendency for robust growth in strains expressing *MtNF-YA3*. A similar behavior could also be observed for prey strains expressing *MtNsp1*, *MtWri5a* and *MtZf1*, each of which were weakly positive with three out of the four baits tested. These cases, in addition to prey strains like those containing *MtGras5* and *Mt25005*, consistently exhibiting strong growth capacity, indicate that the employed Y1H system is subject to disturbances by intrinsic, unknown factors, thus harming its potential validity. Similarly, expression of *MtRam1* and *MtWri5a* consistently appeared as detrimental throughout the experiments.

Still, some observations can be made concerning potential functional systems involved with AM, such as the potential binding of the *MtPalm1* promoter by the MtWRI5-TFs involved with FA-biosynthesis and members of the MtDELLA/NSP/RAD-complex of GRAS-TFs regulating arbuscule formation. Similarly, CBFs involved in early AM-signaling appear to potentially bind to the promoter of *MtZf1* alongside some other key early factors like MtNSP1. Reactions with *pMtZf2* were overall diverse, although *Mt25005* and *MtGRAS5* appeared as specifically strong interaction candidates for this promoter. Interestingly, the promoter of *MtZf3*, despite results from other experiments pointing to a minor role in AM, yielded uniquely positive results with MtRAM1 in this experiment alongside both MtNSP1 and 2, indicating a potential role downstream of these factors in the mature stages of the arbuscule life cycle.

Together, the results from the Y1H assays support binding of promoters belonging to *MtZf*-genes by several AM-related TFs and thus further support the role of these genes in AM-related regulatory circuits.

**Table 25 – Summary of Yeast 1-Hybrid direct mating results**

*S. cerevisiae* YM4271 strains containing fusions of the promoters of *MtPalm1*, *MtZf1*, *MtZf2* and *MtZf3* with reporter genes were mated with 30 Y187 strains expressing putative AM-related TFs fused to activation domains. Promoter binding efficiency was estimated based on growth activity on 3-AT-containing media as well as colorimetric assays via X-Gal. Activity above background in both assays or strong activity in one assay are depicted in light green, whereas strong potential promoter binding, as indicated by clear positive results in both assays is shown in dark green.

	pMtPalm1	pMtZf1	pMtZf2	pMtZf3
Mt15867				
Mt25005				
Mt460730				
MtArf3				
MtArf7				
MtArf25				
MtCbf2				
MtCbf3				
MtDella1				
MtDella2				
MtDella3				
MtGras1				
MtGras4				
MtGras5				
MtGras7				
MtNF-YA1				
MtNF-YA2				
MtNF-YA3				
MtNF-YA4				
MtNF-YA7				
MtNsp1				
MtNsp2				
MtPalm1				
MtRad1				
MtRam1				
MtWri5a				
MtWri5b				
MtWri5c				
MtZf1				
MtZf2				



## 5 Discussion

### 5.1 The four *M. truncatula* Zinc finger genes *MtPalm1*, *MtZf1*, *MtZf2* and *MtZf3* feature distinct activation patterns during AM-development and -maintenance

As part of this work on the AM-related *MtZf*-genes *MtPalm1*, *MtZf1*, *MtZf2* and *MtZf3*, their activity was examined via transcript quantification and promoter-reporter gene studies. When taking these different approaches into account, it becomes clear that these genes likely play roles during separate processes and are not part of a single signaling pathway.

Starting with the known leaf determinant gene *MtPalm1*, its activity in roots could be demonstrated to be almost specifically associated with AM symbiotic structures, as measured in the direct comparison of Myc<sup>-</sup> to Myc<sup>+</sup> roots and as expected from the available RNASeq transcriptome data (Luginbuehl *et. al*, 2017). When solely evaluating the observations from the promoter-*gus* study summarized in Figure 45, this correlation appears to be even more specific to just the arbuscule-containing cells, as was expected based on the cell-specific expression profiles shown in Figure 6. However, the early induction during the mycorrhization time course (Figure 13) contradicts this, possibly due to higher sensitivity of these sqRT-PCR measurements compared to the histochemical staining. Therefore, it remains unclear whether *MtPalm1* might still be slightly induced in cells of the root cortex prior to harboring arbuscules. In contrast, activity during the stages II and III of the arbuscular life cycle could be demonstrated in very young infection units (see Figure 15c, d) and is also indicated by the remaining activity in the *ram1-1* mutants (Figure 16) lacking the capacity for fine branching (Park *et. al*, 2015). This limited, but still present observed activity with non-functional MtRAM1, stands in contrast to the RNASeq time course data by Luginbuehl *et. al* (2017), where *MtPalm1* transcript levels were nearly abolished in *ram1-1* mutants (Figure 6). Perhaps mycorrhization due to the mutant *ram1-1* phenotype was so limited in the RNASeq transcriptome dataset that *MtPalm1* mRNAs were below the detection threshold. Nevertheless, promoter activity of *MtPalm1* appears to peak in cells containing fully formed arbuscules, while old and degenerated arbuscules of stage V do not show strong p*MtPalm1* activity, neither in the WT background nor in *pt4-2* roots exhibiting the PAD-phenotype (Figures 15 and 16). Similarly, as additional evidence of little relevance to processes in senescent arbuscules, transcript amounts of *MtPalm1* were reduced at the latest timepoint of 49 dpi in the mycorrhization time course (Figure 13).

Promoter	Myc-	Myc+	Arbuscule	Hyphae	App.	<i>ram1-1</i>	<i>pt4-2</i> (no PAD)	<i>pt4-2</i> (PAD)
<i>pMtPalm1</i>		Dark Blue	Dark Blue			Light Blue	Light Blue	
<i>pMtZf1</i>		Dark Blue	Dark Blue	Dark Blue	Dark Blue	Dark Blue	Dark Blue	Dark Blue
<i>pMtZf2</i>	Light Blue	Dark Blue	Dark Blue	Light Blue		Light Blue	Light Blue	Light Blue
<i>pMtZf3</i>	Light Blue	Dark Blue	Dark Blue					

**Figure 45 – Patterns of promoter activity observed for the different *MtZf* genes**

Compilation of observations based on the promoter reporter gene studies performed on *MtZf* genes. Strong staining activity is shown in dark blue, weaker, but still present induction in light blue and no consistent promoter activity in white. Myc- was considered positive in cases of visible coloration after regular staining periods without AMF present. Myc+ positivity indicates induction with any AMF structure, which was present in all cases. Arbuscules, hyphae and appressoria stand for association with the respective structures. Finally, overall activity in the *ram1-1* and *pt4-2* mutant lines is indicated (in case of *pt4-2* with additional dependence on prematurely degenerated arbuscules).

As compared to the arbuscule-dependent induction exhibited by *MtPalm1* (see also Figure 46), the gene encoding the RING-domain containing protein MtZf1 displays activity in the presence of all AMF structures observed (see Figure 27 and the outline presented in Figure 45). As such, *MtZf1* in roots appears to be induced in all stages of AM, starting directly with fungal contact. This could be observed both in the mycorrhization time course experiment (Figure 13), exhibiting clear induction in the presence of germinating spores, as well as in the promoter reporter gene study showing a *pMtZf1* response to present hyphopodia (Figure 27g, h). Cell-specific expression data from Hogekamp *et. al* (2011) are in agreement as well (Figure 6). Similarly, GUS-staining activity in the vicinity of intraradical hyphae indicates promoter activation before arbuscules are established. Still, based on the present data, it is unclear whether *MtZf1* activity is induced due to fungal contact or – as indicated by histochemical stains like in Figure 27e, f) – might precede hyphal growth within the roots, in service of a function preparing for the arrival of the symbiotic fungus. Once the AMF begins to colonize individual cortical cells forming arbuscules, *MtZf1* remains active. As evidenced by unimpaired staining in the *ram1-1* mutants, this activity is independent of arbuscules reaching maturity and likely has to do with earlier induction than *MtRam1*. Arbuscule degeneration likewise appears not to fully impair promoter activity observed for *MtZf1*, as both older infections in the WT and arbuscules of the *pt4-2* mutants exhibiting a PAD phenotype were stained (Figure 28). In the WT, however, mature arbuscules elicit a more intense response, while transcript levels were diminished in the later stages of the time course, together indicating that *MtZf1* expression is still downregulated during senescence. In total, *MtZf1* appears active all throughout the arbuscular life cycle and possibly plays a role in the entire AM symbiotic program of *M. truncatula* (Figure 46).

Contrasting with the patterns described for the two prior genes, the gene encoding the C2H2 ZF-TF MtZF2 appears more strongly induced in the later stages of AM symbiosis as well as the arbuscular life cycle as a whole, as illustrated in Figure 45. This is evidenced by the expression of *MtZf2* continually rising even at the latest time point sampled in the sqRT-PCR mycorrhization time course measurements, unlike all other candidate and AM-marker genes examined (Figure 13). Likewise, promoter-*gus* staining results indicate *MtZf2* activity to be highest in older and strongly colonized infection units including degenerated arbuscules. Similarly, the staining observed in the *pt4-2* mutants does not visibly change in intensity irrespective of arbuscules exhibiting a PAD phenotype (Figure 33). Indeed, both in the WT and the *pt4-2* mutant background, colonization density had a much more profound effect on staining activity of p*MtZf2* than the condition of mycorrhization. For *ram1-1* mutants, no clear AM-associated p*MtZf2* activity could be observed, though the vascular staining seen under Myc- conditions was also present. Unfortunately, as with the overall weak response and the high vascular background activity of the *MtZf2* promoter, it is unclear whether these effects are intrinsic or have to do with the likely incomplete nature of the construct due to the unclear exon-intron-structure of the gene annotation and the presence of an upstream ATG possibly affecting the GUS staining (Figures 31 and 32). This could be rectified in future studies by repeating the experiment with constructs of varying lengths of promoter regions to possibly obtain more specific patterns of activity that might more clearly reflect the expected expression levels. Indeed, measured transcript levels are similar between *MtPalm1* and *MtZf2* in the RNASeq and sqRT-PCR approaches, which is not reflected by the observed promoter staining activities (Figure 6 and 13). Still, even with the present data, some additional information can be extracted: induction of *MtZf2* does not appear to fully depend on regulation by RAM1, as demonstrated by promoter GUS-staining and measurable expression in the *ram1-1* mutant line (Figures 6 and 33). Consistent with this, the sole presence of intraradical hyphae appears to still provoke a slight response, though no activity around hyphopodia could be observed.

While appearing especially crucial for *MtZf2* activity, all three genes highlighted above share a feature within their 5'-UTRs in the form of upstream ATGs. These additional upstream ORFs (uORFs), prior to the protein coding regions can act as regulatory elements in various ways and have been observed to be overrepresented in promoter regions of TFs (Yamashita *et. al*, 2003). Overlapping ORFs (oORFs), where the uORF coding region forming a small peptide overlaps with the 5'-region of the CDS, have been demonstrated to contribute to negative translational regulation through competition of the ORFs for ribosomal coverage (Guerra-Almeida *et. al*, 2021). For p*MtPalm1*, such a mechanism appears likely, as the *ver2* promoter-*gus* construct with the putative oORF removed exhibited substantially higher levels of activity (compare Figure 14) in mycorrhized roots. In the future, additional quantitative GUS-assays could add further clarity. As for the putative regulatory mechanism, some very preliminary

analyses predict the ATG of the oORF to part of mRNA secondary structures that might cause this feature to be skipped under certain conditions (data not shown). In the case of *MtZf1*, a similar region was identified encoding a 38 aa peptide from position -14. In its class of RING domain proteins, such features have been documented as a conserved positive regulating mechanism in the form of 5'-introns (Aguilar-Hernández and Guzmán, 2013). Due to the inclusion of these introns via alternative splicing, increased gene expression is achieved through the process of Intron-Mediated Enhancement (IME, Chung *et. al*, 2006). As the activity of the full *pMtZf1-gus* construct was fairly high, such positive regulation appears plausible, but could not be investigated yet in the scope of this work.

In addition to these mechanisms, stop-codons present in uORF regions have been demonstrated to contribute to negative transcriptional regulation through nonsense-mediated mRNA decay. This could be the case for *pMtZf2*, where the full ver1 of the promoter did not yield any activity in the GUS assays. In the 5'-UTR, excluded from the examined ver2 construct, a potential upstream coding region in frame is present with the CDS, but contains a stop after yielding a six aa peptide (see Figure 32a). In addition, small peptides produced from uORFs may play a further role in autoregulation of the downstream genes, as was already demonstrated in the context of root symbiosis for the NF-YA1-TF gene (Combiere *et. al*, 2008). These regulatory uncertainties further highlight the need for further experiments to elucidate the significance of these features, especially with additional versions of the *MtZf2* promoter.

The promoter region of *MtZf3* was the only one examined without a detected uORF. In line with this, the observed expression profile appears clear: Despite the expected and observed considerable background activity, a significant association with arbuscules is still present (Figure 37). Further, this activity appears unimpeded in old and degenerated arbuscules (Figure 37i, j), indicating a role in the mature to later stages IV and V of the arbuscular life cycle, as outlined in Figure 46. Similarly, hyphae alone elicit no increase in *pMtZf3* activity. In contrast to all other candidate genes, this promoter response is fully abolished in arbuscules with impeded nutritional exchange of the *pt4-2* mutants and in the *ram1-1* background unable to form mature arbuscules (Figure 38). This could be due to the activation of *MtZf3* being impeded by a ruptured signaling cascade in these mutants. This pattern would fit to the results obtained from the Y1H assays showing potential direct promoter binding by MtRAM1 (Figure 43). Additionally, both MtNSP1 and 2 showed some activity with *pMtZf3*, which could indicate a whole functional unit of interacting GRAS proteins inducing *MtZf3* transcription. However, the presence of *MtZf3* transcripts at normal levels in the Luginbuehl *et. al* (2017) data contradicts this (Figure 6), perhaps indicating a response to different mycorrhization regimes or a different nutritional status. Experiments using specific nutrient regimes including higher Pi could be used to elucidate this possibility. Likewise, the activity profile obtained from a relatively short length promoter used in these experiments – necessitated by the close proximity of annotated upstream genes – might be misleading.

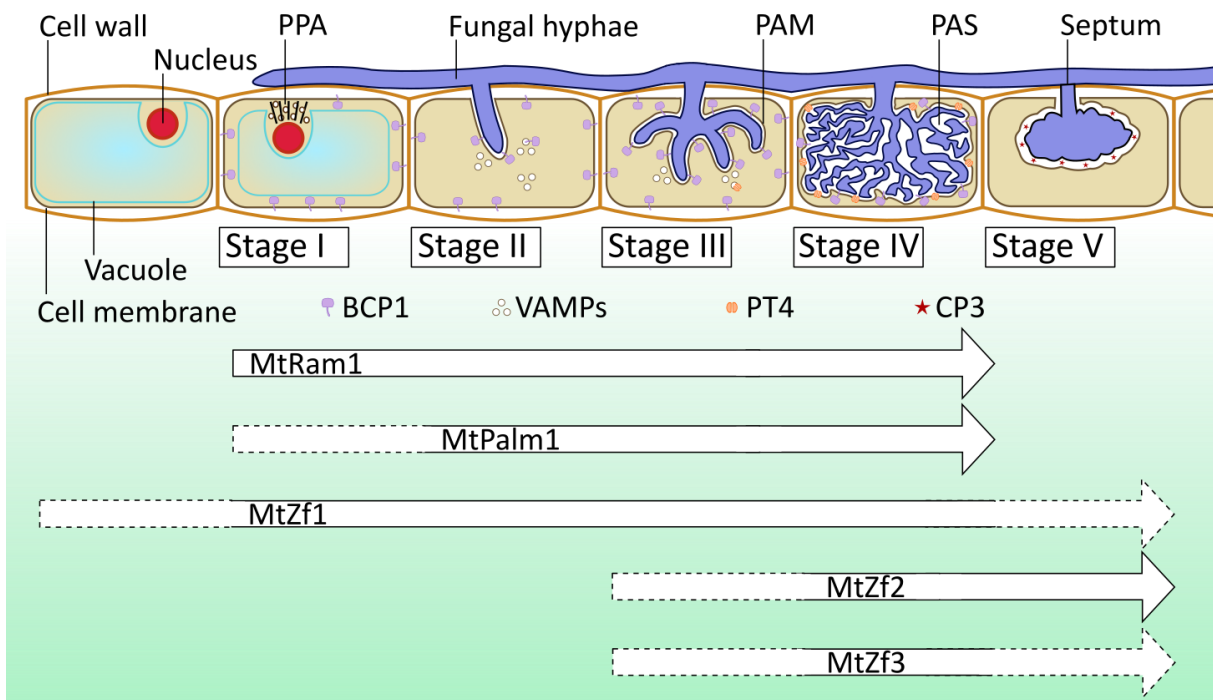


**Figure 46 – Major patterns of *MtRam1* and *MtZf* activity during the arbuscular life cycle**

In comparison to the expression pattern of the key regulatory gene *MtRam1*, which is active prior to the invagination of the fungus into the cell and remains active until the mature stage, *MtPalm1* activity could not be directly observed prior to colonization of individual cells. However, such activity is likely still weakly present (indicated by dotted line), as a slight induction of transcription was observed in the presence of germinating spores. Fully degenerated arbuscules likely show only a residual response of *pMtPalm1*. For *MtZf1*, induction was clearly observed in the presence of hyphae prior to the establishment of arbuscules, though arbuscules also activate this gene. Further observations from histochemical stains indicate possible activity in preparation for a proceeding fungal infection. *MtZf2* gene activity is most strongly induced in arbuscule-containing cells that have reached the mature stage. This activation is retained in the presence of degenerating or degenerated arbuscules as well. Induction independent of RAM1 indicates that it is also present prior to fine hyphal branching in the transition from Stage III to Stage IV. *MtZf3* is clearly induced in arbuscules of the mature stage. Earlier and later activity were occasionally observed in a WT background, but its AM-dependent activity is abolished in the *ram1-1* and *pt4-2* mutant backgrounds, indicating dependence on fully developed arbuscules.

## 5.2 Insights into the involvement of *M. truncatula* ZF proteins in the development and maintenance of the AM-symbiosis

### 5.2.1 The CCCH ZF protein encoded by *MtZf3* plays a minor role during AM-symbiosis

The knockdown experiments performed with *MtZf3* were based on two separate RNAi constructs. Of these, only *MtZf3*-RNAi-1 yielded a significant reduction in transcript levels (Figure 39a-c). Across all three separate repetitions, AM-marker genes including *MtPt4* were only significantly reduced in the second (see Figure 39d-f). A significant, though comparatively minor reduction in arbuscules was observed in this experiment as well. Furthermore, a minor reduction in overall AMF colonization was detected in the first knockdown experiment in spite of no clear reduction in AM marker gene expression. This result was likely only significant due to the sample pooling uniquely done in that round to obtain sufficient material for counting the AM structures, as the small decrease by ~12% would otherwise have been masked by the variation between individual root samples (Figure 39g-i). These slight effects of MtZF3 deficiency point towards some role in the process of AM, as do the results from the promoter activation and potential binding by crucial GRAS factors MtNSP1/2 and MtRAM1 (Figure 43). Still, a weaker involvement compared to the other *MtZf* candidates is likely, especially when also taking into account its much less specific expression profile. It could be hypothesized that *MtZf3* reacts to functional nutritional exchange during AM and leads to an amplifying effect on mycorrhization or enhanced arbuscule maintenance. In this capacity, measured responsiveness to the phytohormone ABA demonstrated by Zhang *et. al.*, (2013) could work as a mediator, as this hormone is involved in stress responses including nutritional stresses. In this context, a connection to signaling involving MtPALM1 could also be examined further. In order to test such claims in the future, it makes sense to study mutant lines, as was done for *MtPalm1* and *MtZf2* in this work. Additionally, such a boosting effect could be further examined in overexpression studies *in planta* as well as potential interaction assays for the MtZF3 protein.

### 5.2.2 The RING-domain protein encoded by *MtZf1* is involved in AM signaling and might contribute to targeted proteolysis in preparation of fungal colonization

During this study, a partially effective RNAi construct was created to achieve a knockdown of *MtZf1* expression in mycorrhized roots. Unfortunately, across the entire samples sets, a significant effect was only observed in one of three experiments performed (Figure 30a-c). When examining individual root samples, approximately half exhibited a strong downregulation of *MtZf1* transcripts as well as AM-marker genes, resulting from strongly hampered mycorrhization (Figures 30d-i and S11). As the *MtZf1* gene is strongly induced due to AM, it is intrinsically unclear whether the absence of MtZF1 is the actual cause for the reduction in mycorrhization or if lower levels of AM-colonization in turn lead to

the diminished expression. Furthermore, while roots with putatively successful knockdowns were strongly reduced in AMF colonization, no specific effects such as arbuscule degeneration or a clear reduction of individual intraradical features such as vesicles or hyphae were seen (Figures 30j and k, Figure S5).

Still, the nearly complete abolishment of *MtZf1* transcripts in individual root samples was uniquely observed in the RNAi group, serving as evidence of this behavior being a genuine knockdown effect intrinsic to the *MtZf1*-RNAi-2 construct. In addition, while a certain level of variability in the efficacy of RNAi-based knockdowns in transgenic root systems is expected (Limpens *et. al*, 2004) and was observed throughout all experiments performed for *MtPalm1*, *MtZf2* and *MtZf3*, the clear effect of either almost no *MtZf1* expression or WT transcript levels was a specific feature of *MtZf1*-RNAi-2 (compare Figures S3, S11, S12 and S13). Normal RNAi variation in the system comes about due to each transgenic root representing a unique insertion event as well as the possible presence of WT roots during growth and mycorrhization that are only fully removed during sample collection. Additionally, the sequences used for the RNAi construct themselves have a strong influence that is still poorly understood. It has been proposed that the expression of small dsRNAs negatively influences the production of siRNAs (Joga *et. al*, 2016), which might explain the complete ineffectiveness of *MtZf1*-RNAi-1, the smallest of the constructs used in this work and lower effectiveness for *MtZf1*-RNAi-2. Still, strong variation in RNAi efficiency between samples has been documented extensively, with approximate knockdown effects in only 50% of individuals occurring commonly (McGinnis, 2010). Overexpression of *MtZf1* yielded no significant effects of any kind, which might additionally point to the basic AM-induced expression levels of the gene to be sufficient to fully serve its function. Conversely, it could be hypothesized that lower knockdown effects in individual roots could stem from remaining *MtZf1*-levels being sufficient for fully normal AM-development. Root samples with substantially effective RNAi, instead might reduce MtZF1 below a functional level, leading to feedback-loop causing the very strong disruptions in mycorrhization observed.

In any case, an attempt to confirm this colonization reduction phenotype in the *Tnt1*-line NF0154 was unsuccessful in this study, as no actual insertion in *MtZf1* could be identified. Other *Tnt1* lines such as NF20003, putatively containing a mutated *MtZf1* gene have become available as part of ongoing efforts by the *M. truncatula* Mutant Database (Tadege *et. al*, 2008). As such, further tests in a similar mutant-complementation assay as with *MtPalm1* and *MtZf2* could be performed in the future to add evidence of the potential AM-reduction phenotype observed in the RNAi. If this is not feasible as for example due to lethality of homozygous mutants, another RNAi approach might be performed as well using either the native promoter (Trung Pham, LUH, unpublished) or an AM-dependent promoter (Devers *et. al*, 2013) acting similarly early in the symbiosis such as p*MtCbf2*.

Results obtained from the Yeast 2-Hybrid Library Mating approach suggest a role of MtZF1 as a protein-binding factor involved in ubiquitination through the observed interactions with a variety of E2 ubiquitin-conjugating enzymes (Table 24). Proteins containing a putative RING domain like MtZF1 have often been described as having ubiquitin-ligation activity. Data from the present Y2H study is able to better support this function than other potential roles such as transcriptional or translational regulation of expression can (Borden, 2000), with only one MADS-box-TF and one ribosomal component being identified as potential interactors. Further, there are some automated KEGG-annotations of MtZF1, which predict a ubiquitination activity of its own due to similarity to the AtATL52-protein.

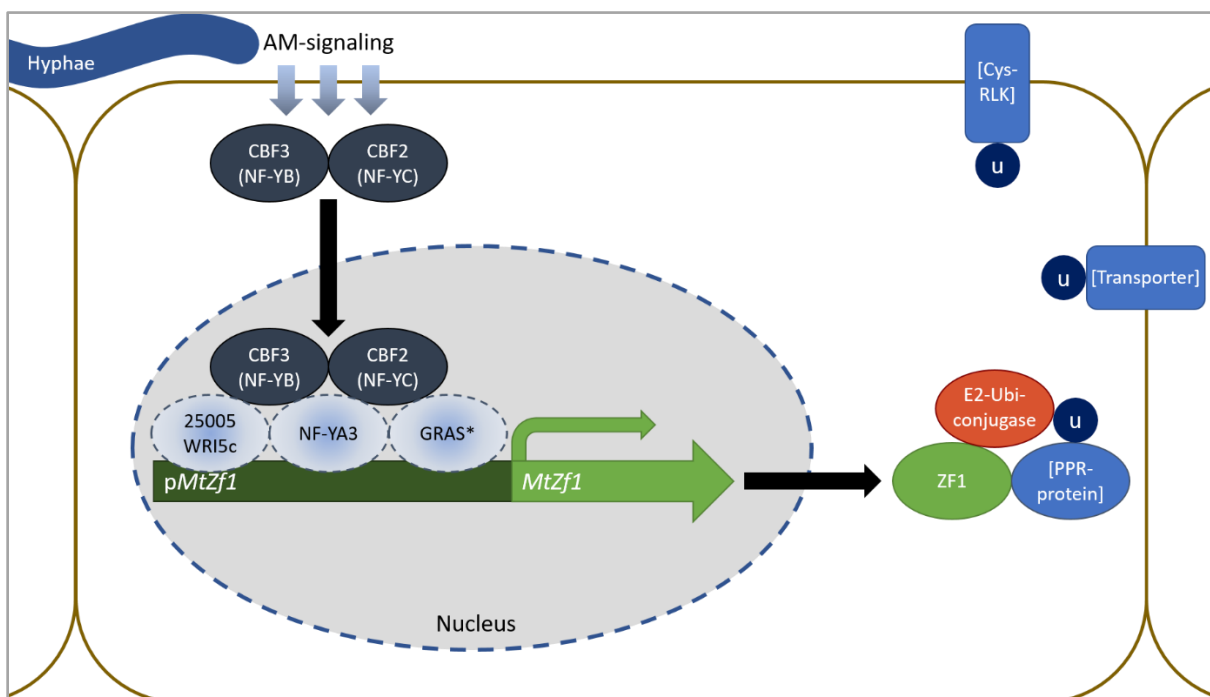


**Figure 47 – Model for the AM-based induction and activity of *MtZf1***

The CCAAT-box binding factors CBF2 and CBF3 (dark blue) are induced as part of the early AM-signaling program in response to AMF contact. They act as NF-YB and -YC-subunits of heteromultimeric NF-Y-TFs, which dimerize in the cytoplasm before translocating into the nucleus (gray) to associate with a DNA-binding NF-YA-subunit. Based on the Y1H data, NF-YA3 could directly bind to the promoter region of *MtZf1* indicated in green, with CBF2 and 3 exhibiting some potential for binding as well. Additionally, AP2/ERF-TFs MtWRI5c and Mt25005 also exhibited such binding potential and have been identified as potential interaction partners with CBF2/3 (Hartung, 2021). Furthermore, a number of GRAS-TFs (marked with \*) such as MtDELLA2, MtNSP2, MtGRAS1 and MtRAD1 are also candidate regulators of *MtZf1*-expression. Once expressed, the MtZF1 protein (green) could act as a E3 ubiquitin ligase for targeted proteolysis in preparation for AM-colonization. Besides binding a number of E2 ubiquitin-conjugases, MtZF1 also associated with potential targets such as Cysteine-rich receptor-like kinases (Cys-RLK), a number of membrane transporters and a pentatricopeptide repeat (PPR) protein (marked with u for potential ubiquitination).



Targeting specific proteins for ubiquitin-based proteolysis has been described as part of symbiotic regulation processes such as the regulation of the LYK3 receptor kinase, a part of the CSSP by the PUB1 E3 ubiquitin ligase (Mbengue *et. al*, 2010; Wang *et. al*, 2021a). Similarly, a RING-H2 domain protein in *M. sativa* had, among exhibiting other effects, an impact on the root nodule symbiosis (Karlowski and Hirsch, 2003). It is therefore possible that MtZF1 binds to specific proteins and directs them towards other ubiquitin ligases or performs this ubiquitination itself. When taking into account the early induction of *MtZf1*, its role illustrated in Figure 47 might involve degradation of specific proteins in preparation of AM-colonization. Some of these potential targets have also been identified in the Y2H data such as several transporters, a component of the respiratory chain and two cysteine-rich repeat containing receptor kinases, one of which has been observed as being potentially involved in nodulation (Wang *et. al*, 2021b). Contrary to this hypothesis, no clearly known or hypothesized negative regulators of AM-symbiosis were identified in the library mating dataset. Interestingly, however, two of the potential MtZF1 interactors were found as differentially expressed in the *MtPalm1*-RNAi RNASeq study, possibly suggesting a connection (see Table 24). Still, repetitions of the Y2H experiment as well as direct confirmations via direct mating approaches and possibly BiFC are needed to obtain more complete results.

The lack of autoactivation for Y2H baits expressing *MtZf1* that enabled these results itself can be seen as further evidence against activity as an expression-enhancing TF: while the C2H2-ZF TFs MtPALM1 and MtZF2 were clearly able to induce reporter gene expression without the presence of a prey containing the activation domain, MtZF1 was not (see Figure 40). Such argumentation for or against activity as a transcriptional activator based on bait autoactivity has been used prior by Heck *et. al* (2016). Contrary to this hypothesis of MtZF1 primarily binding to other proteins is its ability to activate the *MtPalm1* and *MtZf2* promoters, as observed in the Yeast 1-Hybrid assays (see also Figure 40 and Table 25). Such behavior could stem from association with endogenous yeast DNA-binding proteins, as was reported by Hirsch *et. al* (2009).

During the same Y1H assays (Figure 42), p*MtZf1* itself was putatively bound by the CBF proteins MtCBF2 and MtCBF3, encoding for an NF-YC- and NF-YB-TF-subunit, respectively. As part of their mode of action, these proteins are known to form heteromultimeric complexes between each other as well as associating with NF-YA-subunits or other DNA-binding proteins (Mantovani, 1999; Ben-Naim *et. al*, 2006). This has to occur in the heterologous yeast system as well, with previous works suggesting that NF-Y-subunits from other species are able to complete functional complexes (Calvenzani *et. al*, 2012). In the functional context of plants, proteins forming the DNA-binding portions in NF-Y-complexes include the AP2/ERF-TFs Mt25005 and MtWRI5c that also yielded positive results with the baits containing the *MtZf1* promoter (Hartung, 2021). Similarly, actions in concert between NF-Y proteins

and NSP1/2 have been suggested for establishing the root nodule symbiosis (Baudin *et. al*, 2015). Functional analyses of *MtCbf2* and *MtCbf3* showed an early induction during AM-symbiosis and suggested a strong positive effect on the overall mycorrhization (Hogekamp *et. al*, 2011). It is therefore plausible for *MtZf1* to be a positive regulatory target for a complex of CBFs during early AM-signaling, in order to prepare cells for colonization by degrading specific proteins detrimental to the AMF.

Obviously, this hypothesis is, in addition to the expression profiles, mainly based on Y1H and Y2H-results, being limited by potential false positives in a heterologous system. To collect further evidence, direct DNA-binding could be demonstrated more clearly in a pull-down assay. Similarly, a co-overexpression of the *MtCbfs* might show induction of *MtZf1* as a further demonstration of a direct regulation. As for the specific mode of action for MtZF1, besides the additional protein-interaction assays mentioned above, subcellular protein localization studies could help to elucidate its activity and test the prior hypothesis of its concrete role during AM.

### 5.2.3 The C2H2 Zinc finger TFs encoded by *MtPalm1* and *MtZf2* are important for the full functionality of AM symbiotic program

In order to confirm a role of the C2H2 TF MtPALM1, also known to be important for leaf morphology, *MtPalm1* knockdowns were performed via RNAi in mycorrhized *M. truncatula* A17 root systems. Both of the RNAi constructs employed across three separate experiments were successful in significantly reducing the measurable *MtPalm1* transcript levels, with *MtPalm1*-RNAi-1 exhibiting perfectly stable efficacy (Figure S3). *MtPalm1*-RNAi-2, despite showing a stronger effect in successful approaches, was less consistent with two out of three significant knockdowns. In all five sample pools exhibiting the typical >80% *MtPalm1* transcript reductions, expression of the arbuscule marker gene *MtPt4* was likewise strongly and significantly reduced, indicating a negative impact on the AM-symbiosis (Figure 18a-f). Microscopic observations of intraradical AMF structures revealed a clear reduction of overall fungal colonization and an especially strong reduction in the abundance of arbuscules in *MtPalm1*-RNAi roots in four out of six assays (Figure 18g-i). Due to unknown reasons, one set of samples exhibiting a strong AM marker gene reduction did not show any clearly diminished AM-symbiosis on the morphological level, highlighting a need for further confirmation of this otherwise strong indication of a causal relationship between impairment of MtPALM1 and a reduced mycorrhization.

The RNAi assays targeting *MtZf2* were also successful, with both distinct RNAi knockdown constructs yielding a significant knockdown in all sample pools assayed (Figure 35a-c). Due to time constraints, the *MtZf2*-RNAi experiment was only performed twice, compared to all other RNAi target genes in this work. In these mycorrhized roots with reduced *MtZf2* expression, significant reductions of AM marker

gene expression were measured in two out of four cases (Figure 35d-f). When microscopically observing intracellular AMF structures, one out of these two sample pools exhibiting a substantial AM marker gene reduction was also significantly hampered in overall mycorrhization (Figure 35g, h). As such, a clear physiological effect was only obtained in only one assay, indicating a regulatory role of MtZF2 during mycorrhization of *M. truncatula* that is comparatively minor.

Still, to ascertain these initial knockdown results, *M. truncatula* R108 *Tnt1* insertion lines were examined to confirm potential phenotypic effects of the absence of functional MtPALM1 and MtZF2 in mycorrhized roots. To that end, homozygous plants of the NF18424 and NF6681 lines were confirmed to contain KO mutations in the CDS regions of *MtPalm1* and *MtZf2*, respectively, with the former exhibiting the pentafoliate phenotype characteristic of the MtPALM1 deficiency.

In a direct comparison between mycorrhized *MtPalm1-Tnt1* plants and WT controls, the RNAi results were largely confirmed, with the MtPALM1 deficient group exhibiting significant reductions in AM marker gene expression and overall mycorrhization (Figure 19). As with the knockdown assays, this AM reduction phenotype has an especially strong effect on the number of arbuscules observed. Via the introduction of a secondary *MtPalm1* gene from the A17 cultivar into this mutant background, this observed reduction was partially rescued. In this context, this meant slightly reduced mycorrhization levels compared to the WT and more AM colonization compared to the full mutants. As such, the effect of MtPALM1 deficient roots exhibiting an approx. 50% reduction of arbuscule containing cells could be confirmed using this approach (see Figures 18 and 19). However somewhat unexpectedly, this reduction was not clearly stronger than in the knockdown experiments, despite the complete abolishment of *MtPalm1* expression and function. Such results have previously been documented by Jiang *et. al* (2018), where an RNAi-based knockdown yielded overall stronger phenotypic effects on the AM than a potential loss of function mutant.

Interestingly, both in the RNAi-knockdown and in the full mutant lines, *MtPalm1* deficiency caused only quantitative reductions in mycorrhization, while no clear effects on arbuscule morphology were observed, indicating that while arbuscules are reduced in number, their functionality is likely retained. Such phenotypes were previously described for mutants of genes involved in controlling overall AM colonization such as the very early CBFs 1 and 2, NSP1, as well as GA-signaling involving DELLA proteins and DIP1 (Delaux *et. al*, 2013; Yu *et. al*, 2014; Park *et. al*, 2015; Steven Krüger, LUH, unpublished). Many of these TFs integrate hormonal signals (GAs and SLs), potentially suggesting a mode of action for MtPALM1 that will be discussed later.

The same experimental setup used for the *MtZf2-Tnt1* mutants yielded similar results with significant decreases in AM marker gene expression and overall mycorrhization in the roots examined (see Figure

36). As with the prior RNAi experiments, this reduction is more minor in comparison to the results for *MtPalm1* with around 45% reduction in overall AM-colonization and no specific AMF structures being disproportionately affected (compare Figures 19 and 36). Again, the reduction observed in the RNAi roots was stronger as well and the complementation did not fully restore WT mycorrhization levels. This likely results from the expression of the A17 *MtZf2* gene in the R108 background, since it contains a number of differences, especially in the promoter- and intron-regions included as part of the complementation construct. Furthermore, individual transgenic roots representing unique insertion events may have caused complementation with varying expression levels for the constructs as an additional confounding factor. As such, even the more minor influence of reduced or fully abolished MtZF2 on AM could be confirmed.

To further elucidate potential modes of action of *MtZf2* during the AM-symbiosis, results from the overexpression approach can be considered (Figures 17, 29 and 34): Out of the three genes *MtPalm1*, *MtZf1* and *MtZf2* that were overexpressed in mycorrhized *M. truncatula* transgenic roots, only the increase of *MtZf2* transcripts throughout the whole root system had an apparent effect on the AM-colonization. Similar to the RNAi knockdown, transcript amount for the arbuscule marker gene *MtPt4* were significantly reduced (see Figure 34b). However, this was not due to a clear quantitative reduction in mycorrhization, but instead a significant increase in the number of smaller arbuscules in roots overexpressing *MtZf2* (Figure 34c and e). As previously reported, strong overexpression can lead to gene silencing in plants (“cosuppression”), which cannot be fully excluded here as the cause for this observation (Paoli *et. al*, 2009). Nevertheless, it is possible to distinguish the effects of the *MtZf2* knockdown or knockout, which exhibits a generalized reduction in mycorrhization, from the observed changes in arbuscule morphology in the overexpression plants. It is also possible that the added stress of the 16-fold overexpression, indicated by the shorter plants (Figure 34d), could have caused this phenotype. In opposition to this explanation, no such arbuscule phenotype was observed for the other *MtZf* genes in spite of a similar shoot size reduction at least for *MtPalm1*-OE (Figure 17). When related to the expression profile of *MtZf2*, indicating induction later in the arbuscular life cycle, a role in the control of arbuscule degeneration can be hypothesized. To further examine this possibility, transcript measurements of markers for arbuscule degeneration such as *MtMyb1* or *MtCp3* (Floss *et. al*, 2017) could be performed in the future. Similarly, impairment of functionality of the symbiotic exchange would have to be further confirmed in the absence of MtZF2, since this has so far only been indicated by reduced *MtPt4* expression. Based on the present results, it is thus only possible to conclude an apparent requirement for *MtZf2*-expression to be at a particular level for the normal AM-symbiosis program to occur.

Unfortunately, the results from the Y2H studies did not allow for additional insight into the granular processes MtZF2 might be involved in, due to a combination of weak growth of yeast clones and some autoactivity (Figure 40 and Table S3). Still, the endogenous capability of MtZF2 to induce gene expression in yeast serves as evidence for its activity as a transcription factor, as would be characteristic for the C2H2-ZF family. As such, alternative methods of investigating protein-protein interactions would have to be used such as co-immunoprecipitation or targeted BiFC assays.

Similarly, results obtained from the Y1H approach shown in Figure 42 do not allow for clear insights into the position of *MtZf2* within the AM-symbiotic regulatory network. This is in part due to the fact that some of the TFs identified as possible promoter binding partners are not clearly linked to the observed timepoint of *MtZf2* induction, such as the NF-Y-subunits. Additionally, agreement between the colorimetric assay and observed growth performance of the matings involving *pMtZf2* was specifically poor with the strongest staining associated with weak growth.

Such patterns are likely indicative of false positives that can occur due to binding of TFs to other regions around the bait construct on the yeast chromosome. In such cases, this erroneous activation would only occur for one of the reporters and not both, as was occasionally the case throughout these experiments (Reece-Hoyes and Marian Walhout, 2012). In addition to these caveats, some of the observed TF binding could constitute valid interactions in the heterologous yeast assay, that do not occur in the natural system and thus have no functional relevance. Still, some GRAS factors associated with mature arbuscules like MtGRAS1 and MtGRAS5, as well as WR15-TFs stand as potential regulators connected to *MtZf2*. In the future, a library mating could allow for additional regulation candidates including those not directly associated with mycorrhization processes that were not investigated as part of this study, such as the MtMYB1-based arbuscule degeneration program (Floss *et. al*, 2017). Similarly, any potential promoter binding candidates could be further verified by identifying and testing potential binding motifs in subsequent Y1H approaches.

For MtPALM1, its activity as a DNA binding transcriptional regulator has been documented in the context of leaves. Thus, bait autoactivation in the Y2H assays was unsurprising. Still, as with *MtZf2*, alternative methods for the detection of interactions with other proteins would have to be used in future research.

In contrast to the other, novel genes subject to this study, an Auxin Responsive Factor 3-like TF was already known from experiments in leaves to be a regulator of *MtPalm1* (Peng *et. al*, 2017). Throughout the Y1H interactions assays, MtARF3 could be identified as a weak positive. However, no other MtARF active in roots was newly identified as potential regulator of *MtPalm1*. To elucidate a functional relationship in of this regulation in mycorrhized roots, it could be possible in the future to

perform knockdown or overexpression experiments on *MtArf3*, while monitoring mycorrhization overall and *MtPalm1* expression in particular.

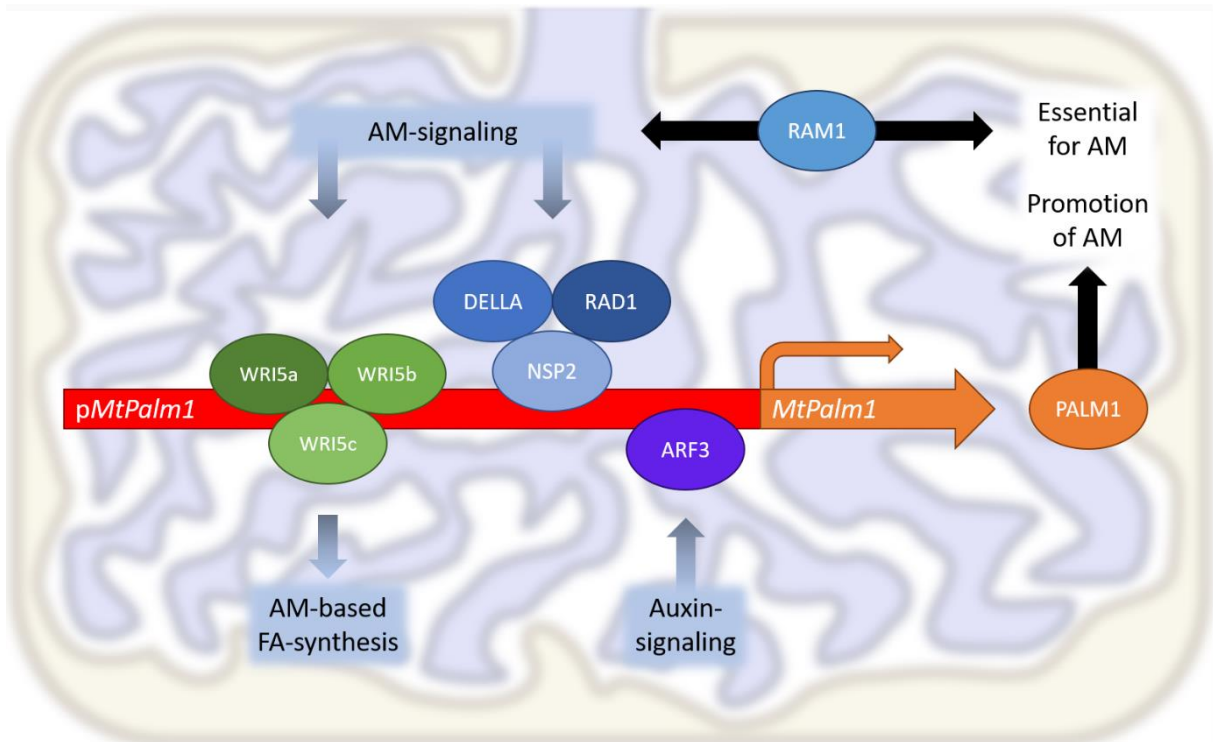


**Figure 48 – Model for the promotion of mycorrhization via the integration of different influences on the activation of *MtPalm1* in arbuscules**

In Y1H interaction studies, the *MtPalm1* promoter (red) was bound by WRIS ERF-TFs (green) involved in AM-dependent fatty acid biosynthesis. Additionally, activation in cortical cells initiating AM colonization or already harboring arbuscules could depend on complexes of GRAS-TFs including DELLA-proteins, NSP2 and RAD1 (blue). From leaves, *pMtPalm1* binding by ARF3 (purple) is known. Via this pathway, *MtPalm1*-activity could depend on auxin-levels in roots as well. The MtPALM1-TF (orange) acts in concert with the essential AM-regulator MtRAM1 during the maintenance of arbuscules and thus promotes mycorrhization.

Instead of the expected MtARF3 regulatory unit, a number of other TFs involved with AM exhibited stronger *MtPalm1* activation, including GRAS-TFs MtDELLA2 and 3, MtNSP2 and MtRAD1. Interestingly, these have been proposed to act in concert in a variety of AM-developmental processes including arbuscule formation, with MtNSPs having specifically been demonstrated to have DNA-binding properties (Hirsch *et. al*, 2009; Pimprikar and Gutjahr, 2018). As such, it is possible to propose a preliminary model in Figure 48, by which *MtPalm1* transcription is induced by an AM-induced complex of GRAS-TFs. Additionally, some binding AP2/ERF-TFs, including the WRIS-TFs, might suggest an additional involvement with AM-dependent FA-biosynthesis (Jiang *et. al*, 2018; Hartung 2021), that could be investigated further.

Interestingly, no interaction with MtRAM1 was observed for *pMtPalm1*, in spite of a functional relationship suggested by reduced activity in *ram1-1* mutants. This indicates no direct regulation of *MtPalm1* by MtRAM1. Moreover, the expression profile for *MtPalm1*-RNAi roots in comparison to MtRAM1-deficient mycorrhized roots showed that the regulatory targets of these two TFs are likely distinct (Figure 23), suggesting that both work in concert to promote AM-symbiosis and arbuscule formation.

### 5.3 MtPALM1 acts as a mediator between AM symbiotic processes and hormonal stimuli, especially auxin

In order to further elucidate the functions of MtPALM1 during AM symbiosis and specifically ascertain downstream effects of its absence, transcriptomes of mycorrhized *MtPalm1*-RNAi and *gus*-control root systems were analyzed via RNASeq. In the data obtained, as expected from the lower rate of mycorrhization in *MtPalm1*-RNAi roots, a number of processes generally associated with AM symbiosis were differentially regulated. As a strategy for obtaining representative information on processes that *MtPalm1* is specifically involved in, genes induced or repressed more strongly in MtPALM1-deficient roots than in a general comparison between mycorrhized and non-mycorrhized conditions were considered in particular as part of GO-enrichments (AM-subtracted dataset, see Figure 23).

This subtraction strategy has a potential weakness, in that a number of genes crucially involved in the AM-symbiosis are not particularly strongly or specifically impacted by varying mycorrhization levels on a transcriptional level, such as for example those encoding MtDELLA proteins. As such, it is possible that the subtraction of AM-induced and -repressed genes based on the intensity of differential regulation in the *MtPalm1*-RNAi samples only produces an incomplete correction. This was counteracted by performing the same GO-enrichment analyses with data on differential regulation in Myc+ vs. Myc- conditions alone (Supplementary Figure S15). This strategy validated the major conclusions from the AM-subtracted *MtPalm1*-RNAi dataset discussed in the paragraph below.

When considering some of the most strongly enriched functional categories of the AM-subtracted dataset, defense- and stress related biological processes appeared as differentially regulated (Figure 24). This includes obvious GO-terms like defense- and immune-response, drought stress but also hydrolase-activity or spermine biosynthesis. Such responses could be related to ABA-signaling, which involves differentially regulated PYR/PYL-receptors, PP2C phosphatases, serine/threonine-protein kinases and ABF-TFs, as outlined in Figure 26. Interestingly, the apparent pattern of regulation observed in the MtPALM1-deficient roots follows the general model of ABA signaling, where ABA binds to and activates PYR/PYL, which causes degradation of the protein phosphatase C that otherwise dephosphorylates SnRK. From there, ABFs can be phosphorylated and are able to act as TFs to regulate

downstream genes (Ali *et. al*, 2020). These differences could be accounted for by upregulation of ABA biosynthesis in the absence of MtPALM1 (Figure 25). Prior studies have shown an involvement of ABA signals with AM, likely acting both as a modulator of stress responses in relation to fungal interactions as well as a potential stimulant on the AM symbiotic fungus itself (Herrera-Medina *et. al*, 2007; Liu *et. al*, 2019). In addition, some possible connections to the biosynthesis of AM-promoting SLs have also been proposed (López-Ráez *et. al*, 2010). These efforts have led to the identification of proteins linking these processes, such as protein phosphatases involved in downstream regulation in response to ABA signals affecting AM colonization (Charpentier *et. al*, 2014). As a whole, the *MtPalm1*-RNAi RNASeq profiles indicate potential involvement of MtPALM1 with ABA signaling and might be a lead for further research in the connection between phytohormones and AM-symbiosis in *M. truncatula*.

Similarly, differentially regulated components of processes related to auxin signaling were uniquely enriched in the AM-subtracted *MtPalm1*-RNAi dataset (Figure 26). Auxin influences on MtPALM1 were also described as part of the processes enabling compound leaf development in *M. truncatula* (summarized in Figure 7b). In this context, local auxin maxima were demonstrated as essential in orchestrating the gene expression patterns required for the organized formation of leaf primordia (Zhou *et. al*, 2011; Mo *et. al*, 2021). As such, prior experimental evidence supports the involvement of *MtPalm1* with response to and the generation of spatiotemporal auxin patterns in tissues of *M. truncatula*, which could help to propose a hypothesis for its role during AM.

As part of this work, a strong induction in arbuscocytes was observed for *MtPalm1*. With the inferred changes in auxin-production and -signaling from the RNASeq transcription profiles, it would be plausible to assume an influence, where MtPALM1 acts as a link between auxin-mediated processes and AM regulation. It has been known for some time that roots with an active AM symbiotic exchange contain elevated levels of auxin, with this phytohormone generally being thought to promote fungal colonization (Jentschel *et. al*, 2007). More recent studies, however, suggest a more complex picture: Chen *et al.* (2021) demonstrated that medium amounts of IAA were ideal in promoting mycorrhization, while auxin-biosynthesis genes in general are downregulated. Conversely, they were also able to show that the putative IAA-amido synthetase encoded by *SIGH3.4* negatively regulates AM in tomato by modulating auxin levels. *MtGH3* genes were also generally downregulated under MtPALM1-deficient conditions and could thus be involved in the local reduction of bioactive IAA-levels. Similarly, activity of the auxin-repressed AUX/IAA protein SI-IAA27 was previously demonstrated to be positively correlated with mycorrhized root sections (Bassa *et. al*, 2013). Interestingly, in further research performed by Guillotin *et. al* (2017), a positive regulation of strigolactone biosynthesis via the induction of *SIDWARF27* could be shown, suggesting a plausible mechanism for the influence of auxin



signals on AM colonization via the activation of the biosynthesis of SLs, phytohormones known to promote AM-progression (Liu *et. al*, 2011).

When integrating this knowledge with the general auxin signaling cascade, the control of compound leaf development (Chen *et. al*, 2021) and the observed differential regulation in *MtPalm1*-deficient mycorrhized roots (see also Figure 26), a potential mechanism as outlined in Figure 49 can be proposed: in mycorrhized root sections, MtPALM1 might function as an autoregulatory component of auxin signaling acting on the production or accumulation of endogenous IAA, as indicated by differential regulation of biosynthesis genes (Figure S9) and a putative PIN-efflux carrier (see Table 20). As a result, AUX/IAA proteins would be downregulated and degraded, which in turn would free ARF proteins to act on downstream promoters. This way, *MtDwarf27* could be stimulated, leading to the increase of SL levels and the promotion of mycorrhization, recapitulating the mechanism demonstrated by Bassa *et. al* (2013) and Guillotin *et. al* (2017). Simultaneously, expression of *MtPalm1* is itself controlled by ARF proteins (Peng *et. al*, 2017). In addition, it is tempting to further speculate that fine-tuning of *MtPalm1*-expression might be achieved via the oORF starting in its 5'-UTR. Finally, GH3 proteins, encoded by genes also downregulated in the absence of *MtPalm1*, can ensure auxin-homeostasis (Chen *et. al*, 2021).

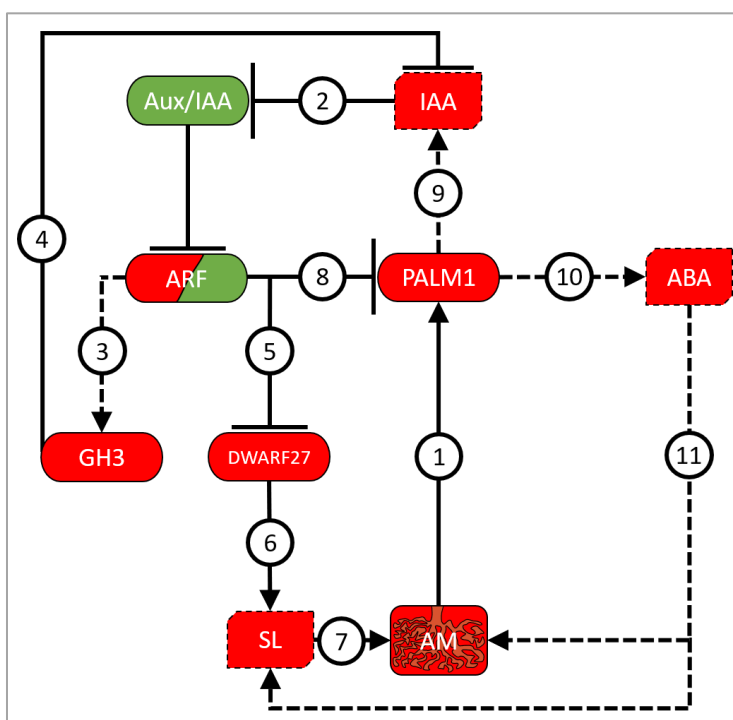


**Figure 49 – Proposed model integrating MtPALM1 with AM-signaling and hormonal stimuli**

Activation of *MtPalm1* (1) by the presence of intraradical AM structures was demonstrated during this work. In *MtPALM1*-deficient mycorrhized roots as shown here, genes encoding Aux/IAA proteins tended to be downregulated (2, negative regulation depicted in green). As a result, certain ARFs might regulate GH3-proteins (3), that in turn act negatively on auxin-levels (4). Downregulated ARF proteins could repress DWARF27 (5), completing a positive regulatory circuit involving IAA proteins proposed by Guillotin *et. al* (2017). As a result, SL levels would be increased (6), promoting AM

(7). *MtPalm1* itself is repressed by ARF3-like proteins (Peng *et. al*, 2017), allowing for its autoregulation (8). Differential regulation of components of the IAA-biosynthesis pathway in *MtPalm1*-RNAi roots could point towards the differences in signaling being caused by altered auxin-content (9). ABA-synthesis and -signaling components were likewise differentially regulated (10) and have been proposed to be able to act directly via the modulation of defense-responses and indirectly through SLs on AM-colonization (11), giving way for a potential autoregulation. Colors indicate possible regulation with red signifying up- and green signifying downregulation under Myc+ conditions in the presence of functional MtPALM1, based on expression data from the *MtPalm1*-RNAi roots.

The up- and downregulated components of this proposed model shown in Figure 49 line up with the observed induction and reduction of gene expression in the *MtPalm1*-RNAi roots outlined in Figure 26. Nevertheless, this explanation makes a number of assumptions: Most importantly, it assumes IAA levels to be either locally or generally reduced in the absence of *MtPalm1*, while genes putatively involved in auxin biosynthesis appearing more upregulated in whole *MtPalm1*-RNAi roots. This discrepancy could be explained by *MtPalm1* activation only in the vicinity of local auxin maxima as observed in leaves (Mo *et. al*, 2021), while the overall hormonal concentration throughout the whole root system shows few differences. Alternatively, IAA levels could indeed be elevated as a result of an attempt of the plant to induce *MtPalm1* expression in the RNAi conditions for downstream regulatory functions. Since no direct measurements of auxin were taken, the actual tissue-specific levels of this hormone in roots are currently unknown and would have to be investigated in the future. In a similar experiment, responsiveness of p*MtPalm1* to IAA could directly be examined in roots, where currently only some evidence for induction exists from transcriptome data (Figure S16; Boschiero *et. al*, 2020). Secondly, while up- and downregulation of components of the model are based on transcriptional data (see 4.2.7, Figures 25 and 26), the individual connections drawn have not always been underpinned by experimental evidence in *M. truncatula*, but are partly based on functional analyses in tomato. Critically, while the connection between an AUX/IAA protein negatively regulating DWARF27 has been observed in tomato, conservation of this functional relationship would still have to be demonstrated, as would the negatively regulating ARF protein placed in between as a mediator in the present model. Similarly, the identification of a crucial GH3 protein in AM symbiosis of *M. truncatula* has yet to be done.

In conclusion, while a necessity for future validation for the model proposed is clear, MtPALM1 represents a strong candidate for the previously missing link between the regulation of AM symbiosis and hormonal signals such as abscisic acid and in particular auxin.

## 5.4 Conclusion and outlook

Transcriptional induction of the *M. truncatula* ZF genes *MtPalm1*, *MtZf1*, *MtZf2* and *MtZf3* was successfully demonstrated in mycorrhized roots. Cell-specific profiles obtained from a promoter-*gus* study confirmed a specific activation of *pMtPalm1* and *pMtZf1* in the vicinity of AMF structures, with *pMtZf2* and *pMtZf3* exhibiting considerable induction in mycorrhized regions above their background activities. For the promoter regions of *MtPalm1*, *MtZf1* and *MtZf2*, upstream ORF regions likely contribute to the regulation of expression, although this could only be clearly demonstrated for *pMtPalm1*. Further experiments with different promoter versions of varying lengths and quantitative *gus*-assays could underpin this data with additional evidence. Particularly in the case of *pMtZf2*, discrepancies between observed transcript levels and promoter activation suggest an incomplete picture, highlighting the potential need for additional experiments concerning the *MtZf2* cell-specific expression profile.

Promoter-binding assays performed via Y1H gave some indications on how this AM-related activation could be achieved, including potential binding of *pMtPalm1* via AM-inducible GRAS-proteins such as NSP2 and DELLA, induction of *pMtZf1* by MtNF-Y-complexes involved in early AM-signaling or direct binding of the key AM-regulator MtrAM1 to *pMtZf3*. These preliminary results would have to be confirmed in future experiments that might also allow the specific binding motifs to be identified, such as targeted pull-down assays.

Expression of all four ZF genes studied was successfully knocked down via RNAi, leading to a major reduction in AM marker gene expression for *MtPalm1*, *MtZf1* and *MtZf2*. As a result, general mycorrhization levels were reduced as well, with the downregulation of *MtPalm1* having the strongest effect, both on the overall colonization and the frequency of arbuscules. These phenotypic defects were confirmed in *Tnt1*-lines carrying loss-of-function mutations in *MtPalm1* and *MtZf2* that were partially rescued via complementation with an additional, functional gene copy. This further proof could not be obtained for *MtZf1*, where a negative impact was observed, but sporadic RNAi effects were an additional confounding factor, necessitating further studies in stable mutant lines.

Ectopic overexpression in mycorrhized root systems was achieved for *MtPalm1*, *MtZf1* and *MtZf2*, resulting in no increases in mycorrhization levels or marker gene expression. On the contrary, higher amounts of MtZF2 led to an increase in smaller arbuscules and lowered *MtPt4* transcript levels, suggesting hampered growth or early degeneration of arbuscules. Hypothetical involvement with the MtMYB1-based program for arbuscule degeneration could be tested in the future, though a general transcriptomics approach might be even better suited to obtain a more general idea of processes controlled by MtZF2.

Involvement in wider protein interaction networks could not be successfully explored for MtPALM1 and MtZF2 in a Y2H approach due to autoactivation and would require the use of alternative methods in subsequent research. Protein interaction results for MtZF1 suggested a potential involvement in targeted proteolysis, indicating a potential role in signaling during the preparation of the symbiotic interaction, when taking into account the early expression of *MtZf1*. This hypothetical involvement would have to be studied further through confirmation of the putative interactions identified in the Y2H library mating via alternative methods.

Transcriptome data from MtPALM1-deficient mycorrhized roots suggest a potential involvement in hormonal regulatory circuits that act in concert with the major AM transcriptional reprogramming involving MtRAM1. Further studies including measurements of the phytohormones SL, auxin and ABA purported to be involved will be required to test the proposed mode of action of MtPALM1.

Table 26 – List of Abbreviations

Full name or designation	Abbreviation
3-Aminotriazole	3-AT
3-hydroxy-3-methylglutaryl coenzyme A reductase 1	HMGR1
5-bromo-4-chloro-3-indolyl- $\alpha$ -D-galactopyranosid	X- $\alpha$ -Gal
5-bromo-4-chloro-3-indolyl- $\beta$ -D-galactopyranoside	X-Gal
5-bromo-4-chloro-3-indolyl glucuronide	X-Gluc
$\beta$ -galactosidase	lacZ
$\beta$ -glucuronidase	GUS
Abscisic acid	ABA
Acetate	Ac
Acyl carrier protein	ACP
Ampicillin	Amp
Apetala 2	AP2
Appressoria	APP
Arbuscocyte	Arb
Arbuscular mycorrhiza	AM
Arbuscular mycorrhiza fungus/fungi	AMF
Ammonium transporter	AMT
Aureobasidin A	Aba
Auxin Response Factor	ARF
Auxin responsive element	Aux-RE
Attachment-site	att
Base pairs	bp
Basic local alignment search tool	BLAST
Binding domain	BD
Bimolecular fluorescence complementation	BiFC
Blue copper protein 1	BCP1
Cauliflower mosaic virus	CMV
CCAAT-box binding factor	CBF
Chitooligosaccharides	COs
Chloramphenicol	Chloro
Codon determining sequence	CDS
Common symbiotic signaling pathway	CSSP
Complementation	Comp
Confocal laser scanning microscope	CLSM
Control	CTRL
copyDNA	cDNA
Cysteine protease 3	CP3
Days post inoculation	dpi
DELLA interacting protein 1	DIP1
Does not Make Infection	DMI
Double dropout	DDO
Empty vector	EV
Epidermal cells	EPI
Ethylene responsive factor	ERF
False discovery rate	FDR
Fat required for arbuscular mycorrhiza symbiosis	FatM
Fatty acid	FA
Flanking Sequence Tag	FST

<u>GAI</u> <u>RGA</u> <u>SCR</u>	GRAS
Gateway	GW
Gene Ontology	GO
Gentamycin	Genta
Gibberellic acid	GA
Gibberelic Acid Insensitive	GAI
H <sup>+</sup> -ATPase	HA1
Hyphae	Hyp
Indole acetic acid	IAA
Inhibitor of rust germ tube differentiation 1	IRG1
Interquartile range	IQR
Intron-mediated enhancement	IME
Interacting protein of DMI3	IPD3
Kanamycin	Kan
Knock out	KO
Kyoto Encyclopedia of Genes and Genomes	KEGG
Laser microdissection and pressure catapulting	LMPC
LB-based Abrobacterium medium	LB-A
Lipo-chitoooligosaccharides	LCOs
Leucine	Leu
Leucine-rich repeat	LRR
Liquid nitrogen	IN <sub>2</sub>
Luria-Bertani Broth	LB
Lysine-motif	LysM
Monosaccharide transporter	MST
<i>Medicago truncatula</i>	Mt
<i>Medicago truncatula</i> Gene Expression Atlas	MtGEA
<i>Medicago truncatula</i> genome version 4/5	Mtv4/5
Monoacylglycerols	MAG
Mycorrhiza	Myc
Mycorrhiza-induced GRAS	MIG1
Multiple cloning site	mcs
Nalidixic acid	Ndx
Nod factor perception	NFP
Nodulation Signaling Pathway	NSP
Nuclear Factor Y	NF-Y
Nucleoporin	Nup
overlapping open reading frame	oORF
Overexpression	OE
Palmate-like pentafofoliata 1	PALM1
Periarbuscular membrane	PAM
Periarbuscular space	PAS
PHANTASTICA	PHAN
(inorganic) phosphate	Pi
Phosphate transporter	PT
Polymerase chain reaction	PCR
Pre-penetration apparatus	PPA
Premature arbuscule degeneration	PAD
Quadruple Dropout Medium	QDO
Real time	RT

Really interesting new gene	RING
Receptor-like kinase	RLK
Red fluorescent protein	RFP
Reduced Arbuscular Mycorrhiza	RAM
Regulator of symbiosome differentiation	RSD
Repressor of GAI	RGA
Required for Arbuscule Development 1	RAD1
Rifampicin	Rif
<i>Rhizophagus irregularis</i>	Ri
RNA-induced silencing complex	RISC
RNA integrity number	RIN
RNA-interference	RNAi
Scarecrow	SCR
Semi-quantitative real-time RT-PCR	sq-RT-PCR
Single leaflet 1	Sgl1
Single dropout	SDO
Short interfering RNAs	siRNA
Spectinomycin	Spec
Streptomycin	Strep
Strigolactone	SL
Stunted arbuscule	STR
Synthetically defined medium	SD
Transcription factor	TF
Transfer-DNA	T-DNA
Translation elongation factor $\alpha$	Tef $\alpha$
Transporter Inhibitor Response 1	TIR1
Transposon from <i>Nicotiana tabacum</i> 1	<i>Tnt1</i>
Tryptone yeast medium	TY
Vesicles	Ves
Vesicle-associated membrane proteins	VAMP
Virulence	vir
Wheat germ agglutinin	WGA
Wild-type	WT
Wrinkled 5	Wri
Yeast 1-Hybrid	Y1H
Yeast 2-Hybrid	Y2H
Yeast peptone dextrose adenine medium	YPDA
Yellow fluorescence protein	YFP
Zinc finger	ZF

## 6 References

- Aguilar-Hernández, V., and Guzmán, P.** (2013). Spliceosomal introns in the 5' untranslated region of plant BTL RING-H2 ubiquitin ligases are evolutionary conserved and required for gene expression. *BMC Plant Biology* **13**: 179.
- Agusti, J., Herold, S., Schwarz, M., Sanchez, P., Ljung, K., Dun, E.A., Brewer, P.B., Beveridge, C.A., Sieberer, T., Sehr, E.M., and Greb, T.** (2011). Strigolactone signaling is required for auxin-dependent stimulation of secondary growth in plants. *PNAS* **108** (50): 20242–20247.
- Akiyama, K., Matsuzaki, K., and Hayashi, H.** (2005). Plant sesquiterpenes induce hyphal branching in arbuscular mycorrhizal fungi. *Nature* **435** (7043): 824–827.
- Alexander, T., Toth, R., Meier, R., and Weber, H.C.** (1989). Dynamics of arbuscule development and degeneration in onion, bean, and tomato with reference to vesicular–arbuscular mycorrhizae in grasses. *Canadian Journal of Botany* **67** (8): 2505–2513.
- Ali, A., Pardo, J.M., and Yun, D.-J.** (2020). Desensitization of ABA-Signaling: The Swing From Activation to Degradation. *Frontiers in Plant Science* **11**: 379.
- Allen, J.W., and Shachar-Hill, Y.** (2009). Sulfur Transfer through an Arbuscular Mycorrhiza. *Plant Physiology* **149** (1): 549–560.
- Ané, J.M., Kiss, G.B., Riely, B.K., Penmetsa, R.V., Oldroyd, G.E., Ayax, C., Lévy, J., Debelle, F., Baek, J.M., Kalo, P., Rosenberg, C., Roe, B.A., Long, Dénarié, J., and Cook** (2004). *Medicago truncatula* DMI1 required for bacterial and fungal symbioses in legumes. *Science (New York, N.Y.)* **303** (5662): 1364–1367.
- Aoyanagi, T., Ikeya, S., Kobayashi, A., and Kozaki, A.** (2020). Gene Regulation via the Combination of Transcription Factors in the INDETERMINATE DOMAIN and GRAS Families. *Genes* **11** (6): 613.
- Bago, B., Pfeffer, P.E., and Shachar-Hill, Y.** (2000). Carbon Metabolism and Transport in Arbuscular Mycorrhizas. *Plant Physiology* **124** (3): 949–958.
- Baier, M.C., Keck, M., Gödde, V., Niehaus, K., Küster, H., and Hohnjec, N.** (2010). Knockdown of the symbiotic sucrose synthase MtSucS1 affects arbuscule maturation and maintenance in mycorrhizal roots of *Medicago truncatula*. *Plant Physiology* **152** (2): 1000–1014.
- Bassa, C., Etemadi, M., Combier, J.-P., Bouzayen, M., and Audran-Delalande, C.** (2013). SI-IAA27 gene expression is induced during arbuscular mycorrhizal symbiosis in tomato and in *Medicago truncatula*. *Plant signaling & behavior* **8** (10): e25637.
- Baudin, M., Laloum, T., Lepage, A., Rípodas, C., Ariel, F., Frances, L., Crespi, M., Gamas, P., Blanco, F.A., Zanetti, M.E., Carvalho-Niebel, F. de, and Niebel, A.** (2015). A Phylogenetically Conserved Group of Nuclear Factor- $\gamma$  Transcription Factors Interact to Control Nodulation in Legumes. *Plant Physiology* **169** (4): 2761–2773.
- Becker, A., Kleickmann, A., Walter, A., and Pühler, A.** (1993). Analysis of the *Rhizobium meliloti* exoH/exoK/exoL fragment: ExoK shows homology to excreted endo- $\beta$ -1,3-1,4-glucanases and ExoH resembles membrane proteins. *Molecular and General Genetics* (238): 145–154.
- Benedetto, A., Magurno, F., Bonfante, P., and Lanfranco, L.** (2005). Expression profiles of a phosphate transporter gene (GmosPT) from the endomycorrhizal fungus *Glomus mosseae*. *Mycorrhiza* **15** (8): 620–627.
- Benedito, V.A., Torres-Jerez, I., Murray, J.D., Andriankaja, A., Allen, S., Kakar, K., Wandrey, M., Verdier, J., Zuber, H., Ott, T., Moreau, S., Niebel, A., Frickey, T., Weiller, G., He, J., Dai, X., Zhao, P.X., Tang, Y., and Udvardi, M.K.** (2008). A gene expression atlas of the model legume *Medicago truncatula*. *The Plant Journal* **55** (3): 504–513.
- Ben-Naim, O., Eshed, R., Parnis, A., Teper-Bamnolker, P., Shalit, A., Coupland, G., Samach, A., and Lifschitz, E.** (2006). The CCAAT binding factor can mediate interactions between CONSTANS-like proteins and DNA. *The Plant Journal* **46** (3): 462–476.



- Beringer, J.E.** (1974). R factor transfer in *Rhizobium leguminosarum*. *Journal of general microbiology* **84** (1): 188–198.
- Berruti, A., Lumini, E., Balestrini, R., and Bianciotto, V.** (2015). Arbuscular Mycorrhizal Fungi as Natural Biofertilizers: Let's Benefit from Past Successes. *Frontiers in Microbiology* **6**: 1559.
- Besserer, A., Puech-Pagès, V., Kiefer, P., Gomez-Roldan, V., Jauneau, A., Roy, S., Portais, J.C., Roux, C., Bécard, G., and Séjalon-Delmas, N.** (2006). Strigolactones stimulate arbuscular mycorrhizal fungi by activating mitochondria. *PLoS biology* **4** (7): e226.
- Blancaflor, E.B., Zhao, L., and Harrison, M.J.** (2001). Microtubule organization in root cells of *Medicago truncatula* during development of an arbuscular mycorrhizal symbiosis with *Glomus versiforme*. *Protoplasma* **217** (4): 154–165.
- Borden, K.L.** (2000). RING domains: master builders of molecular scaffolds? *Journal of molecular biology* **295** (5): 1103–1112.
- Boschiero, C., Dai, X., Lundquist, P.K., Roy, S., Christian de Bang, T., Zhang, S., Zhuang, Z., Torres-Jerez, I., Udvardi, M.K., Scheible, W.-R., and Zhao, P.X.** (2020). MtSSPdb: The *Medicago truncatula* Small Secreted Peptide Database. *Plant Physiology* **183** (1): 399–413.
- Bravo, A., Brands, M., Wewer, V., Dörmann, P., and Harrison, M.J.** (2017). Arbuscular mycorrhiza-specific enzymes FatM and RAM2 fine-tune lipid biosynthesis to promote development of arbuscular mycorrhiza. *The New Phytologist* **214** (4): 1631–1645.
- Bravo, A., York, T., Pumplin, N., Mueller, L.A., and Harrison, M.J.** (2016). Genes conserved for arbuscular mycorrhizal symbiosis identified through phylogenomics. *Nature Plants* **2** (2): 15208.
- Breullin-Sessoms, F., Floss, D.S., Gomez, S.K., Pumplin, N., Ding, Y., Levesque-Tremblay, V., Noar, R.D., Daniels, D.A., Bravo, A., Eaglesham, J.B., Benedito, V.A., Udvardi, M.K., and Harrison, M.J.** (2015). Suppression of Arbuscule Degeneration in *Medicago truncatula* phosphate transporter4 Mutants is Dependent on the Ammonium Transporter 2 Family Protein AMT2;3. *The Plant Cell* **27** (4): 1352–1366.
- Calvenzani, V., Testoni, B., Gusmaroli, G., Lorenzo, M., Gnesutta, N., Petroni, K., Mantovani, R., and Tonelli, C.** (2012). Interactions and CCAAT-binding of *Arabidopsis thaliana* NF-Y subunits. *PLOS ONE* **7** (8): e42902.
- Campanella, J.J., Smith, S.M., Leib, D., Wexler, S., and Ludwig-Müller, J.** (2008). The Auxin Conjugate Hydrolase Family of *Medicago truncatula* and Their Expression During the Interaction with Two Symbionts. *Journal of Plant Growth Regulation* **27** (1): 26–38.
- Camps, C., Jardinaud, M.-F., Rengel, D., Carrère, S., Hervé, C., Debellé, F., Gamas, P., Bensmihen, S., and Gough, C.** (2015). Combined genetic and transcriptomic analysis reveals three major signalling pathways activated by Myc-LCOs in *Medicago truncatula*. *The New Phytologist* **208** (1): 224–240.
- Carbon, S., and Mungall, C.** (2018). Gene Ontology Data Archive (Zenodo).
- Carrere, S., Verdier, J., and Gamas, P.** (2021). MtExpress, a Comprehensive and Curated RNAseq-based Gene Expression Atlas for the Model Legume *Medicago truncatula*. *Plant & cell physiology* **62** (9): 1494–1500.
- Cavagnaro, T.R., Jackson, L.E., Six, J., Ferris, H., Goyal, S., Asami, D., and Scow, K.M.** (2006). Arbuscular Mycorrhizas, Microbial Communities, Nutrient Availability, and Soil Aggregates in Organic Tomato Production. *Plant and Soil* **282**: 209–225.
- Charpentier, M., Bredemeier, R., Wanner, G., Takeda, N., Schleiff, E., and Parniske, M.** (2008). Lotus japonicus CASTOR and POLLUX are ion channels essential for perinuclear calcium spiking in legume root endosymbiosis. *The Plant Cell* **20** (12): 3467–3479.
- Charpentier, M., Sun, J., Vaz Martins, T., Radhakrishnan, G.V., Findlay, K., Soumpourou, E., Thouin, J., Véry, A.-A., Sanders, D., Morris, R.J., and Oldroyd, G.E.D.** (2016). Nuclear-localized cyclic

- nucleotide-gated channels mediate symbiotic calcium oscillations. *Science (New York, N.Y.)* **352** (6289): 1102–1105.
- Charpentier, M., Sun, J., Wen, J., Mysore, K.S., and Oldroyd, G.E.D.** (2014). Abscisic acid promotion of arbuscular mycorrhizal colonization requires a component of the PROTEIN PHOSPHATASE 2A complex. *Plant Physiology* **166** (4): 2077–2090.
- Chen, J., Yu, J., Ge, L., Wang, H., Berbel, A., Liu, Y., Chen, Y., Li, G., Tadege, M., Wen, J., Cosson, V., Mysore, K.S., Ratet, P., Madueño, F., Bai, G., and Chen, R.** (2010a). Control of dissected leaf morphology by a Cys(2)His(2) zinc finger transcription factor in the model legume *Medicago truncatula*. *PNAS* **107** (23): 10754–10759.
- Chen, L.-Q., Hou, B.-H., Lalonde, S., Takanaga, H., Hartung, M.L., Qu, X.-Q., Guo, W.-J., Kim, J.-G., Underwood, W., Chaudhuri, B., Chermak, D., Antony, G., White, F.F., Somerville, S.C., Mudgett, M.B., and Frommer, W.B.** (2010b). Sugar transporters for intercellular exchange and nutrition of pathogens. *Nature* **468** (7323): 527–532.
- Chen, X., Chen, J., Liao, D., Ye, H., Li, C., Luo, Z., Yan, A., Zhao, Q., Xie, K., Li, Y., Wang, D., Chen, J., Chen, A., and Xu, G.** (2021). Auxin-mediated regulation of arbuscular mycorrhizal symbiosis: A role of SLGH3.4 in tomato. *Plant, Cell & Environment* **45** (3): 955–968.
- Chen, X., Liao, D., Yang, X., Ji, M., Wang, S., Gu, M., Chen, A., and Xu, G.** (2017). Three cis-Regulatory Motifs, AuxRE, MYCRS1 and MYCRS2, are Required for Modulating the Auxin- and Mycorrhiza-Responsive Expression of a Tomato GH3 Gene. *Plant & cell physiology* **58** (4): 770–778.
- Cheng, X., Peng, J., Ma, J., Tang, Y., Chen, R., Mysore, K.S., and Wen, J.** (2012). NO APICAL MERISTEM (MtNAM) regulates floral organ identity and lateral organ separation in *Medicago truncatula*. *The New Phytologist* **195** (1): 71–84.
- Choi, J., Summers, W., and Paszkowski, U.** (2018). Mechanisms Underlying Establishment of Arbuscular Mycorrhizal Symbioses. *Annual review of phytopathology* **56**: 135–160.
- Chung, B.Y.W., Simons, C., Firth, A.E., Brown, C.M., and Hellens, R.P.** (2006). Effect of 5'UTR introns on gene expression in *Arabidopsis thaliana*. *BMC Genomics* **7**: 120.
- Combier, J.P., Billy, F. de, Gamas, P., Niebel, A., and Rivas, S.** (2008). Trans-regulation of the expression of the transcription factor MtHAP2-1 by a uORF controls root nodule development. *Genes & Development* **22** (11): 1549–1559.
- Cruz, C., Egsgaard, H., Trujillo, C., Ambus, P., Requena, N., Martins-Loução, M.A., and Jakobsen, I.** (2007). Enzymatic evidence for the key role of arginine in nitrogen translocation by arbuscular mycorrhizal fungi. *Plant Physiology* **144** (2): 782–792.
- Czaja, L.F., Hogekamp, C., Lamm, P., Maillet, F., Martinez, E.A., Samain, E., Dénarié, J., Küster, H., and Hohnjec, N.** (2012). Transcriptional responses toward diffusible signals from symbiotic microbes reveal MtNFP- and MtDMI3-dependent reprogramming of host gene expression by arbuscular mycorrhizal fungal lipochitooligosaccharides. *Plant Physiology* **159** (4): 1671–1685.
- David-Schwartz, R., Koenig, D., and Sinha, N.R.** (2009). LYRATE is a key regulator of leaflet initiation and lamina outgrowth in tomato. *The Plant Cell* **21** (10): 3093–3104.
- Davière, J.M., and Achard, P.** (2016). A Pivotal Role of DELLAs in Regulating Multiple Hormone Signals. *Molecular plant* **9** (1): 10–20.
- Delaux, P.M., Bécard, G., and Combier, J.P.** (2013). NSP1 is a component of the Myc signaling pathway. *The New Phytologist* **199** (1): 59–65.
- Deplancke, B., Dupuy, D., Vidal, M., and Walhout, A.J.M.** (2004). A gateway-compatible yeast one-hybrid system. *Genome Research* **14** (10B): 2093–2101.
- Devers, E.A., Teply, J., Reinert, A., Gaude, N., and Krajinski, F.** (2013). An endogenous artificial microRNA system for unraveling the function of root endosymbioses related genes in *Medicago truncatula*. *BMC Plant Biology* **13**: 82.

- Dharmasiri, N., Dharmasiri, S., and Estelle, M.** (2005). The F-box protein TIR1 is an auxin receptor. *Nature* **435** (7041): 441–445.
- Di Laurenzio, L., Wysocka-Diller, J., Malamy, J.E., Pysh, L., Helariutta, Y., Freshour, G., Hahn, M.G., Feldmann, K.A., and Benfey, P.N.** (1996). The SCARECROW Gene Regulates an Asymmetric Cell Division That Is Essential for Generating the Radial Organization of the Arabidopsis Root. *Cell* **86** (3): 423–433.
- Diédhiou, I., Tromas, A., Cissoko, M., Gray, K., Parizot, B., Crabos, A., Alloisio, N., Fournier, P., Carro, L., Svistoonoff, S., Gherbi, H., Hocher, V., Diouf, D., Laplaze, L., and Champion, A.** (2014). Identification of potential transcriptional regulators of actinorhizal symbioses in *Casuarina glauca* and *Alnus glutinosa*. *BMC Plant Biology* **14**: 342.
- El Ghachtouli, N., Martin-Tanguy, J., Paynot, M., and Gianinazzi, S.** (1996). First-report of the inhibition of arbuscular mycorrhizal infection of *Pisum sativum* by specific and irreversible inhibition of polyamine biosynthesis or by gibberellic acid treatment. *FEBS Letters* **385** (3): 189–192.
- Englbrecht, C.C., Schoof, H., and Böhm, S.** (2004). Conservation, diversification and expansion of C2H2 zinc finger proteins in the *Arabidopsis thaliana* genome. *BMC Genomics* **5**: 39.
- Etemadi, M., Gutjahr, C., Couzigou, J.-M., Zouine, M., Laressergues, D., Timmers, A., Audran, C., Bouzayen, M., Bécard, G., and Combier, J.-P.** (2014). Auxin perception is required for arbuscule development in arbuscular mycorrhizal symbiosis. *Plant Physiology* **166** (1): 281–292.
- Ezawa, T., Smith, S.E., and Smith, F.A.** (2002). P metabolism and transport in AM fungi. *Plant and Soil* **244**: 221–230.
- Favre, P., Bapaume, L., Bossolini, E., Delorenzi, M., Falquet, L., and Reinhardt, D.** (2014). A novel bioinformatics pipeline to discover genes related to arbuscular mycorrhizal symbiosis based on their evolutionary conservation pattern among higher plants. *BMC Plant Biology* **14**: 333.
- Fitter, A.H., and Moyersoen, B.** (1996). Evolutionary trends in root-microbe symbioses. *Philosophical Transactions of the Royal Society London B* **351** (1345): 1367–1375.
- Floss, D.S., Gomez, S.K., Park, H.J., Am MacLean, Müller, L.M., Bhattarai, K.K., Lévesque-Tremblay, V., Maldonado-Mendoza, I.E., and Harrison, M.J.** (2017). A Transcriptional Program for Arbuscule Degeneration during AM Symbiosis Is Regulated by MYB1. *Current Biology* **27** (8): 1206–1212.
- Floss, D.S., Lévesque-Tremblay, V., Park, H.J., and Harrison, M.J.** (2016). DELLA proteins regulate expression of a subset of AM symbiosis-induced genes in *Medicago truncatula*. *Plant signaling & behavior* **11** (4): e1162369.
- Floss, D.S., Levy, J.G., Levesque-Tremblay, V., Pumplun, N., and Harrison, M.J.** (2013). DELLA proteins regulate arbuscule formation in arbuscular mycorrhizal symbiosis. *PNAS* **110** (51): 5025–5034.
- Fonouni-Farde, C., Tan, S., Baudin, M., Brault, M., Wen, J., Mysore, K.S., Niebel, A., Frugier, F., and Diet, A.** (2016). DELLA-mediated gibberellin signalling regulates Nod factor signalling and rhizobial infection. *Nature Communications* **7**: 12636.
- Foo, E., Ross, J.J., Jones, W.T., and Reid, J.B.** (2013). Plant hormones in arbuscular mycorrhizal symbioses: an emerging role for gibberellins. *Annals of botany* **111** (5): 769–779.
- Frank, B.** (1885). Über die auf Wurzelsymbiose beruhende Ernährung gewisser Bäume durch unterirdische Pilze.
- Frenzel, A., Manthey, K., Perlick, A.M., Meyer, F., Pühler, A., Küster, H., and Krajinski, F.** (2005). Combined transcriptome profiling reveals a novel family of arbuscular mycorrhizal-specific *Medicago truncatula* lectin genes. *Molecular Plant-Microbe Interactions* **18** (8): 771–782.
- Fuxman Bass, J.I., Reece-Hoyes, J.S., and Walhout, A.J.M.** (2016a). Colony Lift Colorimetric Assay for  $\beta$ -Galactosidase Activity. *Cold Spring Harb Protoc* **2016** (12): pdb.prot088963.

- Fuxman Bass, J.I., Reece-Hoyes, J.S., and Walhout, A.J.M.** (2016b). Generating Bait Strains for Yeast One-Hybrid Assays. *Cold Spring Harb Protoc* **2016** (12): pdb.prot088948.
- Fuxman Bass, J.I., Reece-Hoyes, J.S., and Walhout, A.J.M.** (2016c). Performing Yeast One-Hybrid Library Screens. *Cold Spring Harb Protoc* **2016** (12): pdb.prot088955.
- Garcia, K., Chasman, D., Roy, S., and Ané, J.-M.** (2017). Physiological Responses and Gene Co-expression Network of Mycorrhizal Roots under K<sup>+</sup> Deprivation. *Plant Physiology* **173** (3): 1811–1823.
- Garcia, K., Doidy, J., Zimmermann, S.D., Wipf, D., and Courty, P.E.** (2016). Take a Trip Through the Plant and Fungal Transportome of Mycorrhiza. *Trends in plant science* **21** (11): 937–950.
- Gaude, N., Bortfeld, S., Duensing, N., Lohse, M., and Krajinski, F.** (2012). Arbuscule-containing and non-colonized cortical cells of mycorrhizal roots undergo extensive and specific reprogramming during arbuscular mycorrhizal development. *The Plant Journal* **69** (3): 510–528.
- Ge, L., Chen, J., and Chen, R.** (2010). Palmate-like pentafoliata1 encodes a novel Cys(2)His(2) zinc finger transcription factor essential for compound leaf morphogenesis in *Medicago truncatula*. *Plant signaling & behavior* **5** (9): 1134–1137.
- Ge, L., Peng, J., Berbel, A., Madueño, F., and Chen, R.** (2014). Regulation of compound leaf development by PHANTASTICA in *Medicago truncatula*. *Plant Physiology* **164** (1): 216–228.
- Genre, A., Chabaud, M., Faccio, A., Barker, D.G., and Bonfante, P.** (2008). Prepenetration apparatus assembly precedes and predicts the colonization patterns of arbuscular mycorrhizal fungi within the root cortex of both *Medicago truncatula* and *Daucus carota*. *The Plant Cell* **20** (5): 1407–1420.
- Genre, A., Chabaud, M., Timmers, T., Bonfante, P., and Barker, D.G.** (2005). Arbuscular mycorrhizal fungi elicit a novel intracellular apparatus in *Medicago truncatula* root epidermal cells before infection. *The Plant Cell* **17** (12): 3489–3499.
- Genre, A., Ivanov, S., Fendrych, M., Faccio, A., Zársky, V., Bisseling, T., and Bonfante, P.** (2012). Multiple exocytotic markers accumulate at the sites of perifungal membrane biogenesis in arbuscular mycorrhizas. *Plant & cell physiology* **53** (1): 244–255.
- Giovanetti, M., and Mosse, B.** (1980). An Evaluation Of Techniques For Measuring Vesicular Arbuscular Mycorrhizal Infection In Roots. *The New Phytologist* **84** (3): 489–500.
- Giovanetti, M., Tolosano, M., Volpe, V., Kopriva, S., and Bonfante, P.** (2014). Identification and functional characterization of a sulfate transporter induced by both sulfur starvation and mycorrhiza formation in *Lotus japonicus*. *The New Phytologist* **204** (3): 609–619.
- Gobbato, E., Marsh, J.F., Vernié, T., Wang, E., Maillet, F., Kim, J., Miller, J.B., Sun, J., Bano, S.A., Ratet, P., Mysore, K.S., Dénarié, J., Schultze, M., and Oldroyd, G.E.D.** (2012). A GRAS-type transcription factor with a specific function in mycorrhizal signaling. *Current Biology* **22** (23): 2236–2241.
- Gobbato, E., Wang, E., Higgins, G., Bano, S.A., Henry, C., Schultze, M., and Oldroyd, G.E.** (2013). RAM1 and RAM2 function and expression during arbuscular mycorrhizal symbiosis and *Aphanomyces euteiches* colonization. *Plant signaling & behavior* **8** (10): e26049.
- Gomez, S.K., Javot, H., Dewatthanawong, P., Torres-Jerez, I., Tang, Y., Blancaflor, E.B., Udvardi, M.K., and Harrison, M.J.** (2009). *Medicago truncatula* and *Glomus intraradices* gene expression in cortical cells harboring arbuscules in the arbuscular mycorrhizal symbiosis. *BMC Plant Biology* **9**: 10.
- Govindarajulu, M., Pfeffer, P.E., Jin, H., Abubaker, J., Douds, D.D., Allen, J.W., Bücking, H., Lammers, P.J., and Shachar-Hill, Y.** (2005). Nitrogen transfer in the arbuscular mycorrhizal symbiosis. *Nature* **435** (7043): 819–823.
- Groth, M., Takeda, N., Perry, J., Uchida, H., Dräxl, S., Brachmann, A., Sato, S., Tabata, S., Kawaguchi, M., Wang, T.L., and Parniske, M.** (2010). NENA, a *Lotus japonicus* homolog of Sec13,

is required for rhizodermal infection by arbuscular mycorrhiza fungi and rhizobia but dispensable for cortical endosymbiotic development. *The Plant Cell* **22** (7): 2509–2526.

- Guerra-Almeida, D., Tschoeke, D.A., and Nunes-da-Fonseca, R.** (2021). Understanding small ORF diversity through a comprehensive transcription feature classification. *DNA Research* **28** (5): 1–18.
- Guillotin, B., Etemadi, M., Audran, C., Bouzayen, M., Bécard, G., and Combier, J.P.** (2017). SI-IAA27 regulates strigolactone biosynthesis and mycorrhization in tomato (var. MicroTom). *The New Phytologist* **213** (3): 1124–1132.
- Gutjahr, C., Banba, M., Croset, V., An, K., Miyao, A., An, G., Hirochika, H., Imaizumi-Anraku, H., and Paszkowski, U.** (2008). Arbuscular mycorrhiza-specific signaling in rice transcends the common symbiosis signaling pathway. *The Plant Cell* **20** (11): 2989–3005.
- Gutjahr, C., and Parniske, M.** (2013). Cell and developmental biology of arbuscular mycorrhiza symbiosis. *Annual review of cell and developmental biology* **29**: 593–617.
- Gutjahr, C., Radovanovic, D., Geoffroy, J., Zhang, Q., Siegler, H., Chiapello, M., Casieri, L., An, K., An, G., Guiderdoni, E., Kumar, C.S., Sundaresan, V., Harrison, M.J., and Paszkowski, U.** (2012). The half-size ABC transporters STR1 and STR2 are indispensable for mycorrhizal arbuscule formation in rice. *The Plant Journal* **69** (5): 906–920.
- Hall, T.M.T.** (2005). Multiple modes of RNA recognition by zinc finger proteins. *Current opinion in structural biology* **15** (3): 367–373.
- Hanlon, M.T., and Coenen, C.** (2011). Genetic evidence for auxin involvement in arbuscular mycorrhiza initiation. *The New Phytologist* **189** (3): 701–709.
- Harrison, M.J., Dewbre, G.R., and Liu, J.** (2002). A phosphate transporter from *Medicago truncatula* involved in the acquisition of phosphate released by arbuscular mycorrhizal fungi. *The Plant Cell* **14** (10): 2413–2429.
- Harrison, M.J., and van Buuren, M.L.** (1995). A phosphate transporter from the mycorrhizal fungus *Glomus versiforme*. *Nature* **378** (6557): 626–629.
- Hartmann, R.M.** (2018). Functional analysis of arbuscular mycorrhiza-related GRAS transcription factor genes of *Medicago truncatula*: Dissertation. Leibniz Universität Hannover.
- Hartmann, R.M., Schaepe, S., Nübel, D., Petersen, A.C., Bertolini, M., Vasilev, J., Küster, H., and Hohnjec, N.** (2019). Insights into the complex role of GRAS transcription factors in the arbuscular mycorrhiza symbiosis. *Scientific Reports* **9** (1): 1–15.
- Hartung, L.** (2021). Ethylene-responsive transcription factors orchestrating AM-dependent fatty acid biosynthesis act in complexes with Nuclear Factor-Y TFs and the key AM regulator RAM1: Dissertation. Leibniz Universität Hannover.
- Hayashi, K.** (2012). The Interaction and Integration of Auxin Signaling Components. *Plant & cell physiology* **53** (6): 965–975.
- Heck, C., Kuhn, H., Heidt, S., Walter, S., Rieger, N., and Requena, N.** (2016). Symbiotic Fungi Control Plant Root Cortex Development through the Novel GRAS Transcription Factor MIG1. *Current Biology CB* **26** (20): 2770–2778.
- Heijden, M.G.A., Martin, F.M., Selosse, M.-A., and Sanders, I.R.** (2015). Mycorrhizal ecology and evolution: the past, the present, and the future. *The New Phytologist* **205** (4): 1406–1423.
- Helber, N., Wippel, K., Sauer, N., Schaarschmidt, S., Hause, B., and Requena, N.** (2011). A versatile monosaccharide transporter that operates in the arbuscular mycorrhizal fungus *Glomus* sp is crucial for the symbiotic relationship with plants. *The Plant Cell* **23** (10): 3812–3823.
- Hellwinkel, B.** (2018). Molecular analysis of *Medicago truncatula* GRAS transcription factor genes in arbuscular mycorrhiza: Bachelor Thesis. Leibniz Universität Hannover.

- Herrera-Medina, M.J., Steinkellner, S., Vierheilig, H., Ocampo Bote, J.A., and García Garrido, J.M.** (2007). Abscisic acid determines arbuscule development and functionality in the tomato arbuscular mycorrhiza. *The New Phytologist* **175** (3): 554–564.
- Hirsch, S., Kim, J., Muñoz, A., Heckmann, A.B., Downie, J.A., and Oldroyd, G.E.** (2009). GRAS Proteins Form a DNA Binding Complex to Induce Gene Expression during Nodulation Signaling in *Medicago truncatula*. *The Plant Cell* **21** (2): 545–557.
- Hogekamp, C., Arndt, D., Pereira, P.A., Becker, J.D., Hohnjec, N., and Küster, H.** (2011). Laser microdissection unravels cell-type-specific transcription in arbuscular mycorrhizal roots, including CAAT-box transcription factor gene expression correlating with fungal contact and spread. *Plant Physiology* **157** (4): 2023–2043.
- Hogekamp, C., and Küster, H.** (2013). A roadmap of cell-type specific gene expression during sequential stages of the arbuscular mycorrhiza symbiosis. *BMC Genomics* **14**: 306.
- Hohnjec, N., Czaja-Hasse, L.F., Hogekamp, C., and Küster, H.** (2015). Pre-announcement of symbiotic guests: transcriptional reprogramming by mycorrhizal lipochitooligosaccharides shows a strict co-dependency on the GRAS transcription factors NSP1 and RAM1. *BMC Genomics* **16**: 994.
- Hohnjec, N., Perlick, A.M., Pühler, A., and Küster, H.** (2003). The *Medicago truncatula* sucrose synthase gene MtSucS1 is activated both in the infected region of root nodules and in the cortex of roots colonized by arbuscular mycorrhizal fungi. *Molecular Plant-Microbe Interactions* **16** (10): 903–915.
- Horstman, A., Tonaco, I.A.N., Boutilier, K., and Immink, R.G.H.** (2014). A cautionary note on the use of split-YFP/BiFC in plant protein-protein interaction studies. *International journal of molecular sciences* **15** (6): 9628–9643.
- Hotton, S.K., and Callis, J.** (2008). Regulation of cullin RING ligases. *Annual review of plant biology* **59**: 467–489.
- Ivanov, S., Fedorova, E.E., Limpens, E., Mita, S. de, Genre, A., Bonfante, P., and Bisseling, T.** (2012). Rhizobium-legume symbiosis shares an exocytotic pathway required for arbuscule formation. *PNAS* **109** (21): 8316–8321.
- Javot, H., Penmetza, R.V., Breuillin, F., Bhattarai, K.K., Noar, R.D., Gomez, S.K., Zhang, Q., Cook, D.R., and Harrison, M.J.** (2011). *Medicago truncatula* mtpt4 mutants reveal a role for nitrogen in the regulation of arbuscule degeneration in arbuscular mycorrhizal symbiosis. *The Plant Journal* **68** (6): 954–965.
- Javot, H., Penmetza, R.V., Terzaghi, N., Cook, D.R., and Harrison, M.J.** (2007). A *Medicago truncatula* phosphate transporter indispensable for the arbuscular mycorrhizal symbiosis. *PNAS* **104** (5): 1720–1725.
- Jentschel, K., Thiel, D., Rehn, F., and Ludwig-Müller, J.** (2007). Arbuscular mycorrhiza enhances auxin levels and alters auxin biosynthesis in *Tropaeolum majus* during early stages of colonization. *Physiologia Plantarum* **129** (2): 320–333.
- Jiang, Q., Fu, C., and Wang, Z.-Y.** (2019). A Unified Agrobacterium-Mediated Transformation Protocol for Alfalfa (*Medicago sativa* L.) and *Medicago truncatula*. *Methods in molecular biology* **1864**: 153–163.
- Jiang, Y., Wang, W., Xie, Q., Liu, N., Liu, L., Wang, D., Zhang, X., Yang, C., Chen, X., Tang, D., and Wang, E.** (2017). Plants transfer lipids to sustain colonization by mutualistic mycorrhizal and parasitic fungi. *Science (New York, N.Y.)* **356** (6343): 1172–1175.
- Jiang, Y., Xie, Q., Wang, W., Yang, J., Zhang, X., Yu, N., Zhou, Y., and Wang, E.** (2018). *Medicago* AP2-Domain Transcription Factor WRI5a Is a Master Regulator of Lipid Biosynthesis and Transfer during Mycorrhizal Symbiosis. *Molecular plant* **11** (11): 1344–1359.

- Jiao, Z., Wang, L., Du, H., Wang, Y., Wang, W., Liu, J., Huang, J., Huang, W., and Ge, L.** (2020). Genome-wide study of C2H2 zinc finger gene family in *Medicago truncatula*. *BMC Plant Biology* **20**: 401.
- Joga, M.R., Zotti, M.J., Smagghe, G., and Christiaens, O.** (2016). RNAi Efficiency, Systemic Properties, and Novel Delivery Methods for Pest Insect Control: What We Know So Far. *Front. Physiol.* **7**: 553.
- Kanamori, N., Madsen, L.H., Radutoiu, S., Frantescu, M., Quistgaard, E.M.H., Miwa, H., Downie, J.A., James, E.K., Felle, H.H., Haaning, L.L., Jensen, T.H., Sato, S., Nakamura, Y., Tabata, S., Sandal, N., and Stougaard, J.** (2006). A nucleoporin is required for induction of Ca<sup>2+</sup> spiking in legume nodule development and essential for rhizobial and fungal symbiosis. *PNAS* **103** (2): 359–364.
- Karlowski, W.M., and Hirsch, A.M.** (2003). The over-expression of an alfalfa RING-H2 gene induces pleiotropic effects on plant growth and development. *Plant Molecular Biology* **52** (1): 121–133.
- Kentsis, A., Dwyer, E.C., Perez, J.M., Sharma, M., Chen, A., Pan, Z.Q., and Borden, K.L.** (2001). The RING domains of the promyelocytic leukemia protein PML and the arenaviral protein Z repress translation by directly inhibiting translation initiation factor eIF4E. *Journal of molecular biology* **312** (4): 609–623.
- Kevei, Z., Lougnon, G., Mergaert, P., Horváth, G.V., Kereszt, A., Jayaraman, D., Zaman, N., Marcel, F., Regulski, K., Kiss, G.B., Kondorosi, A., Endre, G., Kondorosi, E., and Ané, J.-M.** (2007). 3-hydroxy-3-methylglutaryl coenzyme a reductase 1 interacts with NOR1 and is crucial for nodulation in *Medicago truncatula*. *The Plant Cell* **19** (12): 3974–3989.
- Keymer, A., Pimprakar, P., Wewer, V., Huber, C., Brands, M., Bucerius, S.L., Delaux, P.-M., Klingl, V., Röpenack-lahaye, E. von, Wang, T.L., Eisenreich, W., Dörmann, P., Parniske, M., and Gutjahr, C.** (2017). Lipid transfer from plants to arbuscular mycorrhiza fungi. *eLife Sciences Publications, Ltd*: e29107.
- Kim, G.-B., and Nam, Y.-W.** (2013). A novel GRAS protein gene MtSymSCL1 plays a role in regulating nodule number in *Medicago truncatula*. *Journal of Plant Growth Regulation* **71** (1): 77–92.
- Kistner, C., and Parniske, M.** (2002). Evolution of signal transduction in intracellular symbiosis. *Trends in plant science* **7** (11): 511–518.
- Klironomos, J.N., and Hart, M.M.** (2002). Colonization of roots by arbuscular mycorrhizal fungi using different sources of inoculum. *Mycorrhiza* **12** (4): 181–184.
- Kobae, Y., Gutjahr, C., Paszkowski, U., Kojima, T., Fujiwara, T., and Hata, S.** (2014). Lipid droplets of arbuscular mycorrhizal fungi emerge in concert with arbuscule collapse. *Plant & cell physiology* **55** (11): 1945–1953.
- Kobae, Y., Kameoka, H., Sugimura, Y., Saito, K., Ohtomo, R., Fujiwara, T., and Kyojuka, J.** (2018). Strigolactone Biosynthesis Genes of Rice are Required for the Punctual Entry of Arbuscular Mycorrhizal Fungi into the Roots. *Plant & cell physiology* **59** (3): 544–553.
- Kohlen, W., Charnikhova, T., Lammers, M., Pollina, T., Tóth, P., Haider, I., Pozo, M.J., Maagd, R.A. de, Ruyter-Spira, C., Bouwmeester, H.J., and López-Ráez, J.A.** (2012). The tomato CAROTENOID CLEAVAGE DIOXYGENASE8 (SICCD8) regulates rhizosphere signaling, plant architecture and affects reproductive development through strigolactone biosynthesis. *The New Phytologist* **196** (2): 535–547.
- Kosarev, P., Mayer, K.F.X., and Hardtke, C.S.** (2002). Evaluation and classification of RING-finger domains encoded by the Arabidopsis genome. *Genome Biology* **3** (4): 16.1-16.12.
- Krajinski, F., Courty, P.-E., Sieh, D., Franken, P., Zhang, H., Bucher, M., Gerlach, N., Kryvoruchko, I., Zoeller, D., Udvardi, M., and Hause, B.** (2014). The H<sup>+</sup>-ATPase HA1 of *Medicago truncatula* Is Essential for Phosphate Transport and Plant Growth during Arbuscular Mycorrhizal Symbiosis. *The Plant Cell* **26** (4): 1808–1817.

- Kruger, M., Kruger, C., Walker, C., Stockinger, H., and Schussler, A.** (2012). Phylogenetic reference data for systematics and phylotaxonomy of arbuscular mycorrhizal fungi from phylum to species level. *The New Phytologist* **193** (4): 970–984.
- Lakatos, L., Szittyá, G., Silhavy, D., and Burgyán, J.** (2004). Molecular mechanism of RNA silencing suppression mediated by p19 protein of tombusviruses. *The EMBO journal* **23** (4): 876–884.
- Laporte, P., Lepage, A., Fournier, J., Catrice, O., Moreau, S., Jardinaud, M.-F., Mun, J.-H., Larrainzar, E., Cook, D.R., Gamas, P., and Niebel, A.** (2014). The CCAAT box-binding transcription factor NF-YA1 controls rhizobial infection. *Journal of experimental botany* **65** (2): 481–494.
- Lauressergues, D., Delaux, P.-M., Formey, D., Lelandais-Brière, C., Fort, S., Cottaz, S., Bécárd, G., Niebel, A., Roux, C., and Combier, J.-P.** (2012). The microRNA miR171h modulates arbuscular mycorrhizal colonization of *Medicago truncatula* by targeting NSP2. *The Plant Journal* **72** (3): 512–522.
- Liao, D., Wang, S., Cui, M., Liu, J., Chen, A., and Xu, G.** (2018). Phytohormones Regulate the Development of Arbuscular Mycorrhizal Symbiosis. *International journal of molecular sciences* **19** (10): 3146.
- Limpens, E., Ramos, J., Franken, C., Raz, V., Compaan, B., Franssen, H., Bisseling, T., and Geurts, R.** (2004). RNA interference in *Agrobacterium rhizogenes*-transformed roots of *Arabidopsis* and *Medicago truncatula*. *Journal of experimental botany* **55** (399): 983–992.
- Liu, J., Blaylock, L.A., Endre, G., Cho, J., Town, C.D., VandenBosch, K.A., and Harrison, M.J.** (2003). Transcript profiling coupled with spatial expression analyses reveals genes involved in distinct developmental stages of an arbuscular mycorrhizal symbiosis. *The Plant Cell* **15** (9): 2106–2123.
- Liu, S., Lv, Z., Liu, Y., Li, L., and Zhang, L.** (2018). Network analysis of ABA-dependent and ABA-independent drought responsive genes in *Arabidopsis thaliana*. *Genetics and molecular biology* **41** (3): 624–637.
- Liu, W., Kohlen, W., Lillo, A., Op, d.C.R., Ivanov, S., Hartog, M., Limpens, E., Jamil, M., Smaczniak, C., Kaufmann, K., Yang, W.C., Hooiveld, G.J., Charnikhova, T., Bouwmeester, H.J., Bisseling, T., and Geurts, R.** (2011). Strigolactone biosynthesis in *Medicago truncatula* and rice requires the symbiotic GRAS-type transcription factors NSP1 and NSP2. *The Plant Cell* **23** (10): 3853–3865.
- Liu, X., Feng, Z., Zhu, H., and Yao, Q.** (2019). Exogenous abscisic acid and root volatiles increase sporulation of *Rhizophagus irregularis* DAOM 197198 in asymbiotic and pre-symbiotic status. *Mycorrhiza* **29** (6): 581–589.
- López-Pedrosa, A., González-Guerrero, M., Valderas, A., Azcón-Aguilar, C., and Ferrol, N.** (2006). GintAMT1 encodes a functional high-affinity ammonium transporter that is expressed in the extraradical mycelium of *Glomus intraradices*. *Fungal Genetics and Biology* **43** (2): 102–110.
- López-Ráez, J.A., Charnikhova, T., Gómez-Roldán, V., Matusova, R., Kohlen, W., Vos, R. de, Verstappen, F., Puech-Pages, V., Bécárd, G., Mulder, P., and Bouwmeester, H.** (2008). Tomato strigolactones are derived from carotenoids and their biosynthesis is promoted by phosphate starvation. *The New Phytologist* **178** (4): 863–874.
- López-Ráez, J.A., Kohlen, W., Charnikhova, T., Mulder, P., Undas, A.K., Sergeant, M.J., Verstappen, F., Bugg, T.D.H., Thompson, A.J., Ruyter-Spira, C., and Bouwmeester, H.** (2010). Does abscisic acid affect strigolactone biosynthesis? *The New Phytologist* **187** (2): 343–354.
- Luginbuehl, L.H., Menard, G.N., Kurup, S., van Erp, H., Radhakrishnan, G.V., Breakspear, A., Oldroyd, G.E.D., and Eastmond, P.J.** (2017). Fatty acids in arbuscular mycorrhizal fungi are synthesized by the host plant. *Science (New York, N.Y.)* **356** (6343): 1175–1178.
- Luginbuehl, L.H., and Oldroyd, G.E.** (2017). Understanding the Arbuscule at the Heart of Endomycorrhizal Symbioses in Plants. *Current Biology* **27** (17): R952–R963.
- Luo, W., and Brouwer, C.** (2013). Pathview: an R/Bioconductor package for pathway-based data integration and visualization. *Bioinformatics* **29** (14): 1830–1831.



- Luo, W., Pant, G., Bhavnasi, Y.K., Blanchard, S.G., and Brouwer, C.** (2017). Pathview Web: user friendly pathway visualization and data integration. *Nucleic acids research* **45** (W1): W501-W508.
- Maillet, F., Poinot, V., Andre, O., Puech-Pages, V., Haouy, A., Gueunier, M., Cromer, L., Giraudet, D., Formey, D., Niebel, A., Martinez, E.A., Driguez, H., Becard, G., and Denarie, J.** (2011). Fungal lipochitooligosaccharide symbiotic signals in arbuscular mycorrhiza. *Nature* **469** (7328): 58–63.
- Manck-Götzenberger, J., and Requena, N.** (2016). Arbuscular mycorrhiza Symbiosis Induces a Major Transcriptional Reprogramming of the Potato SWEET Sugar Transporter Family. *Frontiers in Plant Science* **7**: 487.
- Mantovani, R.** (1999). The molecular biology of the CCAAT-binding factor NF-Y. *Gene* **239** (1): 15–27.
- Martín-Rodríguez, J.A., Huertas, R., Ho-Plágaro, T., Ocampo, J.A., Turečková, V., Tarkowská, D., Ludwig-Müller, J., and García-Garrido, J.M.** (2016). Gibberellin-Abscisic Acid Balances during Arbuscular Mycorrhiza Formation in Tomato. *Frontiers in Plant Science* **7**: 1273.
- Martín-Rodríguez, J.Á., León-Morcillo, R., Vierheilig, H., Ocampo, J.A., Ludwig-Müller, J., and García-Garrido, J.M.** (2011). Ethylene-dependent/ethylene-independent ABA regulation of tomato plants colonized by arbuscular mycorrhiza fungi. *The New Phytologist* **190** (1): 193–205.
- Mbengue, M., Camut, S., Carvalho-Niebel, F. de, Deslandes, L., Froidure, S., Klaus-Heisen, D., Moreau, S., Rivas, S., Timmers, T., Hervé, C., Cullimore, J., and Lefebvre, B.** (2010). The *Medicago truncatula* E3 ubiquitin ligase PUB1 interacts with the LYK3 symbiotic receptor and negatively regulates infection and nodulation. *The Plant Cell* **22** (10): 3474–3488.
- McGinnis, K.M.** (2010). RNAi for functional genomics in plants. *Briefings in Functional Genomics* **9** (2): 111–117.
- Mi, H., Muruganujan, A., Casagrande, J.T., and Thomas, P.D.** (2013). Large-scale gene function analysis with the PANTHER classification system. *Nature protocols* **8** (8): 1551–1566.
- Miller, R.M., Jastrow, J.D., and Reinhardt, D.R.** (1995). External hyphal production of vesicular-arbuscular mycorrhizal fungi in pasture and tallgrass prairie communities. *Oecologia* **103** (1): 17–23.
- Mo, X., He, L., Liu, Y., Wang, D., Zhao, B., and Chen, J.** (2021). The Genetic Control of the Compound Leaf Patterning in *Medicago truncatula*. *Frontiers in Plant Science* **12**: 749989.
- Montgomery, T.A., Howell, M.D., Cuperus, J.T., Li, D., Hansen, J.E., Alexander, A.L., Chapman, E.J., Fahlgren, N., Allen, E., and Carrington, J.C.** (2008). Specificity of ARGONAUTE7-miR390 interaction and dual functionality in TAS3 trans-acting siRNA formation. *Cell* **133** (1): 128–141.
- Müller, S.** (2012). Functional Analysis of Genes encoding CCAAT-Box Transcription Factors in Arbuscular Mycorrhizal Roots: Dissertation. Leibniz Universität Hannover.
- Nouri, E., Surve, R., Bapaume, L., Stumpe, M., Chen, M., Zhang, Y., Ruyter-Spira, C., Bouwmeester, H., Glauser, G., Bruissson, S., and Reinhardt, D.** (2021). Phosphate Suppression of Arbuscular Mycorrhizal Symbiosis Involves Gibberellic Acid Signaling. *Plant & cell physiology* **62** (6): 959–970.
- Oldroyd, G.E.D.** (2013). Speak, friend, and enter: signalling systems that promote beneficial symbiotic associations in plants. *Nature reviews. Microbiology* **11** (4): 252–263.
- Pan, H., Oztas, O., Zhang, X., Wu, X., Stonoha, C., Wang, E., Wang, B., and Wang, D.** (2016). A symbiotic SNARE protein generated by alternative termination of transcription. *Nature Plants* **2**: 15197.
- Paoli, E. de, Dorantes-Acosta, A., Zhai, J., Accerbi, M., Jeong, D.-H., Park, S., Meyers, B.C., Jorgensen, R.A., and Green, P.J.** (2009). Distinct extremely abundant siRNAs associated with cosuppression in petunia. *RNA* **15** (11): 1965–1970.
- Park, H.-J., Floss, D.S., Levesque-Tremblay, V., Bravo, A., and Harrison, M.J.** (2015). Hyphal Branching during Arbuscule Development Requires Reduced Arbuscular Mycorrhiza1. *Plant Physiology* **169** (4): 2774–2788.

- Park, J., Nguyen, K.T., Park, E., Jeon, J.-S., and Choi, G.** (2013). DELLA proteins and their interacting RING Finger proteins repress gibberellin responses by binding to the promoters of a subset of gibberellin-responsive genes in Arabidopsis. *The Plant Cell* **25** (3): 927–943.
- Parniske, M.** (2008). Arbuscular mycorrhiza: the mother of plant root endosymbioses. *Nature reviews. Microbiology* **6** (10): 763–775.
- Pecrix, Y., Staton, S.E., Sallet, E., Lelandais-Brière, C., Moreau, S., Carrère, S., Blein, T., Jardinaud, M.-F., Latrasse, D., Zouine, M., Zahm, M., Kreplak, J., Mayjonade, B., Satgé, C., Perez, M., Cauet, S., Marande, W., Chantry-Darmon, C., Lopez-Roques, C., Bouchez, O., Bérard, A., Debellé, F., Muñoz, S., Bendahmane, A., Bergès, H., Niebel, A., Buitink, J., Frugier, F., Benhamed, M., Crespi, M., Gouzy, J., and Gamas, P.** (2018). Whole-genome landscape of *Medicago truncatula* symbiotic genes. *Nature Plants* **4** (12): 1017–1025.
- Peng, J., Berbel, A., Madueño, F., and Chen, R.** (2017). AUXIN RESPONSE FACTOR3 Regulates Compound Leaf Patterning by Directly Repressing PALMATE-LIKE PENTAFOLIATA1 Expression in *Medicago truncatula*. *Frontiers in Plant Science* **8**: 1630.
- Peng, J., Carol, P., Richards, D.E., King, K.E., Cowling, R.J., Murphy, G.P., and Harberd, N.P.** (1997). The Arabidopsis GAI gene defines a signaling pathway that negatively regulates gibberellin responses. *Genes & Development* **11** (23): 3194–3205.
- Peng, J., and Chen, R.** (2011). Auxin efflux transporter MtPIN10 regulates compound leaf and flower development in *Medicago truncatula*. *Plant signaling & behavior* **6** (10): 1537–1544.
- Pérez-Torres, C.-A., López-Bucio, J., Cruz-Ramírez, A., Ibarra-Laclette, E., Dharmasiri, S., Estelle, M., and Herrera-Estrella, L.** (2009). Phosphate Availability Alters Lateral Root Development in Arabidopsis by Modulating Auxin Sensitivity via a Mechanism Involving the TIR1 Auxin Receptor. *The Plant Cell* **20** (12): 3258–3272.
- Peterson, R.L., Massicotte, H.B., and Melville, L.H.** (2004). *Mycorrhizas: Anatomy and cell biology* (Ottawa, Wallingford, Oxon, UK: NRC Research Press).
- Pfeffer, Douds, D.D., JR, Becard, and Shachar-Hill** (1999). Carbon uptake and the metabolism and transport of lipids in an arbuscular mycorrhiza. *Plant Physiology* **120** (2): 587–598.
- Pimprikar, P., Carbonnel, S., Paries, M., Katzer, K., Klingl, V., Bohmer, M.J., Karl, L., Floss, D.S., Harrison, M.J., Parniske, M., and Gutjahr, C.** (2016). A CCaMK-CYCLOPS-DELLA Complex Activates Transcription of RAM1 to Regulate Arbuscule Branching. *Current Biology* **26** (8): 987–998.
- Pimprikar, P., and Gutjahr, C.** (2018). Transcriptional Regulation of Arbuscular Mycorrhiza Development. *Plant & cell physiology* **59** (4): 673–690.
- Pirozynski, K.A., and Malloch, D.W.** (1975). The origin of land plants: A matter of mycotrophism. *Biosystems* **6** (3): 153–164.
- Piya, S., Shrestha, S.K., Binder, B., Stewart, C.N., and Hewezi, T.** (2014). Protein-protein interaction and gene co-expression maps of ARFs and Aux/IAAs in Arabidopsis. *Frontiers in Plant Science* **5**: 744.
- Pridmore, R.D.** (1987). New and versatile cloning vectors with kanamycin-resistance marker. *Gene* **56** (2-3): 309-312.
- Pumplin, N., and Harrison, M.J.** (2009). Live-cell imaging reveals periarbuscular membrane domains and organelle location in *Medicago truncatula* roots during arbuscular mycorrhizal symbiosis. *Plant Physiology* **151** (2): 809–819.
- Pumplin, N., Mondo, S.J., Topp, S., Starker, C.G., Gantt, J.S., and Harrison, M.J.** (2010). *Medicago truncatula* Vapyrin is a novel protein required for arbuscular mycorrhizal symbiosis. *The Plant Journal* **61** (3): 482–494.
- Pysh, L.D., Wysocka-Diller, J.W., Camilleri, C., Bouchez, D., and Benfey, P.N.** (1999). The GRAS gene family in Arabidopsis: sequence characterization and basic expression analysis of the SCARECROW-LIKE genes. *The Plant Journal* **18** (1): 111–119.

- Redecker, D., Kodner, R., and Graham, L.E.** (2000). Glomalean Fungi from the Ordovician. *Science* (New York, N.Y.) **289** (5486): 1920–1921.
- Redecker, D., Schüßler, A., Stockinger, H., Stürmer, S.L., Morton, J.B., and Walker, C.** (2013). An evidence-based consensus for the classification of arbuscular mycorrhizal fungi (Glomeromycota). *Mycorrhiza* **23** (7): 515–531.
- Reece-Hoyes, J.S., and Marian Walhout, A.J.** (2012). Yeast one-hybrid assays: a historical and technical perspective. *Methods* **57** (4): 441–447.
- Robinson, J.T., Thorvaldsdóttir, H., Winckler, W., Guttman, M., Lander, E.S., Getz, G., and Mesirov, J.P.** (2011). Integrative genomics viewer. *Nature Biotechnology* **29** (1): 24–26.
- Roth, R., and Paszkowski, U.** (2017). Plant carbon nourishment of arbuscular mycorrhizal fungi. *Current opinion in plant biology* **39**: 50–56.
- Saito, K., Yoshikawa, M., Yano, K., Miwa, H., Uchida, H., Asamizu, E., Sato, S., Tabata, S., Imaizumi-Anraku, H., Umehara, Y., Kouchi, H., Murooka, Y., Szczyglowski, K., Downie, J.A., Parniske, M., Hayashi, M., and Kawaguchi, M.** (2007). NUCLEOPORIN85 is required for calcium spiking, fungal and bacterial symbioses, and seed production in *Lotus japonicus*. *The Plant Cell* **19** (2): 610–624.
- Schaarschmidt, S., Roitsch, T., and Hause, B.** (2006). Arbuscular mycorrhiza induces gene expression of the apoplastic invertase LIN6 in tomato (*Lycopersicon esculentum*) roots. *Journal of experimental botany* **57** (15): 4015–4023.
- Schenck, C.N., and Smith, S.G.** (1982). Additional new and unreported species of mycorrhizal fungi (Endogonaceae) from Florida: [*Glomus* spp., *Gigaspora albida*]. *Mycologia* **74** (1): 77–92.
- Schindelin, J., Arganda-Carreras, I., Frise, E., Kaynig, V., Longair, M., Pietzsch, T., Preibisch, S., Rueden, C., Saalfeld, S., Schmid, B., Tinevez, J.-Y., White, D.J., Hartenstein, V., Eliceiri, K., Tomancak, P., and Cardona, A.** (2012). Fiji: an open-source platform for biological-image analysis. *Nature methods* **9** (7): 676–682.
- Schüssler, A., Martin, H., Cohen, D., Fitz, M., and Wipf, D.** (2006). Characterization of a carbohydrate transporter from symbiotic glomeromycotan fungi. *Nature* **444** (7121): 933–936.
- Senjuti Sinharoy, Ivone Torres-Jerez, Kaustav Bandyopadhyay, Attila Kereszt, Catalina I. Pislariu, Jin Nakashima, Vagner A. Benedito, Eva Kondorosi, and Michael K. Udvardi** (2013). The C2H2 transcription factor REGULATOR OF SYMBIOSOME DIFFERENTIATION represses transcription of the secretory pathway gene VAMP721a and promotes symbiosome development in *Medicago truncatula*. *The Plant Cell* **25** (9): 3584–3601.
- Shaul-Keinan, O., Gadkar, V., Ginzberg, I., Grünzweig, J.M., Chet, I., Elad, Y., Winer, S., Belausov, E., Eshed, Y., Atzmon, N., Ben-Tal, Y., and Kapulnik, Y.** (2002). Hormone concentrations in tobacco roots change during arbuscular mycorrhizal colonization with *Glomus intraradices*. *The New Phytologist* **154** (2): 501–507.
- Shen, C., Yue, R., Sun, T., Zhang, L., Xu, L., Tie, S., Wang, H., and Yang, Y.** (2015). Genome-wide identification and expression analysis of auxin response factor gene family in *Medicago truncatula*. *Frontiers in Plant Science* **6**: 73.
- Sieh, D., Watanabe, M., Devers, E.A., Brueckner, F., Hoefgen, R., and Krajinski, F.** (2013). The arbuscular mycorrhizal symbiosis influences sulfur starvation responses of *Medicago truncatula*. *The New Phytologist* **197** (2): 606–616.
- Smith, S.E., and Smith, F.A.** (2011). Roles of arbuscular mycorrhizas in plant nutrition and growth: new paradigms from cellular to ecosystem scales. *Annual review of plant biology* **62**: 227–250.
- Stracke, S., Kistner, C., Yoshida, S., Mulder, L., Sato, S., Kaneko, T., Tabata, S., Sandal, N., Stougaard, J., Szczyglowski, K., and Parniske, M.** (2002). A plant receptor-like kinase required for both bacterial and fungal symbiosis. *Nature* **417** (6892): 959–962.
- Sun, L., Gill, U.S., Nandety, R.S., Kwon, S., Mehta, P., Dickstein, R., Udvardi, M.K., Mysore, K.S., and Wen, J.** (2019). Genome-wide analysis of flanking sequences reveals that Tnt1 insertion is

- positively correlated with gene methylation in *Medicago truncatula*. *The Plant Journal* **98** (6): 1106–1119.
- Sun, X., Xue, B., Jones, W.T., Rikkerink, E., Dunker, A.K., and Uversky, V.N.** (2011). A functionally required unfolded domain from the plant kingdom: intrinsically disordered N-terminal domains of GRAS proteins are involved in molecular recognition during plant development. *Plant Molecular Biology* **77** (3): 205–223.
- Tadege, M., Wen, J., He, J., Tu, H., Kwak, Y., Eschstruth, A., Cayrel, A., Endre, G., Zhao, P.X., Chabaud, M., Ratet, P., and Mysore, K.S.** (2008). Large-scale insertional mutagenesis using the Tnt1 retrotransposon in the model legume *Medicago truncatula*. *The Plant Journal* **54** (2): 335–347.
- Takatsuji, H.** (1999). Zinc-finger proteins: the classical zinc finger emerges in contemporary plant science. *Plant Molecular Biology* **39** (6): 1073–1078.
- Takeda, N., Handa, Y., Tsuzuki, S., Kojima, M., Sakakibara, H., and Kawaguchi, M.** (2015). Gibberellins interfere with symbiosis signaling and gene expression and alter colonization by arbuscular mycorrhizal fungi in *Lotus japonicus*. *Plant Physiology* **167** (2): 545–557.
- Tang, H., Krishnakumar, V., Bidwell, S., Rosen, B., Chan, A., Zhou, S., Gentzbittel, L., Childs, K.L., Yandell, M., Gundlach, H., Mayer, K.F.X., Schwartz, D.C., and Town, C.D.** (2014). An improved genome release (version Mt4.0) for the model legume *Medicago truncatula*. *BMC Genomics* **15**: 312.
- Tang, N., San Clemente, H., Roy, S., Bécard, G., Zhao, B., and Roux, C.** (2016). A Survey of the Gene Repertoire of *Gigaspora rosea* Unravels Conserved Features among Glomeromycota for Obligate Biotrophy. *Front. Microbiol.* **7**: 233.
- Tisserant, E., Kohler, A., Dozolme-Seddas, P., Balestrini, R., Benabdellah, K., Colard, A., Croll, D., Da Silva, C., Gomez, S.K., Koul, R., Ferrol, N., Fiorilli, V., Formey, D., Franken, P., Helber, N., Hijri, M., Lanfranco, L., Lindquist, E., Liu, Y., Malbreil, M., Morin, E., Poulain, J., Shapiro, H., van Tuinen, D., Waschke, A., Azcón-Aguilar, C., Bécard, G., Bonfante, P., Harrison, M.J., Küster, H., Lammers, P., Paszkowski, U., Requena, N., Rensing, S.A., Roux, C., Sanders, I.R., Shachar-Hill, Y., Tuskan, G., Young, J.P.W., Gianinazzi-Pearson, V., and Martin, F.** (2012). The transcriptome of the arbuscular mycorrhizal fungus *Glomus intraradices* (DAOM 197198) reveals functional tradeoffs in an obligate symbiont. *The New Phytologist* **193** (3): 755–769.
- Tisserant, E., Malbreil, M., Kuo, A., Kohler, A., Symeonidi, A., Balestrini, R., Charron, P., Duensing, N., Frei dit Frey, N., Gianinazzi-Pearson, V., Gilbert, L.B., Handa, Y., Herr, J.R., Hijri, M., Koul, R., Kawaguchi, M., Krajinski, F., Lammers, P.J., Masclaux, F.G., Murat, C., Morin, E., Ndikumana, S., Pagni, M., Petitpierre, D., Requena, N., Rosikiewicz, P., Riley, R., Saito, K., San Clemente, H., Shapiro, H., van Tuinen, D., Bécard, G., Bonfante, P., Paszkowski, U., Shachar-Hill, Y.Y., Tuskan, G.A., Young, J.P.W., Sanders, I.R., Henrissat, B., Rensing, S.A., Grigoriev, I.V., Corradi, N., Roux, C., and Martin, F.** (2013). Genome of an arbuscular mycorrhizal fungus provides insight into the oldest plant symbiosis. *PNAS* **110** (50): 20117–20122.
- Toro, M., Azcon, R., and Barea, J.** (1997). Improvement of Arbuscular Mycorrhiza Development by Inoculation of Soil with Phosphate-Solubilizing Rhizobacteria To Improve Rock Phosphate Bioavailability (32P) and Nutrient Cycling. *Appl. Environ. Microbiol.* **63** (11): 4408–4412.
- Trépanier, M., Bécard, G., Moutoglis, P., Willemot, C., Gagné, S., Avis, T.J., and Rioux, J.-A.** (2005). Dependence of arbuscular-mycorrhizal fungi on their plant host for palmitic acid synthesis. *Appl. Environ. Microbiol.* **71** (9): 5341–5347.
- Trinh, T.H., Ratet, P., Kondorosi, E., Durand, P., Kamaté, K., Bauer, P., and Kondorosi, A.** (1998). Rapid and efficient transformation of diploid *Medicago truncatula* and *Medicago sativa* ssp. *falcata* lines improved in somatic embryogenesis. *Plant Cell Reports* **17** (5): 345–355.

- Uhe, M., Hoge Kamp, C., Hartmann, R.M., Hohnjec, N., and Küster, H.** (2018). The mycorrhiza-dependent defensin MtDefMd1 of *Medicago truncatula* acts during the late restructuring stages of arbuscule-containing cells. *PLOS ONE* **13** (1): e0191841.
- Untergasser, A., Cutcutache, I., Koressaar, T., Ye, J., Faircloth, B.C., Remm, M., and Rozen, S.G.** (2012). Primer3--new capabilities and interfaces. *Nucleic acids research* **40** (15): e115.
- Uppalapati, S.R., Ishiga, Y., Doraiswamy, V., Bedair, M., Mittal, S., Chen, J., Nakashima, J., Tang, Y., Tadege, M., Ratet, P., Chen, R., Schultheiss, H., and Mysore, K.S.** (2012). Loss of Abaxial Leaf Epicuticular Wax in *Medicago truncatula* *irg1/palm1* Mutants Results in Reduced Spore Differentiation of Anthracnose and Nonhost Rust Pathogens. *The Plant Cell* **24** (1): 353–370.
- van de Velde, K., Ruelens, P., Geuten, K., Rohde, A., and van der Straeten, D.** (2017). Exploiting DELLA Signaling in Cereals. *Trends in plant science* **22** (10): 880–893.
- van Ha, C., Leyva-González, M.A., Osakabe, Y., Tran, U.T., Nishiyama, R., Watanabe, Y., Tanaka, M., Seki, M., Yamaguchi, S., van Dong, N., Yamaguchi-Shinozaki, K., Shinozaki, K., Herrera-Estrella, L., and Tran, L.-S.P.** (2014). Positive regulatory role of strigolactone in plant responses to drought and salt stress. *PNAS* **111** (2): 851–856.
- Venkateshwaran, M., Jayaraman, D., Chabaud, M., Genre, A., Balloon, A.J., Maeda, J., Forshey, K., Os, D. den, Kwiecien, N.W., Coon, J.J., Barker, D.G., and Ané, J.-M.** (2015). A role for the mevalonate pathway in early plant symbiotic signaling. *PNAS* **112** (31): 9781–9786.
- Vieweg, M.F., Fruhling, M., Quandt, H.J., Heim, U., Baumlein, H., Puhler, A., Kuster, H., and Andreas, M.P.** (2004). The promoter of the *Vicia faba* L. leghemoglobin gene *VfLb29* is specifically activated in the infected cells of root nodules and in the arbuscule-containing cells of mycorrhizal roots from different legume and nonlegume plants. *Molecular Plant-Microbe Interactions* **17** (1): 62-69.
- Walter, M., Chaban, C., Schütze, K., Batistic, O., Weckermann, K., Näke, C., Blazevic, D., Grefen, C., Schumacher, K., Oecking, C., Harter, K., and Kudla, J.** (2004). Visualization of protein interactions in living plant cells using bimolecular fluorescence complementation. *The Plant Journal* **40** (3): 428-438.
- Wang, B., and Qiu, Y.-L.** (2006). Phylogenetic distribution and evolution of mycorrhizas in land plants. *Mycorrhiza* **16** (5): 299–363.
- Wang, E., Yu, N., Bano, S.A., Liu, C., Miller, A.J., Cousins, D., Zhang, X., Ratet, P., Tadege, M., Mysore, K.S., Downie, J.A., Murray, J.D., Oldroyd, G.E.D., and Schultze, M.** (2014). A H<sup>+</sup>-ATPase That Energizes Nutrient Uptake during Mycorrhizal Symbioses in Rice and *Medicago truncatula*. *The Plant Cell* **26** (4): 1818–1830.
- Wang, H., Chen, J., Wen, J., Tadege, M., Li, G., Liu, Y., Mysore, K.S., Ratet, P., and Chen, R.** (2008). Control of compound leaf development by FLORICAULA/LEAFY ortholog SINGLE LEAFLET1 in *Medicago truncatula*. *Plant Physiology* **146** (4): 1759–1772.
- Wang, P., Jiang, H., Boeren, S., Dings, H., Kulikova, O., Bisseling, T., and Limpens, E.** (2021a). A nuclear-targeted effector of *Rhizophagus irregularis* interferes with histone 2B mono-ubiquitination to promote arbuscular mycorrhization. *The New Phytologist* **230** (3): 1142–1155.
- Wang, Y., and Chen, R.** (2013). Regulation of Compound Leaf Development. *Plants (Basel, Switzerland)* **3** (1): 1–17.
- Wang, Y., Yang, P., Zhou, Y., Hu, T., Zhang, P., and Wu, Y.** (2021b). A proteomic approach to understand the impact of nodulation on salinity stress response in alfalfa (*Medicago sativa* L.). *Plant biology (Stuttgart, Germany)* **24** (2): 323–332.
- Wewer, V., Brands, M., and Dörmann, P.** (2014). Fatty acid synthesis and lipid metabolism in the obligate biotrophic fungus *Rhizophagus irregularis* during mycorrhization of *Lotus japonicus*. *The Plant Journal* **79** (3): 398–412.

- Wright, E., Dixon, R.A., and Wang, Z.-Y.** (2006). *Medicago truncatula* Transformation Using Cotyledon Explants. In *Agrobacterium Protocols*, K. Wang, ed (Totowa, NJ: Humana Press), pp. 129–136.
- Xue, L., Cui, H., Buer, B., Vijayakumar, V., Delaux, P.-M., Junkermann, S., and Bucher, M.** (2015). Network of GRAS transcription factors involved in the control of arbuscule development in *Lotus japonicus*. *Plant Physiology* **167** (3): 854–871.
- Yamashita, R., Suzuki, Y., Nakai, K., and Sugano, S.** (2003). Small open reading frames in 5' untranslated regions of mRNAs. *Comptes Rendus Biologies* **326** (10-11): 987–991.
- Yano, K., Yoshida, S., Müller, J., Singh, S., Banba, M., Vickers, K., Markmann, K., White, C., Schuller, B., Sato, S., Asamizu, E., Tabata, S., Murooka, Y., Perry, J., Wang, T.L., Kawaguchi, M., Imaizumi-Anraku, H., Hayashi, M., and Parniske, M.** (2008). CYCLOPS, a mediator of symbiotic intracellular accommodation. *PNAS* **105** (51): 20540–20545.
- Yoshida, H., Hirano, K., Sato, T., Mitsuda, N., Nomoto, M., Maeo, K., Koketsu, E., Mitani, R., Kawamura, M., Ishiguro, S., Tada, Y., Ohme-Takagi, M., Matsuoka, M., and Ueguchi-Tanaka, M.** (2014). DELLA protein functions as a transcriptional activator through the DNA binding of the indeterminate domain family proteins. *PNAS* **111** (21): 7861–7866.
- Young, N.D., Cannon, S.B., Sato, S., Kim, D., Cook, D.R., Town, C.D., Roe, B.A., and Tabata, S.** (2005). Sequencing the genespaces of *Medicago truncatula* and *Lotus japonicus*. *Plant Physiology* **137** (4): 1174–1181.
- Yu, N., Luo, D., Zhang, X., Liu, J., Wang, W., Jin, Y., Dong, W., Liu, J., Liu, H., Yang, W., Zeng, L., Li, Q., He, Z., Oldroyd, G.E.D., and Wang, E.** (2014). A DELLA protein complex controls the arbuscular mycorrhizal symbiosis in plants. *Cell Research* **24** (1): 130–133.
- Zhang, C., Zhang, H., Zhao, Y., Jiang, H., Zhu, S., Cheng, B., and Xiang, Y.** (2013). Genome-wide analysis of the CCCH zinc finger gene family in *Medicago truncatula*. *Plant Cell Reports* **32** (10): 1543–1555.
- Zhang, Q., Blaylock, L.A., and Harrison, M.J.** (2010). Two *Medicago truncatula* half-ABC transporters are essential for arbuscule development in arbuscular mycorrhizal symbiosis. *The Plant Cell* **22** (5): 1483–1497.
- Zhang, X., Pumplin, N., Ivanov, S., and Harrison, M.J.** (2015). EXO70I Is Required for Development of a Sub-domain of the Periarbuscular Membrane during Arbuscular Mycorrhizal Symbiosis. *Current Biology* **25** (16): 2189–2195.
- Zhou, C., Han, L., Hou, C., Metelli, A., Qi, L., Tadege, M., Mysore, K.S., and Wang, Z.-Y.** (2011). Developmental analysis of a *Medicago truncatula* smooth leaf margin1 mutant reveals context-dependent effects on compound leaf development. *The Plant Cell* **23** (6): 2106–2124.

## 7 Supplements

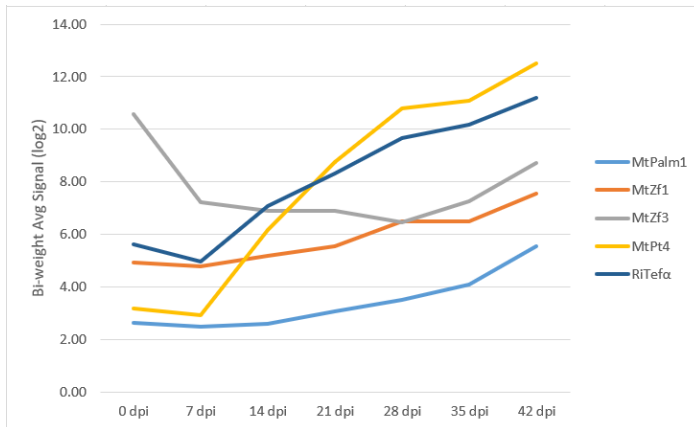


**Figure S1 – Visualization of gene expression over a time course of mycorrhization**

GeneChip expression data over a mycorrhization time course (Hartmann, LUH, unpublished) on the basis of *M. truncatula* A17 roots inoculated with *R. irregularis* spores. Gene expression is depicted as log<sub>2</sub> average signals from multiple probe sets. Roots were either frozen directly after contact with the spores (0 days post inoculation, dpi) or grown for up to six weeks (42 dpi) with weekly samples.

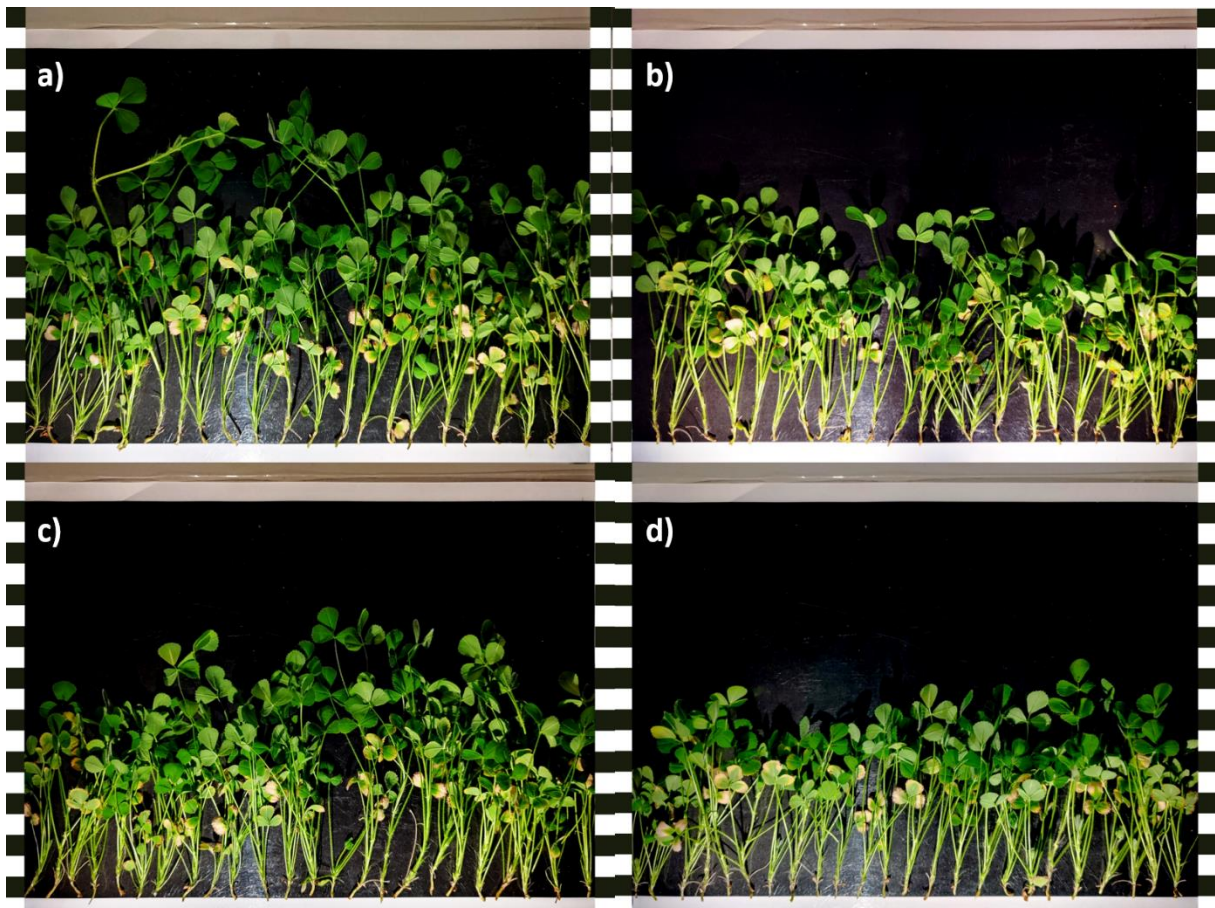


**Figure S2 – Shoot sizes of composite *M. truncatula* plants overexpressing AM-related *MtZf*-genes in transgenic roots**

Composite *M. truncatula* plants overexpressing *MtPalm1*, *MtZf1* and *MtZf2* in transgenic root systems. Mycorrhized roots were harvested for transcriptional and phenotypical analyses, while shoot sizes were captured photographically. Squares on the left and right represent 1 cm each, image distortion was corrected via Adobe Photoshop. Images correspond to the experimental groups as follows: a) Overexpression controls, b) *MtPalm1*-OE, c) *MtZf1*-OE and d) *MtZf2*-OE



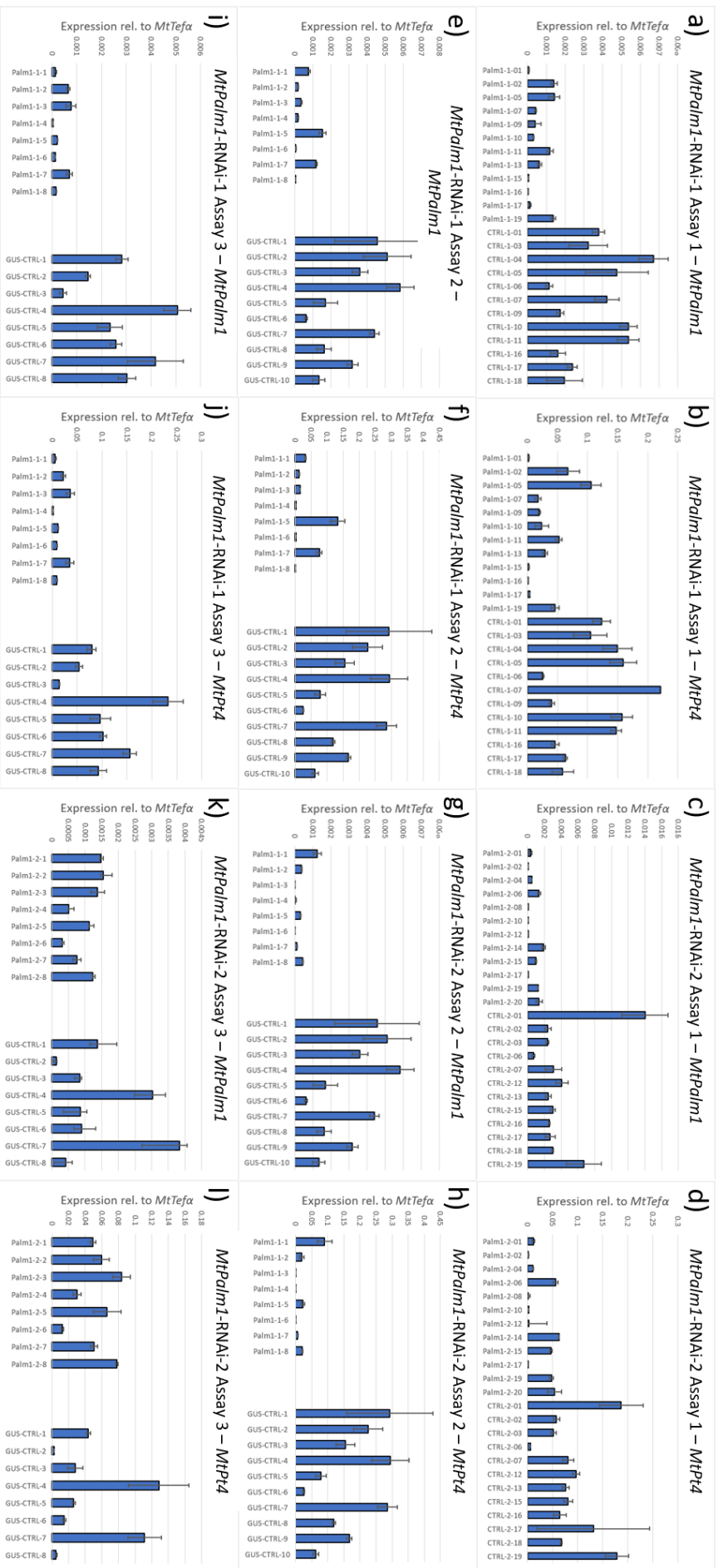


**Figure S3 – Detailed results of the *MtPalm1*-RNAi-knockdown experiments**

Individual *MtPalm1* and *MPT4* expression levels from *MtPalm1*-RNAi roots samples in the three RNAi-assays performed compared to the respective controls as measured via sqRT-PCR relative to *MtTefα*. Error bars represent standard deviation between technical replicates. In the first experiment shown in a)-d), RNA was extracted from the individual roots (12 for each category) compared to pools of three roots making up the samples in trials 2 (e-h) and 3 (i-l).



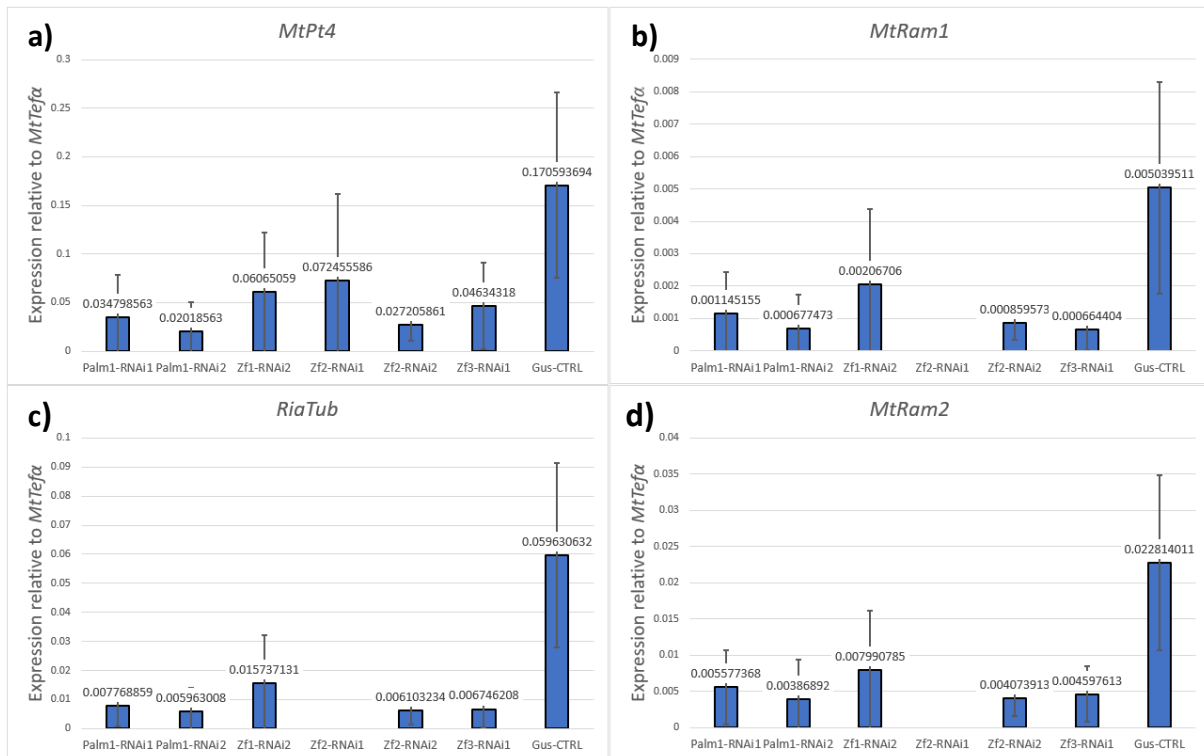


**Figure S4 – AM-marker gene expression in RNAi assay 2**

Expression of the AM-marker genes *MtPt4*, *MtRam1*, *MtRam2* and the fungal gene *RiaTub* in mycorrhized roots expressing RNAi-constructs targeting *MtPalm1*, *MtZf1*, *MtZf2* and *MtZf3* in comparison to *gus*-controls. Shown as bars and numbers are averages of the measured transcript amounts relative to *MtTefα* from eight individual samples of three roots each. Error bars depict standard deviations. Due to being generally less effective in this experiment, not all AM marker genes were measured for *MtZf2*-RNAi-1 samples.

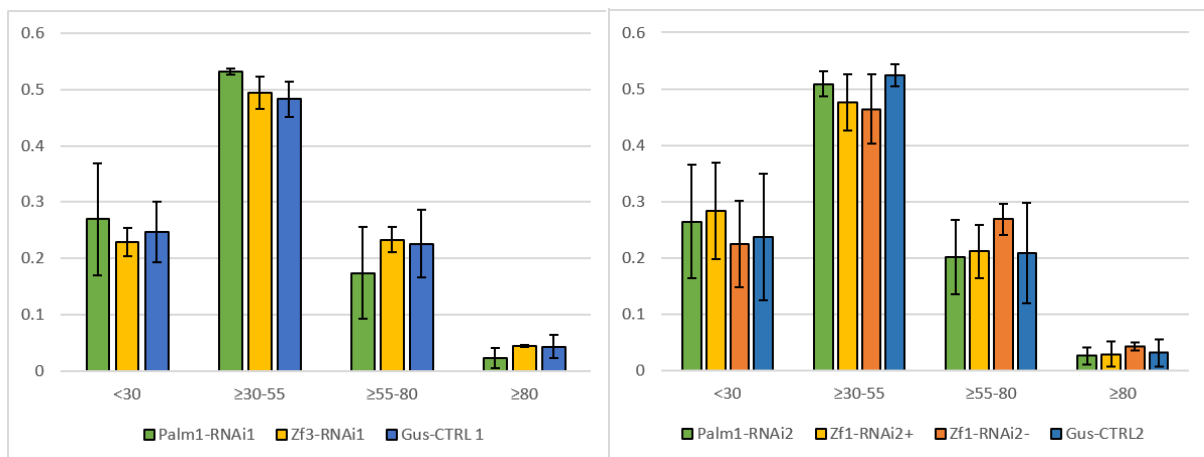


**Figure S5 – Arbuscule size distribution in roots expressing *MtZf*-RNAi constructs**

Longitudinal arbuscules sizes were measured from CLSM images of Alexa488-WGA-stained root fragments of *MtPalm1*-, *MtZf1*-, *MtZf3*-RNAi and *gus*-control roots. Relative distributions into four bins (<30 μm, 30-55 μm, 55-80 μm and >80 μm) are shown, error bars represent standard deviation. Measurements consist of 3x10 root sections for each sample group with an average of 911 arbuscules measured (19,133 in total). Listed under a) is the RNAi-1 construct compared to the *gus*-control 1 set while b) depicts the second set of samples. RNAi-constructs determined to be ineffective in sqRT-PCR measurements were not used in this analysis. No significant differences were observed.

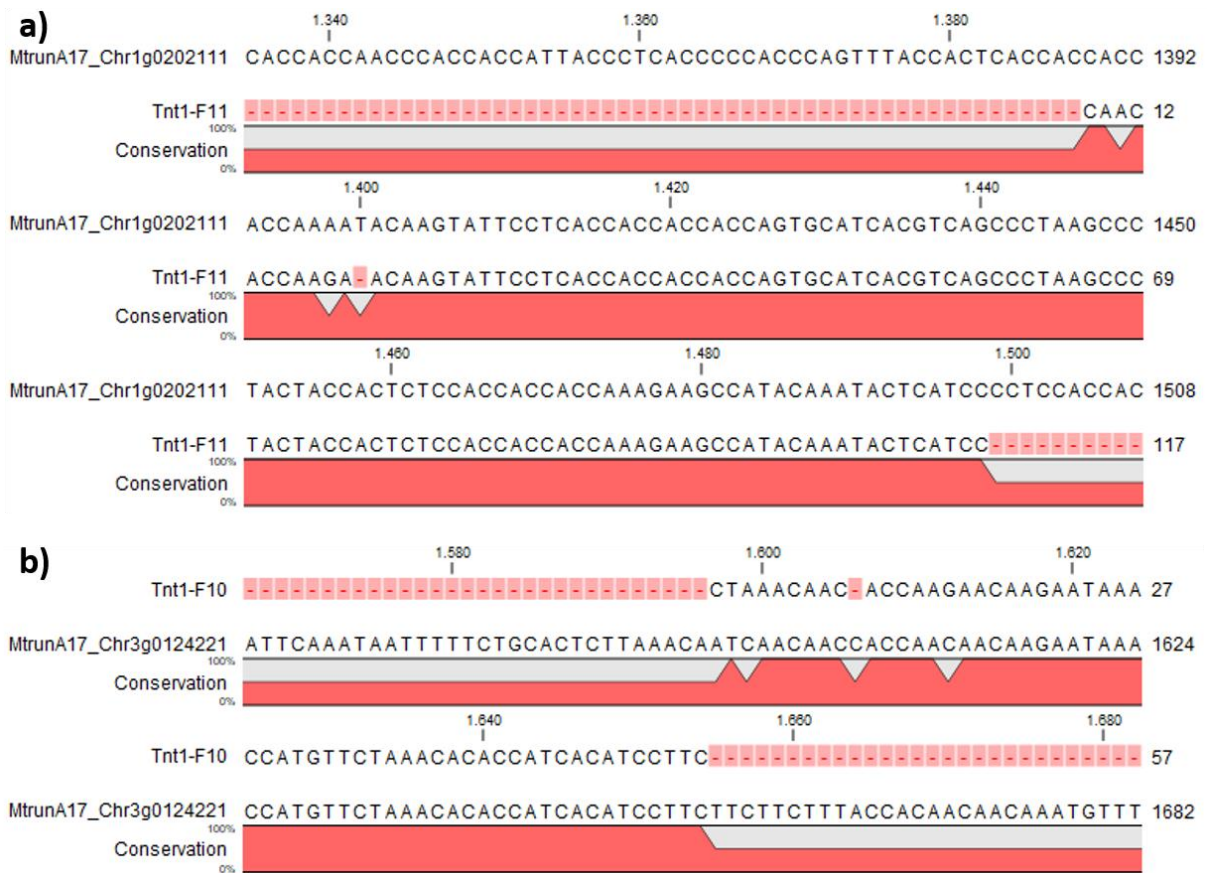


**Figure S6 – Sequencing results of amplicons obtained from *MtPalm1-Tnt1* plants**

Fragments amplified from *MtPalm1-Tnt1* mutants without the complementation construct via the *MtPalm1-Tnt1*-flanking primer pair during sqRT-PCR were subcloned into pGEMTeasy. Several clones obtained were sequenced to obtain information on the genes amplified. No sequences matching with *MtPalm1* were obtained. Instead, BLAST search revealed the fragments to match with MtrungA17\_Chr1g0202111 (a) and MtrungA17\_Chr3g0124221 (b), respectively.

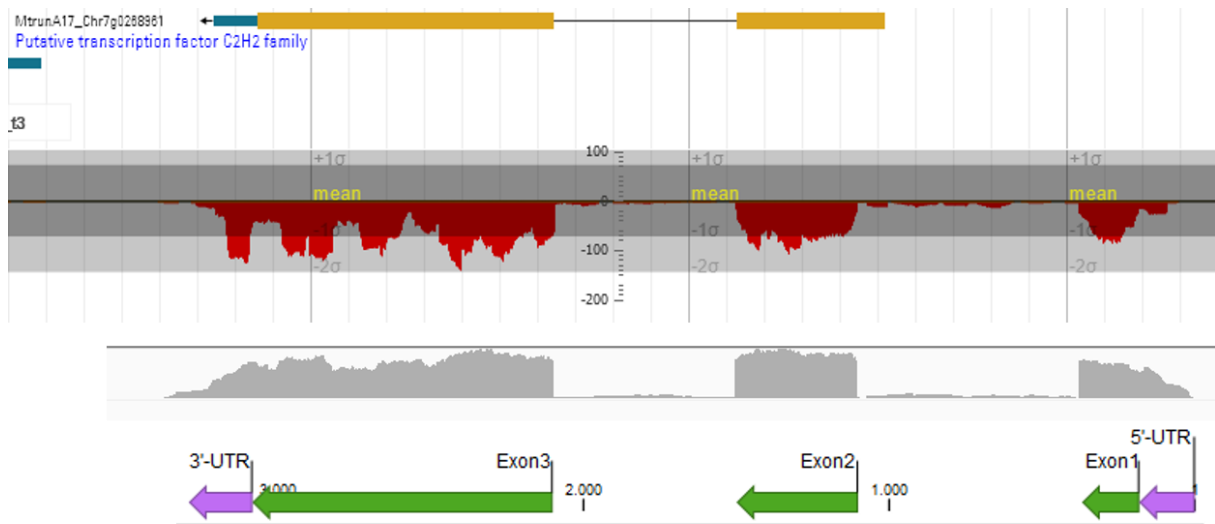


**Figure S7 – *MtZf2* gene annotation compared to data from different RNASeq results**

Shown at the top is the gene annotation of *MtZf2* (MtrunA17\_Chr7g0268961, -Strand) lacking the first Exon. Corresponding RNASeq read mappings from Luginbuehl *et. al* (2017) are shown below in red. Mapped reads from the *MtPalm1*-RNASeq data are shown in grey below in approximate agreement with the other dataset. Intron-exon-structure reconstructed from the cDNA obtained is shown below.

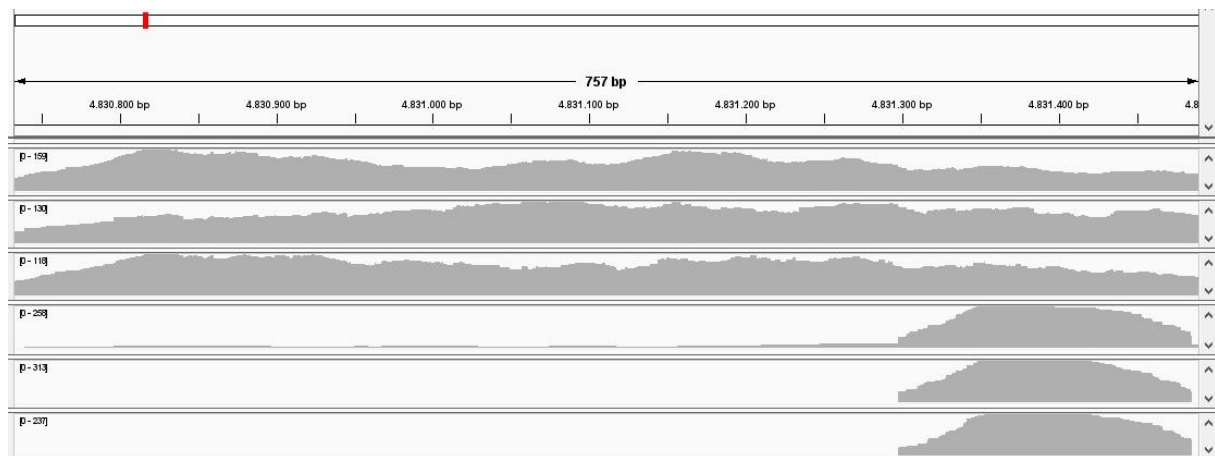


**Figure S8 – Erroneous quantification of *MtPalm1* transcripts in *MtPalm1*-RNAi samples during RNASeq**

Screenshot from Integrative Genomics Viewer depicting reads mapped to *MtPalm1* obtained from the RNASeq analysis. The three controls at the top show the entire mRNA being matched with reads at similar levels, while the RNAi samples at the bottom show predominate read mappings only to the 5'-region corresponding to the RNAi-construct. Few transcripts remain for the first RNAi-samples, while B and C at the bottom did not contain mRNAs corresponding to *MtPalm1*.

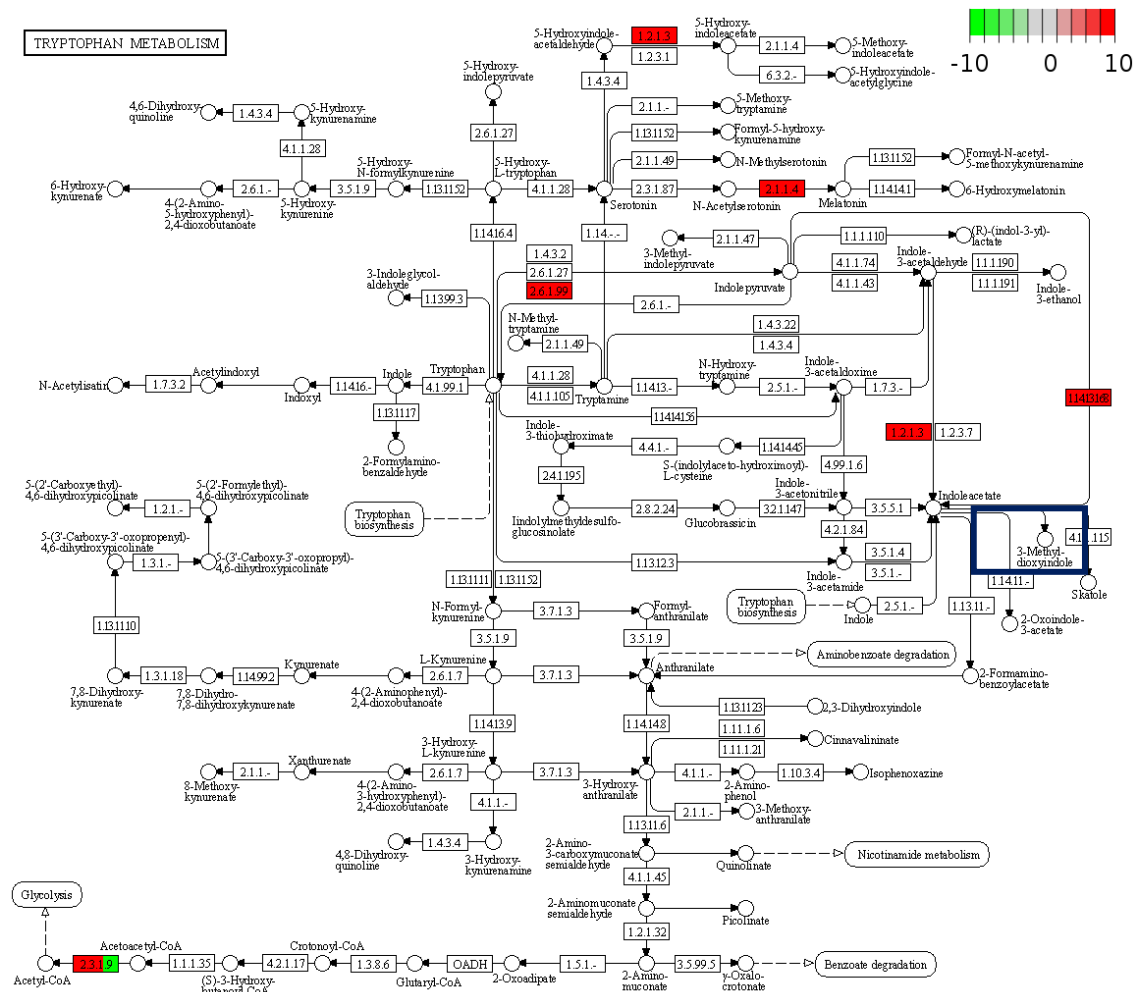
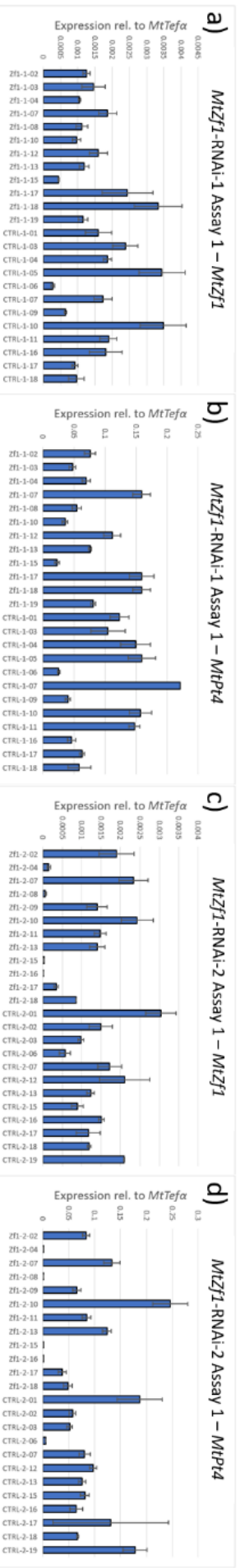


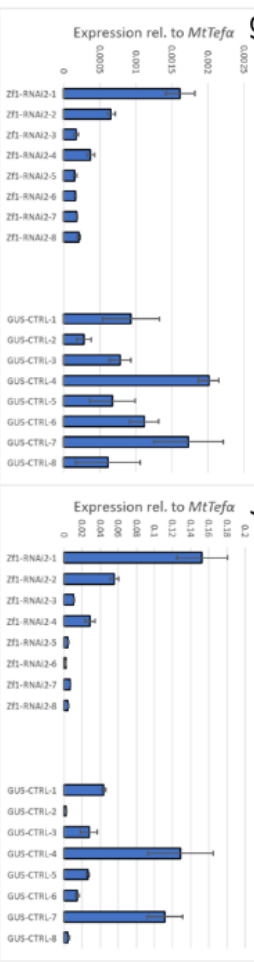
Figure S9 – Differential regulation of components of the tryptophan metabolism leading to indoleacetate (IAA)

Tryptophan metabolic pathway graph rendered in Pathview. Enzymes encoded by genes downregulated under MtPALM1-deficient conditions are shown in green, while those upregulated in the absence of MtPALM1 are depicted in red. Unaffected genes are shown in white. IAA is marked with a blue box.



**Figure S10 – Detailed results of the *MtZf1*-RNAi-knockdown experiments**

Individual *MtZf1* and *MtPr4* expression levels from *MtZf1*-RNAi roots samples in the three RNAi-assay performed compared to the respective controls as measured via qRT-PCR relative to *MtTef4*. Error bars represent standard deviation between technical replicates. In the first experiment shown in a)-d), RNA was extracted from the individual roots (12 for each category) compared to pools of three roots making up the samples in trials 2 (e, f) and 3 (g, h). RNAi-construct 2 was deemed ineffective based on assay 1 and thus not repeated further.



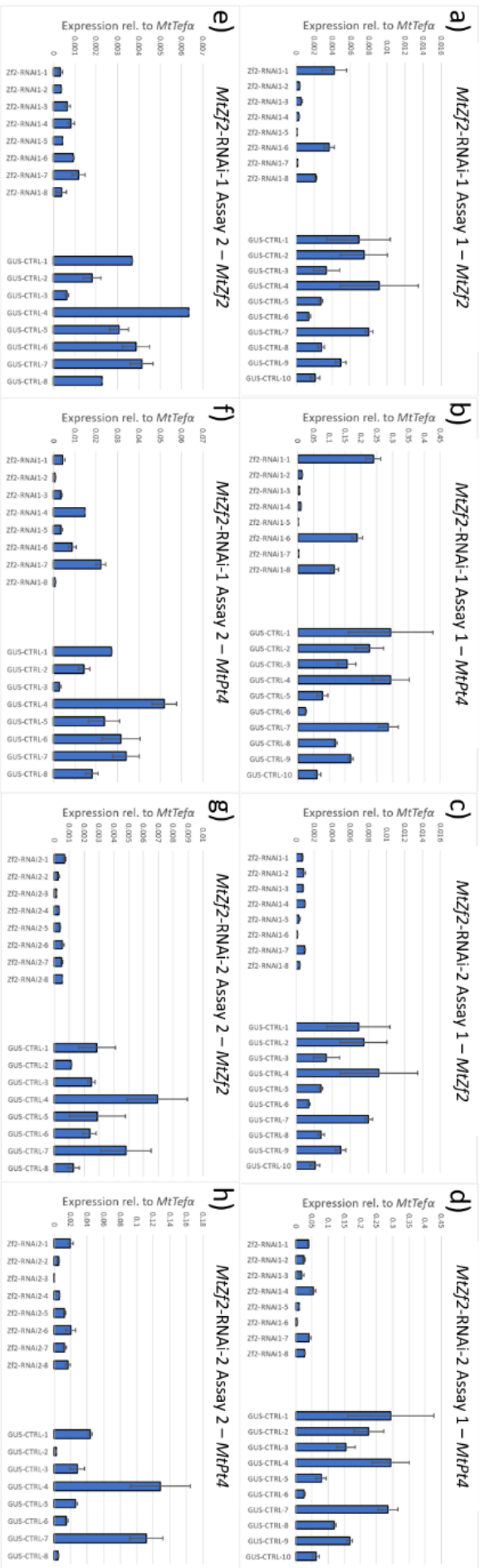


**Figure S11 – Detailed results of the MtZf2-RNAi-knockdown experiments**

Individual *MtZf2* and *MtPrt4* expression levels from *MtZf2*-RNAi roots samples in the three RNAi-assays performed compared to the respective controls as measured via sqRT-PCR relative to *MtTef4*. Error bars represent standard deviation between technical replicates. RNA was extracted from pools of three roots making up the eight samples in trials 1 (a-d) and 2 (e-h).

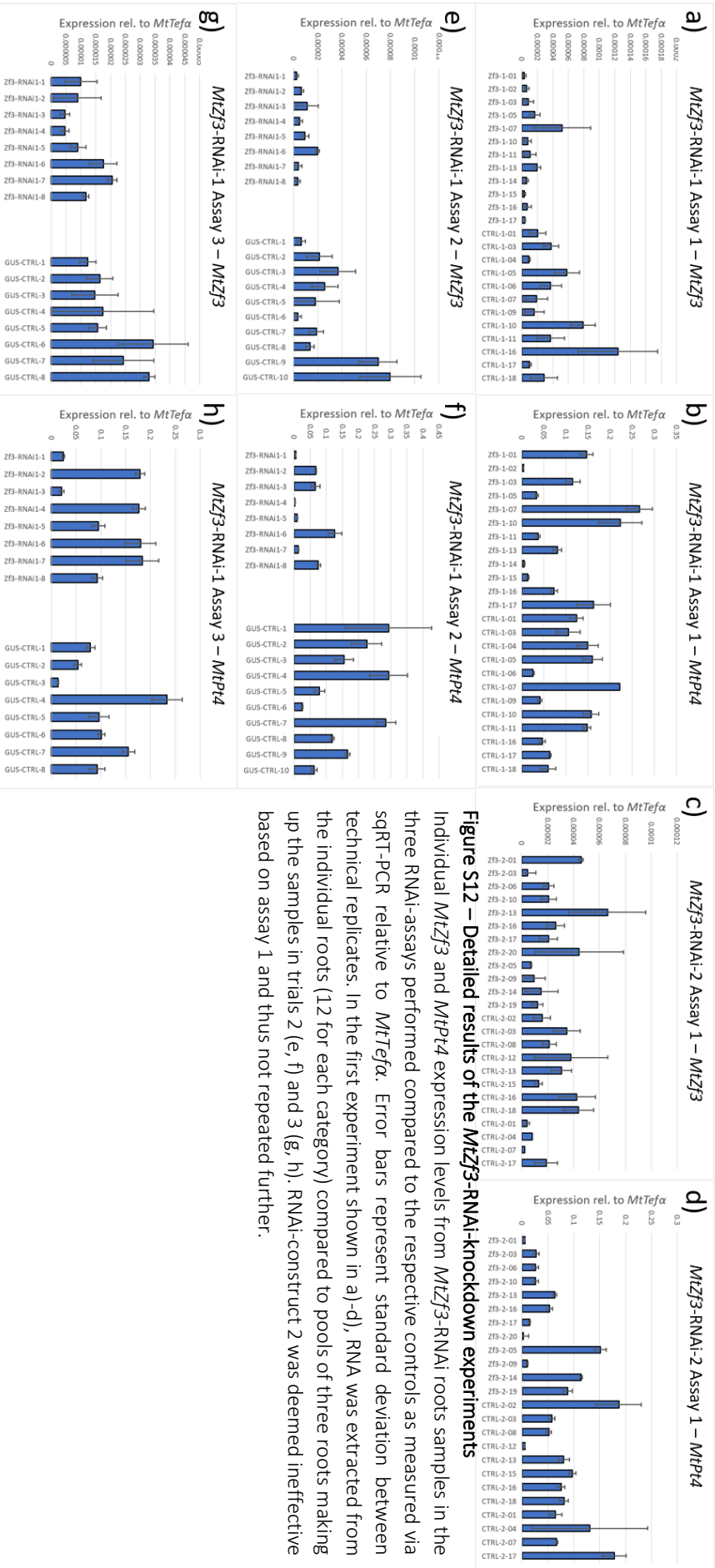


**Figure S12 – Detailed results of the MtZf3-RNAi-knockdown experiments**

Individual MtZf3 and MtPt4 expression levels from MtZf3-RNAi roots samples in the three RNAi-assays performed compared to the respective controls as measured via sqRT-PCR relative to MtTefα. Error bars represent standard deviation between technical replicates. In the first experiment shown in a)-d), RNA was extracted from the individual roots (12 for each category) compared to pools of three roots making up the samples in trials 2 (e, f) and 3 (g, h). RNAi-construct 2 was deemed ineffective based on assay 1 and thus not repeated further.



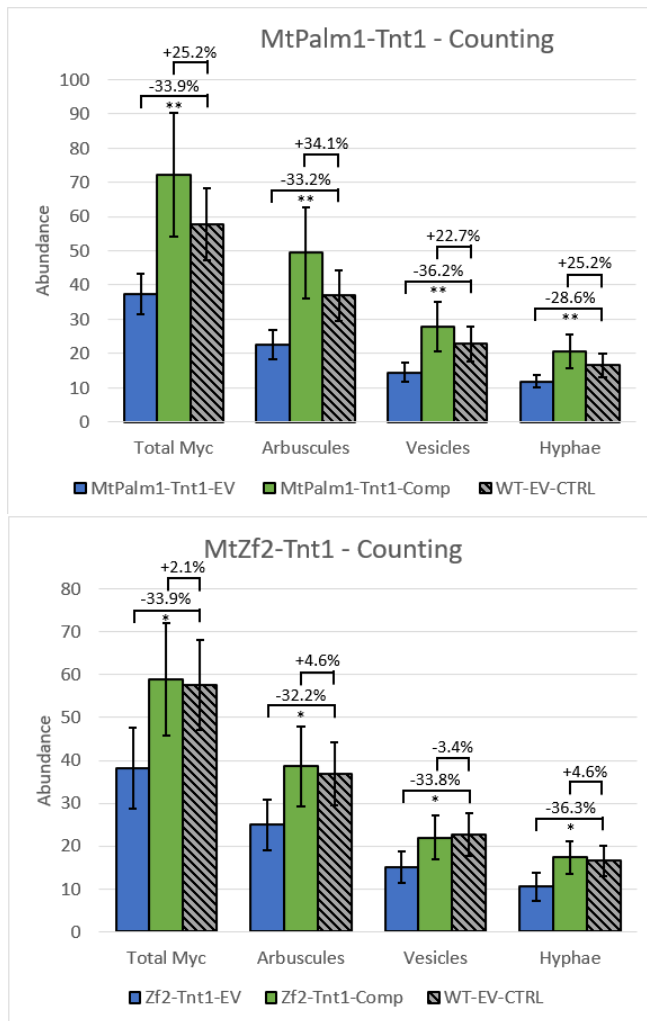


**Figure S13 – Results from counting AM-structures in *MtPalm1*- and *MtZf2-Tnt1* plants**

Mycorrhized root material from *MtPalm1-Tnt1* and *MtZf2-Tnt1* plant with and without the complementation constructs was used for quantification of AMF structures in comparison to the WT-EV controls. Depicted are the total average numbers of intraradical fungal structures observed in 300 root sections per sample (n = 14 for each group). Uncompensated *MtPalm1-Tnt1* roots shown in a) are hampered in overall mycorrhization and in arbuscule counts in particular (p < 0.01 for each structure quantified). The mutants expressing the *MtPalm1*-complementation construct exhibited a trend for slightly elevated mycorrhization levels, though this was not statistically significant. For *MtZf2-Tnt1-EV*, overall mycorrhization levels were approximately 33% reduced in all categories (p < 0.05). These observed effects were fully abolished in the *MtZf2-Tnt1-Comp* group (b), which exhibited WT-levels.

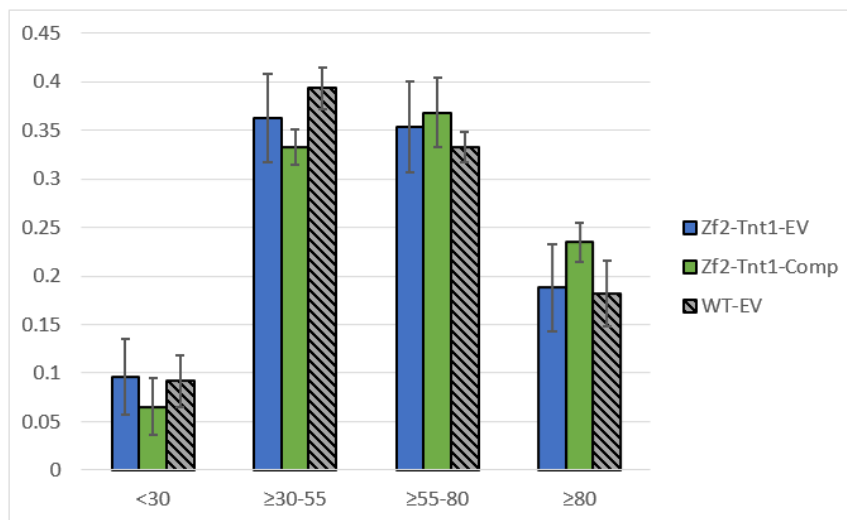


**Figure S14 – Arbuscule size distributions from *MtZf2-Tnt1* plants compared to controls**

Longitudinal arbuscules sizes were measured from LMPC images of CF488-WGA-stained root fragments from *MtZf2-Tnt1-Comp*, *MtZf2-Tnt1-EV* and WT-EV-control roots. Relative distributions into four bins (<30 μm, 30-55 μm, 55-80 μm and >80 μm) are shown, error bars represent standard deviation. Measurements consist of 4x10 root sections for each sample group with an average of 1,058 arbuscules measured (12,694 in total). The only statistically significant differences that were found were between the WT-EV-controls and the *MtZf2-Tnt1-Comp* samples in the 30-55 μm and 80 μm bins.





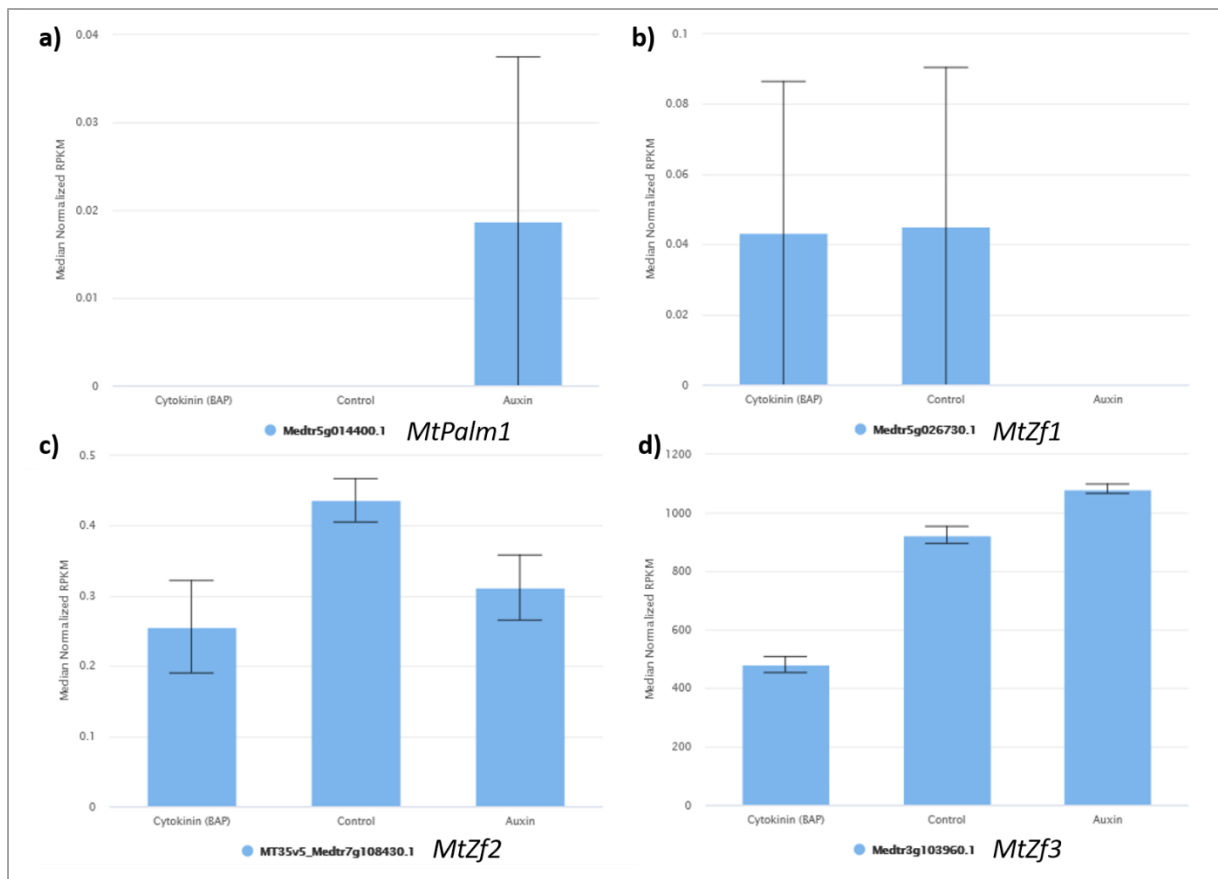


**Figure S16 – Potential phytohormone responsiveness of *MtZf* candidate genes**

RNASeq transcriptome data obtained from the MtSSPdb (Boschiero *et. al*, 2020). Relative expression of *MtPalm1*, *MtZf1*, *MtZf2* and *MtZf3* in *M. truncatula* A17 roots three days post germination under treatment with the cytokinin benzylaminopurin (BAP), IAA (Auxin) or DMSO (control). Bars represent relative transcript amounts as reads per kilobase million (RPKM). Error bars were calculated from three replicates for each condition.

**Table S1 – Genes very strongly downregulated in MtPALM1-deficient mycorrhized roots.**

All genes listed were either fully abolished in all three *MtPalm1*-RNAi samples used in the RNAseq approach or abolished in *MtPalm1*-RNAi\_B and \_C specifically, while being clearly expressed in the controls.

Gene ID	Gene Annotation	Average log change
MTR_5g040755	hypothetical protein	-8.748178149
MTR_6g086575	alpha-galactosidase-like protein	-8.453990373
MtrunA17Chr5g0417221		-8.390075468
MTR_1g086970	GRAS family transcription factor (GRAS7)	-7.605800783
MTR_3g058240	cytochrome P450 family 71 protein	-7.429183434
MTR_1g027560	hypothetical protein	-7.313228011
MTR_3g018920	annexin D8	-7.279262313
MTR_3g081690	ZIP zinc/iron transport family protein (ZIP10)	-7.012069463
MTR_1g098960	plant organelle RNA recognition domain protein	-6.867163438
MTR_6g066010	transmembrane protein%2C putative	-6.71659446
MTR_3g005790	zinc finger%2C C3HC4 type (RING finger) protein	-6.493373617
MTR_4g101460	adenine phosphoribosyltransferase-like protein	-6.444192576
MTR_7g070937	F-box protein interaction domain protein	-6.399831872
MTR_8g020590	auxin-binding protein ABP19a	-6.296223533
MTR_3g056630	NBS-LRR type disease resistance protein	-6.28218366
MTR_8g031170	Ripening related protein family	-6.162070487
MTR_2g102020	chitinase	-6.134602475
MTR_5g095290	cytochrome P450 family 71 protein	-6.128538471
MTR_5g009200	RING-H2 finger ATL21A-like protein	-6.103959625
MTR_5g011980	Lipid transfer protein	-5.994761174
MTR_5g035120	Pmr5/Cas1p GDSL/SGNH-like acyl-esterase family protein	-5.983770765
MTR_6g084320	ABC transporter-like family-protein	-5.944763751
MTR_7g080530	phosphoglycolate phosphatase-like protein	-5.902513613
MTR_1g014160	tubby C 2 protein	-5.851142875
MTR_7g105480	transmembrane protein%2C putative	-5.802244448
MTR_4g019030	verticillium wilt resistance-like protein	-5.801716702
MTR_1g090930	legume lectin beta domain protein	-5.788247045
MTR_2g094450	hypothetical protein	-5.751434089
MTR_4g014220	disease resistance protein (TIR-NBS-LRR class)%2C putative	-5.739003823
MTR_1g077260	hypothetical protein	-5.731493804
MTR_2g083930	papain family cysteine protease	-5.649803459
MTR_5g005290	hypothetical protein	-5.626752186
MTR_3g436170	alpha/beta amylin synthase	-5.615744121
MTR_1g038803	cytochrome P450 family protein	-5.573626029
MTR_4g017720	verticillium wilt disease resistance protein	-5.556307184
MTR_3g091230	hypothetical protein	-5.525738103
MTR_0147s0050	ATP-dependent RNA helicase DDX11-like protein%2C putative	-5.508258792
MTR_7g056300	hypothetical protein	-5.460858938
MTR_3g086070	disease resistance protein RGA4	-5.387620785
MTR_3g086970	hypothetical protein	-5.351046571
MTR_2g063813	RING/FYVE/PHD zinc finger protein	-5.316489193
MtrunA17Chr4g0006141		-5.298128028
MTR_7g039570	UDP-glucosyltransferase putative	-5.291903452
MTR_5g092500	toll interleukin receptor	-5.27378493
MTR_7g094120	SCF ubiquitin ligase SKP1 component	-5.268982037
MTR_0216s0030	albumin-2 protein	-5.25069855
MTR_4g081225	disease resistance protein (TIR-NBS-LRR class)	-5.201766218

MTR_6g038730	disease resistance family protein/LRR protein putative	-5.195007684
MTR_2g078490	transmembrane protein putative	-5.193276459
MTR_8g040250	sulfotransferase domain protein	-5.180609212
MTR_2g008540	chaperone DnaJ domain protein	-5.160047971
MtrunA17Chr2g0297471		-5.153536291
MTR_7g056537	D-mannose-binding lectin protein	-5.140070512
MTR_4g005250	DUF4283 domain protein	-5.139220098
MTR_4g117850	F-box protein interaction domain protein	-5.086948013
MTR_7g098150	peptide transporter	-5.085112899
MTR_3g058260	hypothetical protein	-5.012477287
MTR_0011s0290	hypothetical protein	-4.995068809
MTR_8g015150	LRR receptor-like kinase plant-like protein	-4.929345492
MTR_4g037480	transmembrane protein%2C putative	-4.924459838
MTR_8g013080	acid phosphatase	-4.92158564
MTR_8g027885	UDP-glucosyltransferase family protein	-4.92158564
MTR_4g091110	C3HC4-type RING zinc finger protein	-4.826305498
MTR_5g020900	transmembrane protein putative	-4.81507174
MTR_7g021570	LRR receptor-like kinase	-4.729307592
MTR_2g017875	GDSL-like lipase/acylhydrolase	-4.642059807
MTR_7g077300	Bowman birk trypsin inhibitor	-4.538649698
MTR_7g096660	hypothetical protein	-4.470988752
MTR_7g027610	core histone H2A/H2B/H3/H4	-4.381972906
MTR_1g103670	cytochrome P450 family protein	-4.125820212
MTR_4g049550	disease resistance-responsive2C dirigent domain protein	-4.107165859
MTR_8g074750	ammonium transporter 1 protein (AMT2;3)	-4.018042391
MTR_5g053935	hypothetical protein	-3.949548261
MTR_8g018620	seed linoleate 9S-lipoxygenase	-3.924625281
MTR_5g092520	toll/interleukin-like receptor-protein (TIR)	-3.922619498
MTR_8g060550	Kunitz type trypsin inhibitor	-3.894427955
MTR_8g009170	1-aminocyclopropane-1-carboxylate oxidase-like protein	-3.749679558
MTR_3g028630	stress-induced receptor-like kinase	-3.693186914
MTR_5g062030	hypothetical protein	-3.664692974
MTR_2g438540	hypothetical protein	-3.43758926

Table S2 – Genes very strongly upregulated in MtPALM1-deficient mycorrhized roots.

All genes listed were uniquely expressed in the three *MtPalm1*-RNAi samples, while not being measurable in the controls.

Gene ID	Gene Annotation	Average log change
MTR_4g094508	hypothetical protein	11.06756268
MTR_5g095840	transmembrane protein putative	10.36229633
MTR_8g006920	hypothetical protein	9.680173621
MTR_1g103620	late embryogenesis abundant D-like protein	9.602977615
MTR_8g022720	cytosolic class II small heat-shock protein	9.197222539
MTR_4g094720	1-cys peroxiredoxin PER1	9.00548705
MTR_1g103050	zinc finger C3HC4 type (RING finger) protein	8.600763684
MTR_5g043320	hypothetical protein	8.493997512
MtrunA17Chr6g0468481	hypothetical protein	8.277777616
MTR_3g054060	RNA recognition motif	8.045827796
MTR_1g030230	GDSL-like lipase/acylhydrolase	7.678472393

MTR_5g091100	hypothetical protein	7.678099427
MTR_5g023680	cytochrome P450 family 71 protein	7.654901337
MTR_5g018250	reticulon-like protein	7.610522184
MTR_1g073640	calcosin CLO1-1	7.506464575
MTR_3g072300	peptide/nitrate transporter	7.407618517
MTR_8g028480	late embryogenesis abundant protein	7.066651969
MTR_3g479470	UDP-glucosyltransferase family protein	7.049965526
MTR_3g034650	LRR and NB-ARC domain disease resistance protein	7.023672274
MTR_6g084660	hypothetical protein	6.917188279
MTR_2g075940	transmembrane protein putative	6.91254272
MTR_7g086110	LEM3 (ligand-effect modulator 3) family protein	6.8826749
MTR_7g097000	legumin A2	6.564589458
MTR_3g452940	hypothetical protein	6.210600304
MTR_3g084780	phloem filament protein PP1	6.202005931
MTR_5g038190	peptide/nitrate transporter	6.114914824
MTR_3g106930	core-2/l-branching enzyme	6.065182493
MTR_8g091320	myo-inositol 1-phosphate synthase	6.058659428
MTR_4g126400	hypothetical protein	5.999867974
MTR_2g015545	hypothetical protein	5.974877105
MTR_8g098515	clathrin light chain-like protein	5.815644452
MTR_1g069680	transmembrane protein%2C putative	5.775425387
MTR_7g007710	P-loop nucleoside triphosphate hydrolase superfamily protein	5.763533474
MTR_2g079980	white-brown-complex ABC transporter family protein	5.684454966
MTR_3g054020	tRNA-OTHER	5.629390291
MTR_3g031640	Serine/Threonine kinase plant-type protein	5.546177817
MTR_6g022000	cytosolic class I small heat shock protein	5.472190595
MtrunA17Chr3g0077621	hypothetical protein	5.3814496
MTR_5g022490	NB-ARC domain disease resistance protein	5.27731092
MTR_1g059700	beta-fructofuranosidase	5.172427939
MTR_1g107165	hypothetical protein	5.083866409
MTR_4g132560	F-box protein interaction domain protein	4.979435362
MTR_4g037225	gaba-receptor-associated protein ubiquitin domain protein	4.972245346
MTR_3g071950	hypothetical protein	4.971610087
MTR_0710s0020	aluminum activated malate transporter family protein	4.949088836
MTR_4g092070	dual-specificity kinase domain protein	4.837923128
MTR_4g019790	glutathione S-transferase amino-terminal domain protein	4.77169169
MTR_6g048350	stress up-regulated Nod 19 protein	4.760664502
MTR_5g098530	transmembrane protein putative	4.667403326
MTR_5g042150	phosphate transporter PHO1-like protein	4.515745336
MTR_1g111280	carboxylesterase putative	4.120084357
MTR_2g010610	CAP cysteine-rich secretory protein antigen 5	4.031198949
MTR_6g007633	bidirectional sugar transporter	3.985395345
MTR_4g107030	nonsense-mediated mRNA decay NMD3 family protein	3.97892646

## S1. *MtPalm1* bait-autoactivity was too severe to identify clear interaction partners in direct mating analyses

To obtain possible indications on the concrete role of *MtPalm1*-activity during AM symbiosis, both bait- and prey- strains were mated directly with a variety of different TFs involved with or related to AM-signaling. In spite of the only moderate autoactivation observed for the *MtPalm1*-bait during initial testing, mated strains were nearly always able to grow on the highest stringency QDO+AbA media (see Table S3). Similarly, moderate to intense blue staining was observed in all cases. As such, this test did not allow for the distinction of potentially true interactions for MtPALM1. The prey-strain for *MtPalm1* only reacted positively in two cases: Moderate blue staining was observed for matings with MtGRAS4- and MtWRI5a-baits. For the MtGRAS4-bait, a behavior similar to the MtPALM1-bait was noted, in that occasionally, despite not exhibiting sufficient autoactivity to overcome AbA alone, mated cultures were often able to (Hartmann, 2018). For *MtWri5a*, no such propensity was observed and this interaction might thus be a weak positive. At present, ruling out false positives is not possible due to the unclear data obtained from *MtPalm1*-baits. As such, further protein-interactions studies such as BiFC or EMSA would have to be performed to confirm or falsify these few early indications. Due to the strong autoactivation of any mated cultures, the MtPALM1-bait was not used in a prey-Library screening experiment.

**Table S3 – Y2H direct mating results for MtPALM1**

Results for any prey strains mated with the MtPALM1 bait are indicated in the left half of the table. The right half shows mating results for MtPALM1 prey mated with a variety of different baits. Growth performance is indicated by the stringency level reached: Growth on the DDO (double dropout) mating control medium needed to be observed to be included as a valid result (indicated by -). Growth on DDO+Aureobasidin A (AbA) indicates some potential weak interaction. The highest stringency quadruple dropout medium (QDO) + AbA indicates strong potential interaction partners. Additionally, observed staining intensity is indicated as well. Tests not performed are indicated with three dashes and a red color. Due to the ubiquity of potential interactions with the MtPALM1 bait and little indication for interactions with MtPALM1 prey, the positives are likely false due to increased autoactivation in mated cultures involving MtPALM1-bait.

MtPalm1-bait	prey	bait	MtPalm1-prey
QDO+AbA	Mt15867		---
QDO+AbA	Mt25005	Mt25005	-
QDO+AbA	Mt460730		---
-	MtArf5	MtArf5	-
DDO+AbA	MtArf7	MtArf7	-
DDO+AbA	MtArf25	MtArf25	-
QDO+AbA	MtCbf1	MtCbf1	-
QDO+AbA	MtCbf2	MtCbf2	-
QDO+AbA	MtCbf3	MtCbf3	-
DDO+AbA	MtColE		---
QDO+AbA	MtDella1		---

QDO+AbA	MtDella2		---
QDO+AbA	MtDella3		---
QDO+AbA	MtGras1	MtGras1	-
QDO+AbA	MtGras4	MtGras4	QDO+AbA
QDO+AbA	MtGras5		---
-	MtGras6	MtGras6	-
QDO+AbA	MtGras7	MtGras7	-
QDO+AbA	MtNF-YA1		---
QDO+AbA	MtNF-YA2		---
QDO+AbA	MtNF-YA3		---
QDO+AbA	MtNF-YA4		---
QDO+AbA	MtNF-YA5		---
QDO+AbA	MtNF-YA6		---
QDO+AbA	MtNF-YA7		---
QDO+AbA	MtNF-YA8		---
-	MtNsp1	MtNsp1	-
QDO+AbA	MtPalm1	MtPalm1	QDO+AbA
QDO+AbA	MtRad1		---
QDO+AbA	MtRam1		---
QDO+AbA	MtWri5a	MtWri5a	QDO+AbA
QDO+AbA	MtWri5b	MtWri5b	-
QDO+AbA	MtWri5c	MtWri5c	-
DDO+AbA	MtZf1	MtZf1	-
DDO+AbA	MtZf2	MtZf2	-

## S2. Interaction partners of MtZF2 could not be identified due to sporadic growth of the Y2H bait strain

In order to find potential interactors for the putative C2H2-ZF-TF MtZF2, bait- and prey-strains expressing MtZf2 were mated with a number of yeast strains containing *M. truncatula* TFs related to AM-processes.

Unfortunately, mated bait-strains expressing *MtZf2* uniquely exhibited extremely spotty growth even on the mating control media, making clear growth on higher stringency media unlikely to be detectable. As such, performing a library mating was also not deemed to be viable using this strain.

Prey-strains with *MtZf2* did not have this problem and exhibited normal growth. However, besides the strongly autoactive *MtPalm1*-bait, no clear potential interacting partner was identified (Table S4).

**Table S4 – Y2H direct mating results for MtZF2**

Results for any prey strains mated with the MtZF2 bait are indicated in the right LEFT of the table. The right half shows mating results for MtZF2 prey mated with a variety of different baits. Growth performance is indicated by the stringency level reached: Growth on the DDO (double dropout) mating control medium needed to be observed to be included as a valid result (indicated by -). Growth on DDO+Aureobasidin A (AbA) indicates some potential weak interaction. The highest stringency quadruple dropout medium (QDO) + AbA indicates strong potential interaction partners. Additionally, observed staining intensity is indicated as well. Tests not performed are indicated with three dashes and a red color. One dash and a red color indicates that the matings were not evaluated based on sporadic growth performance during these tests even on the DDO mating control media. The only potential positive was MtPALM1, which is likely due to strong autoactivation of MtPALM1 bait.

MtZf2-bait	prey	bait	MtZf2-prey
-	Mt15867		---
-	Mt25005	Mt25005	-
-	Mt460730		---
-	MtArf5	MtArf5	-
-	MtArf7	MtArf7	-
-	MtArf25	MtArf25	-
-	MtCbf1	MtCbf1	-
-	MtCbf2	MtCbf2	-
-	MtCbf3	MtCbf3	-
-	MtColE		---
-	MtDella1		---
-	MtDella2		---
-	MtDella3		---
-	MtGras1	MtGras1	-
-	MtGras4	MtGras4	-
-	MtGras5		-
-	MtGras6	MtGras6	-
-	MtGras7	MtGras7	-
-	MtNF-YA1		---
-	MtNF-YA2		---
-	MtNF-YA3		---
-	MtNF-YA4		---
-	MtNF-YA5		---
-	MtNF-YA6		---
-	MtNF-YA7		---
-	MtNF-YA8		---
-	MtNsp1	MtNsp1	-
-	MtPalm1	MtPalm1	QDO+AbA
-	MtRad1		---
-	MtRam1		---
-	MtWri5a	MtWri5a	-
-	MtWri5b	MtWri5b	-
-	MtWri5c	MtWri5c	-
-	MtZf1	MtZf1	-
-	MtZf2	MtZf2	-



### S3. BiFC-matrix of AM-related GRAS-proteins reveals novel potential interaction pairs

A number of *M. truncatula* GRAS-TFs upregulated during AM appeared to have fine tuning effects during symbiotic maintenance. However, no concrete functions could be elucidated thus far. Since GRAS-TFs rarely have DNA-binding capabilities on their own and heteromultimeric interactions such as between DELLA, RAM1 and NSP have been observed in the past in this family, further such interactions were deemed likely. A Yeast 2-Hybrid direct mating approach yielded some potential candidates for such interactions (Hartmann, 2018, data not shown). Due to autoactivation of a number of baits strains, however, not all such potential pairs could be examined. Additionally, the potential positives needed to be verified with another approach.

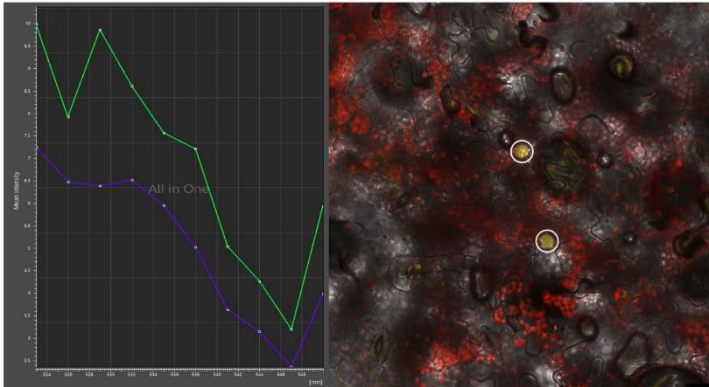
To that end, a Bimolecular fluorescence complementation assay was performed using a matrix of 13 AM-related GRAS-TFs, including the three *M. truncatula* DELLA-proteins, *MtNsp1* and 2, *MtRam1*, *MtRad1* as well as the candidates of thus far unknown function during AM: *MtGras1* (*MtTF80*), *MtGras4*, *MtGras5* (*MtSymScl1*), *MtGras6*, *MtGras7* and *MtGrasX*. In this approach, all potential interaction pairs were assayed at least once in both possible combinations between candidates fused to the respective N- or C-terminal YFP-fragment.

Throughout the assays, the known interaction pair MtNSP1/MtNSP2 consistently gave the strongest signal and was used as a positive control throughout all experiments performed (Figure S17). As expected, based on the available literature, MtNSP2 further exhibited potential for interactions with MtRAM1, MtRAD1, MtDELLA1, 2 and 3 as well as the capacity to form homodimers. MtNSP1 likewise gave a positive signal as a homodimer. Additionally, a potential interaction was observed with MtRAM1, which had not been reported previously. A weak possible signal was also observed in combination with MtGRAS4, representing a potential novel interaction as well.

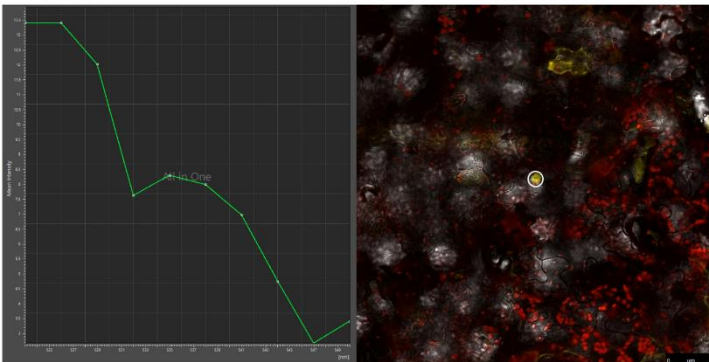
The positive signals for interactions involving MtRAM1 with MtRAD1, MtGRAS1 and itself as previously reported lend further credence as to the validity of this assay (complete results are illustrated in Figure S18).

In addition, the interactions between MtRAD1 and MtDELLA proteins 1 and 2 that were demonstrated before could not be verified here. Weak, but according to the applied scrutiny true YFP signals could occasionally be detected in the combination of C-MtDELLA1/N-MtRAD1, but not in the majority of cases. Additionally, bidirectional positives were not detected. This might indicate that the chosen requirement of signals in both possible orientations could lead to some true interaction pairs being rejected.

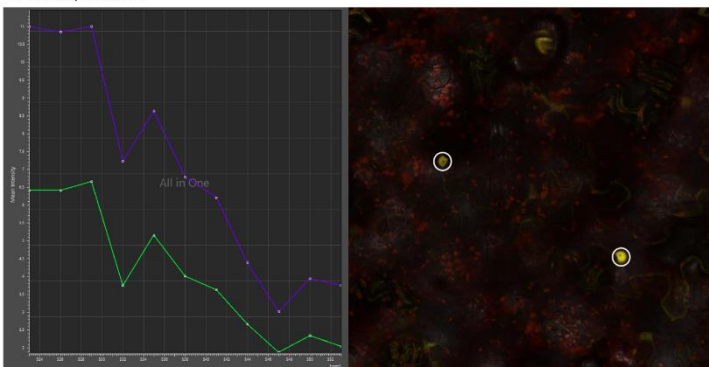
C-Nsp2/N-Nsp1



C-Nsp1/N-Gras4



C-Della3/N-Ram1



C-Rad1/N-Della1

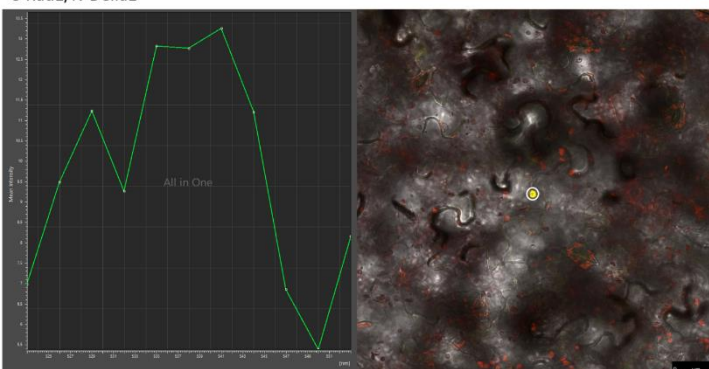
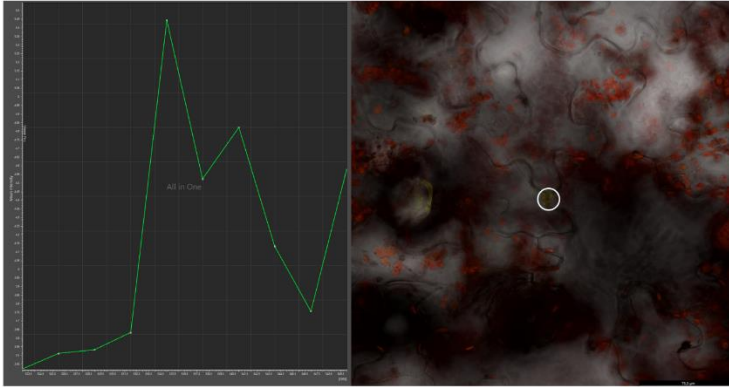


**Figure S17 – Representative collection of nuclear localized YFP-signals and corresponding  $\lambda$ -Scans**

The GRAS-TFs indicated were fused to an N- or C-terminal YFP-fragment and co-expressed in *N. benthamiana* leaves. Positive YFP-signals localized toward the nucleus indicate an interaction between the two proteins expressed. Micrographs with such potentially positive signals are shown to the right. On the left side,  $\lambda$ -Scans are shown of the fluorescence emission in the regions around the potentially positive signals (as indicated by the circles in the microscopic images) measured from 523 nm – 553 nm. For YFP, an emission peak around 228 nm was expected. The combination of MtNSP1 and MtNSP2 consistently gave strong positive signals and was used as a positive control throughout the experiment. Below, the positive signals obtained from the MtNSP1/MtGRAS4 and MtDELLA3/MtRAM1 combinations indicate represent potentially novel interactions between these AM-related GRAS-TFs. The example of a potential signal not considered a positive based on the  $\lambda$ -Scan is given by the combination of C-MtRAD1 and N-MtDELLA1. The previously reported potential interaction between MtRAD1 and MtGRAS4 could not be replicated in this assay.

C-Rad1/N-Gras4



Without this criterion, the putative interaction pairs MtDELLA3/MtGRAS6, MtRAM1/MtGRAS6, MtNSP1/MtGRAS5 as well as MtGRAS4/MtGRAS7 and MtGRAS5/MtGRAS7 would be positive candidates for further interactions studies, as they gave unidirectional YFP-signals as well.

The potential interactions between MtGRAS4 and MtRAD1, MtGRAS4 and MtGRAS1 as well as the dimerization of MtGRAS1 reported in the previous Y2H interaction study could not be verified.

	pSPYCE: MtDella1	pSPYCE: MtDella2	pSPYCE: MtDella3	pSPYCE: MtNsp1	pSPYCE: MtNsp2	pSPYCE: MtRam1	pSPYCE: MtRad1	pSPYCE: MtGras1	pSPYCE: MtGras4	pSPYCE: MtGras5	pSPYCE: MtGras6	pSPYCE: MtGras7	pSPYCE: MtGrasX
pSPYNE: MtDella1					Light Green		Dark Green						
pSPYNE: MtDella2					Light Green		Dark Green						
pSPYNE: MtDella3					Light Green	Yellow							
pSPYNE: MtNsp1				Light Green	Light Green	Yellow			Light Yellow				
pSPYNE: MtNsp2	Light Green	Light Green	Light Green	Light Green	Light Green	Light Green	Light Green						
pSPYNE: MtRam1			Yellow	Yellow	Light Green	Light Green	Light Green	Light Green					
pSPYNE: MtRad1	Dark Green	Dark Green			Light Green	Light Green			Blue				
pSPYNE: MtGras1						Light Green		Blue	Blue				
pSPYNE: MtGras4				Light Yellow			Blue	Blue					
pSPYNE: MtGras5													
pSPYNE: MtGras6													
pSPYNE: MtGras7													
pSPYNE: MtGrasX													

**Figure S18 – Matrix of examined putative interactions between AM-related GRAS-TFs**

The thirteen AM-related GRAS-TF genes *MtDella1*, *2* and *3*, *MtNsp1* and *2*, *MtRam1*, *MtRad1* as well as *MtGras1*, *4*, *5*, *6*, *7* and *X* were translationally fused to N- and C-terminal YFP-fragments contained in the binary vectors pSPYNE/pSPYCE, respectively. All possible combinations of N- and C-terminal fusions were assayed as part of a Bimolecular fluorescence complementation assay in *N. benthamiana* leaves. Positive YFP-signals indicating protein-protein interactions that were previously reported in the literature are presented in light green. Potentially novel interactions pairs identified during this BIFC assay are shown in yellow (lighter tone in the MtNSP1/MtGRAS4-pair signifies relatively low signal strength). Previously obtained positive interaction results from a Y2H direct mating approach are marked in blue and could not be confirmed as part of this experiment. Dark green boxes mark reported interactants that were not considered positives during this experiment. Any positive signals that could not be replicated in the respective opposing orientation were not considered true positives and thus excluded from this overview (e.g.: pSPYCE:*MtDella1*/pSPYNE:*MtRad1* gave a detectable YFP-signal while pSPYCE:*MtRad1*/pSPYNE:*MtDella1* did not).

## 8 Danksagung

Zunächst möchte ich mich bei meinen Betreuern Prof. Dr. Helge Küster und Dr. Natalija Hohnjec bedanken für ihre Mithilfe mit Rat und Tat und selbstverständlich dafür, dass sie mir überhaupt erst die Möglichkeit gegeben haben als Teil ihrer Arbeitsgruppe für meine Dissertation zu forschen. Darüber hinaus danke ich dem ganzen Team der Pflanzengenomforschung, das mich über die insgesamt fünf Jahre dort begleitet hat:

Meine Master-Mitstreiter Daniel Nübel und Jana Vasilev, meine Doktoranden-Kollegen Dr. Lisa Hartung und Steven Krüger, die frühere Generation Dr. Rico Hartmann und Dr. Marian Uhe, das Herz der Gruppe Natascha Köppens und allen weiteren Studierenden die mit uns zusammengearbeitet haben.

Vielen Dank auch an Dr. Sascha Offermann und Prof. Dr. Thomas Debener, die sich netterweise bereiterklärt haben meine Arbeit zu begutachten.

Riesiger Dank geht auch an meine Familie, ohne deren Unterstützung ich niemals die Chance gehabt hätte es in meinem Studium so weit zu bringen!

Zuletzt gebührt noch ganz besonderer Dank meiner Freundin Gwendolin Simper, die mir vor, während und hoffentlich noch lange nach meiner Doktorarbeit trotz aller Widrigkeiten mit Liebe und auch fachlich immer zur Seite stand.

## Curriculum Vitae

Arne Christopher Alexander Petersen

Geboren am 25.09.1992 in Bremen

### Bildungsweg:

- |             |   |
|-------------|---|
| 2017 – 2022 | Doktorand zum Thema “Functional Analysis of Zinc Finger Proteins in the Arbuscular Mycorrhiza Symbiosis of <i>Medicago truncatula</i> Suggests a Regulatory Involvement of the PALM1 Transcription Factor” in der Abteilung für Pflanzengenomforschung am Institut für Pflanzengenetik der Leibniz Universität Hannover |
| 2015 – 2017 | Master of Science in Biologie der Pflanzen an der Leibniz Universität Hannover  |
| 2011 – 2015 | Bachelor of Science in Biologie an der Leibniz Universität Hannover   |
| 1998 – 2011 | Schulbildung bis zum Abitur an der KGS Leeste   |